The structural and dynamic behaviour of coordination cages, rings and chains

Andrew Stephenson

A thesis submitted to The University of Sheffield in partial fulfilment of the requirements for the Degree of Doctor of Philosophy

Department of Chemistry
University of Sheffield
Sheffield S3 7HF
United Kingdom

September 2012

Abstract

This thesis concerns the structural and dynamic behaviour of polyhedral coordination cages and other supramolecular complexes based on a family of bis(pyrazolyl-pyridine) ligands.

Chapter One introduces the general principles governing self-assembly. Examples of self-assembly in nature and coordination chemistry are shown and rationalised. Examples of previous research into coordination cages from groups around the world are discussed including the potential applications.

Chapter Two describes the synthesis of the ligand L^{pp} which is shown to form different polyhedral coordination cages with different metals, namely $[M_{16}(L^{pp})_{24}]^{32+}$ (M = Cd or Zn), $[Cu_6(L^{pp})_9]^{12+}$ and $[Ni_8(L^{pp})_{12}]^{16+}$. The $[Cd_{16}(L^{pp})_{24}]^{32+}$ cage has been shown to undergo a cage-to-cage interconversion in solution to a number of smaller cages, predominantly $[Cd_6(L^{pp})_9]^{12+}$.

Chapter Three describes the synthesis of the related ligand L^{14naph}. $[Cd_{16}(L^{14naph})_{24}]^{32+}$ has been synthesised and shown to be stable in solution. An $[M_3(L^{14naph})_3]^{6+}$ (M = Cd or Cu) complex was synthesised and reacted with L^{mes} in a 1:1 ratio to afford a $[M_{12}(L^{14naph})_{12}(L^{mes})_4]^{24+}$ (M = Cd or Cu) cuboctahedron cage. The ligand L^{14naph} has also been shown to form a new $[Ni_8(L^{14naph})_{12}]^{16+}$ 'cuneane' coordination cage, a geometric isomer of a cube.

Chapter Four describes the synthesis of the ligands L^{fur} and L^{th}, which comprise two chelating pyrazolyl-pyridine termini connected to furan-2,5-diyl or thiophene-2,5-diyl spacers *via* methylene groups. These have been shown to form a range of cube and square structures with first-row transition metal ions. There is also a mononuclear complex and a one-dimensional chain consisting of an infinite sequence of crosslinked $[Cd_2(L^{th})_2]^{4+}$ double helicate units with Cd(II).

Chapter Five describes the coordination chemistry of a series of bis(pyrazolyl-pyridine) ligands with Ag(I). A remarkable series of complexes has been shown and the wide range of structures is due to different interactions dominating in different structures. These include Ag•••Ag interactions, aromatic π-stacking and exocyclic lone pair interactions.

Chapter Six describes the attempted synthesis of Ir-labelled luminescent coordination cages using a tritopic ligand with an $\{Ir(ph\text{-}py)_2\}^+$ unit coordinated to one of the three pyrazolyl-pyridine groups. A $\{Cd_2(L^{mes\text{-}Ir})_2\}^{6+}$ complex based on a double helicate with pendent Ir-groups was among structures afforded. A $\{Cu_3(L^{mes\text{-}Tz})_2\}^{6+}$ capsule with a nitrate in the central cavity was achieved serendipitously and requires the nitrate anion as a template for formation around it.

Acknowledgements

My first thanks go to my supervisor Mike Ward, who has been encouraging, supportive and always full of good ideas. It has been great working in your group and thanks very much for all your help and guidance.

I would like to thank all members of the Ward group, past and present, who I have worked with over the years. These include the (very knowledgeable) Post-Docs Ian, Danoooo, Alex and Martina who always have very useful advice and the PhD students Ben, Methers, AJ, Shida, Adel, Voirrey, Hazel, Nick and Sofia.

Ian Tidmarsh helped me a lot when I first joined the group and taught me about the art of solving and finishing difficult crystal structures so a very big thanks to him. Thanks to Danoooo for his unwavering positivity, help with luminescence [Dan (luminescence)] and for coming up with some excellent ideas! Thanks to Slugger for being a great goalkeeper (sometimes) and for seeming to know something about everything. Also thanks to AJ and Martina for keeping me well up-to-date on the latest gossip and for making the tea far more than I have! Thanks to Ben for an enjoyable three years in the lab and for lots of interesting information about F1. Thanks also to Methers, it was great (trying) to supervise you but it has been even better beating you at pool!

Thanks also to the Brammer group for sharing the lab and office and being a generally good bunch of people and giving us Wardsters all a good laugh.

Thanks to all the Technicians in the department especially Harry Adams for introducing me to X-ray crystallography, Brian and Sue for help with NMRs and Simon and Sharon from mass spec.

I would like to say a big thank you to my parents for their support over the seven years at university, and the rest of my family and friends including my brother Jim. Finally of course, a huge thanks to Laura who has had to put up with living with me for the last four years but has always been there and I hope you've enjoyed it as much as I have!

Contents Page

List of Publications

1. Structures and Dynamic Behaviour of Large Polyhedral Coordination Cages: An Unusual Cage-to-Cage Interconversion; **A. Stephenson**, S. P. Argent, T. Riis-Johannessen, I. S. Tidmarsh, and M. D. Ward, *J. Am. Chem. Soc.*, 2011, **133**, 858–870

2. An octanuclear coordination cage with a 'cuneane' core—a topological isomer of a cubic cage; **A. Stephenson** and M. D. Ward, *Dalton Trans.*, 2011, **40**, 7824-7826

3. Molecular squares, cubes and chains from self-assembly of bisbidentate bridging ligands with transition metal dications; **A. Stephenson** and M. D. Ward, *Dalton Trans.*, 2011, **40**, 10360-10369

4. Structures, host-guest chemistry and mechanism of stepwise self-assembly of new M_4L_6 tetrahedral cage complexes; B. R. Hall, L. E. Manck, I. S. Tidmarsh, **A. Stephenson**, B. F. Taylor, E. J. Blaikie, D. A. Vander Griend and M. D. Ward, *Dalton Trans.*, 2011, **40**, 12132-12145

5. 1-Benzoyl-3-(2-pyridyl)pyrazole; A. H. Shelton, **A. Stephenson**, M. D. Ward and M. B. Kassim, *Acta Cryst E*, 2011, **67**, o2445

6. A triple helix of double helicates: three hierarchical levels of self-assembly in a single structure; **A. Stephenson** and M. D. Ward, *Chem. Commun.*, 2012, **48**, 3605-3607

7. Coordination chemistry of Ag(I) with bridging ligands based on pyrazolyl-pyridine termini: polymers, helicates and a bow-tie; **A. Stephenson** and M. D. Ward, *RSC Adv.*, 2012, **2**, 10844-10853

Abbreviations

M	Metal
L	Ligand
Fac	Facial
Mer	Meridional
NMR	Nuclear Magnetic Resonance
δ	Chemical shift
ppm	Parts per million
J	Coupling constant
Hz	Hertz
s	Singlet
d	Doublet
t	Triplet
m	Multiplet
COSY	Correlation spectroscopy
DOSY	Diffusion-ordered spectroscopy
ESMS	Electrospray Mass Spectrometry
ES	Electrospray
m/z	Mass to charge ratio
EA	Elemental Analysis
2θ	Angles of the diffractometer
Å	Angstrom
a, b, c	Unit cell dimensions
α, β, γ	Unit cell angles

V	Unit cell volume
Z	Formula units per unit cell
μ	Linear absorption correction
F_o, F_c	Observed and calculated structure factors
R_1, wR_2	R-indices (based on F and F^2 respectively)
PyPz	Pyrazolyl-pyridine
PhPy	Phenyl-pyridine
NBS	N-Bromosuccinimide
AIBN	Azobisisobutyronitrile
MeCN	Acetonitrile
$MeNO_2$	Nitromethane
MeOH	Methanol
THF	Tetrahydrofuran
DCM	Dichloromethane
CCl_4	Carbon tetrachloride
$CDCl_3$	Deuterated chloroform
CD_3CN	Deuterated acetonitrile
CD_3NO_2	Deuterated nitromethane

1. Introduction

1.1 Self-assembly

Self-assembly has become increasingly prominent in chemistry in recent times and is a field that although growing rapidly is still far from fully understood. This is because it is only in recent times that the technology has become available to understand and try to mimic the self-assembly that is seen in the natural world.[1]

Self-assembly can be described as a process in which two or more components can spontaneously associate to form a larger, more-ordered structure through weak non-covalent interactions.[2] These interactions can include hydrogen bonding, van der Waals forces and dipole-dipole interactions. Metal-ligand coordinate bonds are also included assuming that they are weak and kinetically labile.[3]

There are many classes of self-assembly although it is possible to separate them into two main types.[4] Strict self-assembly is when the components assemble reversibly, meaning that a change of conditions can lead to the structure going back to its component parts. Self-assembly here is generally driven by relatively weak interactions which are often electrostatic and can include hydrogen bonds and van der Waals forces. The product that forms is under thermodynamic control and has the maximum free energy possible in the system. The alternative is irreversible self-assembly where the interactions are often covalent bonds which are stronger and therefore harder to break. This process is under kinetic control and often requires the component parts to be complementary to each other.

Coordination cages require a strict self-assembly process so that many possible metal/ligand combinations are 'trialled' until the system finds the thermodynamic minimum. At this point there are enough weak interactions reinforcing each other that the assembly becomes kinetically inert and the thermodynamic product is retained.[5]

Self-assembly on the molecular scale has many interesting possibilities for the future. The largest of these could be in nanotechnology where the current method of 'engineering down' to make things smaller is becoming less feasible. The fields of self-

assembly and self-organisation would allow a 'synthesising up' approach, meaning devices can be made much smaller, possibly one day on the molecular scale.[6]

1.2 Examples of self-assembly in nature

Self-assembly plays a very important role in coordination cages but it is also ubiquitous throughout all of chemistry, particularly in nature. A classic example of strict self-assembly in nature is the tobacco mosaic virus (TMV). Protein sub-units spontaneously arrange around a single strand of RNA to form a right handed helix with 16 ⅓ sub-units per helical turn. On changing the temperature, pH or pressure the sub-units will dissociate into their component parts, meaning that assembly of the system is completely reversible.[7] Another example is in lipid bilayers, which form the cell membrane of almost all living organisms and are vital in keeping ions, proteins and other molecules either inside or outside of cells. Lipid bilayers are composed of amphiphilic phospholipids which when exposed to water self-assemble into a two-layered sheet with all of the hydrophobic tails being protected from the water. An interesting elaboration on this natural effect by Nakashima and co-workers was to use C_{60} molecules attached to three alkyl chains and they found that these also self-assembled to give a lipid bilayer structure on electrodes (figure 1.2.1). This is potentially useful due to the electrochemical and optical properties of fullerenes, for example each C_{60} molecule can serve as storage for six electrons.[6, 8]

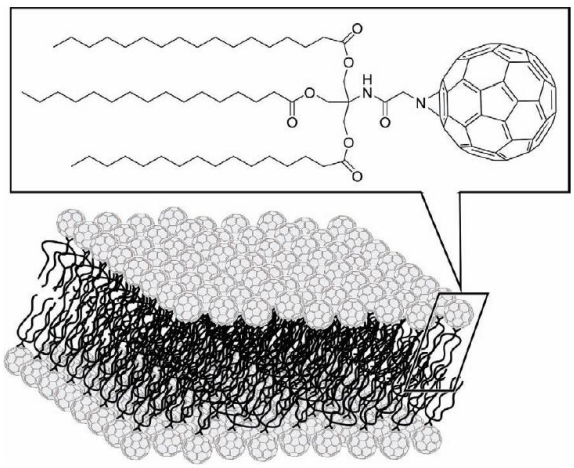

Figure 1.2.1 A lipid bilayer structure of synthetic C_{60} molecules with triple alkyl chains. Reproduced from reference 6.

Self-assembly is also responsible for self-assembled monolayers (SAMs). These also use amphiphilic molecules and are created by the chemisorption of hydrophilic head groups onto a substrate. The monolayers are very tightly packed due to van der Waals forces between neighbouring tails and they can also be functionalised at the end of the tail. These are of interest for a number of reasons and are used in nanotechnology, nanoelectronics and biology. They are a largely separate field though as self-assembly at an air-water interface as is the case with monolayers is very different from self-assembly in a bulk phase.[6]

There is no more important example of self-assembly than DNA.[9] Self-assembly is vital to the formation of DNA as the two polymeric chains of nucleotides come together via complementary hydrogen bonds between base-pairs. The result is a right-handed double helix with guanine – cytosine and adenine – thymine base pairs. The hydrogen bonding in the structure is weak compared to covalent bonds and therefore the double helix can be broken apart and rejoined. This has led to a lot of research in DNA nanotechnology, pioneered by Seeman and co-workers who have shown DNA to be a useful building block in 2D- and 3-D structures, for example a cube[10] as shown in figure 1.2.2. This has been extended to using DNA to synthesise DNA computers[11] and molecular machines.[12]

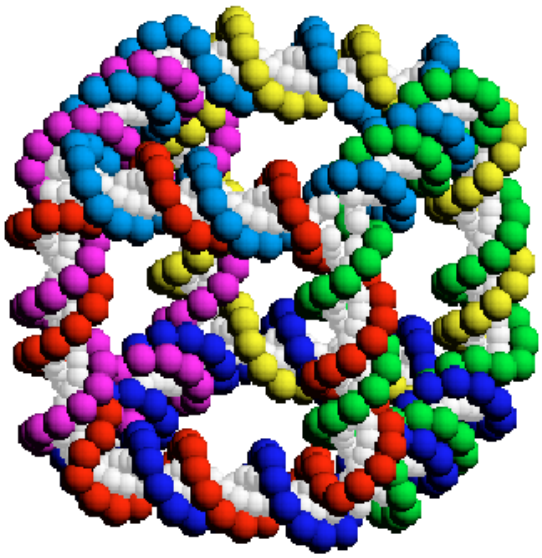

Figure 1.2.2 A representation of a DNA molecule with the connectivity of a cube. Reproduced from reference 13.

1.3 Examples of self-assembly in coordination chemistry

The serendipitous discovery of crown ethers by Pedersen in the 1960s[14] and the subsequent research into cryptands[15] and spherands[16] by Lehn and Cram respectively led to them receiving the Nobel Prize in 1987. These early discoveries led to a great amount of research in supramolecular chemistry based on weak interactions such as hydrogen bonding motifs, ion-ion interactions, van der Waals interactions, π-π interactions and metal-ligand coordination bonds.[17] Metal-ligand coordination bonds have two advantages over weaker interactions; (i) the energies of metal-ligand bonds are weak enough for bonds to break apart until the thermodynamic product is reached, but strong enough to keep this product stable. This means that kinetic intermediates can be 'trialled' until the final product is reached. (ii) The metal and ligand can both have a strong directional and geometrical preference; therefore some design can be applied to achieve a specific product.[18]

One of the first examples of self-assembly in coordination chemistry came from Fujita and co-workers in 1990. He used square-planar palladium (II) ions and a linear 4,4'-bipyridine bridging ligand to form an almost perfect square as shown in figure 1.3.1.[19]

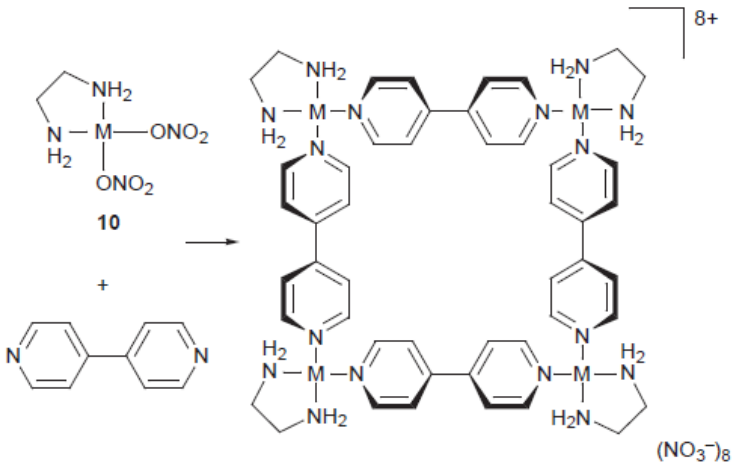

Figure 1.3.1 Fujita's $[Pd(en)(4,4'\text{-bpy})]_4$ $(NO_3)_8$ square. Reproduced from reference 20.

At a similar time Lehn and co-workers were able to show that the self-assembly of helicates was also possible. They synthesised double stranded helicates from oligo-bipyridine ligands and copper (I) cations. They found that mixing different sized oligo-

bipyridine strands with copper ions resulted in very selective formation of different sized helicates.[21] They also showed that by using two differently substituted bipyridine ligands with copper (I) or nickel (II) ions that a double or a triple helix would form exclusively.[22] This was because copper (I) ions are 4-coordinate and nickel (II) ions are 6-coordinate. This is shown in figure 1.3.2.

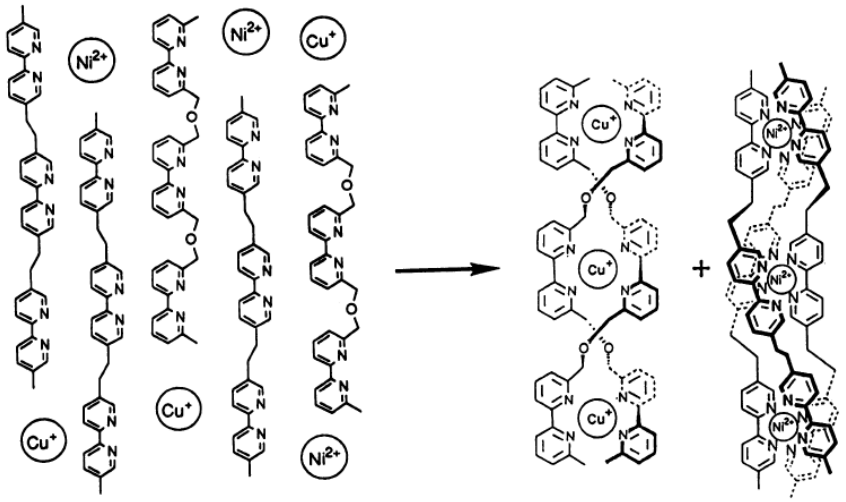

Figure 1.3.2 Lehn's double and triple helices which form almost completely selectively. Reproduced from reference 22.

Stang and co-workers have more recently shown how 2-dimensional structures can predictably self-assemble even when there is a mixture of complexes possible. By using platinum compounds which are pre-determined to form particular polygons, and a linear ligand, they showed that if reacted in the correct ratio all the products would self-assemble. This is shown in figure 1.3.3 where a rectangle, triangle and square are all formed.[23] The pre-determination comes from the bend angle in the square planar platinum unit, for example the angle created from the phenanthrene unit (in blue) is approximately 120 ° and this lends itself to the formation of a triangle.

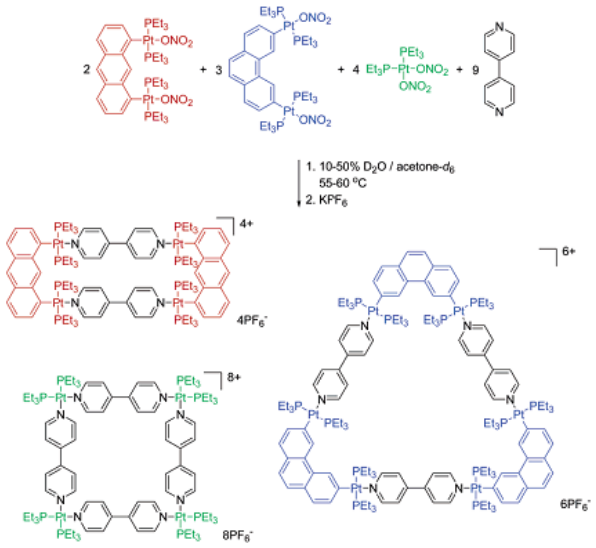

Figure 1.3.3 A combination of three different platinum linkers and a linear bridging ligand leads to three discrete polygons. Reproduced from reference 23.

The first three dimensional cage to be published is thought to be Saalfrank's adamantanoid structure, based on a M_4L_6 tetrahedron with a bridging ligand along each edge. This has the structure shown in figure 1.3.4 and initially used magnesium (II) ions and ethyl malonate as the bridging ligand.[24] Saalfrank later made variations of this structure including using nickel (II), cobalt (II) and iron (III) as the metal ions.[25] He also changed the ligand by including a phenylene spacer between the two diketonate binding sites which expanded the central cavity.[26]

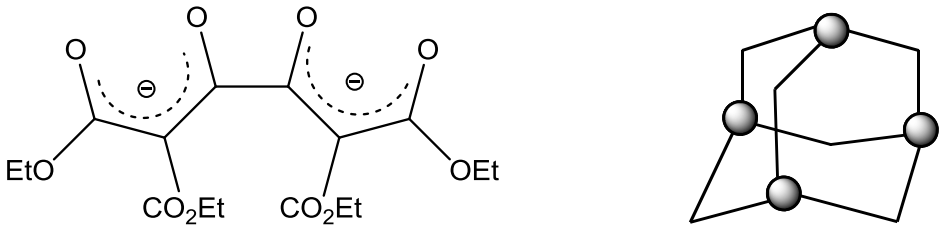

Figure 1.3.4 The ethyl malonate ligand (left) and the basic structure of the M_4L_6 adamantanoid cage (right).

Stang has recently shown that it is possible to design adamantanoid cages by controlling the size and shape of the linkers that form it. He claims that by combining six angular ditopic units and 4 angular tritopic units which all have a 109° angle, then an adamantanoid cage will result.[27] An example of how Stang has done this is shown in

figure 1.3.5. Stang's cage has the same overall adamantanoid structure as Saalfrank's, but is very different in its design. Stang uses the metal ions as the bridging part in the ditopic linker, whereas Saalfrank has the metal ions at the centre of the tritopic linker. This means that although the two structures appear completely different due to the different number of metal ions, clever design strategy by Stang means they still have the same overall topology.

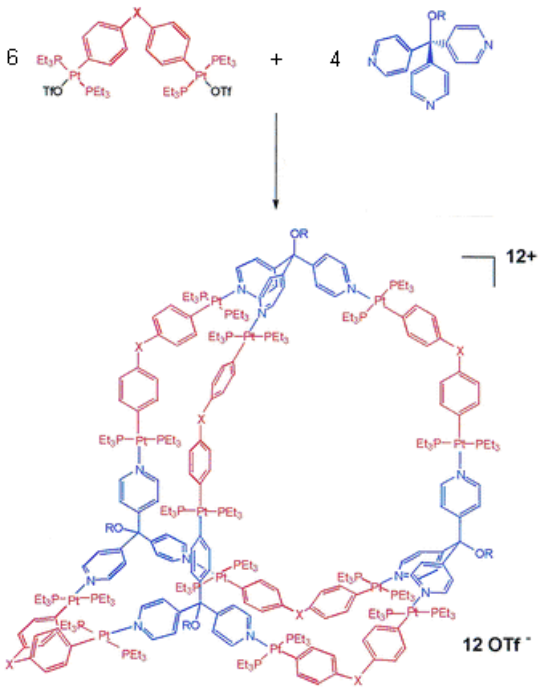

Figure 1.3.5 Stang's pre-designed adamantanoid cage. Reproduced from reference 27.

Fujita and co-workers extended their work on the square complex to form a three-dimensional cage complex.[28] It uses the same square planar $[Pd(en)]^{2+}$ units but a tridentate, triangular ligand as shown in figure 1.3.6. The cage has a M_6L_4 structure based on an octahedron of metal ions with half of the faces capped by triangular ligands. This cage structure has many interesting properties, including that it can be made in a yield of >90 % and is now commercially available. The cage is also amphiphilic with the inside of the cage being hydrophobic and capable of binding to a large number of guest molecules. The outside of the cage is hydrophilic due to the six $\{Pd(en)\}^{2+}$ units, and this also makes the cage water soluble. Chemical reactions are able to occur between molecules bound inside the cavity and these are often accelerated

compared to the same reaction under standard conditions. This will be examined in more detail later.

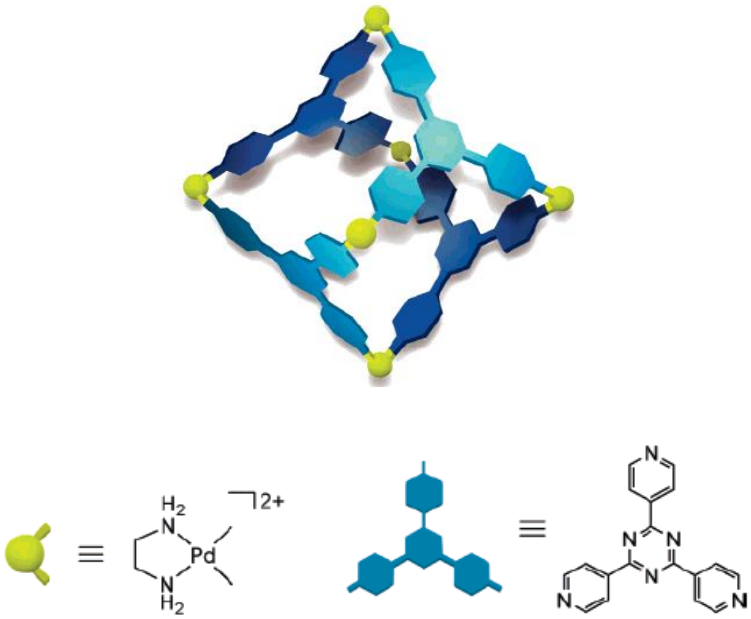

Figure 1.3.6 Fujita's M_6L_4 cage. Reproduced from reference 28.

Another important series of experiments in this field has been undertaken by Raymond and co-workers. Their work is based on bis-catecholate ligands and gallium(III) or iron(III) ions which together form water-soluble tetrahedral M_4L_6 cage complexes. The ligands are tetradentate with the two catecholate groups separated by a spacer and together with a six-coordinate metal ion this gives a M_2:L_3 ratio complex. Although there are many possibilities for complexes that can form with this ratio such as a M_2L_3 dinuclear triple helicate, M_6L_9 trigonal prism or a M_8L_{12} cube, Raymond demonstrated that by using certain ligands a M_4L_6 tetrahedral cage is always the favoured product.

Raymond has found that these anionic cages bind with strong affinity to cationic guests, for example tetraalkylammonium salts[29] and they can also stabilise highly reactive phosphonium salts.[30] More recently the group has also shown that even though the cages are highly anionic, they can also bind neutral n- and cycloalkanes (figure 1.3.7).[31] To do this the hydrophobic effect is used, so when the guest enters the cavity and water molecules are released back into the bulk solution there is an entropic gain for the system. The affinity of binding increases as the guest alkane gets larger because the

entropic gain increases as more water molecules are pushed into the bulk solution. Consequently larger alkanes are favoured as guests over smaller ones.

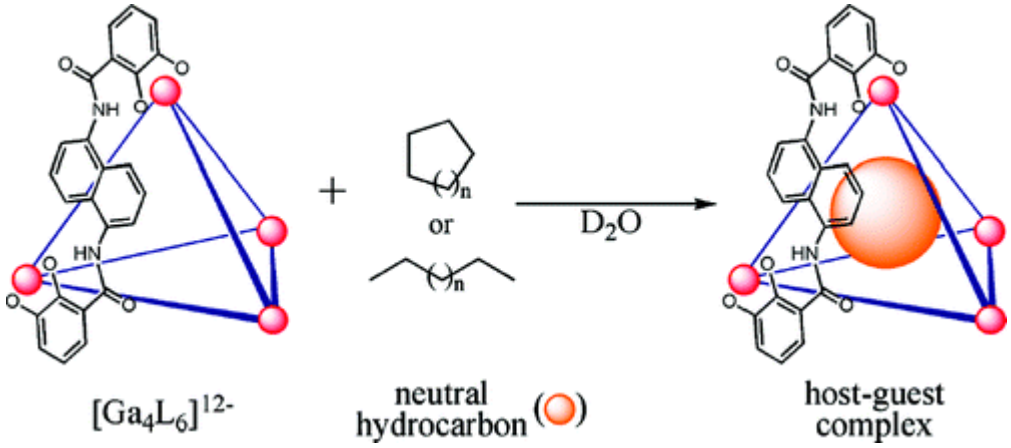

Figure 1.3.7 A water soluble cage complex capable of binding various cationic and neutral guest molecules. Reproduced from reference 31.

A remarkable example of self assembly by Nitschke and co-workers showed that 62 building blocks could be brought together through the formation of 96 new bonds to give one product in a one-pot synthesis.[32] The $Fe_8Pt_6L_{24}$ cube (figure 1.3.8) was the only product using a ligand with pyridine and pyridylimine moieties, even though Pt(II)bis(pyridylimine) and Fe(II)hexakis(pyridine) complexes are known in the literature and theoretically could have formed instead of the cube. The system however is under thermodynamic control and the cube is the most energetically favoured structure.

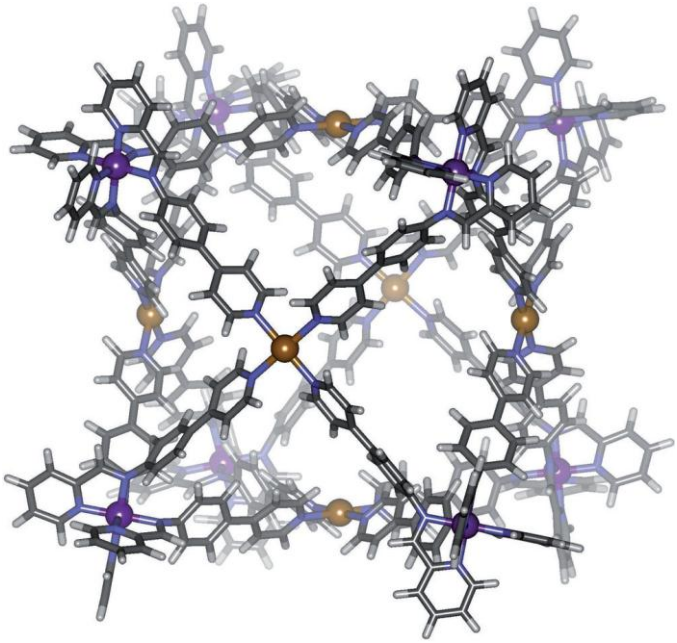

Figure 1.3.8 Energy-minimized model of the $Fe_8Pt_6L_{24}$ cube. Reproduced from reference 32.

The field of metal-organic frameworks (MOFs) is fast expanding due to their potential applications such as gas storage. For example Yaghi and Eddaoudi have reported MOFs capable of storing both methane[33] and hydrogen.[34] MOFs are also largely based on self-assembly and use interactions such as coordination bonds, hydrogen bonds and halogen bonds to create large networks from smaller component parts. Eddaoudi and co-workers have used metal – ligand coordination bonds to self-assemble molecular building blocks (MBBs) into supermolecular building blocks (SBBs) and then the same technique to self-assemble these into a MOF capable of hydrogen storage (figure 1.3.9).

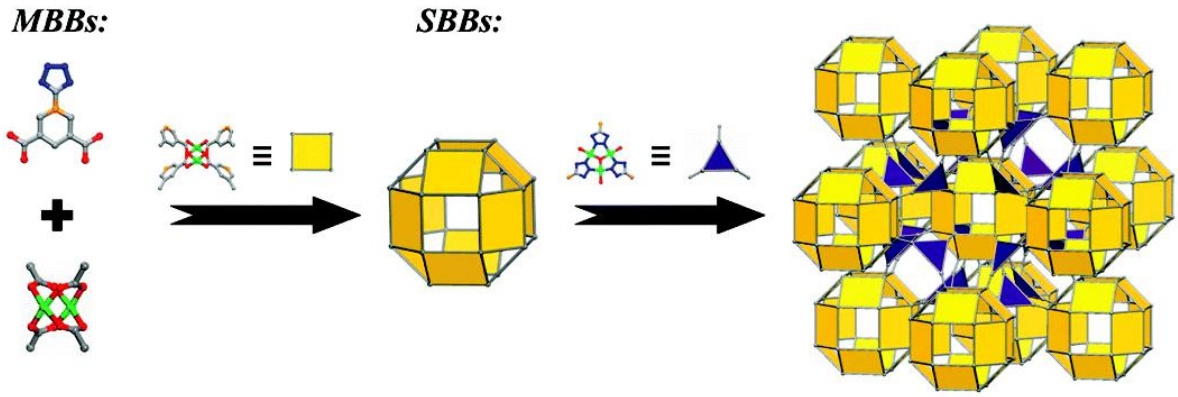

Figure 1.3.9 A schematic showing the path from simple MBBs to a MOF. Reproduced from reference 35.

1.4 Examples of coordination cages from the Ward group

In recent years Ward and co-workers have prepared many examples of cage structures, ranging from simple to more elaborate ones. They are all based on similar ligands, having two bidentate pyrazolyl-pyridine arms connected to a spacer unit via methylene groups. Two of these are shown in figure 1.4.1.

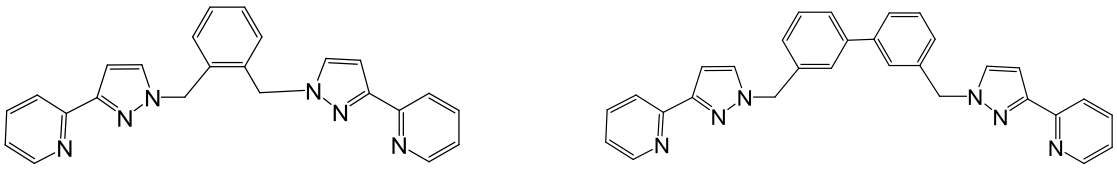

Figure 1.4.1 L-ortho-phenyl (L^{op}) (left) and L-biphenyl (L^{bip}) (right).

The ligands are bis-bidenate, and therefore have a total of four coordination sites. When they are reacted with six-coordinate metal ions this means that a metal-to-ligand ratio of 2 : 3 is required so that all of the coordination sites are saturated. The M_2L_3 ratio is very common in this series although there are exceptions when some metals are used, for example Ag(I) which is generally four-coordinate.

The methylene groups are essential in giving the ligands the flexibility required to form some of the coordination cages. This is also frustrating however because the flexibility makes rational design of cages near impossible. Therefore many of the cages synthesised with these ligands have been achieved serendipitously because it is very

difficult to predict the cage structure arising from a specific metal and ligand combination.

The simplest polyhedral structure based on this ratio is a $[M_4L_6]^{8+}$ tetrahedral cage. An example of this is shown in figure 1.4.2 which incorporates six ligands based on pyrazolyl-pyridine units connected via methylene groups to a phenyl spacer at the ortho positions. Each ligand spans the edge of the tetrahedron, with a cobalt (II) ion at each corner. There is a tetrafluoroborate anion in the centre of the tetrahedron which acts as a template for the synthesis of the cage to form around it.[36]

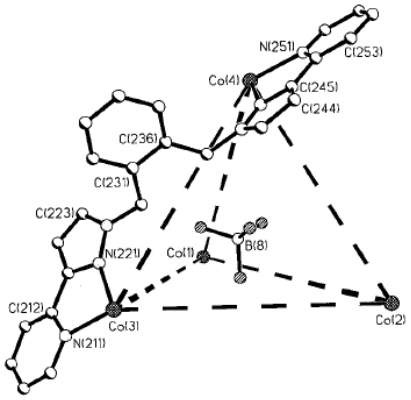

Figure 1.4.2 $[Co_4(L^{op})_6](BF_4)_8$. Reproduced from reference 36.

This ligand L^{op} requires the anion in the central cavity to act as a template for the cage to form. Using the ligand L^{bip} and the same metal ion also gives a tetrahedral cage but there are larger M – M separations due to the larger spacer and the anion is able to freely move in and out of the cavity. In this case the anion is not required for the cage to form and there is no templating effect.[37]

The largest structure found so far by Ward and co-workers is based on a capped truncated tetrahedral core and has the general formula $[M_{16}L_{24}]^{32+}$. There are four triangular faces from when the parent tetrahedron is truncated and these are shown in yellow in figure 1.4.3.

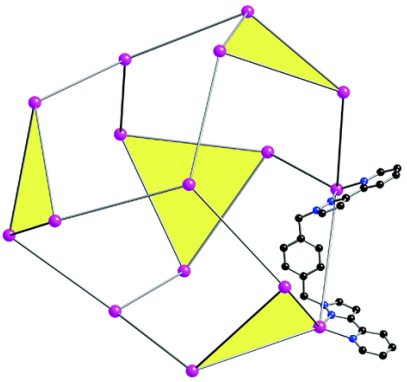

Figure 1.4.3 $[Cd_{16}(L^{PP})_{24}](ClO_4)_{32}$. Reproduced from reference 38.

It has been shown that using different metals with the same ligand can affect the structure of the complex. An example of this is using a ligand with two pyrazolyl-pyridine arms connected to the meta positions of a phenyl spacer via methylene groups (L^{mp}). When combined with zinc (II) ions a $[M_8L_{12}]^{16+}$ cuboidal structure forms (figure 1.4.4), but with cobalt (II) ions a $[M_6L_9]^{12+}$ 'open-book' structure is seen (figure 1.4.5). Both of these structures have a M_2L_3 ratio, although they clearly follow very different self-assembly pathways. It is unclear if the two structures could be in equilibrium with each other, although this is possible as the two structures are thought to be very similar in energy.[39]

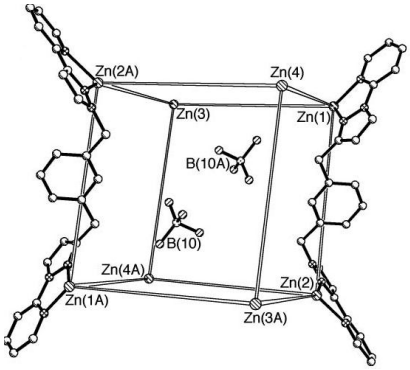

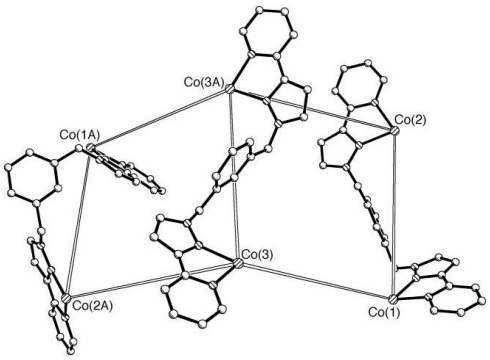

Figure 1.4.4 $[Zn_8(L^{mp})_{12}](BF_4)_{16}$ **Figure 1.4.5 $[Co_6(L^{mp})_9](ClO_4)_{12}$**

Both reproduced from reference 39.

Both tetrafluoroborate and perchlorate anions are commonly used in this work and which anion is present is thought to have little impact in the resulting cage structure. Tetrafluoroborate anions are particularly useful however, because ^{11}B and ^{19}F NMR can be used to probe what environments the anions are in and to look at ion exchange

studies. This was done to look at the tetrahedral cage shown previously in figure 1.4.2, which has a tetrafluoroborate anion in the central cavity. Both the ^{11}B and ^{19}F NMR show a 7:1 ratio of free to encapsulated anions (figure 1.4.6). This is to be expected as eight anions are required to balance the charge but there is only space for one anion within the central cavity.[40]

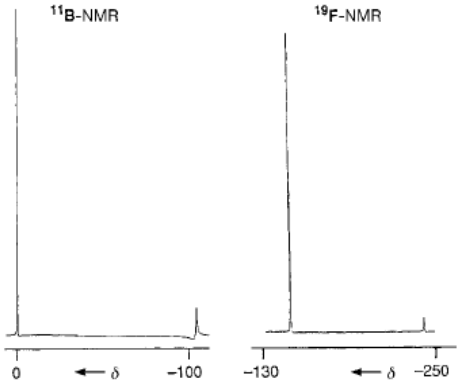

Figure 1.4.6 ^{11}B and ^{19}F NMR showing the free and encapsulated anions. Reproduced from reference 40.

The use of naphthyl spacers in these structures allows the photophysical properties of the cage structures to be investigated. This is because the naphthyl spacer units are fluorescent in their isolated state, but when they form part of a cage structure this fluorescence changes and an 'excimer-like' fluorescence is seen. The fluorescence changes because of the π-stacking of the naphthyl spacers with the pyrazolyl-pyridine units also present in the structure. When they π-stack there is a small transfer of electron density from the relatively electron rich spacer to the relatively electron poor pyrazolyl-pyridine unit. This results in a change of the gap between the HOMO and LUMO, and consequently a different wavelength of fluorescence.[41]

This has been shown previously using a 1,8 naphthyl ligand and slowly adding $Zn(BF_4)_2$ up to a total of 20 equivalents.[41] The fluorescence spectrum shown in figure 1.4.7 clearly shows a loss in the normal naphthyl fluorescence and an increase in the 'excimer-like' fluorescence as the $[Zn_{12}(L^{1,8})_{18}]^{24+}$ cage is formed. This 'excimer-like' fluorescence can be used as a probe to monitor cage assembly. It could monitor this in terms of the metal-to-ligand ratio required for the cage to form, or it could be used to see how quickly the cage forms if continuous measurements are taken from when the

metal salt and ligand are mixed. The π-stacking responsible for the 'excimer-like' emission is shown in figure 1.4.8.

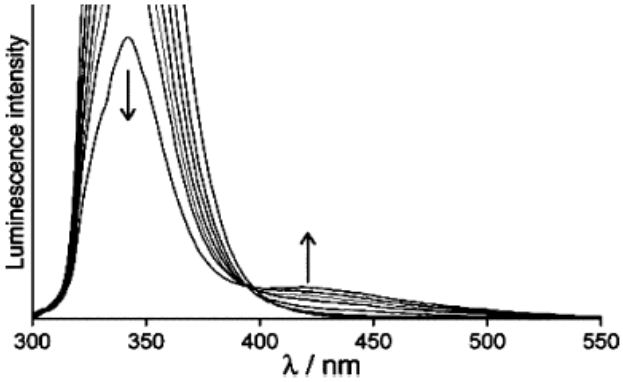

Figure 1.4.7 There is a loss of intensity of normal naphthyl fluorescence (350 nm) and an increase in 'excimer-like' fluorescence (420 nm) as more Zn $(BF_4)_2$ is added to the ligand. Reproduced from reference 41.

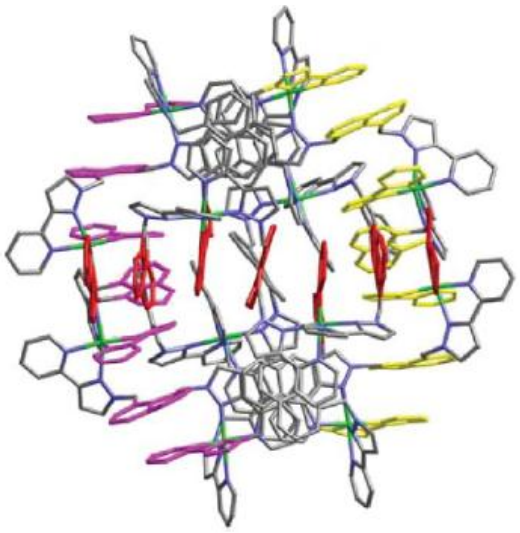

Figure 1.4.8 The $[Zn_{12}(L^{1,8})_{18}](BF_4)_{24}$ cage, with three rows of π-stacking highlighted. Reproduced from reference 41.

The chiroptical properties of these cages have also been investigated by using chiral ligands such as L^{pin} (figure 1.4.9). The ligands have a pinene unit fused onto the normal pyrazolyl-pyridine unit and follow the structure of the 'CHIRAGEN' ligands by von Zelewsky.[42, 43]

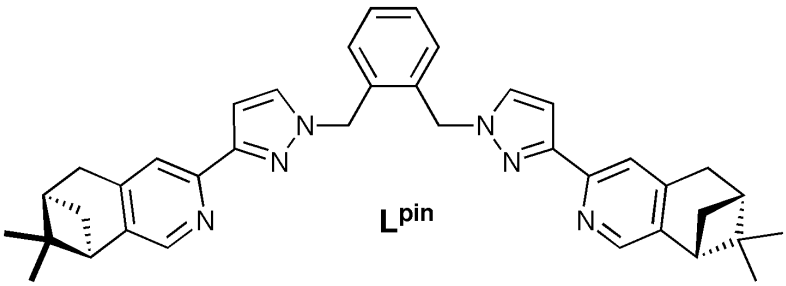

Figure 1.4.9 The chiral ligand L^{pin} (analogous to L^{op}).

Ward and co-workers first investigated these ligands in trying to form a tetrahedral cage structure as previously prepared with the normal pyrazolyl-pyridine ligand L^{op} (figure 1.4.2).[40] This tetrahedral structure was interesting because all four metal centres had the same optical configuration and all six ligands had the same direction of helical twist. The structure possesses *T*-symmetry, and therefore the optical activity of the corresponding chiral structure was expected to be very large not just because of the pinene units but also due to the helical chirality present by the cage superstructure.

The ligand formed exactly the same structure as the analogous pyrazolyl-pyridine ligand, confirmed by electrospray mass spectrometry and X-ray crystallography. The *T*-symmetry of the structure was confirmed by ^{1}H NMR which showed that a single diastereoisomer was formed rather than a racemic mix.[44]

The specific rotation of 589 nm light of both the cage and the ligand were determined. The specific rotation of each was converted to molar values to give a more accurate comparison. The free ligand has a specific molar rotation of -432 °, and the complex -13400 °. This is approximately 30 times greater, and means that the complexation of the six ligands resulted in a five-fold increase in the specific molar rotation compared to six free ligands. This shows that approximately 83 % of the optical rotation arises from chirality of the cage superstructure and 17 % comes from the chirality already present in the ligands.[44]

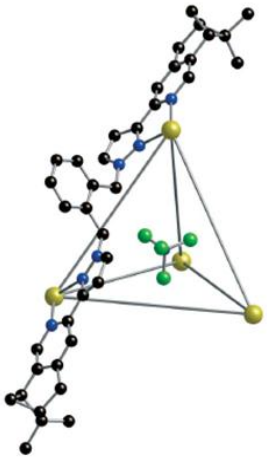

Figure 1.4.10 $[Co_4(L^{pin})_6](BF_4)_8$. Reproduced from reference 44.

More recently, the cubic cage $[Co_8(L^{15naph})_{12}](BF_4)_{16}$ based on the bridging ligand L^{15naph} has been shown to bind coumarin within its central cavity. This binding is very selective as only coumarin was shown to bind out of 23 potential compounds. The windows in the cage are large enough to allow guest exchange, but small enough to provide a kinetic trap.[45]

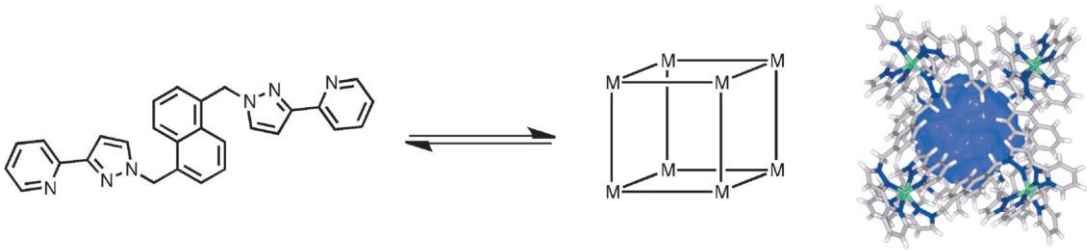

Figure 1.4.11 The ligand L^{15naph} and the cubic coordination cage with the volume in the central cavity highlighted in blue. Reproduced from reference 45.

1.5 Applications of coordination cages

The field of coordination cages has grown rapidly in recent years due to the broad range of applications that are emerging in the field. These include, but are not limited to, catalysis, molecular recognition, sensors, optical devices and drug delivery.[46]

1.5.1 Catalysis

Fujita and co-workers have shown how two normally unreactive molecules can be recognised as a pair inside a central cavity and then be made to react.[47] Triphenylene is an unreactive molecule however it was found that it can undergo the Diels-Alder reaction with *N*-cyclohexylmaleimide when both are in the central cavity of the cage shown in figure 1.3.6. It is thought that due to steric reasons the dienophile is pushed towards one of the benzene rings of the triphenylene (figure 1.5.1.1), therefore promoting a regioselective [2+4] pericyclic reaction. There are no other reports of a similar reaction using triphenylene, therefore showing how powerful catalysis inside coordination cages could potentially be.

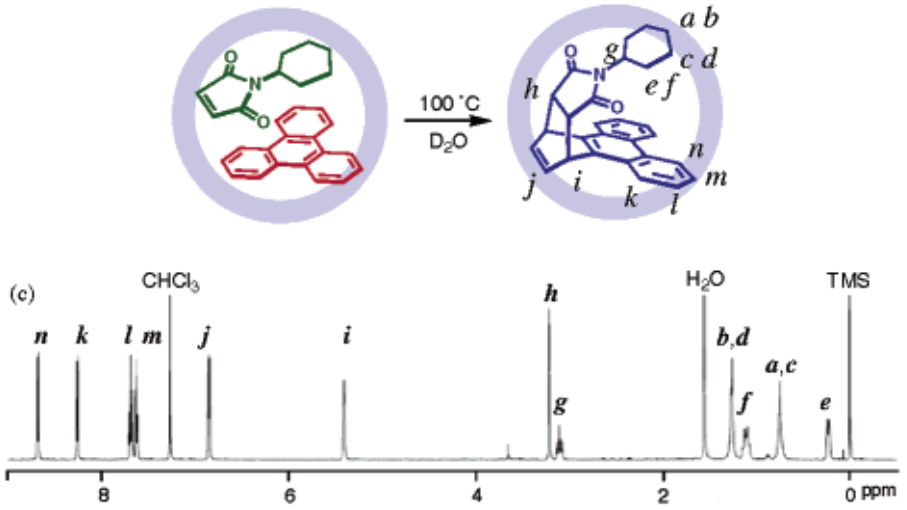

Fig 1.5.1.1 The reaction taking place inside the central cavity and the ^{1}H NMR spectrum showing only one product is produced. Reproduced from reference 47.

Fujita has also shown that it is possible to affect the regioselectivity of catalysis in a Diels-Alder reaction. He has done this by using two different hosts, which result in two very different reactions taking place.[48] The first host is again the structure shown in figure 1.3.6, an M_6L_4 cage. This has been shown to catalyse the Diels-Alder reaction of an anthracene molecule and a maleimide molecule at the 1,4 position on the anthracene. This is unusual as due to the high localisation of π-electron density at the 9,10 site the reaction usually takes place here. However as can be seen in figure 1.5.1.2 the cage pre-organises the two reactants into a position where the C=C bond of the maleimide is in very close proximation with the 1,4 anthracene site. This reaction is also stereoselective,

producing only the syn isomer and is estimated to give a yield of 98%. In the absence of the cage the reaction gave only the 9,10 product in a 44% yield.

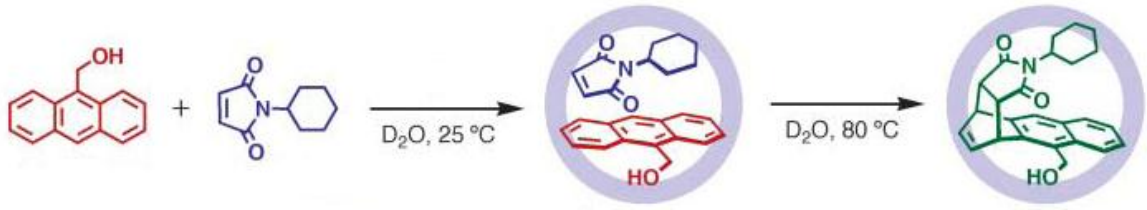

Figure 1.5.1.2 The cage pre-organises the reactants to give an unusual product. Reproduced from reference 48.

The other structure that catalyses this reaction is a square pyramidal bowl, shown in figure 1.5.1.3.[49] This uses the same palladium corner unit as the M_6L_4 cage although using a different tridentate ligand. This has a markedly different effect on the reaction and increases reaction turnover at the 9,10 position.[48] The reaction without the bowl present only proceeded in a 3% yield at room temperature, however with the bowl present there was a greater than 99% yield. Only small amounts of the bowl were needed (less than 10% molar equivalents) showing that it does act as a catalyst. The reason that this system is able to have such a high turnover and not need stoichiometric quantities of the host is due to the aromatic stacking of the host and the guest. Before the reaction proceeds the anthracene and the triazine ligand can π-stack gaining stabilisation for the system. However the Diels-Alder product is bent meaning that this stacking is lost and therefore it is much more favourable for this product to be replaced within the bowl by another anthracene molecule.

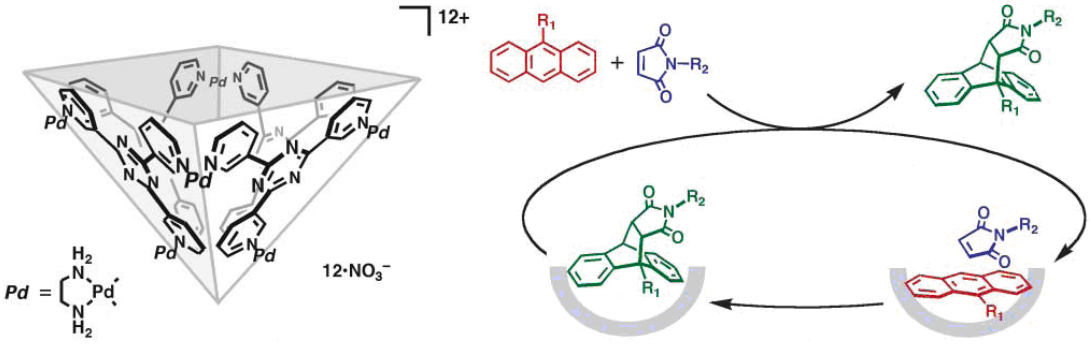

Figure 1.5.1.3 The square pyramidal bowl and the reaction that it catalyses. Reproduced from reference 48.

Other examples of Diels-Alder catalysis inside coordination cages have been shown[50-53] although a common problem is that near stoichiometric amounts of the host are required and this is far from ideal.

Nitschke and co-workers have shown how a cage can be used to *prevent* a Diels-Alder reaction occurring.[54] The water-soluble tetrahedral cage acts as a 'whole molecule protecting group' which encapsulates a furan molecule within its central cavity and prevents it reacting with a maleimide molecule (figure 1.5.1.4). The reaction can proceed when a competing guest such as benzene is added, as this preferentially binds in the central cavity of the cage releasing the furan to react with the maleimide molecule. The benefit of a protecting group such as this one is that it is selective on the basis of size and not chemical functionality. This therefore gives the possibility of allowing the selective protection of one molecule from a mixture of chemically similar molecules with different sizes.

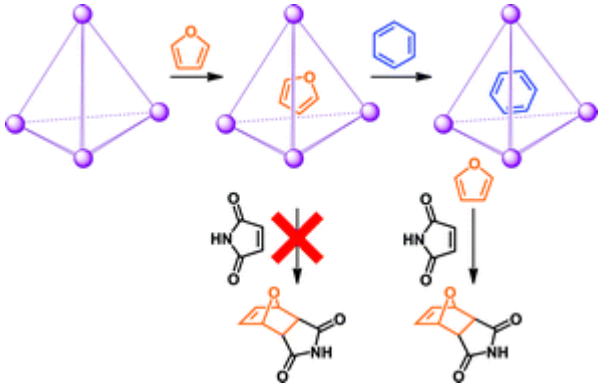

Figure 1.5.1.4 The 'whole molecule protecting group' which prevents the Diels-Alder reaction. Reproduced from reference 54.

Raymond and co-workers have shown that their cages can also be used for catalysis. The tetrahedral cage shown in figure 1.3.7 has been used to catalyse an Aza-Cope rearrangement (figure 1.5.1.5) with an 850-fold rate of acceleration.[55]

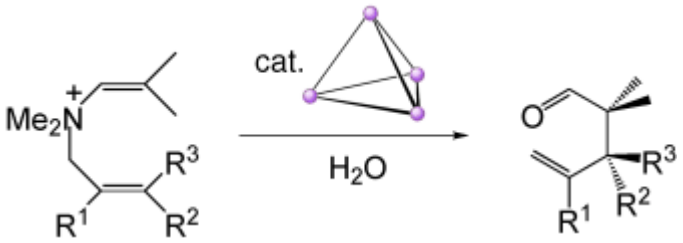

Figure 1.5.1.5 The Aza-Cope rearrangement. Reproduced from reference 55.

Their cages have also been shown to achieve 'enzyme-like' control in the catalysis of the Nazarov reaction.[56] A remarkable rate acceleration of 2×10^6 has been observed for the Nazarov cyclisation of pentadienols to cyclopentadiene.[57]

Other examples of catalysis from this group include an 890-fold acceleration of the acid-catalysed orthoformate hydrolysis in basic solution[58] and the encapsulation of monocationic organometallic species, including half-sandwich iridium complexes,[59] rhodium complexes[60] and gold complexes.[61]

Other examples where coordination cages have been used in catalysis include epoxidation[62], hydroformylation[63] and the Wacker process.[64]

1.5.2 Encapsulation

The encapsulation of molecules and the host-guest chemistry associated with this are very important.

One such area which is being investigated is in the stabilisation of molecules that are either very reactive or sensitive to particular environments. An example of such a molecule is P_4 which is readily oxidised in air and combusts. Nitschke and co-workers have shown how a tetrahedral cage complex (figure 1.5.2.1) can not only stabilise P_4 but also make it water soluble.[65] The cage complex is water-soluble due to the sulfonate groups and if P_4 is mixed with the cage in aqueous solution then the P_4 quickly becomes encapsulated within the central cavity. The cage makes P_4 air stable not because it prevents O_2 molecules from entering the cavity, but because if P_4 were to react with O_2, the intermediate created would be too large for the central cavity. This system is also very useful because the P_4 molecules can be easily displaced from the central cavity with a competing guest such as benzene. The P_4 is oxidised when exposed to air again

and ends up in the aqueous layer as H_3PO_4. The system could prove useful in the future for carrying P_4 safely or cleaning up spillages and it is reusable.

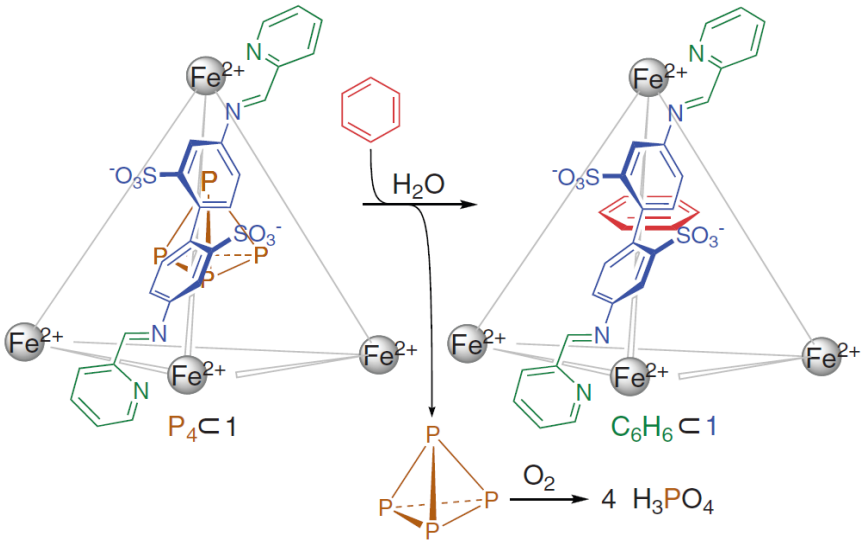

Figure 1.5.2.1 The initial cage with stabilised P_4 (left) and then the substitution with benzene in H_2O (right). Reproduced from reference 65.

The Nitschke group has also shown that the same cage is capable of binding sulphur hexafluoride (SF_6), the most potent greenhouse gas known (figure 1.5.2.2). The cage encapsulates the gas, increases its water solubility and can be readily stored in solution. As with the P_4 example previously, the guest can also be released, this time by three physical or chemical stimuli, including increasing the temperature and addition of acid to the sample.[66]

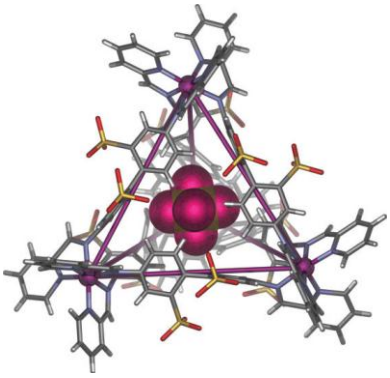

Figure 1.5.2.2 The X-ray crystal structure of SF_6 inside the central cavity of the cage. Reproduced from reference 66.

An extraordinary example of encapsulation was shown by Fujita and co-workers who described a cage that could increase the solubility of C_{60} by more than 30 times that of most organic solvents.[67] The cage contains 24 coronene molecules which due to their high aromaticity increase the solubility of C_{60} (figure 1.5.2.3). The coronene molecules do not stack with each other within the cage but instead act as a 'pseudo solvent' which in normal conditions would not be possible. The ability to generate nanophases such as this means it is possible to use large π-conjugated molecules as solvents and explore their properties.

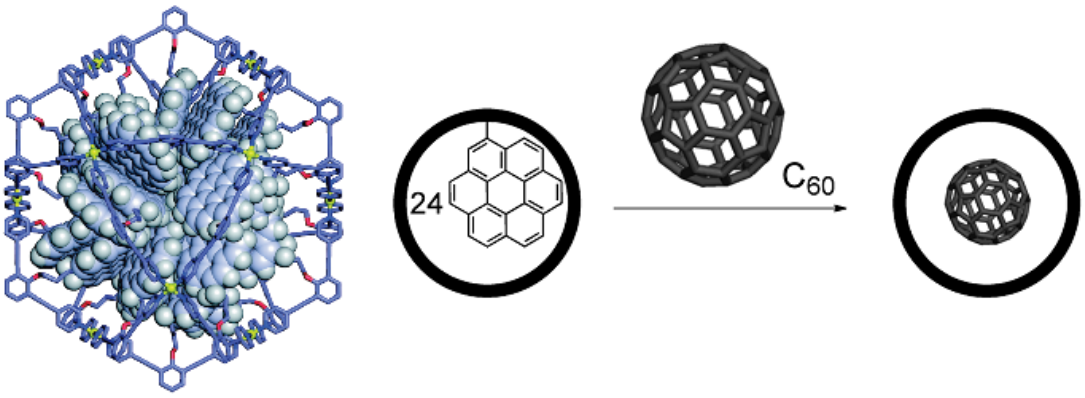

Figure 1.5.2.3 The $M_{12}L_{24}$ cage (left) and and a schematic showing the inclusion of C_{60} (right). Reproduced from reference 67.

Severin and co-workers have reported a trigonal prismatic coordination cage based on three dinuclear ruthenium units connected by two tridentate (2,4,6-tris(pyridin-4-yl)-1,3,5-triazine) ligands (figure 1.5.2.4). The cage is unusual because it has an adaptable

cavity size; the crystal structure without any guest has a compressed structure with the two tridentate ligands in an eclipsed formation, the structure with two coronene molecules in the central cavity has the two tridentate ligands stacked so that the Ru – Ru units are as elongated as possible.[68]

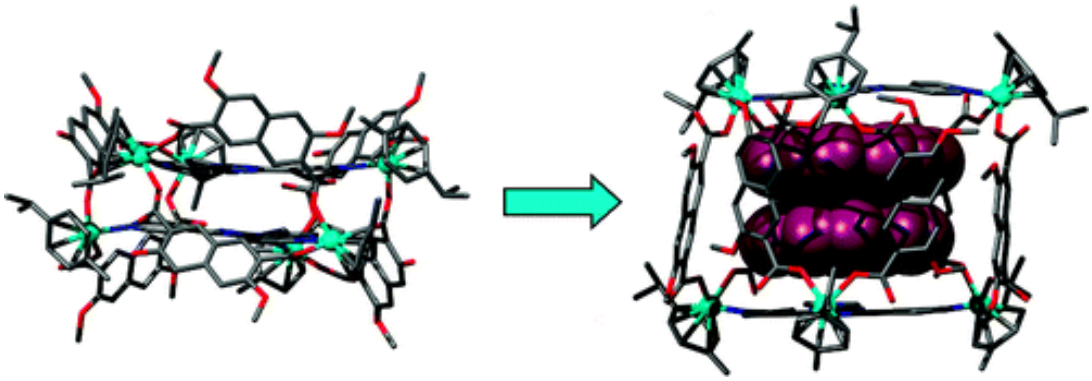

Figure 1.5.2.4 The crystal structure of the Ru_6 cage and the expansion of the central cavity to accommodate two coronene molecules. Reproduced from reference 68.

Fujita and co-workers have shown a system that describes a cationic host encapsulating a cationic guest.[69] This is extremely unusual due to the electrostatic repulsion that would normally prevent a cationic guest from entering a cationic host. However in this case the cage encapsulates four tetrafluoroborate anions and a NBu_4^+ cation as shown in figure 1.5.2.5. The crystal structure shows an onion-like structure with a sphere of negative charge from the tetrafluoroborate anions in between the two sets of positive charge. The alkyl chains of the NBu_4^+ have proved to be very important in stabilising the product as other cations, such as K^+, which also could be complementary do not go into the central cavity.

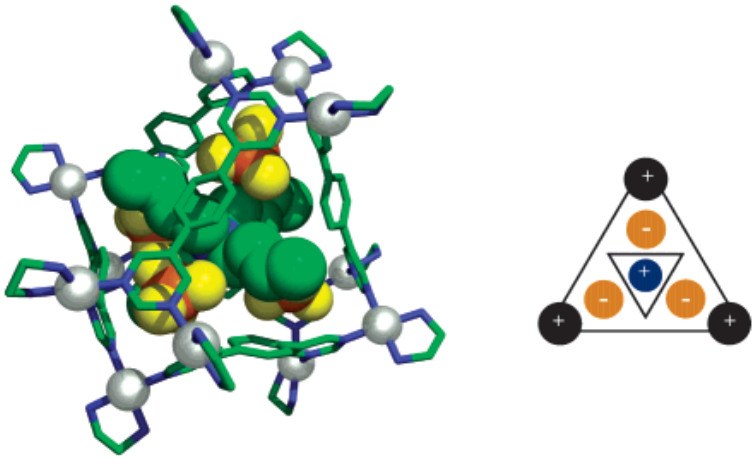

Figure 1.5.2.5 The crystal structure of the complex (left) and a schematic representation of the onion-like structure (right). Reproduced from reference 69.

Clever and co-workers have shown a Pt_2L_4 cage that can accommodate three guests in its central cavity (figure 1.5.2.6).[70] The guests stack alternately, there are two $PtCl_4$ molecules and one $Pt(pyridine)_4$ complex sandwiched in between them. This results in a stack of five platinum (II) ions, similar to what is seen in Magnus' salt. Different anions can be used, for example $PtBr_4$ instead of $PtCl_4$ and the guests stack much more strongly as a trimer than one of them on their own. The Clever group has also shown a similar M_2L_4 cage based on a different ligand that is an interpenetrated dimer of cages[71] and a Pd_3L_6 cage, again based on a different ligand, that has a double-trefoil-knot structure.[72]

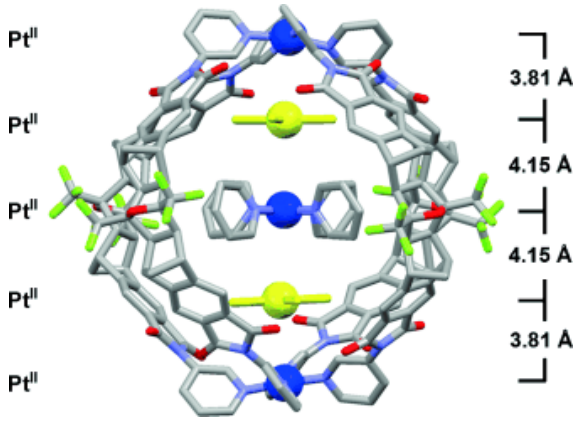

Figure 1.5.2.6 The crystal structure of the Pt_2L_4 cage and the three guests in the central cavity that form the Magnus salt type stack. Reproduced from reference 70.

Custelcean and co-workers have recently reported a urea-functionalised tetrahedral cage based on ligands with two bipyridine units that act as bis-bidentate ligands in much the same way as the pyrazolyl-pyridine ligands from the Ward group.[73] The tetrahedral cage shows preferential binding of tetrahedral oxoanions EO_4^{n-} (E = S, Se, Cr, Mo, W, n = 2; E = P, n = 3) over anions of other shapes or charges. The preference to bind hydrophilic, multicharged anions is unusual and is due to the six inwardly directed urea groups which stabilise the anion via hydrogen bonding interactions.

Lindoy and co-workers have also synthesised a tetrahedral cage based on Fe(II) ions and bis-bidentate quaterpyridine ligands.[74] Their cage shows a preference for binding PF_6^- over BF_4^- and has also been shown to selectively bind $[Fe^{III}Cl_4]^-$ over $[Fe^{II}Cl_4]^{2-}$. This is unusual in that it has mixed Fe(II) and Fe(III) valency and is thought to be the first example of a tetrahalometallate anion in a small supramolecular cage.

Kobayashi and co-workers have shown various methods of encapsulation based on their hydrogen-bonded capsules. They use a combination of metal-ligand coordination bonds and hydrogen bonds to create their capsules. The combination of having stronger and weaker forces is advantageous because the weaker interactions can be broken to allow encapsulation whilst the stronger interactions will still keep the rest of the capsule intact.

This is demonstrated in figure 1.5.2.7 where the group used a cavitand and $[Pt(dppp)(OTf)_2]$ to self assemble into a capsule. No neutral guests were encapsulated by the capsule until tetrabutylammonium triflate was also added.[75] The new interactions with the anion compensated for the enthalpy lost as the hydrogen bonds were broken whilst the guest was encapsulated. Without the anion present the ureide groups would not have turned outwards because the system would have lost enthalpy and so no guest could be encapsulated. Thus it was shown to be possible to control the encapsulation of a neutral guest molecule by changing the amount and/or type of anion or the polarity of the solvent.

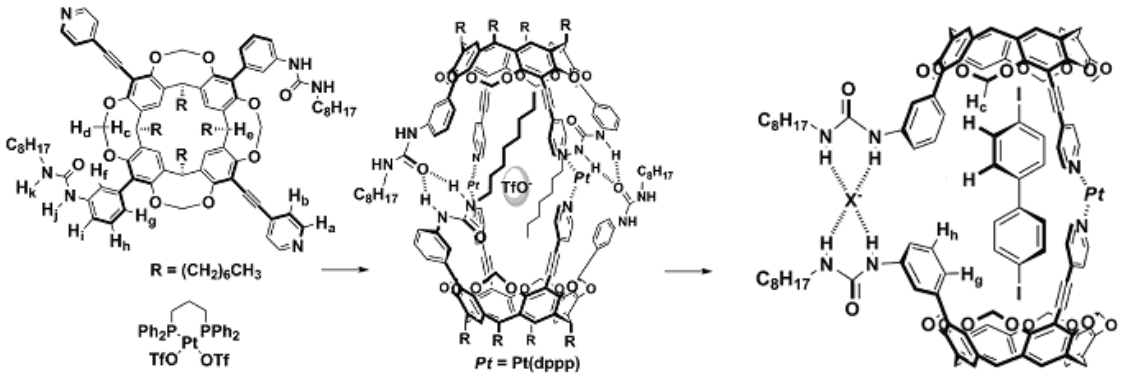

Figure 1.5.2.7 The original cavitand and platinum units (left), the self-assembled capsule (centre) and the capsule with guest and anion stabilising the ureide groups (right). Reproduced from reference 75.

Rebek and co-workers have also undertaken significant work in the field of encapsulation. They generally use two cavitands or calixarenes which come together to form a hydrogen-bonded capsule which is capable of encapsulating small guest molecules in its central cavity. They form reversibly,[76] have been shown to be a good model for alkane recognition,[77] are able to stabilise and amplify reaction intermediates,[78] and can afford previously unseen stereochemistry from reactions within them.[79]

Their group has shown how a reversible reaction can take place inside a capsule of two self-assembled cavitands,[78] (figure 1.5.2.8) and that a different tautomer of the product may be stabilised inside the capsule to what is seen in bulk solution. In fact in some cases a tautomer is stabilised that is not present at all in solution when the capsule is not present (figure 1.5.2.8, right). This is important as the stabilisation of reaction intermediates is a characteristic property of enzymes and is much sought after in catalysts.

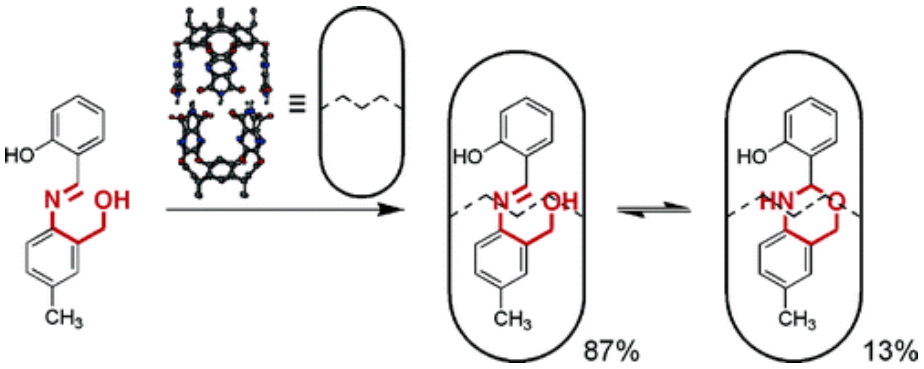

Figure 1.5.2.8 Two cavitands self-assemble and stabilise an intermediate not seen in bulk solution without the capsule present. Reproduced from reference 78.

1.5.3 Photochemistry

There has also been considerable interest in self-assembled coordination cages with regards to photochemistry and the role that they can play. They have been shown to play key roles in photodimerisations, photochemical oxidations and photochemical rearrangements.[80]

An illustrative example of a photochemical oxidation has been shown by Fujita's group. He has demonstrated the first example where a chemical reaction occurs on a guest that is sensitized by the host cage (figure 1.5.3.1).[81] The cage is the M_4L_6 structure shown in figure 1.3.6 and this can contain 4 adamantane molecules as guests. The adamantane molecules are normally inert and it has been shown that they only oxidise when the cage structure is present.

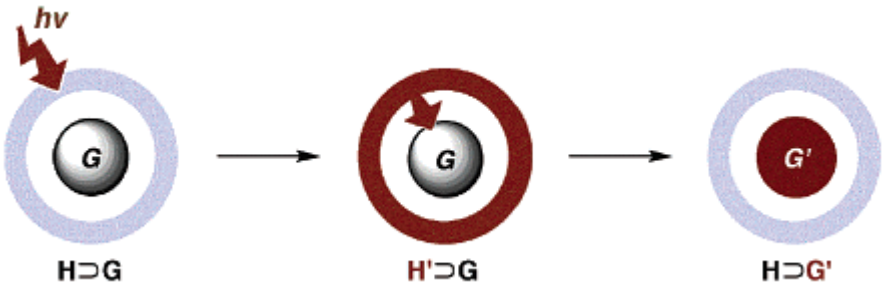

Figure 1.5.3.1 A schematic of the photochemical excitation of the host and then subsequent oxidation of the guest. Reproduced from reference 52.

This system works because the cage is photochemically excited by irradiation, followed by electron transfer from the adamantane guest to the host, giving two 1-adamantyl radicals and a radical species of the cage. The guest is then immediately trapped by O_2 or H_2O to give the oxidised products shown in figure 1.5.3.2.

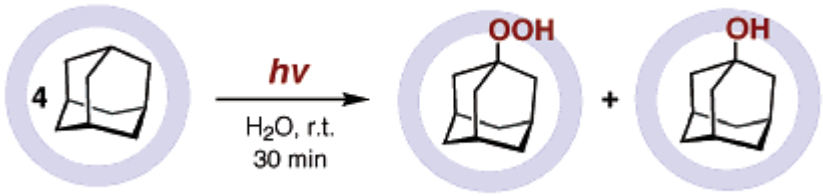

Figure 1.5.3.2 The host guest complex (left) and the oxidised products of the alkane (right). Reproduced from reference 52.

Gibb and co-workers have shown that their hydrophobic capsule shown in figure 1.5.3.3 can also perform a range of photochemical reactions. The capsule only forms in the presence of suitably sized hydrophobic guests and is very flexible. It has been shown to play a key role in the regioselective photochemical oxidation of cycloalkanes,[82, 83] unusual photochemical rearrangements[84-86] and photodimerisations.[87] The majority of these reactions are able to occur because the capsule pre-organises the guest in the central cavity, therefore promoting particular regioselectivities or unusual reactions.

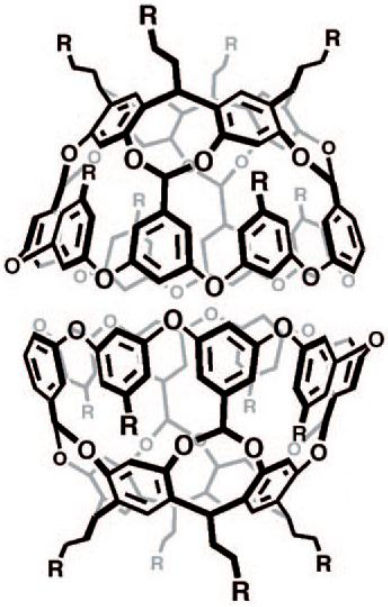

Figure 1.5.3.3 Gibb's self-assembling hydrophobic capsule.[88] Reproduced from reference 52.

Coordination cages have also shown promise as photo-optical devices. An example from Fujita's group has shown that a known red fluorescent emission from tetraazaporphine (TAP) is not quenched when it becomes encapsulated by the cage (figure 1.5.3.4). In fact the cage improves TAPs water solubility and prevents its aggregation both in the solution and solid state.[89] The system is made more impressive as the fluorescence can be turned on and off by switching between acid and base conditions. By simple addition of NEt_3 the TAP was deprotonated and the fluorescence was quenched. On return to acidic conditions the fluorescence turned back on and this process was repeatable.

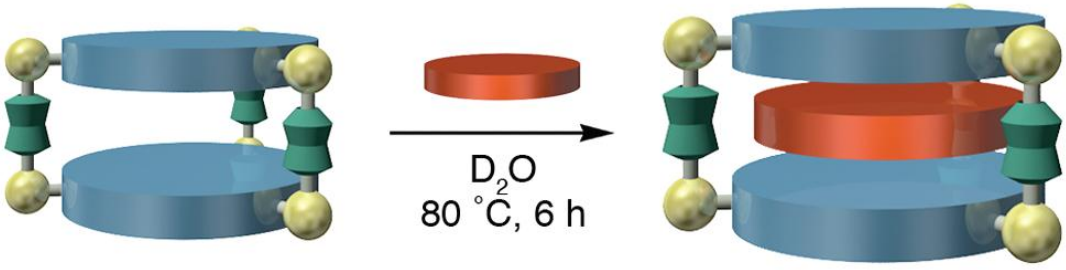

Figure 1.5.3.4 TAP remains highly fluorescent in the cage. Reproduced from reference 89.

1.5.4 Drug Delivery

Another area where coordination cages could potentially have useful applications is in biological recognition and drug delivery. Examples of this from supramolecular chemistry have been shown by Fujita who has shown that different coordination cages can recognise different peptides,[90, 91] or in DNA recognition as shown by Thomas (metallomacrocycles),[92] Hannon (helices)[93] and Therrien (metallo-boxes).[94] Therrien has shown how his ruthenium metalla-boxes such as in figure 1.5.4.1 can interact with duplex and human telomeric quadruplex DNA. The boxes show promise as quadruplex DNA stabilisers and show selectivity for quadruplex over duplex.[95]

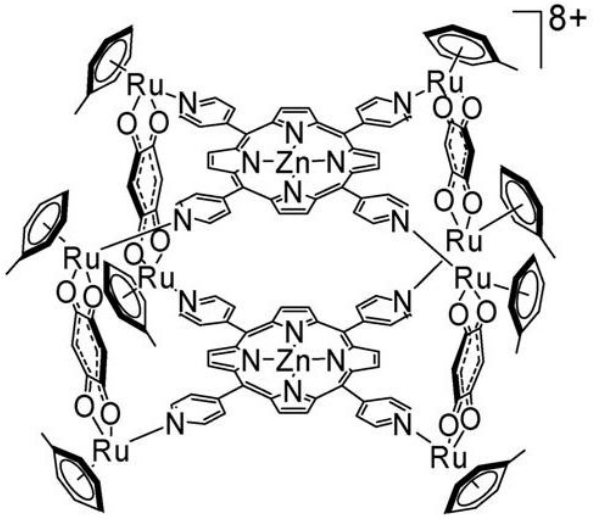

Figure 1.5.4.1 The ruthenium box that interacts strongly with DNA. Reproduced from reference 94.

Therrien has also described a family of complexes based on hexanuclear ruthenium cages which are capable of binding hydrophobic molecules in their central cavity (figure 1.5.4.2).[96] The guests such as M(acetylacetate)$_2$ (M = Pd or Pt) are biologically inactive in cells because they are insoluble in water. The cage itself does have some toxicity towards cancerous cells however the toxicity of the host-guest complex is much greater. It is thought that the cage water solubilises the guest molecule within its cavity and then is broken down within the cancerous cell, therefore releasing the guest molecule.

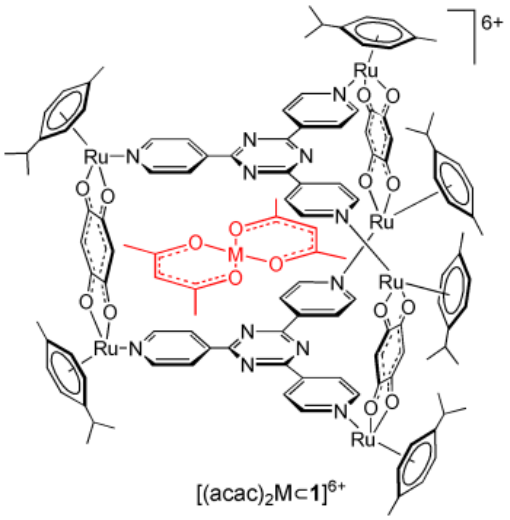

Figure 1.5.4.2 The 'trojan horse': $M(acac)_2$ encapsulated within the central cavity of the hexanuclear cage. Reproduced from reference 96.

Coordination cages have shown promise for drug delivery because theoretically they could carry a drug in their central cavity to a desired location and then release the drug as a 'payload'. An example of a cage that showed promise in this sense was from Nitschke and co-workers who described an unlockable-relockable tetrahedral cage.[97] The cage was shown to be unlockable by addition of acid and relockable by addition of base, therefore meaning that a guest in the central cavity could be released at a specific pH.

Crowley and co-workers extended this principle using a Pd_2L_4 cage which they showed could encapsulate two cisplatin molecules as shown in figure 1.5.4.3.[98] They showed that the cage could be disassembled and reassembled by addition of competing ligands, therefore allowing controlled release of the cisplatin molecules.

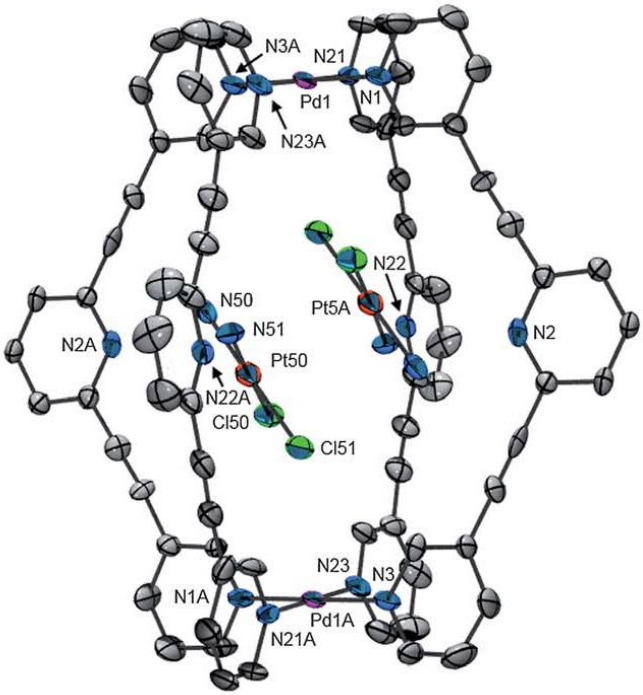

Figure 1.5.4.3 The crystal structure of the Pd_2L_4 cage with two cisplatin molecules inside the central cavity. Reproduced from reference 98.

Similar drug delivery applications have been shown with other supramolecular scaffolds such as rotaxanes,[99] catenanes[100] and dendrimers.[101]

1.6 Aims of this work

This introduction has given a brief overview of the field of coordination cages and some of the potential applications that they possess. It is still a relatively young field and undoubtedly more applications will emerge in the future. The aims of this work are to synthesise new ligands which when combined with transition metal ions afford new coordination cages. The solid state structures will be investigated by X-ray crystallography and solution studies will be undertaken using ^{1}H NMR spectroscopy and ESMS. The cages that are stable in solution with central cavities will have their host-guest chemistry investigated to see if they can accommodate molecules in the central cavity.

1.7 References

1. B. J. Holliday and C. Mirkin, *Angew. Chem. Int. Ed*., 2001, **40**, 2022.

2. J.-M. Lehn, *Supramolecular Chemistry*, VCH, 1995.

3. M. D. Ward, *Annu. Rep. Prog. Chem., Sect. A*, 2000, **96**, 345.

4. J. W. Steed and J. L. Atwood, *Supramolecular Chemistry*, 2nd Edition, Wiley, 2009, ch. 10, 592.

5. D. L. Caulder and K. N. Raymond, *Acc. Chem. Res*., 1999, **32**, 975.

6. K. Ariga, J. P. Hill, M. V. Lee, A. Vinu, R. Charvet and S. Acharya, *Sci. Technol. Adv. Mater*., 2008, **9**, 141.

7. A. Klug, *Phil. Trans. R. Soc. Lond. B.*, 1999, **354**, 531.

8. H. Murakami, Y. Watanabe and N. Nakashima, *J. Am. Chem. Soc.*, 1996, **118**, 4484.

9. J. D. Watson and F. H. C. Crick, *Nature*, 1953, **171**, 737.

10. J. Chen & N. C. Seeman, *Nature*, 1991, **350**, 631.

11. L. M. Adleman, *Science*, 1994, **266**, 1021.

12. B. Yurke, A. J. Turberfield, A. P. Mills Jr, F. C. Simmel and J. L. Neumann, *Nature*, 2000, **406**, 605.

13. N. C. Seeman, H. Wang, X. Yang, F. Liu, C. Mao, W. Sun, L. Wenzler, Z. Shen, R. Sha, H. Yan, M. H. Wong, P. Sa-Ardyen, B. Liu, H. Qiu, X. Li, J. Qi, S. M. Du, Y. Zhang, J. E Mueller, T.-J. Fu, Y. Wang and J. Chen, *Nanotechnology*, 1998, **9,** 257.

14. C. J. Pedersen, *J. Am. Chem. Soc*., 1967, **89**, 2495.

15. B. Dietrich, J.-M.Lehn, J.-P. Sauvage, *Tetrahedron Lett.*, 1969, 2885.

16. E. P. Kyba, M. G. Siegel, L.R. Sousa, G. D. Y. Sogah, D. J. Cram, *J. Am. Chem. Soc.*, 1973, ***95***, 2691.

17. R. Chakrabarty, P. S. Mukherjee, P. J. Stang, *Chem. Rev*., 2011, **111**, 6810.

18. M. D. Ward and P. R. Raithby, *Chem. Soc. Rev*., DOI: 10.1039/c2cs35123d.

19. M. Fujita, J. Yazaki, and K. Ogura, *J. Am. Chem. Soc.*, 1990, **112**, 5645.

20. M. Fujita, *Chem. Soc. Rev.*, 1998, **27**, 417.

21. J.-M. Lehn, A. Rigault, J. Siegel, J. Harrowfield, B. Chevriert & D. Morast, *Proc. Natl. Acad. Sci. U.S.A.*, 1987, **84**, 2565.

22. R. Kramer, J.-M. Lehn, A. Marquis-Rigault, *Proc. Natl. Acad. Sci. U.S.A.*, 1993, **90**, 5394.

23. C. Addicott, N. Das, and P. J. Stang, *Inorganic Chemistry*, 2004, **43**, 5335.

24. R. W. Saalfrank, A. Stark, K. Peters and H. G. von Schnering, *Angew. Chem. Int. Ed. Engl*., 1988, **27**, 851.

25. R. W. Saalfrank, A. Stark, M. Bremer and H.-U. Hummel, *Angew. Chem. Int. Ed. Engl*., 1990, **29**, 311.

26. R. W. Saalfrank, B. Horner, D. Stalke and J. Salbeck, *Angew. Chem. Int. Ed. Engl*., 1993, **32**, 1179.

27. M. Schweiger, S. Seidel, M. Schmitz, and P. J. Stang, *Org. Lett.*, 2000, **2**, 1255.

28. M. Fujita, M. Tominaga, A. Hori, and B. Therrien, *Acc. Chem. Res*., 2005, **38**, 369.

29. D. L. Caulder, C. Brückner, R. E. Powers, S. Künig, T. N. Parac, J. A. Leary, K. N. Raymond, *J. Am. Chem. Soc.*, 2001, **123**, 8923.

30. M. Ziegler, J. Brumaghim, K. N. Raymond, *Angew. Chem. Int. Ed.*, 2000, **39**, 4119.

31. S. M. Biros, R. G. Bergman and K. N. Raymond, *J. Am. Chem. Soc.*, 2007, **129**, 12094.

32. M. M. Smulders, A. Jiminez, and J. R. Nitschke, *Angew. Chem. Int. Ed.*, 2012, **51**, 6681.

33. M. Eddaoudi, J. Kim, N. L. Rosi, D. T. Vodak, J. Wachter, M. O'Keeffe and O. M. Yaghi, *Science*, 2002, **295**, 469.

34. N. L. Rosi, J. Eckert, M. Eddaoudi, D. T. Vodak, J. Kim, M. O'Keeffe and O. M. Yaghi, *Science*, 2003, **300**, 1127.

35. F. Nouar, J. F. Eubank, T. Bousquet, L. Wojtas, M. J. Zaworotko, and M. Eddaoudi, *J. Am. Chem. Soc.*, 2008, **130**, 1833.

36. J. S. Fleming, K. L. Mann, C-A. Carraz, E. Psillakis, J. C. Jeffery, J. A. McCleverty, and M. D. Ward, *Angew. Chem. Int. Ed*., 1998, **37**, 1279.

37. R. L. Paul, S. P. Argent, J. C. Jeffrey, L. P. Harding, J. M. Lynam, and M. D. Ward, *Dalton Trans*., 2004, 3453.

38. S. P. Argent, H. Adams, T. Riis-Johannessen, J. C. Jeffery, L. P. Harding, and M. D. Ward, *J. Am. Chem. Soc*., 2006, **128**, 72.

39. S. P. Argent, H. Adams, L. P. Harding, and M. D. Ward, *Dalton Trans*., 2006, 542.

40. J. S. Fleming, K. L. Mann, C-A. Carraz, E. Psillakis, J. C. Jeffery, J. A. McCleverty, and M. D. Ward, *Angew. Chem. Int. Ed*., 1998, **37**, 1279.

41. N. K. Al-Rasbi, C. Sabatini, F. Barigelletti, and M. D. Ward, *Dalton Trans*., 2006, 4769.

42. O. Mamula, F. L. Monlien, A. Porquet, G. Hopfgartner, A. E. Merbach and A. von Zelewsky, *J. Chem. Eur*., 2001, **7**, 533.

43. L. E. Perret-Aebi, A. von Zelewsky, C. D. Dietrich-Buchecker and J.-P. Sauvage, *Angew. Chem. Int. Ed*., 2004, **43**, 4482.

44. S. P. Argent, T. Riis-Johannessen, J. C. Jeffery, L. P. Harding and M. D. Ward, *Chem. Commun*., 2005, 4647.

45. S. Turega, M. Whitehead, B. R. Hall, M. F. Haddow, C. A. Hunter and M. D. Ward, *Chem. Commun*., 2012, **48**, 2752.

46. J. D. Crowley and P. H. Bandeen, *Dalton Trans.*, 2010, **39**, 612.

47. Y. Nishioka, T. Yamaguchi, M. Yoshizawa, and M. Fujita, *J. Am. Chem. Soc*. 2007, **129**, 7000.

48. M. Yoshizawa, M. Tamura, M. Fujita, *Science*, 2006, **312**, 251.

49. S.-Y. Yu, T. Kusukawa, K. Biradha, and M. Fujita, *J. Am. Chem. Soc.*, 2000, **122**, 2665.

50. J. Kang, J. Rebek, Jr., *Nature,* 1997, **385**, 50.

51. J. Kang, J. Santamaria, G. Hilmersson, J. Rebek Jr., *J. Am. Chem. Soc*., 1998, **120**, 7389.

52. M. Yoshizawa, J. Klosterman, M. Fujita, *Angew. Chem. Int. Ed.,* 2009, **48**, 3418.

53. M. Marty, Z. Clyde-Watson, L. J. Twyman, M. Nakash, J. K. Sanders, *Chem. Commun*., 1998, 2265.

54. M. M. Smulders and J. R. Nitschke, *Chem. Sci.*, 2012, **3**, 785.

55. D. L. Fiedler, R. G. Bergman and K. N. Raymond, *Angew. Chem. Int. Ed*., 2004, **43**, 6748.

56. C. J. Hastings, M. P. Backlund, R. G. Bergman and K. N. Raymond, *Angew. Chem. Int. Ed*., 2011, **50**, 10570.

57. C. J. Hastings, M. D. Pluth, R. G. Bergman and K. N. Raymond, *J. Am. Chem. Soc.*, 2010, **132**, 6938.

58. M. D. Pluth, R. G. Bergman, K. N. Raymond, *Science*, 2007, **316**, 85.

59. D. H. Leung, R. G. Bergman, and K. N. Raymond, *J. Am. Chem. Soc.*, 2006, **128**, 9781.

60. D. H. Leung, R. G. Bergman, and K. N. Raymond, *J. Am. Chem. Soc.*, 2007, **129**, 2746.

61. Z. J. Wang, C. J. Brown, R. G. Bergman, K. N. Raymond, and F. D. Toste, *J. Am. Chem. Soc.*, 2011, **133**, 7358.

62. M. L. Merlau, M. P. Mejia, S. T. Nguyen, J. T. Hupp, *Angew.Chem. Int. Ed. Engl.*, 2001, **40**, 4239.

63. A. W. Kleij, M. Lutz, A. L. Spek, P. W. van Leeuwen and J. N. Reek, *Chem. Commun.*, 2005, 3661.

64. H. Ito, T. Kusukawa, M. Fujita, *Chem. Lett.*, 2000, **29**, 598.

65. P. Mal, B. Breiner, K. Rissanen, J. R. Nitschke, *Science*, 2009, **324**, 1697.

66. I. A. Riddell, M. M. Smulders, J. K. Clegg and J. R. Nitschke, *Chem. Commun.*, 2011, **47**, 457.

67. K. Suzuki, K. Takao, S. Sato, and M. Fujita, *J. Am. Chem. Soc.*, 2010, **132**, 2544.

68. S. Mirtschin, A. Slabon-Turski, R. Scopelliti, A. H. Velders, and K. Severin, *J. Am. Chem. Soc.*, 2010, **132**, 14004.

69. J.-P. Bourgeois, M. Fujita, M. Kawano, S. Sakamoto, and K. Yamaguchi, *J. Am. Chem. Soc*., 2003, **125**, 9260.

70. G. H. Clever, W. Kawamura, S. Tashiro, M. Shiro, and M. Shionoya, *Angew. Chem. Int. Ed*., 2012, **51**, 2606.

71. S. Freye, J. Hey, A. Torras-Galan, D. Stalke, R. Herbst-Irmer, M. John, and G. H. Clever, *Angew. Chem. Int. Ed.*, 2012, **51**, 2191.

72. D. M. Engelhard, S. Freye, K. Grohe, M. John, and G. H. Clever, *Angew. Chem. Int. Ed.*, 2012, **51**, 4747.

73. R. Custelcean, P. V. Bonnesen, N. C. Duncan, X. Zhang, L. A. Watson, G. Van Berkel, W. B. Parson, and B. P. Hay, *J. Am. Chem. Soc.*, 2012, **134**, 8525.

74. C. R. Glasson, J. K. Clegg, J. C. McMurtrie, G. V. Meehan, L. F. Lindoy, C. A. Motti, B. Moubaraki, K. S. Murray and J. D. Cashion, *Chem. Sci*., 2011, **2**, 540.

75. M. Yamanaka, N. Toyoda, and K. Kobayashi, *J. Am. Chem. Soc*., 2009, **131**, 9880.

76. M. M. Conn and J. Rebek, Jr., *Chem. Reviews*, 1997, **97**, 1647.

77. M. P. Schramm, J. Rebek, Jr., *Chem. Eur. J.*, 2006, **12**, 5924.

78. T. Iwasawa, E. Mann, J. Rebek, Jr., *J. Am. Chem. Soc.*, 2006, **128**, 9308.

79. A. Shivanyuk, J. Rebek, Jr., *J. Am. Chem. Soc.*, 2002, **124**, 12074.

80. M. Yoshizawa, J. K. Klosterman, and M. Fujita, *Angew. Chem. Int. Ed*., 2009, **48**, 3418.

81. M. Yoshizawa, S. Miyagi, M. Kawano, K. Ishiguro and M. Fujita, *J. Am. Chem. Soc*., 2004, **126**, 9172.

82. A. Greer, *Nature*, 2007, **447**, 273.

83. A. Natarajan, L. S. Kaanumalle, S. Jockusch, C. L. Gibb, B. C. Gibb, N. J. Turro, V. Ramamurthy, *J. Am. Chem. Soc.*, 2007, **129**, 4132.

84. L. S. Kaanumalle, C. L. Gibb, B. C. Gibb, V. Ramamurthy, *J. Am. Chem. Soc*., 2004, **126**, 14366.

85. C. L. Gibb, A. Sundaresan, V. Ramamurthy, B. C. Gibb, *J. Am. Chem. Soc*., 2008, **130**, 4069.

86. L. S. Kaanumalle, C. L. Gibb, B. C. Gibb, V. Ramamurthy, *Org. Biomol. Chem*., 2007, **5**, 236.

87. Z. R. Laughrey, C. L. Gibb, T. Senechal, B. C. Gibb, *Chem. Eur. J*., 2003, **9**, 130.

88. C. L. Gibb and B. C. Gibb, *J. Am. Chem. Soc*., 2004, **126**, 11408.

89. K. Ono, J. K. Klosterman, M. Yoshizawa, K. Sekiguchi, T. Tahara and M. Fujita, *J. Am. Chem. Soc*., 2009, **131**, 12526.

90. S. Tashiro, M. Fujita, *Bull. Chem. Soc. Jpn*., 2006, **79**, 833.

91. S. Tashiro, M. Tominaga, M. Kawano, B. Therrien, T. Ozeki, M. Fujita, *J. Am. Chem. Soc*., 2005, **127**, 4546.

92. D. Ghosh, H. Ahmad and J. A. Thomas, *Chem. Commun*., 2009, 2947.

93. M. J. Hannon, *Chem. Soc. Rev*., 2007, **36**, 280.

94. B. Therrien, *Eur. J. Inorg. Chem.*, 2009, 2445.

95. N. H. Barry, N. Abd Karim, R. Vilar, B. Therrien, *Dalton Trans*., 2009, 10717.

96. B. Therrien, G. Suss-Fink, P. Govindaswamy, A. K. Renfrew, and P. J. Dyson, *Angew. Chem. Int. Ed*., 2008, **47**, 3773.

97. P. Mal, D. Schultz, K. Beyeh, K. Rissanen and J. R. Nitschke, *Angew. Chem. Int. Ed.*, 2008, **47**, 8297.

98. J. E. M. Lewis, E. L. Gavey, S. A. Cameron and J. D. Crowley, *Chem. Sci.*, 2012, **3**, 778.

99. T. D. Nguyen, Y. Liu, S. Saha, K. C.-F. Leung, J. F. Stoddart and J. I. Zink, *J. Am. Chem. Soc.*, 2007, **9**, 627.

100. R. Klajn, L. Fang, A. Coskun, M. A. Olson, P. J. Wesson, J. F. Stoddart and B. A. Grzybowski, *J. Am. Chem. Soc.*, 2009, **131**, 4233.

101. F. Marchioni, M. Venturi, A. Credi, V. Balzani, M. Belohradsky, A. M. Elizarov, H.-R. Tseng, and J. F. Stoddart, *J. Am. Chem. Soc.*, 2004, **126**, 568.

2. Coordination chemistry with the ligand L^{pp} – an unusual cage-to-cage interconversion

2.1 Introduction

The bis-bidentate bridging ligand L^{pp} {α,α′-bis[3-(2-pyridyl)pyrazol-1-yl]-1,4-dimethylbenzene}(figure 2.1.1), which contains two chelating pyrazolyl-pyridine units connected to a 1,4-phenylene spacer *via* flexible methylene units, has been synthesised. It reacts with transition metal dications to form a range of polyhedral coordination cages based on a M_2:L_3 ratio in which a metal ion occupies each vertex of a polyhedron, a bridging ligand lies along every edge, and all metal ions are octahedrally coordinated.[1] The complexes formed include a large $[M_{16}(L^{pp})_{24}](X)_{32}$ cage [M = Cd(II) or Zn(II), X = BF_4 or ClO_4] which exhibits interesting dynamic behaviour in solution.

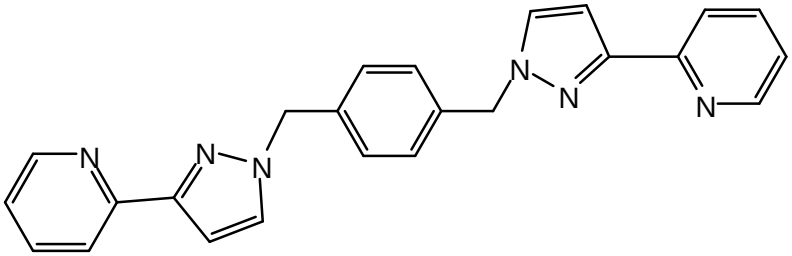

Figure 2.1.1 Structure of the ligand L^{pp}.

Polyhedral coordination cages have been the subject of intense research in recent years as they show promising applications in many areas. These areas include host-guest chemistry such as encapsulation,[2] catalysis,[3-7] and reactivity modification[8] where the cages act as 'microreactors'.

Supramolecular structures which can be switched between two different conformations are of interest due to their potential applications.[9, 10] Examples of this phenomenon are relatively limited in the field of coordination cages, although two examples have been shown which use solvents as the stimuli for the conformational change.

Severin and co-workers have shown a dramatic change in structure with a very small change in solvent polarity.[11] In chloroform they obtained a Ru(II) metallabox based on

four dinuclear metallacrown complexes, however in dichloromethane the cage rearranges to give a tetranuclear complex (figure 2.1.2). The rearrangement is thought to occur because the two complexes provide solvent-specific binding pockets for the corresponding solvents.

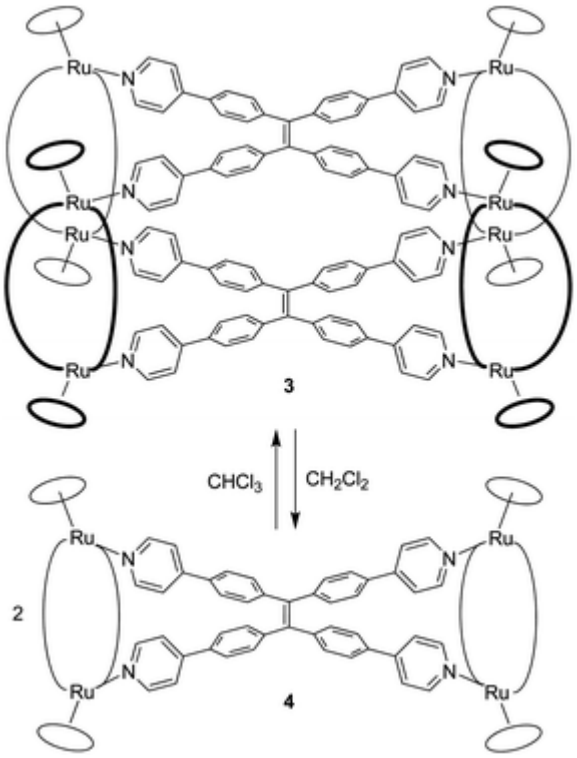

Figure 2.1.2 Solvent induced rearrangement. Reproduced from reference 11.

A similar conformational switch has been shown by Fujita and co-workers. They showed a system where Pd_4L_8 and Pd_3L_6 'boxes' could be interconverted by adding or removing the MeCN solvent.[12] The conversion can be performed reversibly and repeatedly, and was attributed to favourable DMSO/nitrate interactions in the cavity of the Pd_4L_8 box when the MeCN solvent was removed. The entropic benefit of the Pd_3L_6 box appears to dominate with MeCN present as the DMSO/nitrate interactions were lost with MeCN molecules seen in the central cavity.

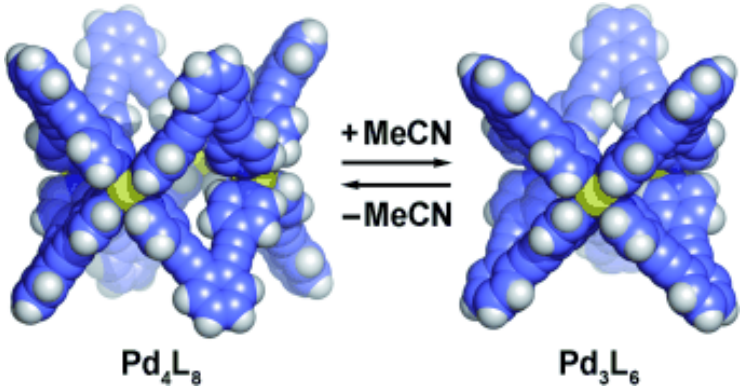

Figure 2.1.3 The solvent dependent rearrangement. Reproduced from reference 12.

There have not been any structural rearrangements or interconversions seen in the cages from the Ward group. However as shown in figure 1.4.4 and 1.4.5 earlier, different complexes have been seen with the same ligand, and the two structures are thought to be very similar in energy and could be in equilibrium with each other.[13] This increases the chance of the structures rearranging with an external stimulus such as a change in solvent.

The ligand L^{pp} has been synthesised previously and been shown to form a $[M_{16}(L^{pp})_{24}](X)_{32}$ cage with either Cd(II) or Zn(II).[14] This was the largest cage seen by the Ward group and therefore has a high possibility of host-guest chemistry within its central cavity. Its behaviour in solution will be studied in detail in this work, as this is an essential prelude to studies on host-guest chemistry.

2.2 Results and Discussion

2.2.1 Solid-state studies

The crystal structure of $[Cd_{16}(L^{pp})_{24}](ClO_4)_{32}$ has been published previously,[14] and $[Zn_{16}(L^{pp})_{24}](BF_4)_{32}$ is isostructural and essentially identical. The crystal structures of these two complexes were collected by previous members of the Ward group however further studies were required to understand how the complexes behave in solution. In order to do this the solid state structure needs to be understood in detail and some of the key points will be outlined here.

The structure is best described as containing a tetra-capped truncated tetrahedral core. This is achieved by slicing off each apex of a tetrahedron to reveal triangular faces [shown in yellow in figure 2.2.1.1(left)], and then twisting all four triangular faces in the same sense such that the mirror planes through the truncated tetrahedron are removed but the C_3 axes are retained. A capping atom is added to the original four faces to give the M_{16} polyhedral array with noncrystallographic T-symmetry with four C_3 axes as the only symmetry elements. The cage has a very large cavity (estimated to be approximately 700 $Å^3$) which contains at least eight disordered anions and six solvent molecules. It has been shown by NMR spectroscopy however that these are able to enter and leave the cage quite freely as there are large windows within the cage complex [figure 2.2.1.1 (right)].

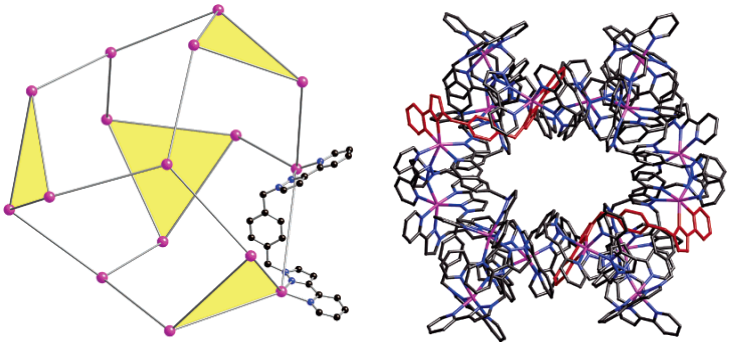

Figure 2.2.1.1 Two views of $[Cd_{16}(L^{pp})_{24}](ClO_4)_{32}$. Reproduced from reference 14.

The twelve Cd(II) centres associated with the four triangular faces all have a *mer* tris-chelate coordination geometry [figure 2.2.1.2(a)], whereas the four capping ions have a *fac* tris-chelate geometry [figure 2.2.1.2(b)]. Therefore the result is two ligand environments, one around the edges of the triangular face connecting two *mer* metal centres, and one connecting the triangular faces to the capping ions connecting *mer* and *fac* metal centres. The four Cd_3 triangular faces have $M_3(\mu\text{-}L^{pp})_3$ cyclic helical structures. This trinuclear cyclic helicate unit appears in many different structures from these types of ligand and appears to be an important structural feature. This point will be examined in more detail later.

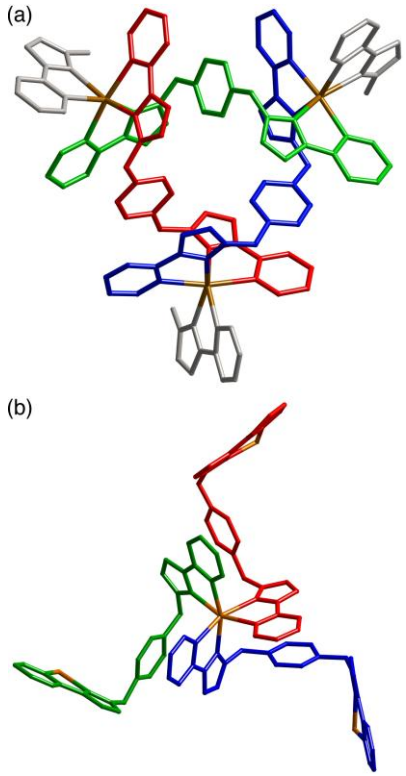

Figure 2.2.1.2 (a) The $Cd_3(L^{pp})_3$ cyclic helical unit in which all centres are *mer* tris-chelate and (b) one of the *fac* tris-chelate capping ions.

The new work described in this chapter with this ligand therefore involved investigating the solution behaviour of the large $M_{16}(L^{pp})_{24}$ cages and determining what structures were afforded with other metal ions such as Cu(II) and Ni(II).

The ligand L^{pp} was combined with $Cu(BF_4)_2$ in a 3:2 ratio and the mixture stirred at room temperature for 24 hours. After recrystallisation using MeCN and $^{i}Pr_2O$, the crystal structure proved to be $[Cu_6(L^{pp})_9](BF_4)_{12}$. This is a rare example of a hexanuclear trigonal prism which is effectively two $Cu_3(L^{pp})_3$ cyclic helicates connected by three pillar ligands [shown in figure 2.2.1.3(a)]. The cage only has approximate trigonal prismatic geometry because the two triangular faces are offset such that the basic core structure is distorted towards a trigonal antiprism [figure 2.2.1.3(b)]. The $Cu_3(L^{pp})_3$ cyclic helical faces are homochiral and all six metal centres have the same optical tris-chelate geometry. All six metal centres have *mer* tris-chelate coordination geometry as was seen in the $Cd_3(L^{pp})_3$ cyclic helicates in the $M_{16}(L^{pp})_{24}$ cage.

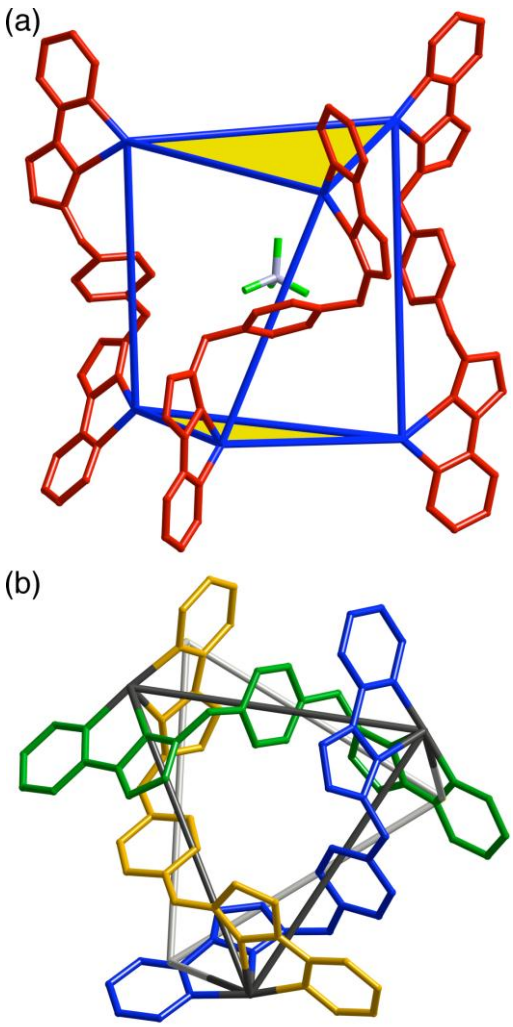

Figure 2.2.1.3 Two views of the hexanuclear $[Cu_6(L^{pp})_9](BF_4)_{12}$ trigonal prismatic cage.

The Cu•••Cu separations average 10.20 Å around the two triangular faces and 10.56 Å for the three edges between the two triangular faces. The Cu – N distances are between 1.95 and 2.45 Å, the large variations being caused by Jahn-Teller distortion. There is an elongation along the pyrazole – pyrazole axis and in every case one of the pyrazole rings in question is part of the pillar ligand. There is also quite a large conformational difference between the ligands in the triangular units and the pillar ligands. The ligands around the triangular faces have a 'U' conformation as can be seen quite clearly in figure 2.2.1.4 (a). In this case the methylene groups orientate the PyPz units so that they are both on the same side of the phenylene group. The pillar ligands though have an 'S' conformation where the methylene groups orientate the PyPz units to be on the opposite side of the phenylene group. This can be seen in figure 2.2.1.4 (b) and helps to explain

why the Cu•••Cu separations are longer between the triangular helical units compared to those within them. The conformations are such that the phenylene groups of every ligand are involved in π-stacking. The phenylene groups from the ligands in the trinuclear cyclic helicate faces are all stacked between two PyPz units from the other two ligands in the unit. This is exactly the same as with the trinuclear fragments of the $Cd_{16}(L^{pp})_{24}$ cage. The pillar ligand is orientated such that the phenylene unit is stacked with one of the PyPz units on one of the helical ligands. This is shown in figure 2.2.1.4 (b).

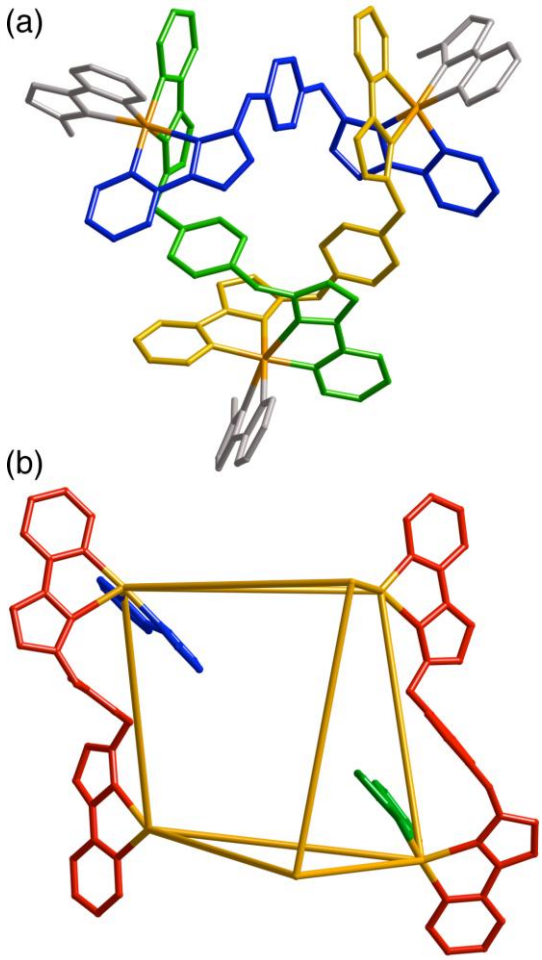

Figure 2.2.1.4 (a) The $Cu_3(L^{pp})_3$ cyclic helical unit [note the similarity with figure 2.2.1.2 (a)] and (b) the interligand aromatic stacking between the pillar ligands and the fragments of the ligands around the triangular faces.

There is one $[BF_4]^-$ anion located in the central cavity, shown in figure 2.2.1.3(a). The anion has a network of CH•••F hydrogen-bonding interactions which anchor it in place.

The C•••F distances are in the range 2.89 – 3.37 Å to inwardly directed CH protons from ligands.

Assuming that the structure relaxes in solution, there would be overall D_3 symmetry, with a C_3 axis running perpendicular to the cyclic helical face and three C_2 axes perpendicular to this, so that each one bisects one of the pillar ligands and projects through to the opposite rectangular face. Unfortunately Cu(II) complexes are not suitable for ^{1}H NMR spectroscopy, however these symmetry principles will be very important later on.

This is the first time that a trigonal prismatic cage has been seen with this series of ligands, and this structure fills an obvious gap. There have been many examples of M_4L_6 tetrahedra and M_8L_{12} cubes based on pyrazolyl-pyridine ligands. Interestingly both of these are Platonic solids, whereas the trigonal prism is not. The Platonic solid with six vertices is an octahedron with 12 edges and therefore would not fit into this series of cages which are all based on a M_2:L_3 ratio. The trigonal prismatic arrangement is sterically less favoured than the octahedral arrangement because the two triangular faces are eclipsed and not staggered. This may be the reason why structures based on Platonic solids are more common than the trigonal prisms and also why examples of trigonal prismatic cages in the literature are relatively rare. Examples that are known are generally based on rigid triangular ligands that provide the top and bottom faces of the assembly and therefore direct the 3 fold symmetry. Examples of this type have been shown from Stang,[15-17] Kaim[18, 19] and Mukherjee.[20] The closest example to this structure appears to be $[\{Mo(CO)_3\}_6(\mu\text{–}CN)_9]^{9-}$ which also has six octahedral metals and nine bridging ligands.[21]

L^{pp} was combined with $Ni(BF_4)_2$ in a 3:2 ratio in MeOH using the solvothermal method. The metal salt and ligand were combined in a Teflon-lined autoclave, heated to 100 °C for twelve hours and then slowly cooled to room temperature. This yielded small purple crystals which were too small for X-ray crystallography and so were recrystallised by diffusion of diethyl ether into a solution of the complex in nitromethane. The resulting crystals were suitable for X-ray diffraction, and the X-ray structure was determined and found to be $[Ni_8(L^{pp})_{12}](BF_4)_{12}(SiF_6)_2$ (figure 2.2.1.5). It is a slanted cube with a metal ion at each vertex and a bridging ligand along each edge.

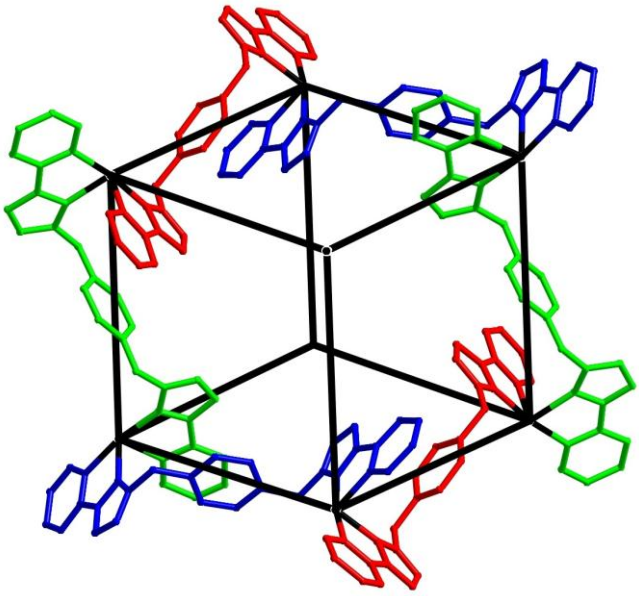

Figure 2.2.1.5 Structure of the complex cation of $[Ni_8(L^{pp})_{12}]$ with half of the ligands shown. Symmetry equivalent ligands are shown in the same colour.

The Ni – Ni – Ni angles are 79.79 °, 97.73 °, and 102.52 °, the average is 90.00 °. There are only two different Ni•••Ni distances due to the high symmetry of the structure, these are 10.20 Å and 10.57 Å. The cube has S_6 symmetry with diagonally opposite Ni(II) ions being equivalent as shown in figure 2.2.1.6. Two of the eight Ni(II) ions have a facial geometry (labelled A), the other six have a meridional geometry (labelled B). The metal centres at opposite corners, for example A and A*, are enantiomers of each other and the different ligand environments are coloured separately. There is no significant difference between the two geometries with respect to bond distances and angles. The average Ni – N bond length is 2.11 Å, and the average N – Ni – N bond angle is 78.26 °.

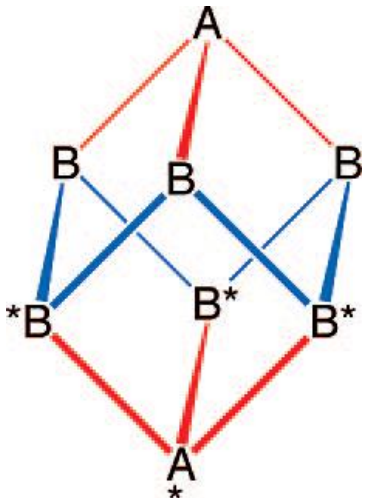

Figure 2.2.1.6 Sketch showing the S_6 symmetry of the cube. Reproduced from reference 22.

There is one disordered counter ion that can be seen in the centre of the cage from the crystal structure. This and other counter ions associated with the cage are shown in figure 2.2.1.7, including a $[SiF_6]^{2-}$ ion which must have arisen by liberation of fluoride from BF_4^- followed by reaction with the glass reaction vessel; this has happened before.[23]

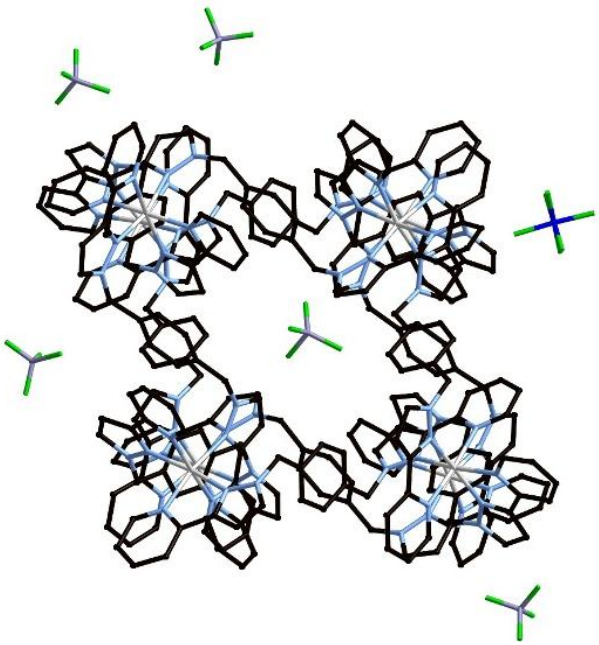

Figure 2.2.1.7 The anions associated with the cage including one tetrafluoroborate anion in the central cavity (disorder not shown).

The ligands are, as usual, all arranged in a way as to maximise π-stacking between them. In this structure eighteen of the twenty four pyrazolyl-pyridine units are involved in a π-stacking arrangement, with only one (on each meridional Ni(II) ion) not being involved. All twelve of the phenyl spacers are involved. The units are arranged in six stacks of five, two examples of which are highlighted in figure 2.2.1.8. These stacks all contain three pyrazolyl-pyridine units and two phenyl spacers. As with the other cages they always alternate when they stack due to their relative electron rich / electron poor character.

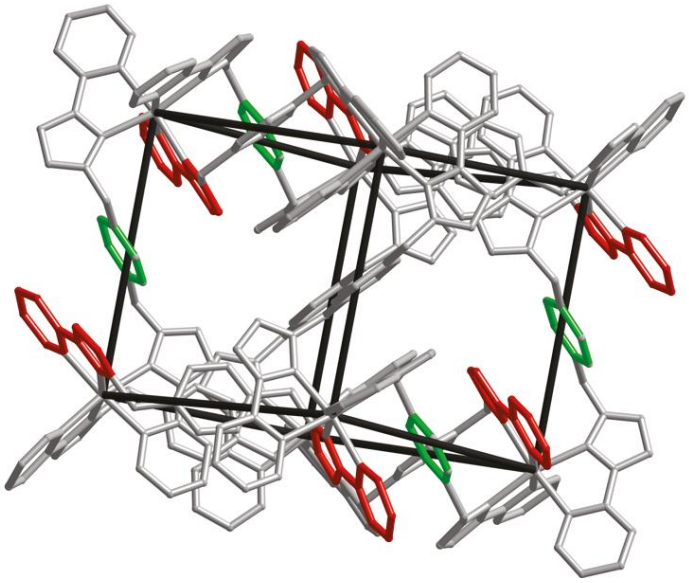

.

Figure 2.2.1.8 Two of the six sets of aromatic stacking in the structure.

This type of cubic octanuclear assembly with S_6 symmetry, containing two facial and six meridional metal centres has been seen before.[22, 24]

The cuboidal structure is different from the M_{16} tetra-capped truncated tetrahedron and the M_6 trigonal prism that have also been synthesised using this ligand because it does not contain the $M_3(L^{pp})_3$ cyclic helical unit. A reason for this may be that Ni(II) has a smaller ionic radius than Cd(II) and Cu(II), and so formation of an M_3L_3 cyclic helicate fragment may be sterically difficult.

2.2.2 Some underlying structural principles

It has already been noted that the M_3L_3 cyclic helical unit has appeared in two different structures with this ligand. These structures both contain the M_3L_3 unit, although they are connected together in different ways to give structures that have no apparent similarities. There are also other structures that have been previously reported by the Ward group which also contain this M_3L_3 unit but again have a different overall structure. The M_6L_9 trigonal prism structure described earlier is the easiest way that more than one of the M_3L_3 units could be connected together [figure 2.2.2.1 (a)]. A similar but more complex example is seen in the truncated tetrahedral $M_{12}L_{18}$ cage structure [figure 2.2.2.1 (b)]. As with the trigonal prism this uses a simple bis-bidentate bridging ligand to connect the M_3L_3 units, however in this case four of the units are connected together by six bridging ligands. An example of this type of cage structure has been seen with a ligand with a 1,8-naphthyl core.[25]

The $M_{16}L_{24}$ cage [figure 2.2.2.1 (d)] described earlier also contains the M_3L_3 units, but connected together by *fac*-ML_3 units. These *fac*-ML_3 units effectively act as a triply bridging 'complex ligand' with three bidentate coordination sites. Each *fac*-ML_3 unit connects to one vertex of three separate M_3L_3 units, and likewise each M_3L_3 is connected to three different *fac*-ML_3 units. There is a very clear relationship between this structure and the previously reported mixed ligand cuboctahedral cage $[M_{12}(L^{pp})_{12}(L^{mes})_4]^{24+}$[figure 2.2.2.1 (c)].[26] This structure combined the edge-bridging ligand L^{pp} and the bis-tridentate face capping ligand L^{mes}. It was found that in this mixed ligand species, the ligand L^{pp} formed the M_3L_3 units, four of which were connected together by four triply-bridging L^{mes} ligands in the same way as the *fac*-ML_3 unit does in the $M_{16}L_{24}$ cage.

The common structural feature in all these apparently very different structures suggests that an underlying design principle may be determined with these ligands. It is also interesting to see how the M_3L_3 units can be connected with ditopic and tritopic connecting pieces to give a range of different structures.

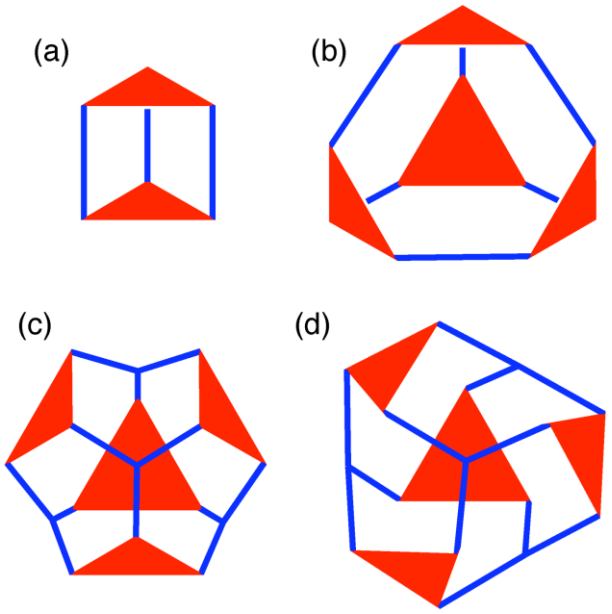

Figure 2.2.2.1 Different cage structures which all contain the M_3L_3 helical unit.

2.2.3 Solution Studies

The behaviour of all these complexes in solution is very important if they are to prove useful in the future for applications such as host-guest chemistry. Consequently, both ESMS and where possible NMR studies will be undertaken to determine if the structure observed by x-ray crystallography is maintained in solution.

The $[Cd_{16}(L^{pp})_{24}](BF_4)_{32}$ complex has been characterised by ^{1}H NMR and ^{113}Cd NMR spectroscopy and ESMS to determine its stability in solution. It was found that the structure was stable in solution, at least long enough to get a clean NMR spectrum and ES mass spectrum. The crystal structure of the cage was collected using $Cd(ClO_4)_2$ as the metal salt however all the solution studies have been undertaken using the tetrafluoroborate salt which has been proven to be isostructural by crystallography.[14]

The ^{1}H NMR spectrum measured immediately after dissolution of crystals reveals 40 different proton environments as shown in figure 2.2.3.1. This is exactly as would be expected with the $Cd_{16}L_{24}$ structure which has two ligand environments, each contributing 20 independent proton environments. There are 12 ligands involved in the $Cd_3(L^{pp})_3$ helical units and 12 more ligands involved in connecting the *fac*-Cd(II) ions to the $Cd_3(L^{pp})_3$ units. The chirality of the complex ensures that in every ligand the two

termini are inequivalent, giving 20 inequivalent protons for each of the two ligand environments.

The COSY spectrum allows easy identification of the methylene protons and pyrazolyl protons. There are four pairs of diastereotopic CH_2 protons, labelled a – d, associated with the two independent, non-symmetric ligand environments. These are doublets with characteristically large coupling constants. There are also four different types of pyrazolyl ring environment, leading to eight doublets, or four coupled pairs of signals. These are labelled p1 – p4 in figure 2.2.3.1 and have characteristically small coupling constants of less than 2 Hz.

The ^{113}Cd NMR spectrum is shown in figure 2.2.3.1 (b) and shows the expected two peaks in a 3:1 ratio. This is because there are twelve Cd(II) ions with a *mer* tris-chelate geometry and four with a *fac* tris-chelate geometry.

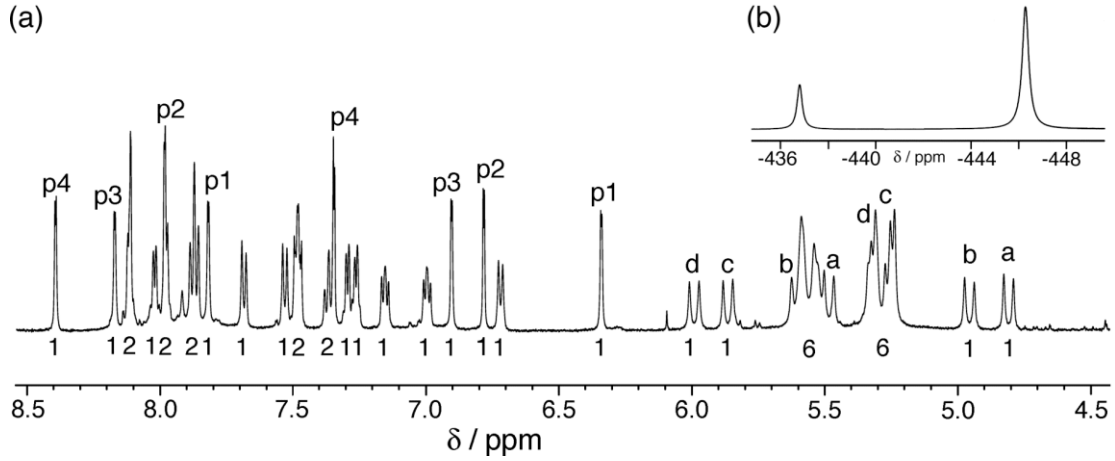

Figure 2.2.3.1 (a) The 500 MHz ^{1}H NMR spectrum of $[Cd_{16}(L^{pp})_{24}](BF_4)_{32}$ immediately after dissolution of crystals in CD_3CN. Integrals are given under each individual peak. (b) The ^{113}Cd spectrum also run immediately after dissolution in CD_3CN.

The complex has also been characterised by ESMS. There is a very clear sequence of peaks corresponding to the $Cd_{16}(L^{pp})_{24}$ cage, as shown in figure 2.2.3.2. The isotope spacing of the peaks confirm that they correspond to the $Cd_{16}(L^{pp})_{24}$ cage and not a smaller cage that could possibly have peaks at the same m/z value.

All the NMR and ESMS evidence therefore confirms that the solid-state molecular structure is retained in solution, at least for a few hours.

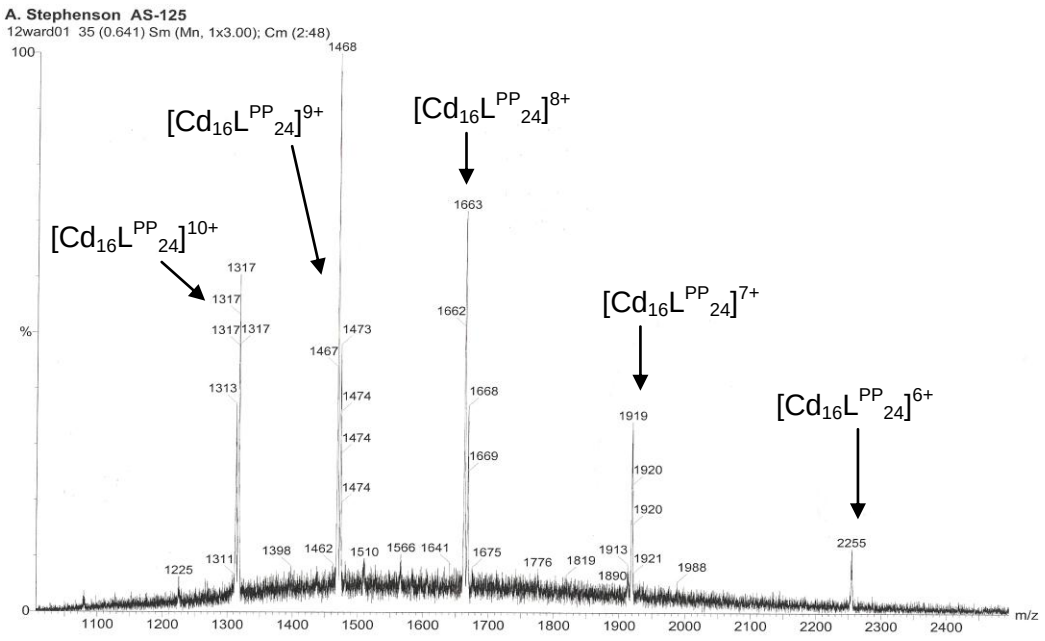

Figure 2.2.3.2 ESMS of redissolved crystals of $[Cd_{16}(L^{pp})_{24}](BF_4)_{32}$.

The $[Zn_{16}(L^{pp})_{24}](BF_4)_{32}$ structure was also investigated by ^{1}H NMR and ESMS. The ESMS showed a clear sequence of peaks corresponding to the intact cage however the ^{1}H NMR was poorly resolved containing more than the expected 40 signals. This appears to show that although the cage is stable in solution to a point, there is a large degree of dissociation or rearrangement that occurs immediately after dissolution.

The $[Cu_6(L^{pp})_9](BF_4)_{12}$ and $[Ni_8(L^{pp})_{12}](BF_4)_{16}$ complexes could not be characterised by ^{1}H NMR spectroscopy but ESMS studies were undertaken. The $[Cu_6(L^{pp})_9](BF_4)_{12}$ cage gave a clear sequence of peaks at *m/z* 2391, 1565, 1152 and 904 corresponding to $\{Cu_6(L^{pp})_9(BF_4)_{12-n}\}^{n+}$ (n = 2, 3, 4, 5). The spectrum showed no peaks corresponding to other cages and the spectrum also did not change over time. This appears to show that the cage is therefore stable in solution.

The ESMS studies of $Ni_8(L^{pp})_{12}$ were less clear-cut however. The spectrum did show weak peaks at *m/z* 3197 and 2102, corresponding to $\{[Ni_8(L^{pp})_{12}](BF_4)_{16-n}\}^{n+}$ (n = 2, 3). However there was a more intense set of peaks corresponding to the hexanuclear complex $\{Ni_6(L^{pp})_9(BF_4)_{12-n}\}^{n+}$ at *m/z* 2376, 1554 and 1144 (n = 2, 3, 4), which are

assumed to arise from a trigonal prismatic cage. These peaks were again identified unambiguously via the isotope spacings, which proved for example that the peak at *m/z* 1554 was $\{Ni_6(L^{pp})_9(BF_4)_9\}^{3+}$ and not $\{Ni_8(L^{pp})_{12}(BF_4)_{12}\}^{4+}$ which would appear at the same *m/z* value. It appears from this spectrum that there is a mixture of products in solution, although the trigonal prismatic structure seems to dominate. This would require the cube to rearrange in solution to the trigonal prism, which again would mean that this structure has the $M_3(L^{pp})_3$ units which seem common with this ligand. A different structure between the solid-state and solution has been shown before in a different example of a cage in this series.[24]

As mentioned earlier, $[Cd_{16}(L^{pp})_{24}](BF_4)_{32}$ cage was shown to be stable in solution by ^1H and ^{113}Cd NMR spectroscopy at least on the time scale of the measurements. However it was observed that when the same sample was measured again a day later, a new set of peaks slowly became apparent in the ^1H NMR and the original peaks reduced in intensity. The changes occurred over about two months at room temperature and appear to show a cage-to-cage interconversion in solution.

The original ^1H NMR spectrum and one after 27 days are shown in figure 2.2.3.3. From this comparison it is clear that the original set of peaks has been replaced by a new sequence in a relatively clean conversion. The new peaks grow in at the same rate and are of equal intensity to each other, therefore suggesting it is one product that the original cage is converting to. After 27 days a COSY spectrum was collected which allowed identification of the methylene and pyrazolyl protons. These are labelled in the spectrum as α, β and γ and p1 – p3 respectively. The phenylene protons from the new structure have also been labelled as A and a coupled pair B and B'.

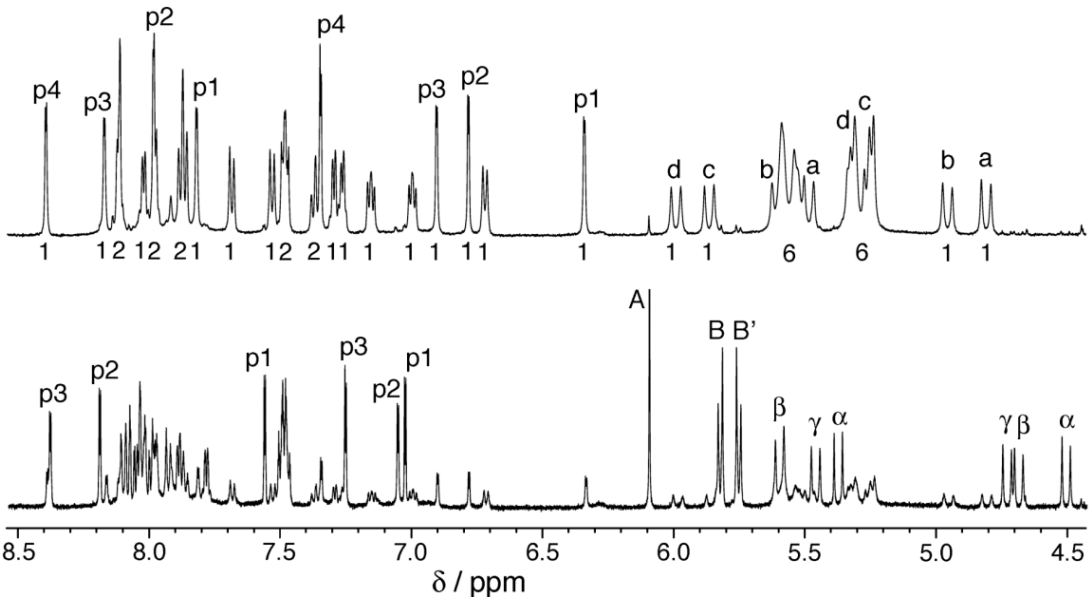

Figure 2.2.3.3 The original ^{1}H NMR spectrum in CD_3CN (top) and the same sample after 27 days showing a new sequence of peaks (bottom).

The changes in the spectrum are quite apparent from just the methylene signals in the spectrum, shown in figure 2.2.3.4, which are relatively easy to interpret. After 5 days [figure 2.2.3.4 (b)] the new peaks and the old peaks are approximately the same intensity, and then after 27 days [figure 2.2.3.4 (c)] the new peaks clearly dominate.

The information from the new peaks is enough to be able to identify the new product in solution. The new complex has six signals for methylene protons and the same for pyrazolyl protons (three coupled pairs of each), and two coupled doublets and a singlet for the phenylene protons. There is only one type of cage structure that could give such a ^{1}H NMR spectrum, and that is a D_3-symmetric trigonal prism, the same as the crystal structure seen with $Cu(BF_4)_2$ and L^{pp}. If this structure relaxes in solution so it is assumed that it has ideal symmetry then it has a C_3 axis and three C_2 axes. The structure would have two different ligand environments; one for the six ligands in the M_3L_3 helical units and one for the three pillar ligands. The ligands in the helical units have no internal symmetry – because of the chirality of the complex – but the three pillar ligands do have internal symmetry as they lie on C_2 axes. Therefore we would expect to see two pairs of coupled methylene protons from the helical ligands and one pair from the pillar

ligands, each of the same intensity (nominally 6H). The total of six pairs of methylene protons of equal intensity is what is observed [labelled as α, β and γ in figure 2.2.3.4 (c)]. This structure would also require three independent environments for the pyrazolyl rings (meaning three coupled pairs of protons) for the same reasons as above, and this is also seen (labelled p1 – p3 in figure 2.2.3.3). Further information can be gained from the phenylene proton signals. The trigonal prismatic structure would result in a coupled pair of doublets for the phenylene protons in the ligands in the helical unit and a singlet for the protons on the pillar ligands as these all become equivalent in solution. This is what is observed and the peaks are labelled as A for the singlet and B and B' for the coupled pair in figure 2.2.3.4(c). These peaks have double the intensity (nominally 12H) of the methylene and pyrazolyl protons.

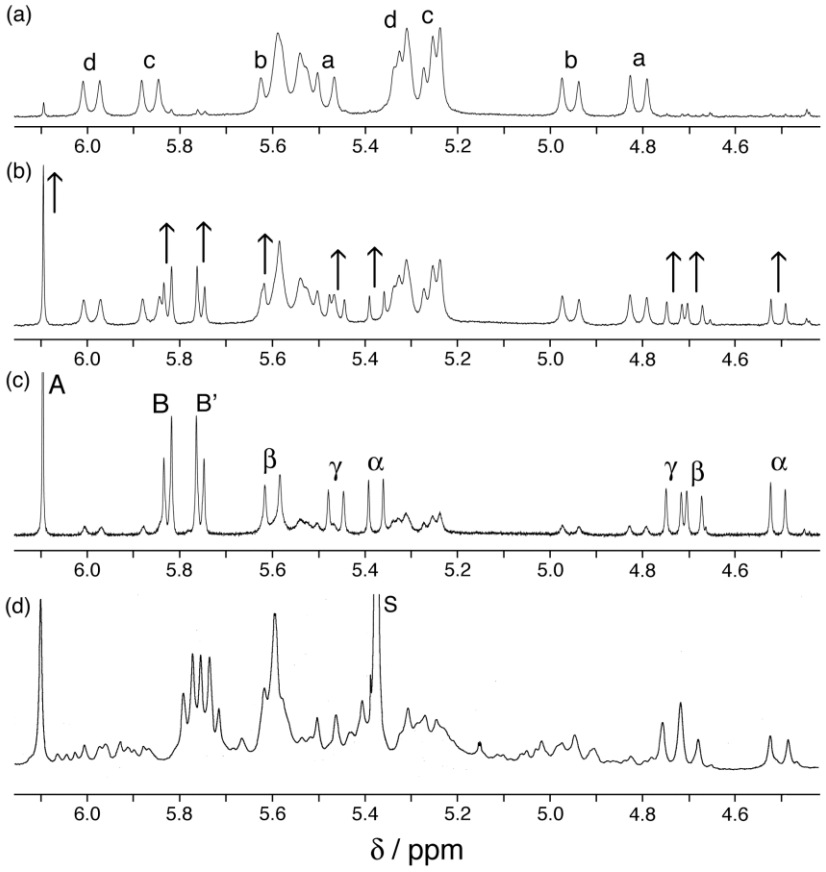

Figure 2.2.3.4 (a) The original ^{1}H NMR spectrum in CD_3CN after dissolution, (b) the same sample after 5 days showing the grow-in of peaks, (c) the same sample after 27 days, (d) the partial spectrum after mixing $Cd(BF_4)_2$ and L^{pp} in a 2:3 ratio. S = residual solvent peak.

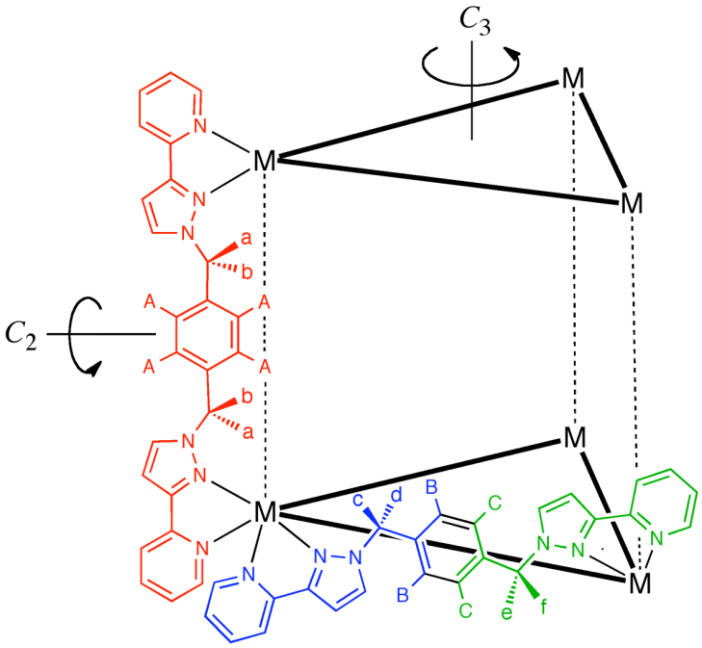

Figure 2.2.3.5 Sketch of a $M_6(L^{pp})_9$ complex showing the symmetry axes present.

The evidence for the existence of the $[Cd_6(L^{pp})_9]^{12+}$ complex in solution was further supported by diffusion coefficient (DOSY) measurements. When the new and old peaks were of comparable intensity the diffusion coefficients of several well-isolated signals for both species were measured. The values obtained were 3.74 x 10^{-10} and 5.21 x 10^{-10} $m^2 \cdot s^{-1}$ for the $[Cd_{16}(L^{pp})_{24}]^{32+}$ and $[Cd_6(L^{pp})_9]^{12+}$ cages respectively. Putting these values into the Stokes-Einstein equation gives a molecular weight ratio of $(5.21 / 3.74)^3$ which equals a ratio of 2.7:1 between starting material and product. Although the equation assumes the products are approximately spherical, the result agrees very well with the required 16:6 ratio (or 2.667:1). The Stokes-Einstein equation can also be used to estimate the hydrodynamic radii of the molecules. This gives radii of 15.9 Å for the Cd_{16} complex and 11.4 Å for the Cd_6 complex. These values are likely to be smaller than the real radii of the complexes which will not be completely spherical. However, measuring the radii (from the crystal structures of Cd_{16} and the Cu_6 complexes) gave good agreement with these estimations as they were approximately 18 Å and 12 Å respectively. Therefore the hydrodynamic radii estimated from the diffusion coefficients are fully consistent with the observed structures.

The conversion of $[Cd_{16}(L^{pp})_{24}]^{32+}$ to $[Cd_6(L^{pp})_9]^{12+}$was also followed by ESMS using redissolved crystals. The initial sequence of peaks due to the Cd_{16} cage slowly diminished in intensity and peaks of smaller cages grew in over time. After about two

months, which was when the conversion appeared to have finished by NMR, the series of peaks corresponding to the $[Cd_{16}(L^{pp})_{24}]^{32+}$ cage had almost disappeared and been replaced by several new peaks. These could be assigned to the tetranuclear species $\{Cd_4(L^{pp})_6(BF_4)_{8-n}\}^{n+}$ (at *m/z* 3412, 1662, 1079, 788 and 613 for n = 1, 2, 3, 4, 5), the hexanuclear species $\{Cd_6(L^{pp})_9(BF_4)_{12-n}\}^{n+}$ (at *m/z* 1225 and 963 for n = 4, 5) and the octanuclear species $\{Cd_8(L^{pp})_{12}(BF_4)_{16-n}\}^{n+}$ (at *m/z* 2247, 1662 and 1313 for n = 3, 4, 5). Other smaller fragmentation products were also present at lower *m/z* values however it is likely that these are just fragments caused by the ESMS conditions. The identification of all peaks named above could be made unambiguously due to the isotope spacings between the peaks which allow identification of the charge of the species. At some *m/z* values there are more than one peak at the same value however it is possible to see more than one species. For example expansion of the isotope cluster at *m/z* 1662 clearly confirms the presence of three distinct species with charges of +1, +2 and +4, ascribed to $\{Cd_2(L^{pp})_3(BF_4)_3\}^{+}$, $\{Cd_4(L^{pp})_6(BF_4)_6\}^{2+}$ and $\{Cd_8(L^{pp})_{12}(BF_4)_{12}\}^{4+}$ (figure 2.2.3.6).

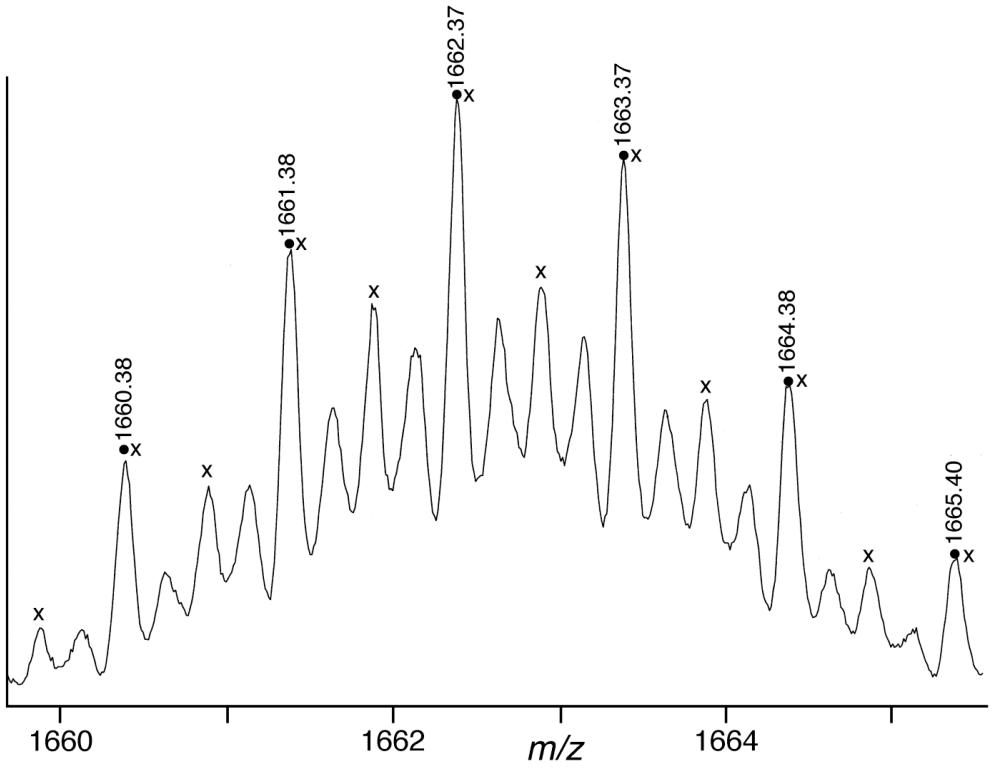

Figure 2.2.3.6 Partial ESMS showing isotope spacings of 1 unit (labelled •), 0.5 units (labelled x) and 0.25 units (all peaks), corresponding to a mixture of fragments $\{Cd_2(L^{pp})_3(BF_4)_3\}^{+}$, $\{Cd_4(L^{pp})_6(BF_4)_6\}^{2+}$ and $\{Cd_8(L^{pp})_{12}(BF_4)_{12}\}^{4+}$ which all have the same *m/z* value.

The cage-to-cage interconversion was also followed at higher temperature to see if the rate of conversion changed. A large batch of crystals of $[Cd_{16}(L^{pp})_{24}]^{32+}$ was dissolved in deuterated MeCN and then split into two samples whose ^{1}H NMR spectra were measured at the same time, with one kept at room temperature and one kept at 60 °C in an oven. The sample at room temperature followed the conversion at the rate expected, however the sample at 60 ºC showed the same evolution but on a much faster timescale. After just 2 days the conversion was 90 % complete but after this point the sample started to decompose and a white solid appeared in the NMR tube. This is presumed to be a mixture of Cd(II)-fluoride complexes which arose from the decomposition of the tetrafluoroborate anion. This has been known to happen before in other BF_4^- complexes of Cd^{2+}, but importantly it was proven that the rate of conversion is affected by temperature as expected.

It was also investigated what would happen if $Cd(BF_4)_2$ and L^{pp} were mixed in a 2:3 ratio and the assembly followed from first principles by ^{1}H NMR and ESMS. This is important as it would show if the same product (the Cd_6 cage) was favoured in solution from assembly of the ligand and metal salt as well as disassembly of the larger cage. It would also prove whether the Cd_{16} cage was purely an artefact of crystallisation, which would be the case if it is not seen during the assembly experiment in solution.

The ^{1}H NMR spectrum approximately thirty minutes after mixing $Cd(BF_4)_2$ and L^{pp} is shown in figure 2.2.3.4 (d). The spectrum is quite poorly resolved, however there are clearly peaks that are the same as the ones that appear during the disassembly experiment. The methylene proton doublets at 4.5 – 4.7 ppm and the phenylene signals at 5.7 – 6.1 ppm are clearly very similar to the peaks of the Cd_6 complex obtained after the conversion has finished in figure 2.2.3.4(c). The spectrum changes little over time, suggesting that the preferred product is reached in the first thirty minutes, and also suggesting that the Cd_6 cage is the preferred product.

The same experiment was performed and followed by ESMS. Thirty minutes after mixing the ligand and metal salt the mixture is dominated by smaller fragments, however there are peaks that can be assigned to the tetranuclear $[Cd_4(L^{pp})_6](BF_4)_8$, hexanuclear $[Cd_6(L^{pp})_9](BF_4)_{12}$ and octanuclear $[Cd_8(L^{pp})_{12}](BF_4)_{16}$ cages. After one month the same solution was measured again and there were significantly less small

fragments and a greater number of intense peaks corresponding to all three cages. The most intense peaks of all corresponded to the tetranuclear cage however the intensity of peaks in an ESMS is not necessarily a reliable guide to abundance in solution. At no point throughout the experiment were there any peaks that could be assigned to $[Cd_{16}(L^{pp})_{24}]^{32+}$, and therefore this appears only to form during crystallisation.

Similar experiments were also performed using L^{pp} with $Cu(BF_4)_2$ and $Ni(BF_4)_2$. The mixture of L^{pp} and $Cu(BF_4)_2$ was measured straight after mixing and showed a strong sequence of peaks at peaks at *m/z* 1565, 1152, 904, 739 and 621 corresponding to the series $\{Cu_6(L^{pp})_9(BF_4)_{12-n}\}^{n+}$ (n = 3, 4, 5, 6, 7). The spectrum did not change and therefore showed that the hexanuclear structure is the most dominant product and is stable in solution. This is consistent with what is observed in the ES mass spectrum of pre-formed crystals.

The assembly experiment with $Ni(BF_4)_2$ and L^{pp} was more complicated (as with the disassembly experiment), with a mixture of products being seen in the mass spectra. Straight after mixing, the spectrum was fairly complicated and peaks were assigned to species including $[Ni_2(L^{pp})_3]^{4+}$, $[Ni_2(L^{pp})_4]^{4+}$, $[Ni_3(L^{pp})_4]^{6+}$, $[Ni_3(L^{pp})_5]^{6+}$, $[Ni_4(L^{pp})_6]^{8+}$ and $[Ni_6(L^{pp})_9]^{12+}$ species. At this stage no peaks could be seen which corresponded to the M_8L_{12} octanuclear cube which was seen in the crystal structure. This mixture did change over time however, and after two weeks the spectrum looked quite different. The most intense peaks were at *m/z* 1555, 1144, 898, 734 and 617, corresponding to the hexanuclear species $\{Ni_6(L^{pp})_9(BF_4)_{12-n}\}^{n+}$ (n = 3, 4, 5, 6, 7). A weaker series of peaks was also present in the spectrum at *m/z* 1227, 1008 and 851 which corresponded to the octanuclear species $\{Ni_8(L^{pp})_{12}(BF_4)_{16-n}\}^{n+}$ (n = 5, 6, 7). This result again agrees with the disassembly experiment which also shows that the hexanuclear structure is the dominant species in solution, although the octanuclear cubic species does persist to a degree. The cube however appears to be the favoured crystallisation product, presumably for the same reasons as the Cd/L^{pp} system has a different favoured crystallisation product compared to what is more stable in solution.

It is important to understand why the rearrangement of $[Cd_{16}(L^{pp})_{24}]^{32+}$ to $[Cd_6(L^{pp})_9]^{12+}$ is occurring in solution and why the favoured crystallisation product is not always stable in solution. It appears to be the case with the Cd complex and to a lesser extent the Ni

complex, that a larger cage which is the crystallisation product converts to one or more smaller cages in solution. This conversion can be understood by the principles of equilibria. Looking at the Cd cage conversion as an example, the conversion of the Cd_{16} cage to the Cd_6 cage can be explained purely on entropic grounds. This states that if all other things are equal (for example no significant change in enthalpy from the change in Cd – N bonds) then a larger number of smaller assemblies will be favoured over a smaller number of larger assemblies. Assuming the conversion is clean then the equilibrium could be given as :

$$Cd_{16}\ \text{cage} = 2.67\ (Cd_6\ \text{cage}) \quad (1)$$

$$[Cd_{16}\ \text{cage}] = K[Cd_6\ \text{cage}]^{2.67} \quad (2)$$

The associated equilibrium constant therefore implies that as the concentration increases the balance shifts towards the Cd_{16} cage. For example, for every factor of 10 increase in the concentration of Cd_6, an increase of the Cd_{16} concentration by $10^{2.67}$ (468) is required to maintain equilibrium. This means that a shift from millimolar to molar in concentration (or effectively solution to solid) will favour the larger cage by a factor of 10^8, which is enough to give a complete switch from >99.99% smaller Cd_6 cage to >99.99% larger Cd_{16} cage and this completely explains the observations.

The conversion (figure 2.2.3.7) is therefore explained on entropic grounds and can be viewed as the kinetic crystallisation product converting to the thermodynamic product which is more stable in solution. Interestingly both the cages in the Cd_{16}/Cd_6 conversion contain the M_3L_3 triangular face units which quite possibly stay intact during the conversion. This appears to be a very stable unit and the trigonal prism is the simplest combination of M_3L_3 units where all metals are coordinatively saturated. It is also interesting that the most stable product in solution with all metals is the hexanuclear trigonal prism, again suggesting that both the M_3L_3 unit and the trigonal prismatic structure as a whole are particularly stable.

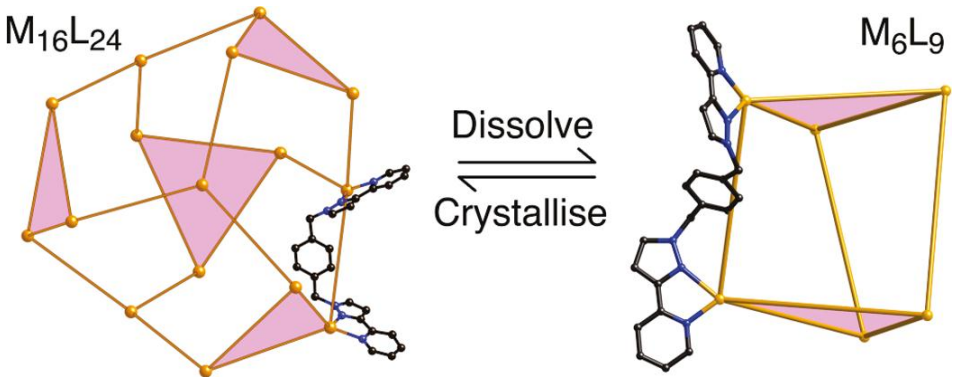

Figure 2.2.3.7 Schematic diagram of the cage-to-cage interconversion.

2.3 Conclusion

The bis-bidentate bridging ligand L^{pp} forms three different types of coordination cage with different metal ions. The crystal structures all have the same 2:3 metal-to-ligand ratio with octahedral metal ions at the vertex and bridging ligands along each edge. The reason for the difference in solid state structures may be ascribed to the different ionic radii of the metals used and also in the case of Cu(II) the Jahn-Teller effect which results in significantly distorted tris-chelate geometries. The structure with Cu(II) is a $[Cu_6(L^{pp})_9]^{12+}$ trigonal prism, with Ni(II) a $[Ni_8(L^{pp})_{12}]^{16+}$ cube, and with Cd(II) or Zn(II) a $[M_{16}(L^{pp})_{24}]^{32+}$ tetra-capped truncated tetrahedron.

The complexes show very interesting behaviour in solution as characterised by NMR spectroscopy and ESMS. The $[Cu_6(L^{pp})_9]^{12+}$ complex is stable in solution and forms after minutes, appearing to be the only product. The $[Ni_8(L^{pp})_{12}]^{16+}$ complex has been shown to form a mixture of products in solution with both the $[Ni_8(L^{pp})_{12}]^{16+}$ and more abundantly the $[Ni_6(L^{pp})_9]^{12+}$ structures persisting in solution. This was confirmed by both assembly and disassembly experiments. The $[Cd_{16}(L^{pp})_{24}]^{32+}$ cage did not persist in solution and underwent a cage-to-cage interconversion to a $[Cd_6(L^{pp})_9]^{12+}$ species. This was confirmed by ESMS and ^1H NMR spectroscopy and has been rationalised on the grounds of entropy. The thermodynamic minimum of the system is an equilibrium between the Cd_{16} and Cd_6 species in which both components are present. The position of the equilibrium shifts depending on concentration which changes when the system is in solution or in the solid-state. At higher concentration the $[Cd_{16}(L^{pp})_{24}]^{32+}$ cage is the favoured product and converts in solution at lower concentration into the smaller

$[Cd_6(L^{pp})_9]^{12+}$ cage. The most abundant species in solution for all metals is the $[M_6(L^{pp})_9]^{12+}$ complex, suggesting that this dominates the equilibrium in solution in all cases.

The $[M_6(L^{pp})_9]^{12+}$ and $[M_{16}(L^{pp})_{24}]^{32+}$ structures both consist of $M_3(L^{pp})_3$ cyclic helical units which appear to be very stable and are common in many of the structures throughout the series. Interestingly the favoured thermodynamic product, the trigonal prism is the simplest way of connecting $M_3(L^{pp})_3$ units so that all metals are coordinatively saturated and the M_2:L_3 ratio is maintained.

2.4 Experimental

The ligand was synthesised as previously reported.[14]

Synthesis of $[Ni_8(L^{pp})_{12}](BF_4)_{16}$

A Teflon lined autoclave was charged with $Ni(BF_4)_2$ (0.029 g, 0.085 mmol), L^{pp} (0.050 g, 0.127 mmol) and methanol (9 mL). Heating to 100 °C for twelve hours followed by slow cooling to room temperature yielded a crop of purple crystals. These were not suitable for X-ray determination and were therefore recrystallised by slow diffusion of diethyl ether into a solution of the complex in nitromethane.

ESMS: *m/z* 3197, $\{[Ni_8(L^{pp})_{12}](BF_4)_{14}\}^{2+}$; 2102, $\{[Ni_8(L^{pp})_{12}](BF_4)_{13}\}^{3+}$; 1555, $\{[Ni_8(L^{pp})_{12}](BF_4)_{12}\}^{4+}$.

Elemental analytical data of vacuum-dried samples were consistent with the presence of water of crystallisation due to the desolvated material being hygroscopic, as follows. Found: C, 50.2; H, 3.8; N, 14.6. Required for $[Ni_8(L^{pp})_{12}](BF_4)_{16}\bullet 15H_2O$: C, 50.6; H, 4.0; N, 14.7%.

$[Cu_6(L^{pp})_9](BF_4)_{12}$, $[Cd_{16}(L^{pp})_{24}](BF_4)_{32}$ and $[Zn_{16}(L^{pp})_{24}](BF_4)_{32}$ were all synthesised using the following method:

Synthesis of $[Cu_6(L^{pp})_9](BF_4)_{12}$

A solution of $Cu(BF_4)_2$ (0.023 g, 0.10 mmol) in MeOH (7 cm^3) was added to a solution of L^{pp} (0.058 g, 0.15 mmol) in CH_2Cl_2 (7 cm^3). The mixture was stirred at room temperature for 24 h, and the resultant precipitate was filtered off, washed with both MeOH and CH_2Cl_2, and dried *in vacuo* to give $[Cu_6(L^{pp})_9](BF_4)_{12}$ as a green powder in 90% yield. X-ray quality crystals were grown by slow diffusion of isopropyl ether into a solution of the complex in acetonitrile or nitromethane.

ESMS: *m/z* 2391, $\{[Cu_6(L^{pp})_9](BF_4)_{10}\}^{2+}$; 1565, $\{[Cu_6(L^{pp})_9](BF_4)_9\}^{3+}$; 1152, $\{[Cu_6(L^{pp})_9](BF_4)_8\}^{4+}$; 904, $\{[Cu_6(L^{pp})_9](BF_4)_7\}^{5+}$.

Elemental analytical data of vacuum-dried samples were consistent with the presence of water of crystallisation due to the desolvated material being hygroscopic, as follows.

Found: C, 50.2; H, 3.6; N, 14.3%. Required for $[Cu_6(L^{pp})_9](BF_4)_{12}\bullet 10H_2O$: C, 50.5; H. 3.9; N, 14.7%.

2.5 X-Ray Crystallography

Crystals were removed from the mother liquor, coated with oil, and transferred to a stream of cold N_2 on the diffractometer as quickly as possible to prevent decomposition due to solvent loss. The structures of $[Cd_{16}(L^{pp})_{24}](ClO_4)_{32}$ and $[Zn_{16}L_{24}](BF_4)_{32}$ were collected at the University of Bristol by previous members of the Ward group using a Bruker PROTEUM diffractometer equipped with Cu-Kα radiation from a rotating anode generator. The Cd structure was previously published,[14] however additional work was done on the refinement of the Zn structure (including a 'Squeeze' as explained later) so that this was also publishable. The structure of $[Cu_6(L^{pp})_9](BF_4)_{12}$ was determined at the University of Sheffield on a Bruker APEX-2 diffractometer equipped with Mo-Kα radiation from a sealed-tube source; and the structure of $[Ni_8(L^{pp})_{12}](BF_4)_{12}(SiF_6)_2$ was determined at the EPSRC National Crystallography Service at the University of Southampton, using a Nonius Kappa-CCD diffractometer equipped with Mo-Kα radiation from a Bruker-Nonius FR-591 rotating anode generator. Details of the crystal parameters, data collection and refinement are summarised. After integration of the raw data, and before merging, an empirical absorption correction was applied (SADABS)[27] based on comparison of multiple symmetry-equivalent measurements. The structures were solved by direct methods and refined by full-matrix least squares on weighted F2 values for all reflections using the SHELX suite of programs.[28] In all cases there were extensive areas of residual electron density which could not sensibly be modelled as solvent or anions, which were removed via application of the 'Squeeze' function in PLATON.[29] Full details of these issues and how they were handled is given in the individual CIFs.

Crystal Data Tables

Summary of crystallographic data for the new crystal structures:

Compound	**$[Ni_8(L^{pp})_{12}](BF_4)_{12}(SiF_6)_2$• 18MeNO$_2$**	**$[Cu_6(L^{pp})_9](BF_4)_{12}$**
Formula	$C_{306}H_{294}B_{12}O_{36}Si_2N_{90}F_{60}Ni_8$	$C_{216}H_{180}B_{12}Cu_6F_{48}N_{54}$
Molecular weight	7603.89	4955.10
T / *K*	120(2)	150(2)
Crystal system	Hexagonal	Orthorhombic
Space group	*R*–3c	*I*ba2
a / Å	26.0607(3)	31.7261(11)
b / Å	26.0607(3)	56.9758(17)
c / Å	98.7782(14)	29.7638(9)
α / °	90	90
β / °	90	90
γ / °	120	90
V / Å^3	58098.3(13)	53802(3)
Z	6	8
ρ / g cm^{-3}	1.300	1.095
μ / mm^{-1}	0.485	0.535
Data, restraints, parameters, R_{int}	14798 / 13 / 652 / 0.0494	54501 / 2673 / 2071 / 0.1517
Final *R*1, *wR*2[a]	0.129, 0.410	0.107, 0.323

[a] The value of *R*1 is based on 'observed' data with $I>2\sigma(I)$; the value of *wR*2 is based on all data.

2.6 References

1. M. D. Ward, *Chem. Commun.*, 2009, 4487.

2. P. Mal, B. Breiner, K. Rissanen, J. R. Nitschke, *Science,* 2009, **324**, 1697.

3. J. Kang, J. Rebek, Jr., *Nature,* 1997, **385**, 50.

4. J. Kang, J. Santamarıa, G. Hilmersson, J. Rebek Jr., *J. Am.Chem. Soc*., 1998, **120**, 7389.

5. M. Yoshizawa, J. K. Klosterman, M. Fujita, *Angew. Chem. Int. Ed.*, 2009, **48**, 3418.

6. M. Marty, Z. Clyde-Watson, L. J. Twyman, M. Nakash, J. K. Sanders, *Chem. Commun*., 1998, 2265.

7. C. J. Hastings, D. Fiedler, R. G. Bergman, K. N. Raymond, *J. Am. Chem. Soc.*, 2008, **130**, 10977.

8. M. Yoshizawa, M. Tamura, M. Fujita, *Science*, 2006, **312**, 251.

9. M. M. Boyle, R. A. Smaldone, A. C. Whalley, M. W. Ambrogio, Y. Y. Botros and J. F. Stoddart, *Chem. Sci*., 2011, **2**, 204.

10. C. G. Oliveri, P. A. Ulmann, M. J. Wiester and C. A. Mirkin, *Acc. Chem. Res.*, 2008, **41**, 1618.

11. B. Kilbas, S. Mirtschin, R. Scopellitia and K. Severin, *Chem. Sci*., 2012, **3**, 701.

12. K. Suzuki, M. Kawano and M. Fujita, *Angew. Chem. Int. Ed.*, 2007, **46**, 2819.

13. S. P. Argent, H. Adams, L. P. Harding, and M. D. Ward, *Dalton Trans*., 2006, 542.

14. S. P. Argent, H. Adams, T. Riis-Johannessen, J. C. Jeffery, L. P. Harding, and M. D. Ward, *J. Am. Chem. Soc*., 2006, **128**, 72.

15. C. J. Kuehl, Y. K. Kryschenko, U. Radhakrishnan, S. R. Seidel, S. D.Huang, P. J. Stang, *Proc. Natl. Acad. Sci.,* 2002, **99**, 4932.

16. C. J. Kuehl, T. Yamamoto, S. R. Seidel, P. J. Stang, *Org. Lett.,* 2002, **4**, 913.

17. Y.-R. Zheng, H.-B. Yang, K. Ghosh, L. Zhao, P. J. Stang, *Chem. Eur. J.*, 2009, **15**, 7203.

18. C.-Y. Su, Y.-P. Cai, C.- L. Chen, F. Lissner, B. S. Kang, W. Kaim, *Angew. Chem. Int. Ed.*, 2002, **41**, 3371.

19. C.-Y. Su, Y.-P. Cai, C.- L. Chen, M. D. Smith, W. Kaim, H.-C. zur Loye, *J. Am. Chem. Soc.*, 2003, **125**, 8595.

20. S. Ghosh, P. S. Mukherjee, *Organometallics*, 2008, **27**, 316.

21. S. M. Contakes, T. B. Rauchfuss, *Angew. Chem. Int. Ed.*, 2000, **39**, 1984.

22. I. S. Tidmarsh, T. B. Faust, H. Adams, L. P. Harding, L. Russo, W. Clegg, M. D. Ward, *J. Am. Chem. Soc.*, 2008, **130**, 15167.

23. B. R. Hall, H. Adams, M. D. Ward, *Supramolecular Chemistry*, 2012, **7**, 499.

24. A. M. Najar, I. S. Tidmarsh, H. Adams, M. D. Ward, *Inorg. Chem.*, 2009, **48**, 11871.

25. S. P. Argent, H. Adams, T. Riis-Johannessen, J. C. Jeffery, L. P. Harding, O. Mamula, M. D. Ward, *Inorg. Chem.*, 2006, **45**, 3905.

26. N. K. Al-Rasbi, I. S. Tidmarsh, S. P. Argent, H. Adams, L. P. Harding, M. D. Ward, *J. Am. Chem. Soc.*, 2008, **130**, 11641.

27. G. M. Sheldrick, *SADABS*: *A program for absorption correction with the Siemens SMART system*, University of Gottingen, Germany, 1996.

28. G. M. Sheldrick, *Acta Crystallogr. Sect. A*, 2008, **64**, 112.

29. A. L. Spek, *J. Appl. Cryst.*, 2003, **36**, 7.

3. Hierarchical self-assembly of luminescent coordination cages and a 'cuneane' with the ligand L^{14naph}

3.1 Introduction

The ligand L^{14naph} (figure 3.1.1) has been synthesised and its coordination chemistry investigated. The ligand has many similarities to L^{pp},[1] with the additional benefit of the naphthyl unit being luminescent. This means that a series of luminescent groups, with high-energy excited states, can surround the central cavity of a cage. This in turn could allow the use of a coordination cage to act as an antenna group to trigger photochemically induced reactions in an encapsulated guest.[2,3]

The cages formed with this ligand are expected to be similar to the structures with L^{pp} as the geometric arrangement of the two bis-bidentate pyrazolyl-pyridine units is identical. The naphthyl unit should provide more efficient π-stacking compared to the phenyl analogue and the naphthyl unit is obviously larger although it is unlikely that it is large enough to make a difference to the cage formed.

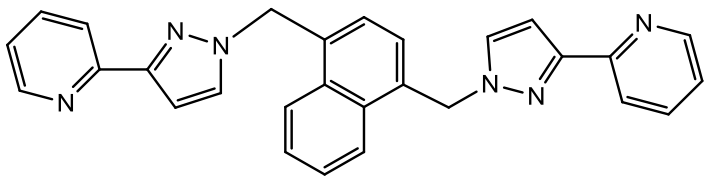

Figure 3.2.1.1 The ligand L^{14naph}.

The 1,4-naphthalene core unit has been used extensively in coordination chemistry before. It has previously been used with imidazole units,[4] triazole units[5] and pyrazole units[6] to form bis-monodentate ligands. The 1,4-naphthalenedicarboxylate building block has also found many applications including in MOFs,[7] polymeric structures linked via hydrogen bonds,[8] and complexes containing lanthanides.[9]

Hierarchical self-assembly uses small pre-assembled building blocks to create larger self-assembled architectures and has the potential to be a powerful tool in supramolecular chemistry. It is often difficult to achieve because the building block must not only be self-assembled itself but must have the capacity for further self-

assembly either through metal-ligand coordination bonds or favourable intermolecular interactions such as hydrogen bonding or metallophilic interactions. The hierarchical self-assembly of coordination cages could be achieved by forming a complex such as a metallacycle that will act as a building block for the coordination cage. The metallacycle needs to have vacant coordination sites in the metal ions which will initially be filled by solvent molecules but can then be easily displaced by a second ligand. This would result in a mixed ligand coordination cage, self-assembled in a stepwise manner via the metallacycle building block.

Meehan and co-workers have shown an example of hierarchical self-assembly based on $[M_3L_3]$ triangles which can then be reacted on further to give a metal-organic framework (MOF).[10] The $[M_3L_3]$ triangle (M = Cu or Co) based on bis-bidentate diketonate ligands with a biphenyl spacer has six pyridine solvent molecules filling the coordination sites in the crystal structure. These solvent molecules could then be displaced by hexamethylenetetramine (hmt), a tris-bidentate ligand, which connected three of these triangles together to form the MOF (figure 3.1.2). The assembly is a nice example of how a 2D metallacycle can be assembled into a 3D structure via hierarchical self-assembly. The MOF is porous and gas sorption measurements have shown it can adsorb different gases.

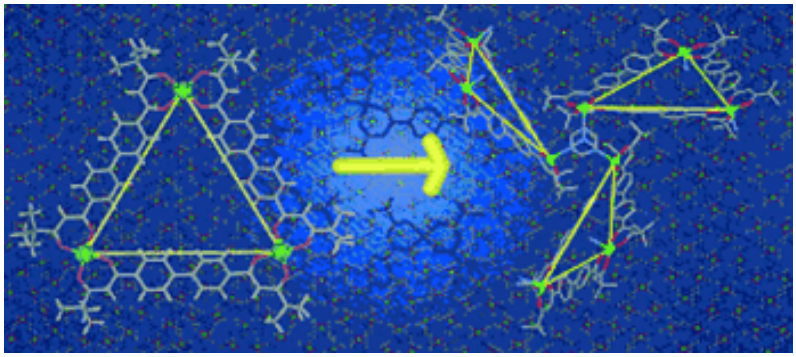

Figure 3.1.2 The $[M_3L_3(py)_6]$ triangle and corresponding MOF. Reproduced from reference 10.

Hong and co-workers have shown an example of a one-pot synthesis of a truncated octahedral coordination cage (figure 3.1.3).[11] The cage is composed of six tetranuclear shuttlecock-shaped units which are formed first in situ and form the vertices of the octahedron. These are then connected by twelve linear BDC^{2-} ligands through a [6 + 12]

condensation reaction. The cage is porous and has been shown to adsorb H_2, N_2 and CO_2. This cage requires hierarchical self-assembly similar to the previous example, however in this case everything happens in a one pot synthesis.

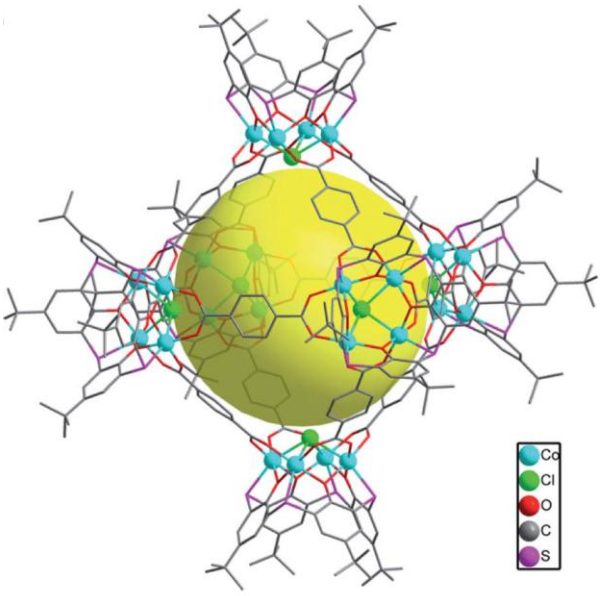

Figure 3.1.3 The anionic $[Co_{24}(BTC4A)_6(\mu_4\text{-}Cl)_6(BDC)_{12}]^{6-}$ coordination cage. Reproduced from reference 11.

3.2 Results and Discussion

3.2.1 Synthesis of L^{14naph}

The ligand was prepared by the usual method of brominating the dimethyl precursor and then reacting 3(2-pyridyl)pyrazole with 1,4-bis(bromomethyl)naphthalene under basic conditions. Further details are given in the experimental section.

This is a newly synthesised ligand and the crystal structure has also been determined (figure 3.2.1.1). The structure is fairly standard for ligands of this type with the pyrazolyl-pyridine units having a transoid arrangement to avoid the two N lone pairs being directed towards each other. The ligand packs in the crystal to maximise favourable aromatic stacking.

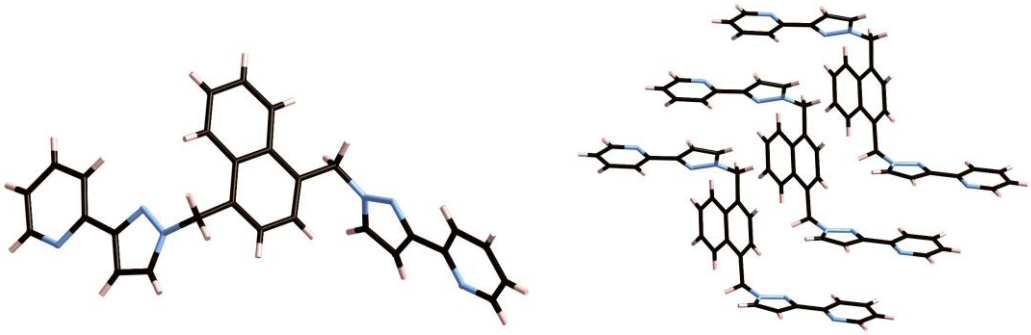

Figure 3.2.1.1 Crystal structure of the ligand L^{14naph}.

3.2.2 A luminescent coordination cage: $[Cd_{16}(L^{14naph})_{24}](BF_4)_{32}$

$Cd(BF_4)_2$ and L^{14naph} were mixed in a 2:3 ratio, stirred at room temperature and the resultant white powder recrystallised using MeCN and isopropyl ether. This gave colourless block crystals, which proved by Xray-crystallography to be $[Cd_{16}(L^{14naph})_{24}](BF_4)_{32}$. The crystal structure is shown in figure 3.2.2.1, and is essentially isostructural to the $[Cd_{16}(L^{pp})_{24}](BF_4)_{32}$ complex described earlier however with naphthalene groups in place of the phenylene groups. The complex has 12 *meridional* tris-chelate Cd(II) centres and four *facial* tris-chelate metal centres. The twelve *meridional* centres form four $[Cd_3(L^{14naph})_3]^{6+}$ trinuclear cyclic helical units and these are connected by the four capping *facial* Cd(II) ions. As with the previous $[Cd_{16}(L^{pp})_{24}](BF_4)_{32}$ complex this leads to two ligand environments, with twelve ligands in each.

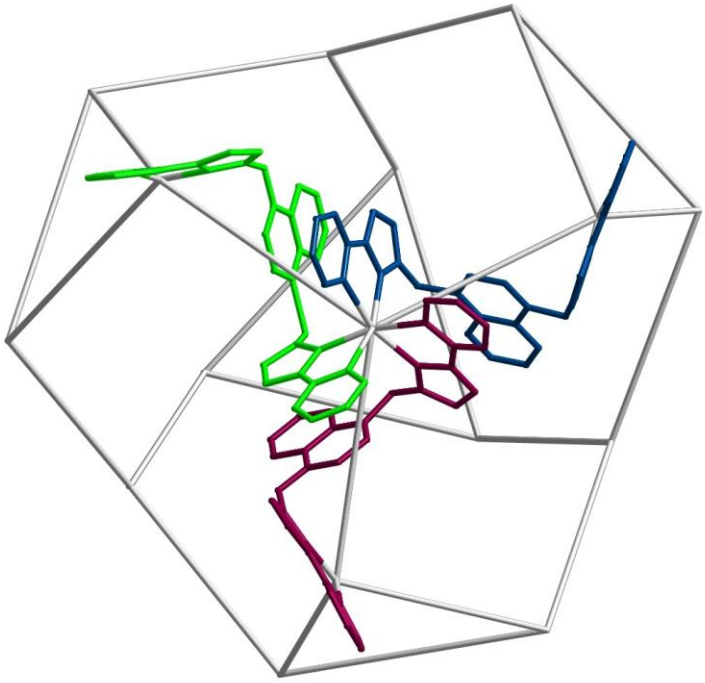

Figure 3.2.2.1 The core structure of the complex cation of $[Cd_{16}(L^{14naph})_{24}](BF_4)_{32}$ with only the ligand of one *fac*-$Cd(L^{14naph})_3$ centre shown.

The complex crystallised in the space group *P-1*, with the whole molecule being crystallographically unique. The cage has non-crystallographic *T*-symmetry with four C_3 axes as the only symmetry elements. The cage has a central cavity of similar size to the analogous $[Cd_{16}(L^{pp})_{24}](BF_4)_{32}$ complex which, based on the H•••H contacts across the middle of the cavity, is approximately 1300 $Å^3$. The cavity contains at least nine tetrafluoroborate anions and some anions and acetonitrile solvent molecules are located in the cage windows. The anions in the central cavity are shown in spacefilling view in figure 3.2.2.2 to emphasise the volume of the cavity that they occupy. Two of the anions are located near to the *facial* tris-chelate Cd(II) ions, as can be seen in figure 3.2.2.2. These sites have been shown to be capable of more favourable interactions than the *meridional* metal sites due to the presence of the three methylene groups being favourably oriented for hydrogen bonds to the fluorine atoms of the tetrafluoroborate anion.[12]

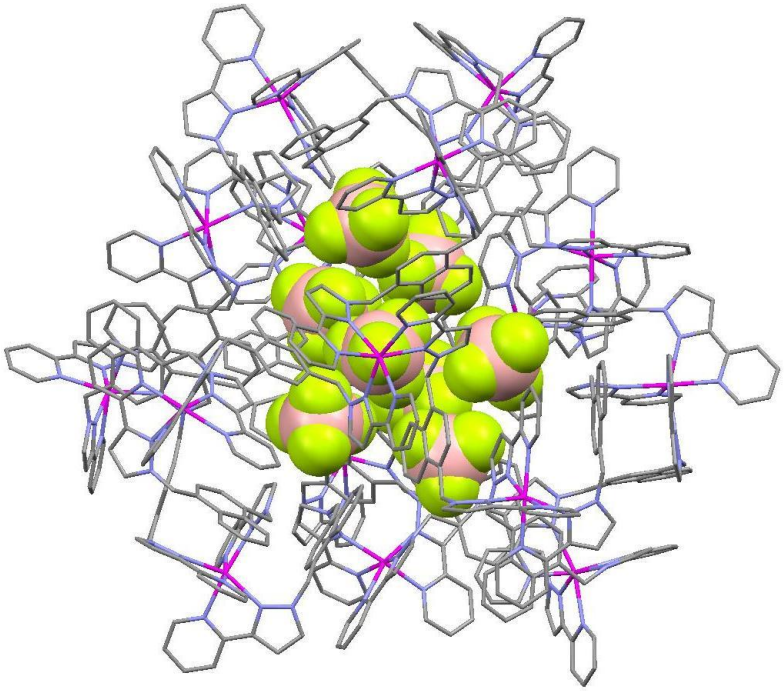

Figure 3.2.2.2 The full $[Cd_{16}(L^{14naph})_{24}](BF_4)_{32}$ cage with the anions in space-filling view.

The Cd – Cd separations are consistently longer between the *mer* – *mer* metal centres – around the edges of the $[Cd_3(L^{14naph})_3]^{6+}$ triangular units – where they are in the range 10.007 – 10.463 Å. From the *mer* – *fac* metal centres the Cd – Cd distances lie in the range 9.172 – 9.568 Å. The 96 Cd – N bond distances are all fairly regular and lie in the range 2.247 – 2.404 Å. The Cd(II) ions have fairly standard octahedral geometry and all sixteen tris-chelate metal centres have the same optical configuration, however the complex as a whole is racemic.

The complex is stabilised by π-stacking which is prevalent throughout the crystal structure. The structure contains twelve stacks of five units, each containing three pyrazolyl-pyridine groups and two naphthalene groups (figure 3.2.2.3). These are stacked so that relatively electron rich (naphthalene) and relatively electron poor (pyrazolyl-pyridine) groups alternate. The result is that all twenty four naphthalene units contribute to a stack and thirty six of the forty eight pyrazolyl-pyridine groups do. One pyrazolyl-pyridine group on each meridional Cd(II) ion is not involved in the π-stacking. The result is 48 favourable π-stacking interactions which presumably assist formation of the large complex which is unfavoured in terms of entropy compared to a

larger number of small complexes. The ΔH contribution from the stacking must help to compensate for the unfavourable ΔS term.

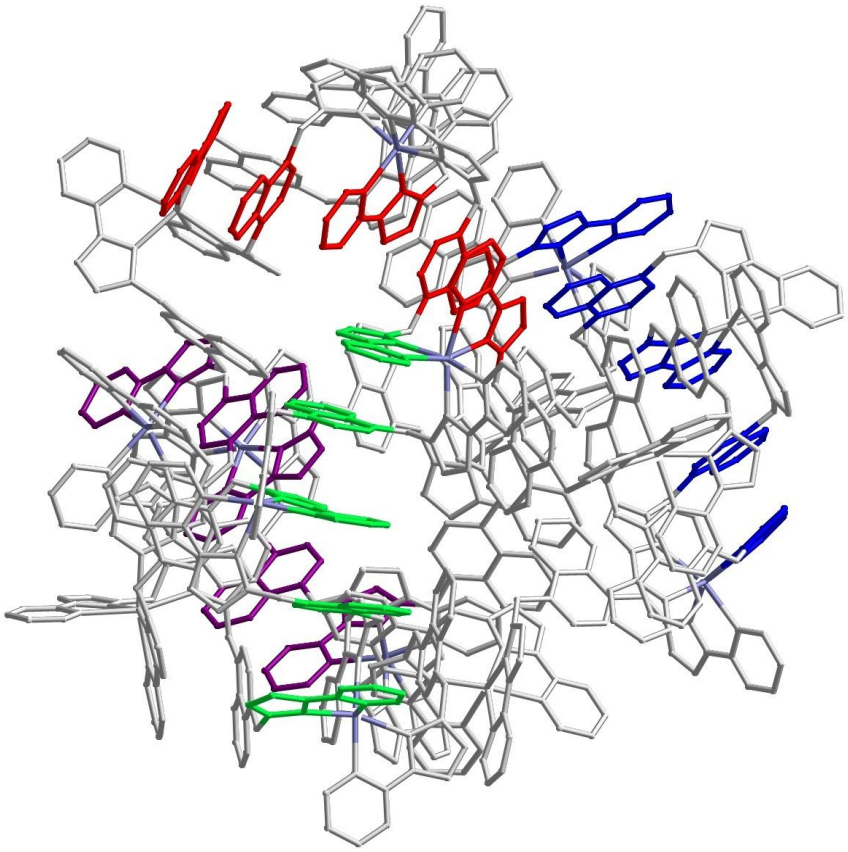

Figure 3.2.2.3 Four rows of π-stacking present in the $[Cd_{16}(L^{14naph})_{24}](BF_4)_{32}$ cage.

The behaviour of $[Cd_{16}(L^{14naph})_{24}](BF_4)_{32}$ in solution was studied by ^{1}H NMR spectroscopy and ESMS. Unlike the $[Cd_{16}(L^{pp})_{24}](BF_4)_{32}$ structure described in chapter 2, the complex with L^{14naph} is stable in solution by both methods of characterisation. The ^{1}H NMR spectrum shows 44 signals, corresponding to 22 protons from each of the two ligand environments. As with $[Cd_{16}(L^{pp})_{24}](BF_4)_{32}$, there are two ligand environments arising due to the presence of *fac* and *mer* metal centres. A COSY spectrum has allowed easy identification of the pairs of methylene and pyrazolyl protons. There are four pairs of diastereotopic methylene protons (labelled m1 – m4 in figure 3.2.2.4) and four pairs of pyrazolyl protons (labelled pz1 – pz4), which confirms the presence of two different, chiral, ligand environments as required.

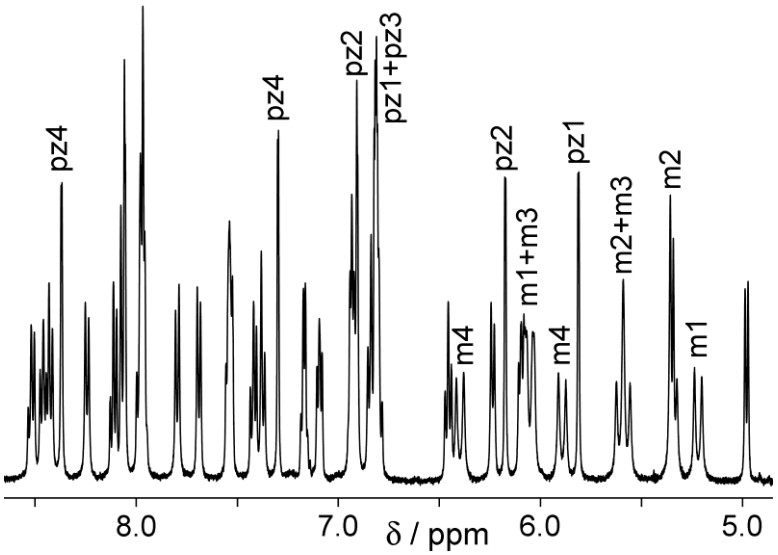

Figure 3.2.2.4 The 500 MHz ^{1}H NMR spectrum of $[Cd_{16}(L^{14naph})_{24}](BF_4)_{32}$ in CD_3CN with the pyrazolyl and methylene pairs labelled. Only 42 of the 44 peaks are shown with two additional doublets due to naphthalene protons at 4.1 and 3.6 ppm which have been assigned from the COSY spectrum.

There is further confirmation that the structure is retained in solution because the ^{113}Cd NMR spectrum (figure 3.2.2.5) shows two environments in an approximate 1:3 ratio. This is as expected due to there being twelve Cd(II) ions with *mer* tris-chelate geometry and four Cd(II) ions with *fac* tris-chelate geometry.

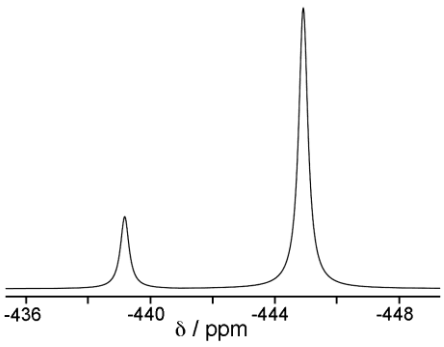

Figure 3.2.2.5 The ^{113}Cd NMR spectrum of $[Cd_{16}(L^{14naph})_{24}](BF_4)_{32}$ with the expected 1:3 ratio of signals.

The complex structure has also been confirmed by ESMS with a clear sequence of peaks corresponding to $\{[Cd_{16}(L^{14naph})_{24}](BF_4)_{32-x}\}^{x+}$ (x = 4-8). In each case the isotope spacings of the peaks were as expected and confirmed the presence of the intact

complex, and not a smaller cage or fragment whose value could appear at the same *m/z* value.

The large difference between $[Cd_{16}(L^{14naph})_{24}](BF_4)_{32}$ and $[Cd_{16}(L^{pp})_{24}](BF_4)_{32}$ is the stability that the cage has in solution. Whereas $[Cd_{16}(L^{pp})_{24}](BF_4)_{32}$ is not stable in solution and undergoes a cage-to-cage interconversion over a period of days at room temperature, $[Cd_{16}(L^{14naph})_{24}](BF_4)_{32}$ is stable for a period of at least several weeks at room temperature. The same ^{1}H NMR sample was measured for seven weeks with no noticeable change to the spectrum. The ESMS of the same sample was also measured over the same time period and again no change was seen. We ascribe this to greater π-stacking arising from replacement of the phenyl spacer by the naphthyl spacer in the ligand framework.

Interestingly the $[Cd_{16}(L^{14naph})_{24}](BF_4)_{32}$ complex also assembles by itself in solution without the need for crystallisation. The complex $[Cd_{16}(L^{pp})_{24}](BF_4)_{32}$ described in chapter 2 only ever formed in solution by dissolution of crystals and slowly rearranged. It was never seen in assembly experiments where the metal salt and ligand were mixed together in the solvent. In contrast when L^{14naph} and $Cd(BF_4)_2$ were mixed together in a 3:2 ratio in DCM and MeOH, the sequence of peaks in the ES mass spectrum was unequivocally assigned to the $[Cd_{16}(L^{14naph})_{24}](BF_4)_{32}$ complex, meaning that this is the thermodynamically favoured product due to the extra ΔH from π-stacking.

The stability of the complex in solution makes it an excellent potential candidate for host-guest chemistry. The cage structure has a large central cavity with large rectangular 'windows', approximately 3 x 10 Å in diameter. The crystal structure (figure 3.2.2.2) shows that anions and solvent molecules lie in the central cavity of the cage. The problem for performing host-guest chemistry with this complex may be that the windows are too large and it is simply too easy for any guest to leave the cage. Initial screening of potential guests by ^{1}H NMR spectroscopy has so far proved unsuccessful although further attempts are going to be made.

3.2.3 The trinuclear complex $[Cd_3(L^{14naph})_3(BF_4)_4(EtOAc)_2](BF_4)_2$

With the M_3L_3 cyclic helicate unit appearing so important in the formation of many of the coordination cages in the Ward group, it was decided to see if this structure could be formed and isolated if a metal-to-ligand ratio of 1:1 was used. This complex would have

vacant coordination sites which would presumably be filled by coordinating anions or solvent molecules, but then these theoretically could easily be replaced by ligands in the future. In this sense if the M_3L_3 unit can be isolated then it could be a good candidate for hierarchical self-assembly, similar to the Meehan example described earlier.[10]

When $Cd(BF_4)_2$ and L^{14naph} were combined in a 1:1 ratio, $[Cd_3(L^{14naph})_3(BF_4)_4(EtOAc)_2](BF_4)_2$ was isolated. The complex has a $\{Cd_3(L^{14naph})_3\}^{6+}$ trinuclear cyclic helicate structure as expected, with four tetrafluoroborate anions and two ethyl acetate solvent molecules filling the coordination sites on the Cd(II) ions, shown in figure 3.2.3.1. The structure was solved in the monoclinic space group *C2/c*, with only half of the complex in the asymmetric unit. The Cd – Cd distances are 10.167 (twice) and 10.131 Å with the Cd – Cd – Cd angles 60.11 (twice) and 59.77 ° making it an almost perfect equilateral triangle. The Cd – N bond distances range between 2.257 and 2.308 Å, the Cd – F distances are between 2.203 and 2.372 Å and the Cd – O bond distance is 2.423 Å for both crystallographically equivalent ethyl acetate molecules.

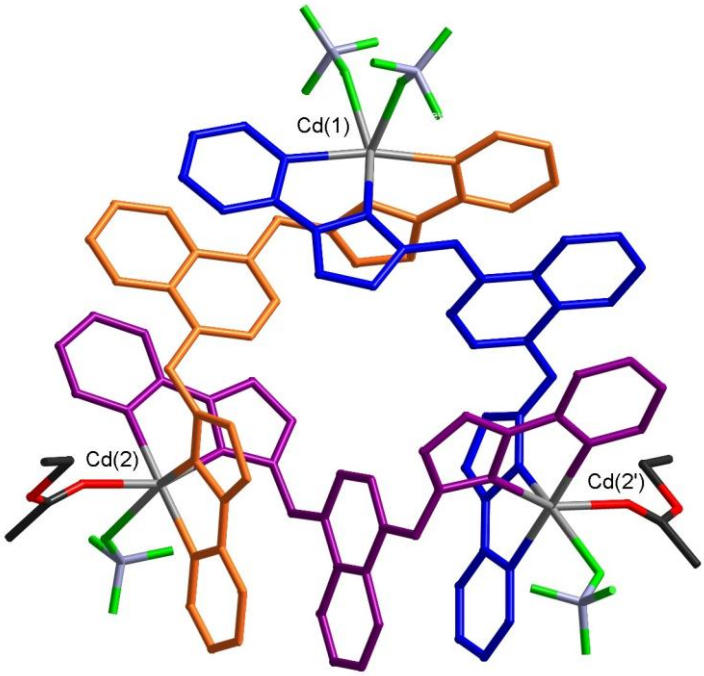

Figure 3.2.3.1 The complex cation of $[Cd_3(L^{14naph})_3(BF_4)_4(EtOAc)_2]$. The disorder of the tetrafluoroborate anions is not shown.

The octahedral coordination geometry around the Cd(II) ions is non-ideal, largely due to the tetrafluoroborate anions being slightly angled away from the pyrazolyl-pyridine

groups, probably to maximise the favourable F•••H interactions with neighbouring complexes. This will be examined in more detail later.

There is aromatic π-stacking within the $\{Cd_3(L^{14naph})_3\}^{6+}$ unit which is essentially the same as when this unit is present within the larger Cd_{16} cage superstructure. The ligands are oriented so that the naphthyl group is stacked between the pyrazolyl-pyridine groups from the two adjacent ligands. This occurs three times, around each edge of the triangle, so that every aromatic unit is involved in the stacking. This interaction must be largely responsible for the complex forming, rather than a complex with the usual 2:3 metal-to-ligand ratio. There is also intermolecular π-stacking between triangular complexes. The triangles stack with each other into infinite lines, with two of the three stacks from each triangular complex involved. The intermolecular π-stacking is shorter between complexes than within complexes, the smallest distance being 3.336 Å compared to 3.479 Å. One example of such stacking is shown in figure 3.2.3.2, where the two complexes are stacking together as highlighted by the stacked groups being shown in blue. Another favourable interaction from the two complexes getting into such close proximity is that CH•••F interactions are present, shown by the dashed lines in figure 3.2.3.2. Although the anions in this interaction are disordered the CH•••F interactions are as short as 2.273 Å.

The third stack within the triangular complex - between Cd(2) and Cd(2') - that is not involved in the intermolecular π-stacking is prevented from doing so by the ethyl acetate molecules which are both orientated in that direction and block any possible stacking.

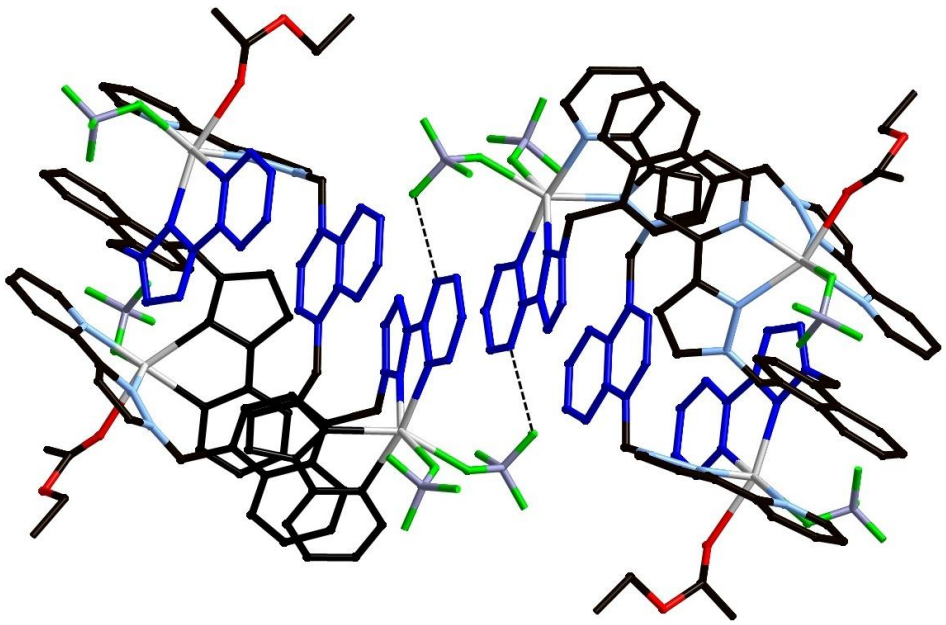

Figure 3.2.3.2 The aromatic stacking and hydrogen bonding interactions between $[Cd_3(L^{14naph})_3(BF_4)_4(EtOAc)_2]^{2+}$ complexes.

The behaviour of the complex in solution was far more complicated than for $[Cd_{16}(L^{14naph})_{24}](BF_4)_{32}$. The complex was characterised by ^1H NMR spectroscopy and ESMS, and both showed that a mixture of two products was present in solution.

A ^1H NMR spectrum of redissolved crystals of $[Cd_3(L^{14naph})_3(BF_4)_4(EtOAc)_2]^{2+}$ in CD_3NO_2 solution clearly shows two sets of signals of different intensity (in about a 2:1 ratio), each set consisting of 11 signals with the methylene protons inequivalent and coupled to one another. This is what would be expected for a mixture of two complexes, each of which contains ligands in a twofold symmetric environment such that the two halves of each ligand are equivalent, and which are chiral such that the CH_2 protons are diastereotopic. A COSY spectrum allows each set of signals to be fully assigned (figure 3.2.3.3), even overlapping components.

The major component protons are labelled A and the minor component B. The pyrazolyl protons are labelled pz, the pyridyl protons py3 – py6, the methylene protons m and the naphthyl protons nap. From the integrals it is clear that the major component is present in double the quantity of the minor component.

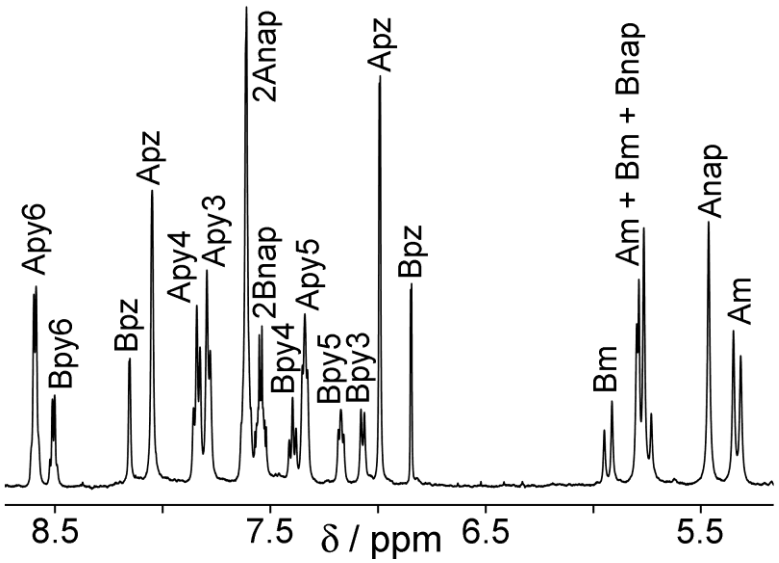

Figure 3.2.3.3 The ^{1}H NMR spectrum of redissolved crystals of $[Cd_3(L^{14naph})_3(BF_4)_4(EtOAc)_2]^{2+}$ with all protons labelled and distinguished into the major and minor components.

The ES mass spectrum of the complex shows a mixture of products. There are peaks that can be assigned to the intact $[Cd_3(L^{14naph})_3]$ complex, $[Cd_2(L^{14naph})_2]$ complex and also mononuclear $[Cd_1(L^{14naph})_1]$ complex. There are a series of peaks at each charge for the $[Cd_3(L^{14naph})_3]$ and $[Cd_2(L^{14naph})_2]$ complexes due to dissociation of varying numbers of anions; the tetrafluoroborate anions are replaced by fluoride anions in varying amounts for example *m/z*; 2098.8, $\{[Cd_3(L^{14naph})_3](BF_4)_5\}^{1+}$; 2031.5, $\{[Cd_3(L^{14naph})_3](BF_4)_4(F)\}^{+}$; 1956.2, $\{[Cd_3(L^{14naph})_3](BF_4)_3(F)_2\}^{+}$.

The ^{1}H NMR spectrum is in agreement with the ES mass spectrum that the two products in solution are the $\{Cd_3(L^{14naph})_3\}^{6+}$ trinuclear cyclic helicate and a $\{Cd_2(L^{14naph})_2\}^{4+}$ complex, presumably a double helix. It is unlikely that a $\{Cd_1(L^{14naph})_1\}^{2+}$ complex would be stable in solution because with the pyrazolyl-pyridine groups being in the 1 and 4 positions of the naphthyl spacer it is very difficult for them to both coordinate to the same metal ion. It is also not possible that there is a $\{Cd_1(L^{14naph})_1\}^{2+}$ complex with only one pyrazolyl-pyridine group coordinated to the Cd(II) ion as this would render both ends of the ligand inequivalent. The $\{Cd_3(L^{14naph})_3\}^{6+}$ cyclic helical cation could be one of the species: relaxed in solution (free of any crystallographically-imposed reductions in symmetry associated with packing) it will have D_3 symmetry, with a twofold rotation axis through each of the ligands in the triangular plane perpendicular to

the C_3 axis. Any other cyclic helicate of D_n symmetry would likewise be consistent with the observed ^{1}H NMR spectrum An example of a M_3L_3 crystal structure and a mixture of M_3L_3 and M_2L_2 structures in solution has been seen before by Hannon although using Cu(I) and bidentate ligands therefore there were no vacant coordination sites.[13]

3.2.4 Tri-nuclear cyclic helicate: $[Cu_3(L^{14naph})_3(BF_4)(MeCN)_2](BF_4)_5$

When $Cu(BF_4)_2$ and L^{14naph} were combined in a 1:1 ratio, the product afforded was again a trinuclear cyclic helicate with the core structure $\{Cu_3(L^{14naph})_3\}^{6+}$. In this crystal structure the Cu(II) ions are all five-coordinate, therefore having only one vacant coordination site at each Cu(II) ion which is filled by one tetrafluoroborate anion and two MeCN solvent molecules. The ligands adopt the same structure as in the $\{Cd_3(L^{14naph})_3\}^{6+}$ complex, with each ligand going 'over and under' an adjacent pair of metal ions.

The complex crystallised in the monoclinic space group *Cc*, with two complete $[Cu_3(L^{14naph})_3(BF_4)(MeCN)_2]^{5+}$ complexes in the asymmetric unit. Both complex units are very similar with two MeCN solvent molecules and one tetrafluoroborate anion coordinated to the Cu(II) ions of each complex. The Cu – Cu distances are 9.550, 9.670 and 9.674 Å for one complex and 9.541, 9.585 and 9.914 Å for the other complex. The Cu – Cu – Cu angles are 59.17, 60.40 and 60.43 ° for the first complex and 58.56, 59.00 and 62.44 ° for the second complex. The complexes are still very close to having an equilateral triangular structure although they are more distorted than in the $\{Cd_3(L^{14naph})_3\}^{6+}$ complex. One of the complex cations is shown in figure 3.2.4.1.

The Cu – N distances for the pyrazolyl-pyridine ligands are in the range 1.948 – 2.228 Å. The Cu(II) ions have a slightly distorted trigonal bipyramidal coordination geometry, with the two pyridine rings in the axial position in each case. There is no Jahn-Teller distortion which usually occurs in these complexes when the Cu(II) ions are six coordinate. The Cu – F bond lengths in the two complexes are 1.999 and 2.011 Å and the Cu – N bond lengths for the MeCN molecules are in the range 1.968 – 2.014 Å.

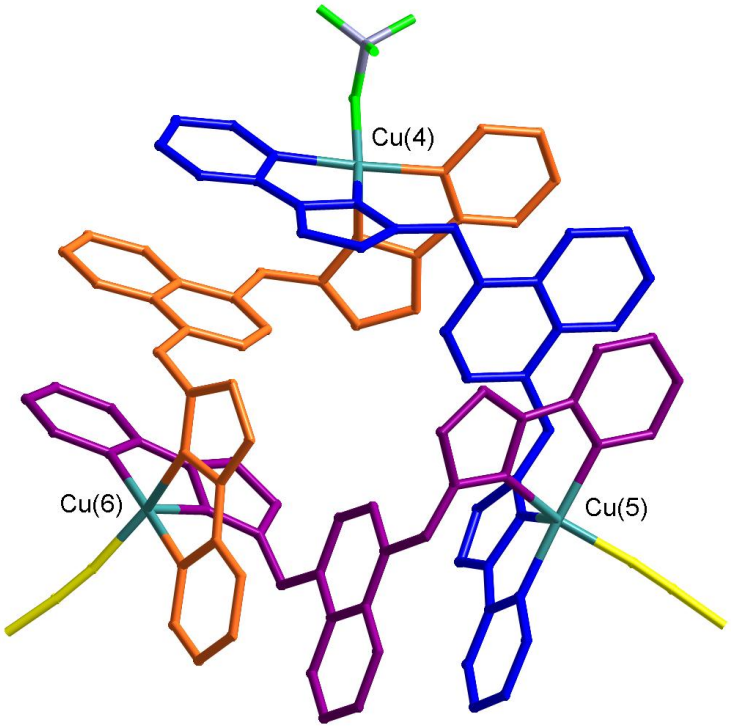

Figure 3.2.4.1 One of the complex cations of $[Cu_3(L^{14naph})_3(BF_4)(MeCN)_2]$.

As with the $\{Cd_3(L^{14naph})_3\}^{6+}$ complex earlier, there is aromatic π-stacking present in the structure with each naphthyl group sandwiched between two pyrazolyl-pyridine groups, one from each neighbouring ligand. There are also intermolecular aromatic π-stacking interactions between complexes, as with the $\{Cd_3(L^{14naph})_3\}^{6+}$ complex. In this case all three stacks within a complex are further stacked with other complexes. This is because the Cu(II) ions are only five coordinate and the MeCN molecules are relatively small so that intermolecular contacts are not blocked in any direction unlike in $\{Cd_3(L^{14naph})_3\}^{6+}$. The distance between the aromatic stacking units within a complex is 3.212 Å and the distance of the stacking between complexes is 3.274 Å. An example of two series of stacks is shown in figure 3.2.4.2, the third stack is in the direction into the page and is not shown.

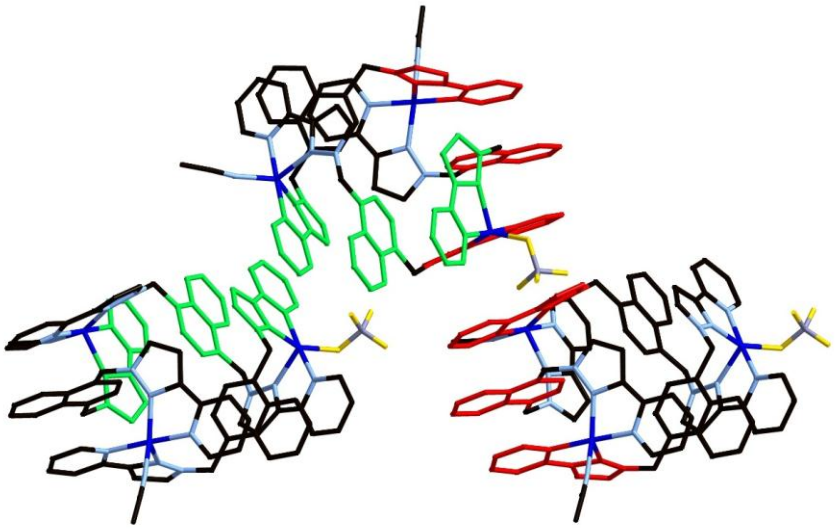

Figure 3.2.4.2 Three of the $[Cu_3(L^{14naph})_3(BF_4)(MeCN)_2]$ complexes involved in two series of aromatic stacking.

The complex again has CH•••F interactions from the coordinated tetrafluoroborate anions that stabilise the close proximity complexes. In this complex there is only one coordinated tetrafluoroborate anion per complex, compared to four per $[Cd_3(L^{14naph})_3]^{6+}$ complex, so there are also CH•••F interactions from uncoordinated tetrafluoroborate anions. An example of this is shown in figure 3.2.4.3 where a tetrafluoroborate anion is anchored in place by numerous CH•••F interactions to methylene protons, pyrazolyl-pyridine protons and naphthyl protons. The shortest CH•••F distance is 2.362 Å.

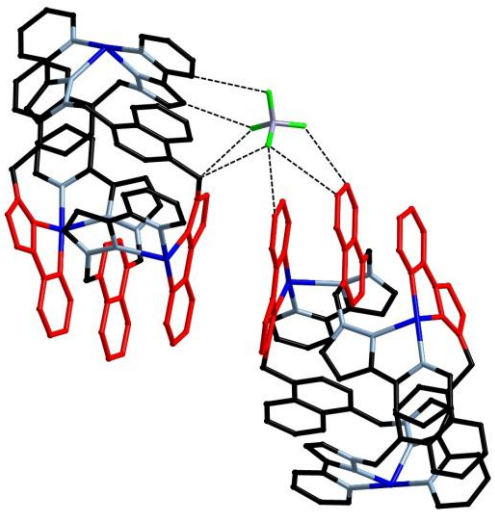

Figure 3.2.4.3 Two $[Cu_3(L^{14naph})_3(BF_4)(MeCN)_2]^{2+}$ complexes stacked together with a tetrafluoroborate anion involved in CH•••F interactions with each complex.

The complex behaves in solution quite differently from $\{Cd_3(L^{14naph})_3\}^{6+}$. Although ^1H NMR spectroscopy is not possible with Cu(II) complexes due to the paramagnetic nature of the metal ion, the ES mass spectrum was quite informative. There is a sequence of peaks that can be unequivocally assigned to $\{[Cu_2(L^{14naph})_2](BF_4)_{4-x}\}^{x+}$ (x = 1 and 2). As with the Cd(II) analogue described previously, there is clearly fragmentation and in all cases there are peaks due to fluoride anions replacing tetrafluoroborate anions: for example the series $\{[Cu_2(L^{14naph})_2](BF_4)_{3-x}(F)_x\}^{+}$ (x = 1 - 5). One large difference between the ES mass spectra of the two complexes is that the Cu(II) complex does not show peaks that are unequivocally assignable to the $\{Cu_3(L^{14naph})_3\}^{6+}$ cation. There is however a sequence of peaks for $\{[Cu_6(L^{14naph})_6](BF_4)_{10-x}(F)_x\}^{2+}$ (x = 2 - 6). This is possibly an aggregate of two $\{Cu_3(L^{14naph})_3\}^{6+}$ complexes, possibly bridged by fluoride or tetrafluoroborate anions, rather than indicating a $\{Cu_6(L^{14naph})_6\}^{12+}$ complex is forming in solution. It is also possible that the $\{[Cu_3(L^{14naph})_3](BF_4)_{5-x}(F)_x\}^{+}$ peaks are hidden underneath the $\{[Cu_6(L^{14naph})_6](BF_4)_{10-x}(F)_x\}^{2+}$ peaks which would appear at the same *m/z* value. There is also a clear sequence of peaks due to $\{[Cu_4(L^{14naph})_4](BF_4)_{6-x}(F)_x\}^{2+}$ complexes. These could arise from the association of two $\{Cu_2(L^{14naph})_2\}^{4+}$ complexes or could be from a tetranuclear cyclic helicate. The tetranuclear cyclic helicate has been seen before as part of a cubic coordination cage,[2, 14] where two of these units are connected by four pillar ligands. It is possible that in the 1:1 metal-to-ligand ratio this complex is present to some degree in solution.

3.2.5 A mixed ligand cuboctahedral cage: $[Cu_{12}(L^{14naph})_{12}(L^{mes})_4](BF_4)_{24}$

The trinuclear cyclic helicate $\{Cu_3(L^{14naph})_3\}^{6+}$ has one vacant coordination site on each Cu(II) ion, although due to the ability of Cu(II) to be five or six coordinate, this could potentially be a bidentate coordination site. By using a bidentate ligand such as pyrazolyl-pyridine it is expected that the Cu(II) ions will change from being five coordinate to six coordinate. To test this theory and see if the $\{Cu_3(L^{14naph})_3\}^{6+}$ unit could be used as a building block of a larger cage, it was reacted with the tritopic ligand L^{mes}.

When $[Cu_3(L^{14naph})_3](BF_4)_6$ was combined with L^{mes} in a 1:1 ratio the product afforded is a cuboctahedral cage with the formula $[Cu_{12}(L^{14naph})_{12}(L^{mes})_4](BF_4)_{24}$. This cage includes four $[Cu_3(L^{14naph})_3]^{6+}$ units, three of which are connected by each L^{mes} ligand

which acts in a similar way to the *facial*-Cd(L^{14naph})$_3$ unit in the [Cd_{16}(L^{14naph})](BF_4)$_{32}$ cage. The cage is isostructural to one seen previously in the Ward group but with L^{pp} in place of L^{14naph}. This was made from a one-pot reaction in which Cu(BF_4)$_2$, L^{pp} and L^{mes} were all reacted together in the appropriate ratio.[15,16] The complex crystallised in the space group *C2/c*, with only half the molecule in the asymmetric unit. The full complex cation of the cage is shown in figure 3.2.5.1, with each {Cu_3(L^{14naph})$_3$}$^{6+}$ unit shown in a different colour and the L^{mes} ligands shown in red.

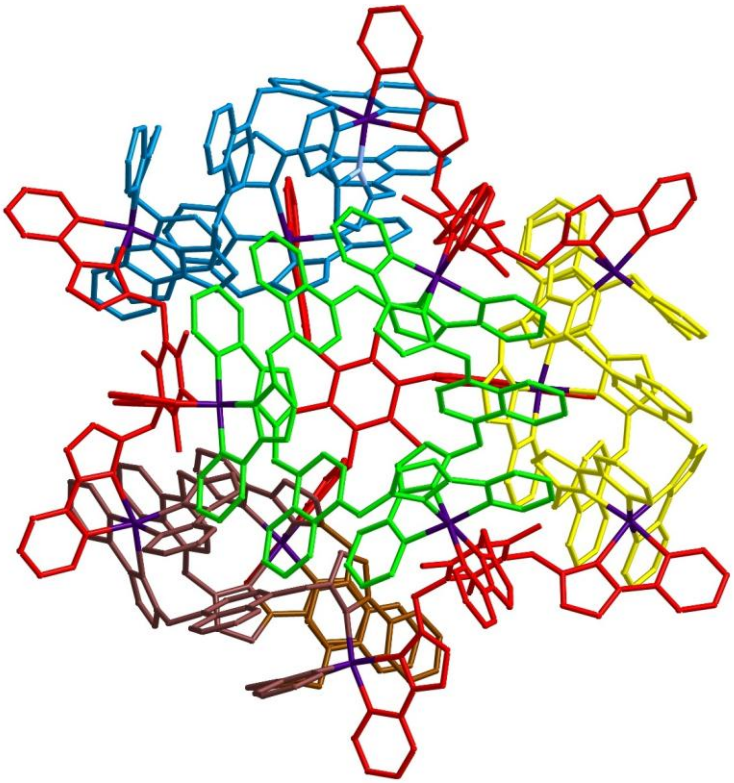

Figure 3.2.5.1 The full complex cation of [Cu_{12}(L^{14naph})$_{12}$(L^{mes})$_4$](BF_4)$_{24}$.

The cuboctahedral structure has eight triangular faces and four square faces. It is derived from slicing the eight corners from a cube and the triangular faces meeting in the centre of what used to be the centre of the edge. The eight triangular faces are made up from four [Cu_3(L^{14naph})$_3$]$^{6+}$ units and four Cu(L^{mes}) units, where L^{mes} acts as a face capping ligand rather than an edge bridging ligand. The Cu – Cu distances are 9.678, 9.854 and 10.060 for one [Cu_3(L^{14naph})$_3$]$^{6+}$ triangular unit and 9.773, 10.058 and 10.103 for the other in the asymmetric unit. The Cu – Cu distances are 11.287, 11.540 and 12.174 and 11.355, 11.695 and 11.829 for the triangular faces created by L^{mes}. Clearly the triangular faces made from the [Cu_3(L^{14naph})$_3$]$^{6+}$ units are smaller, however they are

slightly larger than in the complex $[Cu_3(L^{14naph})_3(BF_4)(MeCN)_2]^{5+}$ described earlier. Presumably the triangular unit has increased in size to allow for the extra pyrazolyl-pyridine group coordinated to each Cu(II) ion. The triangular faces can be seen in figure 3.2.5.2, with four shown in blue and the other four based on the L^{mes} face-capping ligand.

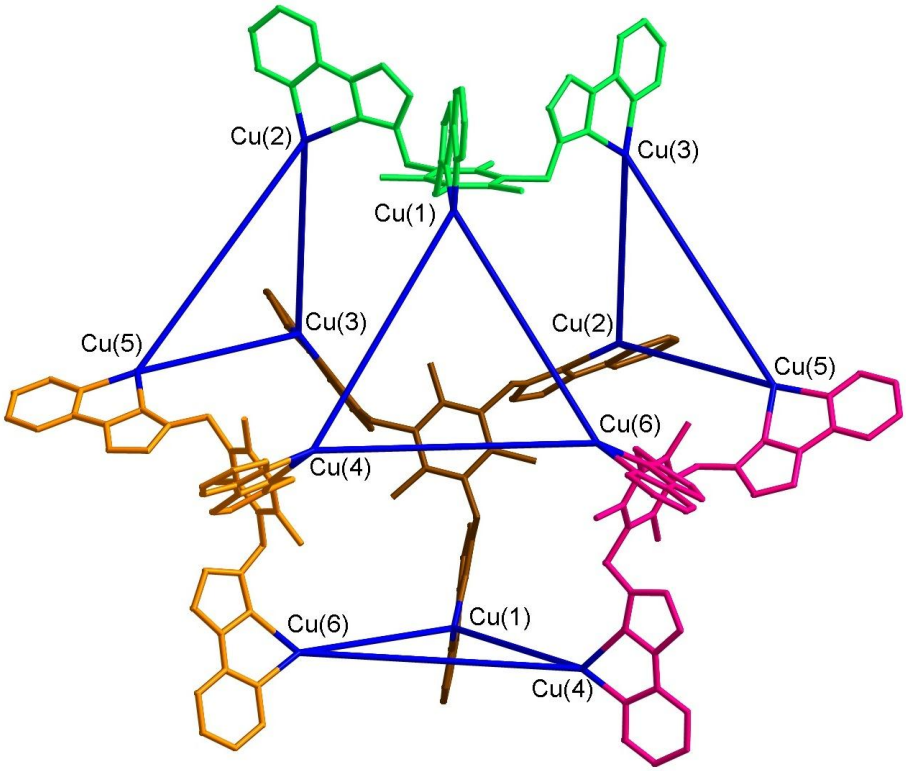

Figure 3.2.5.2 The cage structure with only L^{mes} ligands shown.

Each $[M_3(L^{14naph})_3]^{6+}$ unit in the cuboctahedron (figure 3.2.5.3) has essentially the identical structure to the $\{Cu_3(L^{14naph})_3\}^{6+}$ unit isolated separately, with the three ligands all going 'over and under' to form the cyclic helicate, and each naphthyl group being sandwiched in stacking interactions between two pyrazolyl-pyridine units.

The large difference between the triangular 'panel' on its own and the same fragment in the cuboctahedral complex is that the Cu(II) ions have gone from being five coordinate to six coordinate, with the loss of the solvent or anion and gain of an extra pyrazolyl-pyridine group. This has changed the geometry of the Cu(II) ions from distorted trigonal bipyramidal to an octahedral geometry and they now also show Jahn-Teller distortion. In each case the bond lengths along the pyrazole – pyrazole axis are elongated compared to the other four bonds. The Cu – N bond lengths for the elongated pyrazolyl

– pyrazolyl axis are in the range 2.260 – 2.460 Å, the shorter Cu – N bonds are in the range 1.971 – 2.120 Å.

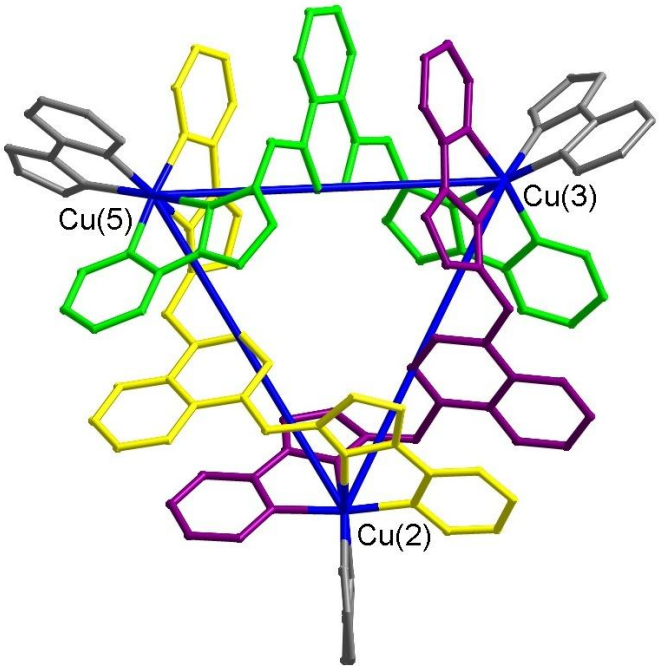

Figure 3.2.5.3 One of the four $Cu_3(L^{14naph})_3$ units.

The cage does not have any anions or solvent molecules that could be located in the central cavity in the crystal structure. There are anions and toluene solvent molecules in the windows around the periphery of the cage as can be seen in figure 3.2.5.4. The anions are all involved in a series of CH•••F hydrogen bonding interactions to pyrazolyl, pyridyl and methylene protons, the shortest of which are 2.46 Å. It is perhaps surprising that no anions could be located in the central cavity in the crystal structure given that the central cavity is estimated to have an approximate volume of 500 $Å^3$. This could however be due to severe disorder, with any electron density that could not be modelled being removed by the 'Squeeze' program in Platon.

There is no additional aromatic π-stacking in the structure, other than within the $[Cu_3(L^{14naph})_3]^{6+}$ units as described previously. There are however weak attractive CH – π interactions from the methyl groups on L^{mes}. The methyl group is oriented towards a pyridyl ring of a L^{14naph} ligand in each case, with the C – pyridyl mean plane distances in the range 3.284 – 3.859 Å.

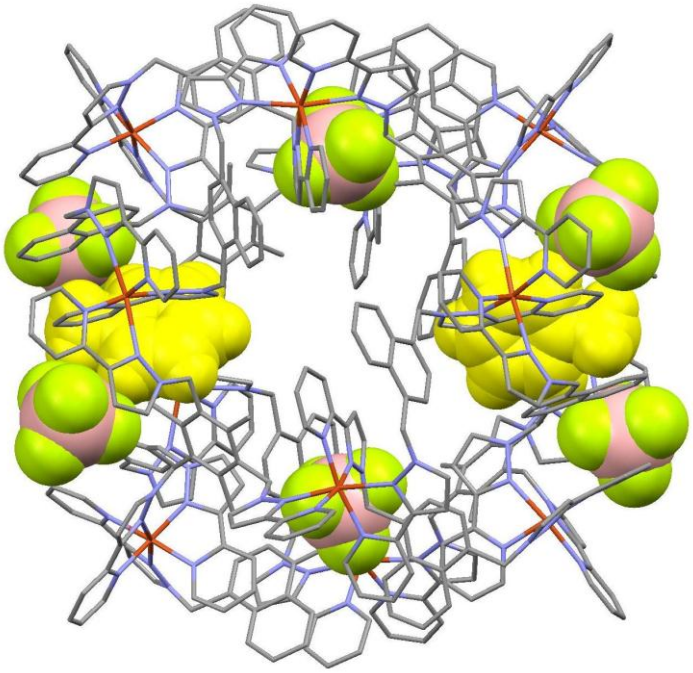

Figure 3.2.5.4 The full complex cation of $[Cu_{12}(L^{14naph})_{12}(L^{mes})_4](BF_4)_{24}$ with the anions and solvent molecules located in the windows shown in space-filling view.

The complex was studied by ESMS in solution and shows a very clear sequence of peaks corresponding to $\{[Cu_{12}(L^{14naph})_{12}(L^{mes})_4](BF_4)_{24-x}\}^{x+}$ (x = 4-10). The peaks dominate the spectrum, and there are no other assignable peaks – apart from free ligand – suggesting that the cage is stable in solution and is the single product formed in the reaction.

A similar reaction was tried by combining $[Cd_3(L^{14naph})_3(BF_4)_4(EtOAc)_2](BF_4)_2$ and L^{mes} in a 1:1 ratio. The expected product $[Cd_{12}(L^{14naph})_{12}(L^{mes})_4](BF_4)_{24}$ was seen by ESMS, although the peaks were of a low intensity and the spectrum was dominated by peaks at lower mass. These peaks could not be assigned apart from the peaks for free L^{14naph} and free L^{mes}. The fact that no other metal-ligand complexes were assignable and that free ligands dominated the ES mass spectrum suggest that a high degree of fragmentation has occurred. A crystal structure could not be obtained despite numerous attempts and the ^1H NMR spectrum of the crude sample was messy with more peaks than would be expected given the symmetry of the complex. It seems that whereas the $[Cu_{12}(L^{14naph})_{12}(L^{mes})_4](BF_4)_{24}$ cuboctahedral complex with L^{14naph} and L^{mes} is stable in solution, the $[Cd_{12}(L^{14naph})_{12}(L^{mes})_4](BF_4)_{24}$ analogue is not.

3.2.6 Luminescence studies on the complexes

As mentioned earlier the use of luminescent ligands such as L^{14naph} allows for the possibility that the coordination cage can act as an antenna group to trigger photochemically induced reactions in a guest in the central cavity. The host-guest chemistry can also be monitored, for example some guests may quench the emission from the cage when they are in the central cavity.

The absorption spectrum of L^{14naph} was measured and gave a broad band in the region 240 – 300 nm. The luminescence measurements were undertaken at 280 nm where the naphthyl chromophore strongly absorbs and dominates compared to the other chromophore, the pyrazolyl-pyridine group. The absorption spectra of $[Cd_{16}(L^{14naph})_{24}](BF_4)_{32}$ and $[Cd_3(L^{14naph})_3(BF_4)_4(EtOAc)_2](BF_4)_2$ were then also measured, until all complexes were isoabsorbing at 280 nm. All measurements were done in MeCN in standard aerated conditions.

The luminescence spectrum of the free ligand L^{14naph} was measured and, as expected, shows a broad naphthalene-based emission between 300 and 400 nm.[3] The luminescence spectra of $[Cd_{16}(L^{14naph})_{24}](BF_4)_{32}$ and $[Cd_3(L^{14naph})_3](BF_4)_6$ were then also measured, and all three are shown in figure 3.2.6.1. There is a clear change in the emission between all three complexes. The $[Cd_3(L^{14naph})_3(BF_4)_4(EtOAc)_2](BF_4)_2$ spectrum shows that the most dominant emission from this complex is still the usual naphthalene emission, but there is a clear low-energy tail which is not present for free L^{14naph}. This is due to the stacking of the naphthyl group with pyrazolyl-pyridine groups as seen in the crystal structure, which changes the origin of the emission. The emission in the free ligand and the dominant component in $[Cd_3(L^{14naph})_3(BF_4)_4(EtOAc)_2](BF_4)_2$ is due to a purely naphthalene based π-π^* fluorescence. The red-shifted, lower-energy emission, arises from a naphthyl (donor) → pyrazolyl-pyridine (acceptor) charge-transfer excited state associated with the π-stacked arrays.

The luminescence spectrum of $[Cd_{16}(L^{14naph})_{24}](BF_4)_{32}$ was very different to $[Cd_3(L^{14naph})_3(BF_4)_4(EtOAc)_2](BF_4)_2$ and L^{14naph}, showing a large shift in the majority of the emission. The normal naphthyl emission is visible as a small shoulder, but the majority of the emission is from the red-shifted component due to the naphthyl → pyrazolyl-pyridine charge-transfer excited state.

The reason for the large difference in the spectra of the two Cd(II) complexes may be that the π-stacking is more extensive in $[Cd_{16}(L^{14naph})_{24}]^{32+}$. It has already been shown by NMR spectroscopy and ESMS that this complex is completely stable in solution, and the crystal structure proves that every naphthyl ring is involved in 5-component stacks alternating with pyrazolyl-pyridine groups. $[Cd_3(L^{14naph})_3(BF_4)_4(EtOAc)_2](BF_4)_2$ on the other hand has been shown to have a mixture of products in solution by both NMR spectroscopy and ESMS and it is possible that the stacking is not as extensive and therefore less of the lower-energy emission component is present.

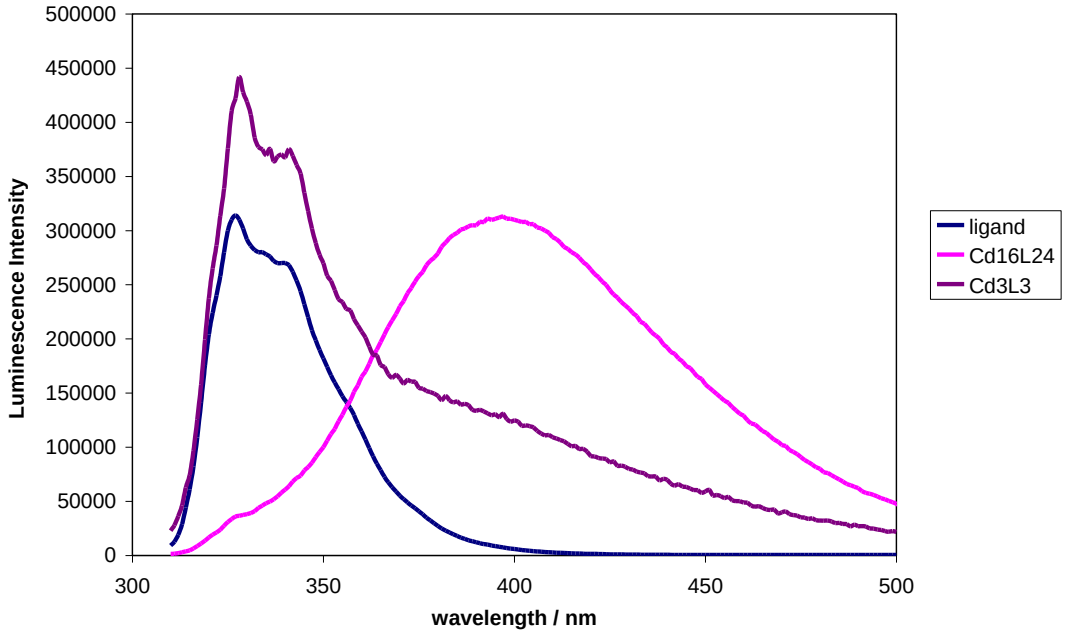

Figure 3.2.6.1 The luminescence spectrum of L^{14naph}, $[Cd_{16}(L^{14naph})_{24}](BF_4)_{32}$ and $[Cd_3(L^{14naph})_3(BF_4)_4(EtOAc)_2](BF_4)_2$.

3.2.7 A $[Ni_8(L^{14naph})_{12}](BF_4)_{16}$ 'cuneane' coordination cage

$Ni(BF_4)_2$ and L^{14naph} were mixed in a 2:3 ratio in MeOH and DCM, yielding a purple solid which ESMS revealed to have a $[Ni_8(L^{14naph})_{12}](BF_4)_{16}$ structure. This was initially presumed to be a cubic structure as has been seen many times before,[17] however X-ray crystallography revealed a different structure. The single-crystal structure revealed a $[Ni_8(L^{14naph})_{12}](BF_4)_{16}$ structure in agreement with the ESMS, however the structure was based on a 'cuneane' core. This is a topological isomer of a cube with eight vertices, all

of which are three connected. The structure has C_{2v}-symmetry and the complex cation is shown in figure 3.2.7.1.

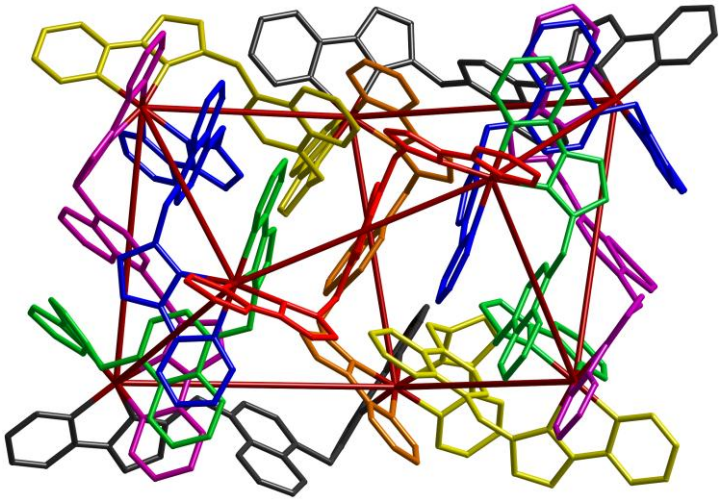

Figure 3.2.7.1 The full complex cation of the cuneane with each ligand shown in a different ligand for clarity.

The Ni•••Ni separations along the edges of the cuneane span the range 9.77 - 11.21 Å and the coordination geometry about each Ni(II) ion is unremarkable with Ni – N bond distances in the range 2.04 – 2.14 Å. All eight Ni(II) centres have a meridional tris-chelate geometry arising from the pyrazolyl-pyridine chelates, with one axis containing two pyridyl ligands, one containing two pyrazolyl ligands, and one axis containing one donor of each type. Ni(1) – Ni(7) are homochiral, with Ni(8) being the sole metal centre that has the opposite chirality. The structure contains two $[Ni_3(L^{14naph})_3]^{6+}$ units, emphasised in figure 3.2.7.2.

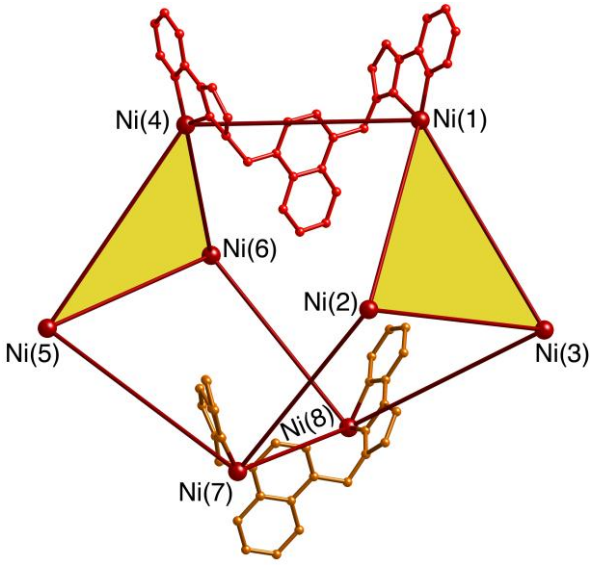

Figure 3.2.7.2 A view of the Ni_8 core to emphasise the structure and the two $[Ni_3(L^{14naph})_3]^{6+}$ triangular faces present.

As is typical of the cage structures,[18] there is extensive inter-ligand π- stacking with the stacks containing an alternating sequence of naphthyl (electron-rich) and pyrazolyl-pyridine (electron-deficient) components. The longest stack contains seven components (figure 3.2.7.3), and in addition to this there are several other such alternating stacks around the periphery of the complex, for example the threefold stacks around the two triangular faces which have the structures of $[Ni_3(L^{14naph})_3]^{6+}$ trinuclear helicates.

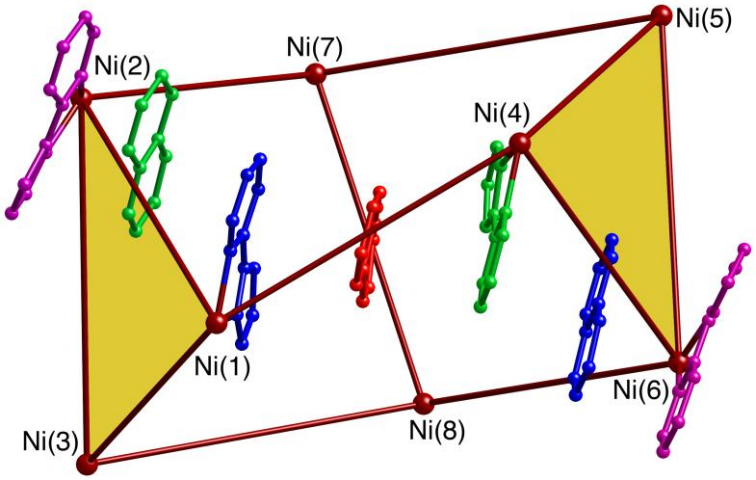

Figure 3.2.7.3 The stack of seven alternating pyrazolyl-pyridine / naphthyl units.

The trinuclear $[M_3L_3]^{6+}$ circular helical unit (figure 3.2.7.4) is a recurring feature in many of the cages in this family as was mentioned in both the previous chapter and in

this one. The only large polyhedral coordination cage seen so far in this series not to contain this $[M_3L_3]^{6+}$ unit as one triangular face of a polyhedron is the $[M_8L_{12}]^{16+}$ cube. It is interesting that with this ligand where this unit appears particularly stable (given the $[Cd_3(L^{14naph})_3(BF_4)_4(EtOAc)_2]^{2+}$ and $[Cu_3(L^{14naph})_3(BF_4)(MeCN)_2]^{5+}$ examples earlier) that the $[M_8L_{12}]^{16+}$ species seen with Ni(II) is the cuneane structure for the first time and not the cube as was the case with L^{pp}. The stability of the $[M_3(L^{14naph})_3]^{6+}$ unit and the possibility that this unit forms as a precursor to the cuneane cage could be the main reason why the cuneane structure was favoured in this case.

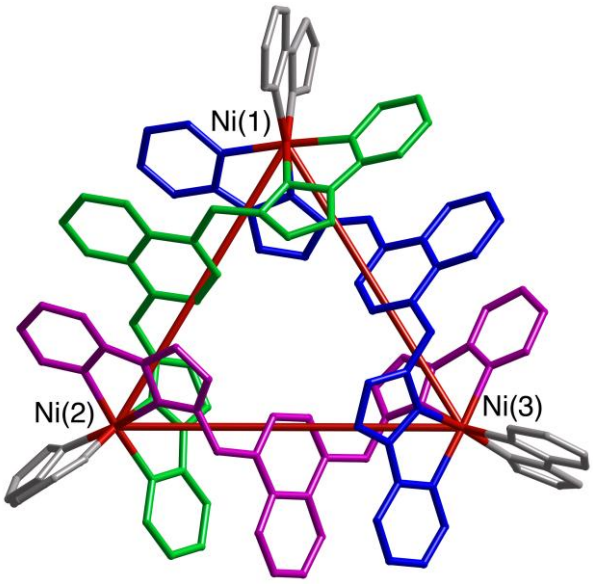

Figure 3.2.7.4 The $[Ni_3(L^{14naph})_3]^{6+}$ cyclic helical unit.

The core structure can be derived from a cube by rearrangement of two of the twelve edges as shown in figure 3.2.7.5, resulting in a C_{2v} symmetric 'wedge-shaped' structure which contains two triangular faces, two approximately rectangular faces, and two approximately pentagonal faces, with three different vertex environments in a 2:4:2 ratio.[19] Examples of this structure are very rare, particularly containing metal ions. The most well characterised example is a derivative of the hydrocarbon 'cubeane' (the cubic molecule C_8H_8) which can be converted into the lower-symmetry 'cuneane' analogues. This can be done via metal catalysed s-bond rearrangements, with the driving force being a considerable relief of strain energy.[19, 20] Calculations on possible structures of the cluster P_8 have shown that, of the structures based purely on single bonds, the cuneane-type arrangement will be lower in energy than the alternative D_{2d} (intermediate

in energy) and cubic (highest energy) possibilities.[21, 22] the most similar example is an octanuclear Ni/phosphido cluster that has been described as being based on a cuneane-type Ni_6P_2 core with additional capping atoms on some faces.[23]

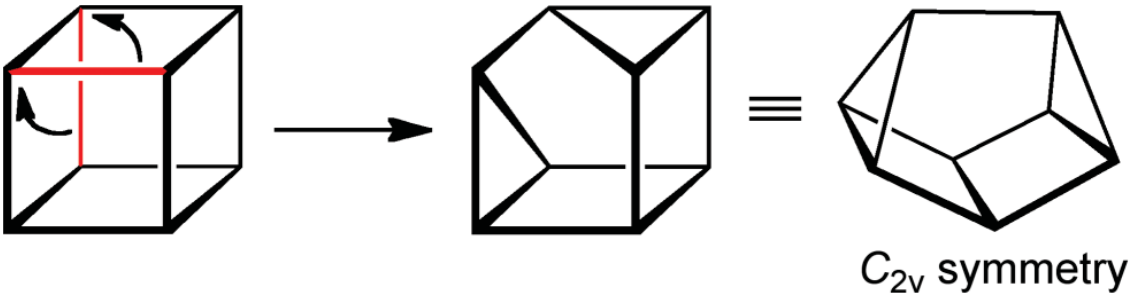

Figure 3.2.7.5 The relationship between the cube and cuneane.

The rarity of the cuneane-type C_{2v}-symmetric structure arises because it requires that all vertices are precisely three-connected. The six-coordinate metal ion / bis-bidentate bridging ligand combination associated with our polyhedral cages require a connectivity of three at each vertex. In this respect our cages have the same topological requirements as (CH)n[19, 20] and Pn[21, 22] cages in which the CH or P fragment at each vertex has the capacity to form three single bonds, and therefore they must form polyhedra containing only three-connected vertices.

Importantly, of the 257 possible polyhedra with eight vertices,[24] the cuneane structure is the only member (apart from a cube) whose vertices are all only three-connected; therefore for a polyhedral octanuclear cage such as $[Ni_8(L^{14naph})_{12}](BF_4)_{16}$ the cuneane-type structure that we observe is the only structural possibility apart from a cube. On that basis it is perhaps surprising that we have not observed a cuneane-type cage earlier, especially given the facts that (i) we have observed numerous examples of octanuclear cubic cages, (ii) according to calculations on both organic cuneanes[19, 20] and P_8 clusters,[21, 22] the cuneane structure is considerably more stable than that of a cube, and (iii) the $M_3(L^{14naph})_3$ unit which is so common in this series of cages is present in the cuneane structure but not the cube.

3.3 Conclusion

The luminescent ligand L^{14naph} has been combined with various metal salts, and a series of coordination cages and trinuclear cyclic helicates have arisen. The clear similarities between this ligand and L^{pp} have resulted in the same types of cage being formed, with the notable exception of Ni(II) which has formed an unprecedented 'cuneane' type octanuclear structure with this ligand. The $[Ni_8(L^{14naph})_{12}]^{16+}$ 'cuneane' core is a geometric isomer of a cube, with C_{2v} symmetry, and appears to have formed in preference due to the stability of the $[M_3(L^{14naph})_3]^{6+}$ trinuclear cyclic helicate unit which is so common in this series of cages.

L^{14naph} has been shown to form a $[Cd_{16}(L^{14naph})_{24}](BF_4)_{32}$ coordination cage when mixed with $Cd(BF_4)_2$ in a 3:2 ratio, isostructural to the cage with L^{pp}. The crystal structure of the cage is essentially identical to that of the L^{pp} analogue with 12 *meridional* tris-chelate metal centres forming four triangular faces, and four *facial* tris-chelate metal centres that act as capping ions. The major difference between the two cages however is their behaviour in solution; the $[Cd_{16}(L^{pp})_{24}](BF_4)_{32}$ cage was shown to interconvert to the $[Cd_6(L^{pp})_9](BF_4)_{12}$ trigonal prism, but $[Cd_{16}(L^{14naph})_{24}](BF_4)_{32}$ is stable in solution by both ^1H NMR and ESMS. Initial host-guest screenings with the cage have been unsuccessful, however further possible guests will be studied in the future.

It has also been shown in this chapter that the $[Cd_3(L^{14naph})_3(BF_4)_4(EtOAc)_2]^{2+}$ and $[Cu_3(L^{14naph})_3(BF_4)(MeCN)_2]^{5+}$ complexes can be isolated when a 1:1 metal-to-ligand ratio is employed. These complexes adopt a mixture of products in solution and in both cases appear to be in equilibrium with a $\{M_2(L^{14naph})_2\}^{4+}$ complex. It has been shown that the pre-formed $\{Cu_3(L^{14naph})_3\}^{6+}$ triangular unit can be reacted further with a different ligand, L^{mes}, to form a larger coordination cage $[Cu_{12}(L^{14naph})_{12}(L^{mes})_4]^{24+}$ via (at least to some degree) hierarchical self-assembly in which the four L^{mes} ligands interconnect four $[Cu_3(L^{14naph})_3]^{6+}$ fragments. The $\{Cu_3(L^{14naph})_3\}^{6+}$ unit is not the only product seen in solution, and due to Cu(II) being labile it is possible that the complex could interconvert in solution as was seen with the $Cd(BF_4)_2$ and L^{pp} complex. However it is clear that the $\{Cu_3(L^{14naph})_3\}^{6+}$ is stable in solution to at least some degree and when the L^{mes} is added this may bring the equilibrium towards this structure rather than the $\{Cu_2(L^{14naph})_2\}^{4+}$ and in this case it could be considered as hierarchical self-assembly.

The $\{Cu_3(L^{14naph})_3\}^{6+}$ complex appears to be a good building block for larger supramolecular architectures, either for coordination cages or metal-organic frameworks. The Cu(II) ions can be five or six coordinate so the complex could be reacted with either mono or bidentate ligands in the future. This is something that will be investigated in more detail in the future.

3.4 Experimental

Synthesis of 1,4-bis(bromomethyl)naphthalene

1,4-dimethylnaphthalene (2.00 g, 13 mmol) was brominated by reaction with N-bromosuccinimide (5.00 g, 28 mmol) in carbon tetrachloride (80 mL). The mixture was refluxed for 1 hour at 90 °C in the presence of azobisisobutyronitrile (AIBN) (0.02 g) which acts as a radical catalyst and was activated using a tungsten lamp. Progress of the reaction was monitored by thin-layer chromatography, (eluent: hexane:dichloromethane, 80:20). The succinimide was filtered off by vacuum filtration and the solution dried using magnesium sulphate. The solvent was removed under vacuum, and then the solid was heated and recrystallised in a minimum amount of toluene. The solid was then filtered, washed with cold toluene and dried resulting in a white powder (2.31 g, 7.4 mmol, 57 %).

Synthesis of $L^{1,4naph}$

1,4-bis(bromomethyl)naphthalene (1.00 g, 3.2 mmol) was refluxed for 20 hours with two equivalents of 3-(2-pyridyl)pyrazole (0.93 g, 6.4 mmol) in THF (60 mL) and aqueous sodium hydroxide (2.57g in 5 mL H_2O). The solution was filtered, dried through $MgSO_4$ and reduced to dryness to yield a white powder which was washed with diethyl ether and dried (1.10 g, 2.5 mmol, 78 %).

^{1}H NMR (400MHz, $CDCl_3$): δ 8.65 (2H, ddd, J = 5.2, 1.2 and 0.8 Hz, pyridyl H^6), 8.10 (2H, m, naphthyl $H^{5 \text{ or } 6}$), 8.00 (2H, dt, J = 7.9 and 1.0, pyridyl H^3), 7.75 (2H, td, J = 7.9 and 1.8, pyridyl H^4), 7.57 (2H, m, naphthyl $H^{5 \text{ or } 6}$), 7.32 (2H, d, J = 2.3 Hz, pyrazolyl H^5), 7.27 (2H, s, naphthyl H^2), 7.23 (2H, m, pyridyl H^5), 6.90 (2H, d, J = 2.3 Hz, pyrazolyl H^4), 5.90(4H, s, CH_2). ESMS: *m*/*z* 443 $(M + H)^+$, 465 (M + Na). Anal. Calcd for $C_{28}H_{22}N_6$: C 76.0; H, 5.0; N, 19.0% Found: C, 75.9; H, 4.9; N, 18.9%.

Synthesis of $[Cd_{16}(L^{14naph})_{24}](BF_4)_{32}$

A solution of $Cd(BF_4)_2$ (0.024 g, 0.06 mmol) in MeOH (7 cm^3) was added to a solution of L^{14naph} (0.040 g, 0.09 mmol) in CH_2Cl_2 (7 cm^3). The mixture was stirred at room temperature for 24 h, and the resultant precipitate was filtered off, washed with both MeOH and CH_2Cl_2, and dried *in vacuo* to give $[Cd_{16}(L^{14naph})_{24}](BF_4)_{32}$ as a white

powder in 67% yield. X-ray quality crystals were grown by slow diffusion of isopropyl ether into a solution of the complex in acetonitrile.

1H NMR: Total of 44 H peaks as expected – Pz and CH_2 peaks assigned via COSY spectrum.

^{113}Cd NMR: -439 ppm (4 Cd *fac* ions), -445 ppm (12 Cd *mer* ions)

The same NMR sample was recorded for 7 weeks without any noticeable change to the spectrum, suggesting the structure is stable in solution for at least this length of time.

ESMS: *m*/*z*; 3712.4, $\{[Cd_{16}(L^{14naph})_{24}](BF_4)_{28}\}^{4+}$; 2952.5, $\{[Cd_{16}(L^{14naph})_{24}](BF_4)_{27}\}^{5+}$; 2446.0, $\{[Cd_{16}(L^{14naph})_{24}](BF_4)_{26}\}^{6+}$; 2084.1, $\{[Cd_{16}(L^{14naph})_{24}](BF_4)_{25}\}^{7+}$; 1812.8, $\{[Cd_{16}(L^{14naph})_{24}](BF_4)_{24}\}^{8+}$. Anal. Calcd for $C_{672}H_{528}B_{32}F_{128}N_{144}Cd_{16}$: C, 53.0; H, 3.5; N, 13.3% Found: C, 52.6; H, 3.7; N, 13.1%.

Synthesis of $[Cd_3(L^{14naph})_3(BF_4)_4(EtOAc)_2](BF_4)_2$

A solution of $Cd(BF_4)_2$ (0.031 g, 0.09 mmol) in MeOH (7 cm^3) was added to a solution of L^{14naph} (0.040 g, 0.09 mmol) in CH_2Cl_2 (7 cm^3). The mixture was stirred at room temperature for 24 h, and the resultant precipitate was filtered off, washed with both MeOH and CH_2Cl_2, and dried *in vacuo* to give $[Cd_3(L^{14naph})_3(BF_4)_4](BF_4)_2$ as a white powder in 77% yield. X-ray quality crystals were grown by slow diffusion of ethyl acetate into a solution of the complex in nitromethane.

^{1}H NMR (500MHz, CD_3NO_2): δ8.59 (2H, ddd, **A**py^6), δ 8.50 (2H, ddd, **B**py^6), 8.15 (2H, d, **B**pz), 8.05 (2H, d, **A**pz), 7.84 (2H, dt, **A**py4), 7.78 (2H, td, **A**py3), 7.61 (4H, m, 2 x **A**nap), 7.54 (4H, m, 2 x **B**nap), 7.40 (2H, dt, **B**py4), 7.34 (2H, dt, **A**py5), 7.17 (2H, dt, **B**py5), 7.07 (2H, dt, **B**py3), 6.99 (2H, d, **A**pz), 6.85 (2H, d, **B**pz), 5.93 (2H, d, **B**CH_2), 5.79 (2H, m, **B**nap), 5.78 (2H, d, **A**CH_2), 5.74 (2H, d, **B**CH_2), 5.46 (2H, m, **A**nap), 5.33 (2H, d, **A**CH_2).

ESMS: *m*/*z*; 2098.8, $\{[Cd_3(L^{14naph})_3](BF_4)_5\}^{1+}$; 2031.5, $\{[Cd_3(L^{14naph})_3](BF_4)_4(F)\}^{+}$; 1956.2, $\{[Cd_3(L^{14naph})_3](BF_4)_3(F)_2\}^{+}$; 1370.4, $\{[Cd_2(L^{14naph})_2](BF_4)_3\}^{+}$; 1303.4, $\{[Cd_2(L^{14naph})_2](BF_4)_2(F)\}^{+}$; 1235.4, $\{[Cd_2(L^{14naph})_2](BF_4)(F)_2\}^{+}$; 1006.0, $\{[Cd_3(L^{14naph})_3](BF_4)_4\}^{2+}$; 641.7, $\{[Cd_3(L^{14naph})_3](BF_4)_3\}^{3+}$. Anal. Calcd for $C_{84}H_{66}B_6F_{24}N_{18}Cd_3$: C, 46.2; H, 3.0; N, 11.5% Found: C, 35.5; H, 3.3; N, 8.8%.

Synthesis of $[Cu_3(L^{14naph})_3(BF_4)(MeCN)_2](BF_4)_5$

A solution of $Cu(BF_4)_2$ (0.029 g, 0.09 mmol) in MeOH (7 cm^3) was added to a solution of L^{14naph} (0.040 g, 0.09 mmol) in CH_2Cl_2 (7 cm^3). The mixture was stirred at room temperature for 24 h, and the resultant precipitate was filtered off, washed with both MeOH and CH_2Cl_2, and dried *in vacuo* to give $[Cu_3(L^{14naph})_3(BF_4)_4(MeCN)_2](BF_4)_2$ as a green powder in 74% yield. X-ray quality crystals were grown by slow diffusion of toluene into a solution of the complex in acetonitrile.

ESMS: *m*/*z*; 1884.5, $\{[Cu_6(L^{14naph})_6](BF_4)_8(F)_2\}^{2+}$; 1850.5, $\{[Cu_6(L^{14naph})_6](BF_4)_7(F)_3\}^{2+}$; 1816.5, $\{[Cu_6(L^{14naph})_6](BF_4)_6(F)_4\}^{2+}$; 1782.5, $\{[Cu_6(L^{14naph})_6](BF_4)_5(F)_5\}^{2+}$; 1750.5, $\{[Cu_6(L^{14naph})_6](BF_4)_4(F)_6\}^{2+}$; 1204.3, $\{[Cu_2(L^{14naph})_2](BF_4)_2(F)\}^{+}$; 1204.3, $\{[Cu_4(L^{14naph})_4](BF_4)_4(F)_2\}^{2+}$; 1170.3, $\{[Cu_4(L^{14naph})_4](BF_4)_3(F)_3\}^{2+}$; 1137.3, $\{[Cu_2(L^{14naph})_2](BF_4)(F)_2\}^{+}$; 1137.3, $\{[Cu_4(L^{14naph})_4](BF_4)_2(F)_4\}^{2+}$; 525.1, $\{[Cu_2(L^{14naph})_2](F)_2\}^{2+}$; 343.8, $\{[Cu_2(L^{14naph})_2](F)\}^{3+}$. Anal. Calcd for $C_{84}H_{66}B_6F_{24}N_{18}Cu_3$: C, 49.5; H, 3.3; N, 12.4% Found: C, 43.1; H, 3.6; N, 10.7%.

Synthesis of $[Cd_{12}(L^{14naph})_{12}(L^{mes})_4](BF_4)_{24}$

A solution of $[Cd_3(L^{14naph})_3(BF_4)_4](BF_4)_2$ (0.020 g, 0.10 mmol) in MeOH (7 cm^3) was added to a solution of L^{mes} (0.015 g, 0.025 mmol) in CH_2Cl_2 (7 cm^3). The mixture was stirred at room temperature for 24 h, and the resultant precipitate was filtered off, washed with both MeOH and CH_2Cl_2, and dried *in vacuo* to give $[Cd_{12}(L^{14naph})_{12}(L^{mes})_4](BF_4)_{24}$ as a white powder in 61% yield.

No crystal structure could be obtained despite numerous attempts. The structure was only characterised by ESMS.

ESMS: *m*/*z*; 2690.5, $\{[Cd_{12}(L^{14naph})_{12}(L^{mes})_4](BF_4)_{20}\}^{4+}$; 2135.0, $\{[Cd_{12}(L^{14naph})_{12}(L^{mes})_4](BF_4)_{19}\}^{5+}$; 1764.7, $\{[Cd_{12}(L^{14naph})_{12}(L^{mes})_4](BF_4)_{18}\}^{6+}$; 1500.2, $\{[Cd_{12}(L^{14naph})_{12}(L^{mes})_4](BF_4)_{17}\}^{7+}$; 1301.9, $\{[Cd_{12}(L^{14naph})_{12}(L^{mes})_4](BF_4)_{16}\}^{8+}$. Anal. Calcd for $C_{480}H_{396}B_{24}F_{96}N_{108}Cd_{12}$: C, 51.9; H, 3.6; N, 13.6% Found: C, 51.8; H, 3.4; N, 13.2%.

Synthesis of $[Cu_{12}(L^{14naph})_{12}(L^{mes})_4](BF_4)_{24}$

A solution of $[Cu_3(L^{14naph})_3(BF_4)_4](BF_4)_2$ (0.020 g, 0.10 mmol) in MeOH (7 cm^3) was added to a solution of L^{mes} (0.015 g, 0.025 mmol) in CH_2Cl_2 (7 cm^3). The mixture was stirred at room temperature for 24 h, and the resultant precipitate was filtered off, washed with both MeOH and CH_2Cl_2, and dried *in vacuo* to give $[Cu_{12}(L^{14naph})_{12}(L^{mes})_4](BF_4)_{24}$ as a green powder in 56% yield. X-ray quality crystals were grown by slow diffusion of toluene into a solution of the complex in acetonitrile.

ESMS: *m*/*z*; 2543.9, $\{[Cu_{12}(L^{14naph})_{12}(L^{mes})_4](BF_4)_{20}\}^{4+}$; 2017.8, $\{[Cu_{12}(L^{14naph})_{12}(L^{mes})_4](BF_4)_{19}\}^{5+}$; 1667.0, $\{[Cu_{12}(L^{14naph})_{12}(L^{mes})_4](BF_4)_{18}\}^{6+}$; 1416.5, $\{[Cu_{12}(L^{14naph})_{12}(L^{mes})_4](BF_4)_{17}\}^{7+}$; 1228.6, $\{[Cu_{12}(L^{14naph})_{12}(L^{mes})_4](BF_4)_{16}\}^{8+}$; 1082.4, $\{[Cu_{12}(L^{14naph})_{12}(L^{mes})_4](BF_4)_{15}\}^{9+}$. Anal. Calcd for $C_{480}H_{396}B_{24}F_{96}N_{108}Cu_{12}$: C, 54.8; H, 3.8; N, 14.4% Found: C, 55.2; H, 4.1; N, 14.6%.

$[Ni_8(L^{14naph})_{12}](BF_4)_{16}$

A solution of $Ni(BF_4)_2$ (0.026 g, 0.075 mmol) in MeOH (7 cm^3) was added to a solution of L^{14naph} (0.050 g, 0.11 mmol) in CH_2Cl_2 (7 cm^3). The mixture was stirred at room temperature for 24 h, and the resultant precipitate was filtered off, washed with both MeOH and CH_2Cl_2, and dried *in vacuo* to give $[Ni_8(L^{14naph})_{12}](BF_4)_{16}$ as a purple powder in 78% yield. X-ray quality crystals were grown by slow diffusion of isopropyl ether into a solution of the complex in acetonitrile.

ESMS: *m*/*z*; 2303.3, $\{[Ni_8(L^{14naph})_{12}][BF_4]_{13}\}^{3+}$; 1705.2, $\{[Ni_8(L^{14naph})_{12}][BF_4]_{12}\}^{4+}$; 1346.8, $\{[Ni_8(L^{14naph})_{12}][BF_4]_{11}\}^{5+}$; 1108.1, $\{[Ni_8(L^{14naph})_{12}][BF_4]_{10}\}^{6+}$; 937.5, $\{[Ni_8(L^{14naph})_{12}][BF_4]_9\}^{7+}$. Anal. Calcd for $C_{336}H_{264}B_{16}F_{64}N_{72}Ni_8$: C, 56.3; H, 3.7; N, 14.1%. Found: C, 56.0; H, 3.5; N, 14.0%.

Luminescence Studies

UV/vis absorption spectra were measured on a Cary 50 spectrophotometer and luminescence spectra on a Jobin-Yvon Fluoromax 4 fluorimeter using air-equilibrated CH_3CN solutions at room temperature.

3.5 X-Ray Crystallography

Details of the crystal, data collection and refinement parameters are summarised. Data were corrected for absorption using empirical methods (SADABS)[25] based upon symmetry-equivalent reflections combined with measurements at different azimuthal angles. The structures were solved by direct methods and refined by full-matrix least squares on weighted F^2 values for all reflections using the SHELX suite of programs.[26] Non-hydrogen atoms were refined anisotropically. Hydrogen atoms were placed in calculated positions, refined using idealized geometries (riding model) and were assigned fixed isotropic displacement parameters.

The structures of $[Cd_{16}(L^{14naph})_{24}](BF_4)_{32}$, $[Cu_{12}(L^{14naph})_{12}(L^{mes})_4](BF_4)_{24}$ and $[Ni_8(L^{14naph})_{12}](BF_4)_{16}$ were collected at the National Crystallography Service at the University of Southampton. The 'Squeeze' function in PLATON was used to eliminate regions of diffuse electron density in solvent-accessible voids in each structure, information is given in the CIF.

In each other case a suitable crystal was mounted in a stream of cold N_2 on a Bruker APEX-2 or SMART CCD diffractometers (at the University of Sheffield) equipped with graphite-monochromated Mo-Kα radiation from a sealed-tube source. Details of each structure are given in their individual CIFs.

Crystal Data Tables

Summary of crystallographic data for the new crystal structures:

Compound	**$L^{1,\ 4naph}$**	**$[Cd_{16}(L^{14naph})_{24}](BF_4)_{32}$ •11(MeCN)**	**$[Cd_3(L^{14naph})_3(BF_4)_4(EtOAc)_2](BF_4)_2$ •2$(MeNO_2)_2$**
Formula	$C_{28}H_{22}N_6$	$C_{694}H_{561}B_{32}Cd_{16}F_{128}N_{155}$	$C_{94}H_{88}B_6Cd_3F_{24}N_{20}O_8$
Molecular weight	442.52	15648.30	2483.90
T / *K*	130 (2)	120(2)	100(2)
Crystal system	Monoclinic	Triclinic	Monoclinic
Space group	P2(1)	P-1	C2/c
a / Å	14.49 (9)	34.450(4)	28.1552(15)
b / Å	4.93 (3)	36.508(4)	25.0616(15)
c / Å	15.40 (10)	44.278(5)	16.5885(9)
α / °	90.00	75.080(8)	90
β / °	99.66 (4)	73.819(9)	110.493(5)
γ / °	90.00	64.522(9)	90
V / $Å^3$	1084.5 (12)	47669(9)	10964.3(11)
Z	2	2	4
ρ / g cm^{-3}	1.355	1.090	1.505
μ / mm^{-1}	0.084	0.424	0.679
Data, restraints, parameters, R_{int}	2471 / 1 / 307 / 0.0552	164233 / 8555 / 6653 / 0.0651	7862 / 719 / 642 / 0.1120
Final *R*1, *wR*2[a]	0.0399, 0.0731	0.1211, 0.3272	0.0916, 0.2609

Compound	**$[Cu_3(L^{14naph})_3(BF_4)(MeCN)_2](BF_4)_5$•2(MeCN)**	**$[Cu_{12}(L^{14naph})_{12}(L^{mes})_4](BF_4)_{24}$ •4(C_7H_8)**	**$[Ni_8(L^{14naph})_{12}](BF_4)_{16}$•8(MeCN)**
Formula	$C_{184}H_{156}B_{12}Cu_6F_{48}N_{44}$	$C_{508}H_{428}B_{24}Cu_{12}F_{96}N_{108}$	$C_{352}H_{288}B_{16}F_{64}N_{80}Ni_8$
Molecular weight	4406.49	10891.50	7497.26
T / *K*	100(2)	100(2)	120(2)
Crystal system	Monoclinic	Monoclinic	Monoclinic
Space group	Cc	C2/c	P2(1)/c
a / Å	33.9274(10)	38.98(4)	26.972(3)
b / Å	19.5014(5)	40.03(4)	36.793(4)
c / Å	33.3186(10)	44.99(4)	40.869(6)
α / °	90	90	90
β / °	94.534(2)	102.36(2)	109.165(3)
γ / °	90	90	90
V / $Å^3$	21975.7(11)	68570(11)	38311(8)
Z	4	4	4
ρ / g cm^{-3}	1.332	1.055	1.300
μ / mm^{-1}	0.668	1.045	0.478
Data, restraints, parameters, R_{int}	27760 / 1618 / 1800 / 0.1003	47693 / 2963 / 2335 / 0.1101	30705 / 4268 / 3483 / 0.0767
Final *R*1, *wR*2[a]	0.0963, 0.2433	0.1445, 0.3760	0.1559, 0.3690

[a] The value of *R*1 is based on 'observed' data with $I>2\sigma(I)$; the value of *wR*2 is based on all data.

3.6 References

1. A. Stephenson, S. P. Argent, T, Riis-Johannessen, I. S. Tidmarsh and M. D. Ward, *J. Am. Chem. Soc.*, 2011, **133**, 858.

2. I. S. Tidmarsh, T. B. Faust, H. Adams, L. P. Harding,W. Clegg and M. D. Ward, *J. Am. Chem. Soc.*, 2008, **130**, 15167.

3. N. K. Al-Rasbi, C. Sabatini, F. Barigelletti and M. D. Ward, *Dalton Trans.*, 2006, 4769.

4. C-Y. Li, C-S. Liu, J-R. Li, and X-H. Bu, *Crystal Growth & Design*, 2007, **7**, 287.

5. D-Z. Wang, T-L. Hu, J-P. Zhao, X-H. Bu, *CrysEngComm.*, 2010, **12**, 3587.

6. H. Fenton, I. S. Tidmarsh and M. D. Ward, *CrystEngComm.*, 2011, **13**, 1432.

7. D. T. Vodak, M. E. Braun, J. Kim, M. Eddaoudi and O. M. Yaghi, *Chem. Commun.*, 2001, 2534.

8. J. Y. Lu and V. Schauss, *CrystEngComm.*, 2002, 4623.

9. X-J. Zheng, L-P. Jin, S. Gao and S-Z. Lu, *New J. Chem.*, 2005, **29**, 798.

10. J. K. Clegg, S. S. Iremonger, M. J. Hayter, P. D. Southon, R. B. Macquart, M. B. Duriska, P. Jensen, P. Turner, K. A. Jolliffe, C. J. Kepert, G. V. Meehan, and L. F. Lindoy, *Angew. Chem. Int. Ed.*, 2010, **49**, 1075.

11. K. Xiong, F. Jiang, Y. Gai, D. Yuan, L. Chen, M. Wu, K. Su and M. Hong, *Chem. Sci.*, 2012, **3**, 2321.

12. S. Turega, M. Whitehead, B. R. Hall, M. F. Haddow, C. A. Hunter and M. D. Ward, *Chem. Commun.*, 2012, **48**, 2752.

13. L. J. Childs, N. W. Alcock and M. J. Hannon, *Angew. Chem. Int. Ed.*, 2002, **41**, 4244.

14. A. Stephenson and M. D. Ward, *Dalton Trans.*, 2011, 40, 10360.

15. S. P. Argent, H. Adams, T. Riis-Johannessen, J. C. Jeffery, L. P. Harding and M. D. Ward, *J. Am. Chem. Soc.*, 2006, **128**, 72.

16. N. K. Al-Rasbi, I. S. Tidmarsh, S. P. Argent, H. Adams, L. P. Harding and M. D. Ward, *J. Am. Chem. Soc.*, 2008, **130**, 11641.

17. A. M. Najar, I. S. Tidmarsh, H. Adams and M. D. Ward, *Inorg. Chem*., 2009, **48**, 11871.

18. M. D. Ward, *Chem. Commun*., 2009, 4487.

19. L. Cassar, P. E. Eaton and J. Halpern, *J. Am. Chem. Soc*., 1970, **92**, 6366.

20. M. V. Roux, J. Z. Dávalos, P. Jiménez, R. Notario, O. Castaño, J. S. Chickos, W. Hanshaw, H. Zhao, N. Rath, J. F. Liebman, B. S. Farivar and A. Bashir-Hashemi, *J. Org. Chem*., 2005, **70**, 5461.

21. M. Häser, U. Schneider and R. Ahlrichs, *J. Am. Chem. Soc*., 1992, **114**, 9551.

22. B. M. Gimarc and D. S. Warren, *Inorg. Chem*., 1993, **32**, 1850.

23. D. F. Rieck, A. D. Rae and L. F. Dahl, *Chem. Commun*., 1993, 585.

24. D. Britton and J. D. Dunitz, *Acta Cryst. A*, 1973, **29**, 362.

25. G. M. Sheldrick, *SADABS*: *A program for absorption correction with the Siemens SMART system*, University of Göttingen, Germany, 1996.

26. G. M. Sheldrick, *Acta Crystallogr. Sect. A*, 2008, **64**, 112.

4. Coordination chemistry with the ligands L^{fur} and L^{th}

4.1 Introduction

Two new ligands, L^{fur} and L^{th} (figure 4.1.1) have been synthesised consisting of two chelating pyrazolyl-pyridine termini connected to a furan-2,5-diyl or thiophene-2,5-diyl spacers *via* methylene groups.

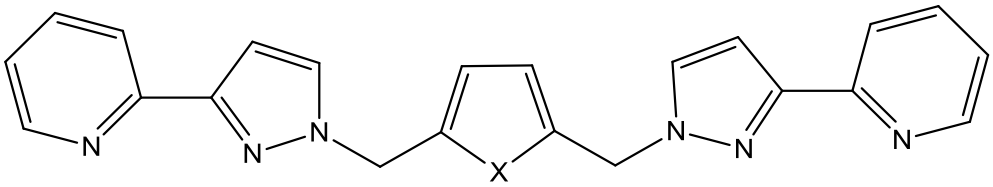

L^{fur}: X = O

L^{th}: X = S

Figure 4.1.1 The two new ligands synthesised.

These are similar to previous ligands from this group in the fact that they are bis-bidentate but they also have some important differences. Firstly the presence of the exocyclic lone pair on the oxygen and the sulphur atoms could be used to modify the environment inside the coordination cage. For example, the lone pair on the furan is a reasonable nucleophile and can act as a hydrogen bond acceptor.[1] This could encourage guests that are hydrogen bond donors to bind in the central cavity of the cage. The thiophene lone pair is less nucleophilic, although sulphur does have some interesting properties of its own which will be further discussed later.

The angle between the methylene groups, which is approximately 144°, is different to any previously synthesised ligands in the group. Previous examples of different ligands suggest that a new angle between the two coordinating arms could result in new or unusual structures. For example the para, meta and ortho substituted phenyl ligands give rise to $[M_{16}L_{24}]^{32+}$, $[M_8L_{12}]^{16+}$ and $[M_4L_6]^{8+}$ respectively.

The final important point about these ligands is that because the central spacer is more electron rich – due to the exocyclic lone pair – this should encourage and increase the π-stacking seen between the electron-rich spacer and the electron deficient pyrazolyl-

pyridine unit. This in turn should favour cage formation over other possibilities such as mononuclear structures where no stacking is required.

Furan and thiophene based ligands have been used before in molecular self assembly. Fujita and co-workers have shown how the subtle change in angle between the furan and thiophene spacers in his bidentate ligands can make a dramatic difference in the final complex. Using dipyridylfuran and $Pd(NO_3)_2$ they found that a $M_{12}L_{24}$ cage self-assembled,[2] however when dipyridylthiophene was used with the same metal unit, a much larger $M_{24}L_{48}$ cage was formed (figure 4.1.2).[3] The reason for the different cages forming is the difference in 'bend' angle between the two pyridyl units which are 127 º and 149 º for the furan and thiophene ligands respectively. This bend angle is vitally important because the ligand is rigid and it is this angle which ultimately dictates the final product by controlling the curvature of the pseudo-spherical surface. Surprisingly when a mixture of ligands was used only pure $M_{12}L_{24}$ or $M_{24}L_{48}$ cage were seen, never a mixture of the two. This proved that it is the average bend angle of the sub-components which is instrumental in deciding the final product.

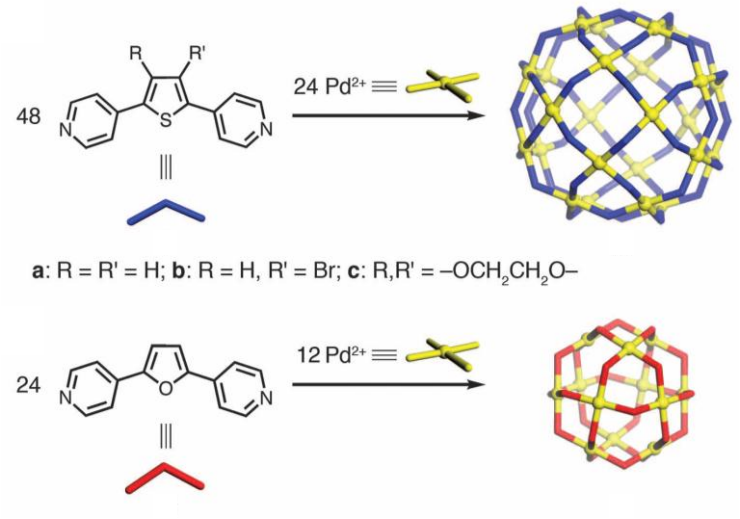

Figure 4.1.2 The furan and thiophene ligands give markedly different structures. Reproduced from reference 3.

Other work from Stang and co-workers also used furanyl-based linkers and a square-planar platinum unit to form a near rectangle (figure 4.1.3) which has inwardly directing furanyl oxygen atoms.[4] The ligand is slightly strained to create the near rectangle,

however it does have interesting features as it is cationic yet possesses hydrogen bond acceptors within its central cavity.

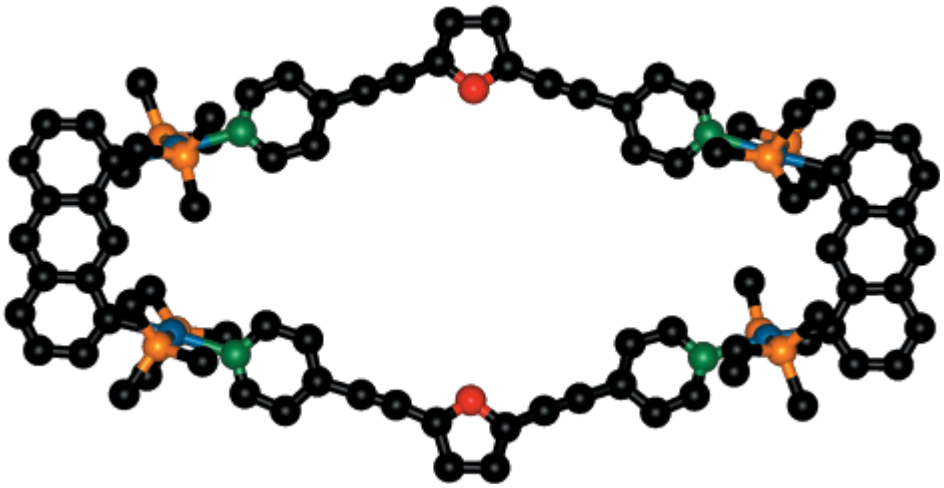

Figure 4.1.3 A 'rectangle' with inwardly directed furanyl oxygens (red). Reproduced from reference 4.

Sathiyendiran and co-workers have used furan substituents to decorate neutral Re(I) 2-D rectangles and 3-D trigonal prisms on the exterior of the complexes (figure 4.1.4).[5] By decorating the exterior of a cage or metallacycle with biologically or materially useful organic motifs, these can interact not only with the complex but with its surroundings too. Furan is a good choice as it is frequently a subunit in biologically active molecules[6] and has been used as a communicating moiety in molecular materials.[7] In fact, both furan and thiophene have been shown to possess useful properties such as electrochemical and optical[8] and electrochromic[9] properties. Thiophene units are also potentially useful because they are well known as being able to bind to surfaces,[10] as well as having other potential applications, for example in photo-switches.[11]

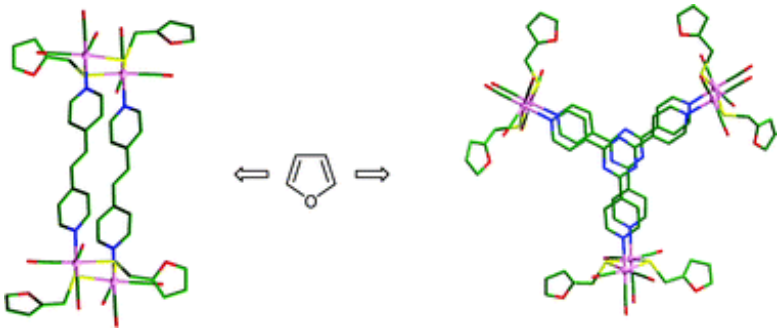

Figure 4.1.4 The 2-D rectangle (left) and the 3-D trigonal prism (right) with 4 and 6 exterior furan units respectively. Reproduced from reference 5.

The coordination chemistry of the ligands L^{fur} and L^{th} has been extensively studied with six-coordinate transition metals and it is expected that the usual M_2:L_3 ratio will be favoured given that the ligands are tetradentate. This ratio is fulfilled, as usual, by having an octahedral metal ion at each vertex and a bridging ligand spanning each edge. The difference in 'bite' angle between the two ligands is expected to have less of an impact here than in Fujita's examples as the methylene groups mean that the ligands are not rigid and have an inherent flexibility which makes the structure of the resulting cages harder to predict.

4.2 Results and Discussion

4.2.1 Ligand syntheses

The ligands L^{fur} and L^{th} were both synthesised in the same way. 2,5-dimethyl furan or 2,5-dimethyl thiophene were brominated using NBS and AIBN in CCl_4,[12] and the resulting intermediate was then immediately reacted with 3(2-pyridyl)pyrazole under basic conditions in THF to give the desired product (Scheme 4.2.1). The bis(bromomethyl) intermediates were reacted straight away due to their instability, as they are prone to self-reacting. The product was purified using column chromatography, and was analysed by ^{1}H NMR spectroscopy, ES mass spectrometry and elemental analysis. Further information is given in the Experimental section.

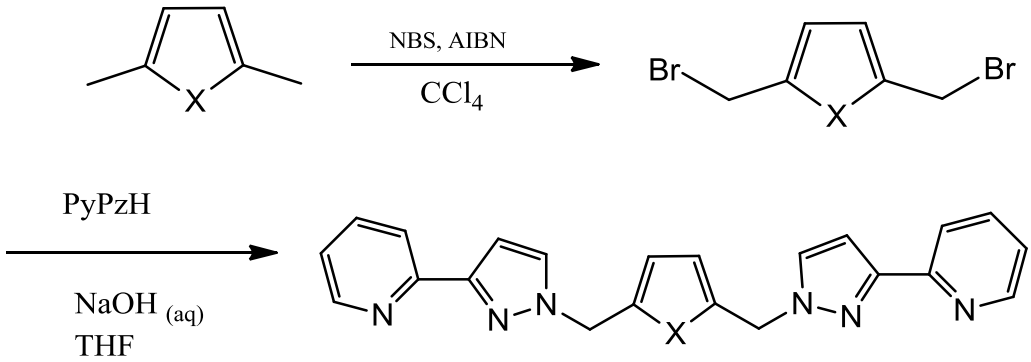

L^{fur}: X = O

L^{th}: X = S

Scheme 4.2.1 The general synthesis of the two ligands.

Once synthesised, the ligands were combined with transition metal dications as their tetrafluoroborate or perchlorate salts. Two methods were used; stirring in solution at room temperature and a high temperature solvothermal method (tetrafluoroborate salts only). The metal ions used included Co(II), Ni(II), Cu(II), Zn(II) and Cd(II). Once combined the resulting complexes were redissolved in either MeCN or $MeNO_2$, and then di(isopropyl) ether vapour was diffused into these solutions, affording X-ray quality crystals.

4.2.2 Complexes of L^{fur} with first-row transition metal dications: crystal structures of cubes and a square

With Co(II), Cu(II) and Zn(II) the crystal structure of the complex with L^{fur} in each case is a $[M_8(L^{fur})_{12}]X_{16}$ cube (M = Cu, X = BF_4; M = Co and Zn, X = ClO_4). The structure of $[Cu_8(L^{fur})_{12}](BF_4)_{16}$ (figure 4.2.2.1) is an irregular cube which has twofold symmetry such that it contains four independent Cu(II) ions.

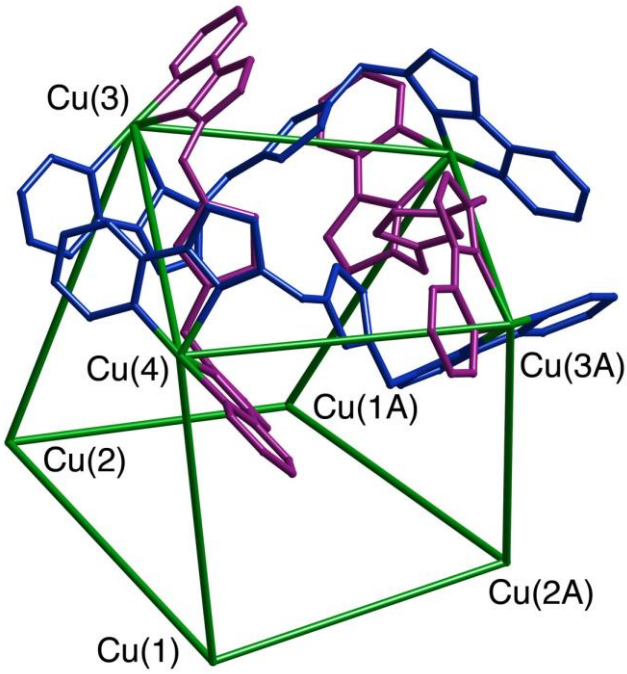

Figure 4.2.2.1 The irregular cubic array of $[Cu_8(L^{fur})_{12}](BF_4)_{16}$ with four of the ligands shown around one Cu_4 face.

There are Cu•••Cu separations of 9.24 – 10.17 Å and each Cu(II) ion has meridional tris-chelate geometry. Therefore at each metal centre there are two mutually trans pyrazolyl rings, two mutually trans pyridyl rings and one pyrazolyl trans to a pyridyl ring. The cube may be considered as two tetranuclear $M_4(L^{fur})_4$ cyclic helicates linked

together by 4 vertical pillars (emphasised in figure 4.2.2.2). The helicates are found around the Cu(1)/Cu(2)/Cu(1A)/Cu(2A) face (figure 4.2.2.3) and one around the Cu(3)/Cu(4)/Cu(3A)/Cu(4A) face (blue and purple ligands in figure 4.2.2.1). The two helicates have the same chirality, meaning that all eight metal centres are homochiral.

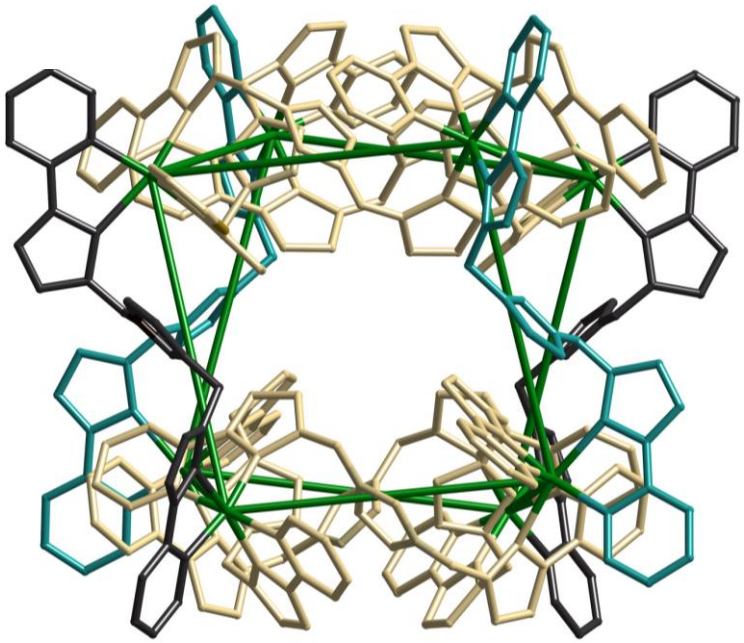

Figure 4.2.2.2 A view showing all twelve ligands although emphasising the four pillar ligands (grey and cyan) which link the two $Cu_4(L^{fur})_4$ cyclic helicates.

The cube has overall approximate D_4 molecular symmetry and the entire cage is chiral. The Cu(II) ions all exhibit the expected elongation along one axis due to the Jahn-Teller effect. This results in a pseudo-octahedral geometry; in every case the elongation occurs along the axis with the trans pair of pyrazolyl ligands, where the average Cu – N bond length is 2.30 Å, compared to an average of 2.03 Å for the other four Cu – N bonds.

Although many cubic complexes have been seen in previous work by this group, this is in fact the first with this symmetry. The majority of cubic cages characterised in this series have a mixture of meridional and facial tris-chelate metal centres and have approximate S_6 symmetry with an inversion centre at the centre of the cubic array.[13,14] In the only other example of a cube which also has two tetranuclear $M_4(L^{fur})_4$ helicates, the two helicates were of opposite chirality resulting in approximate C_{4h} symmetry.[14] The cube in this case did not possess any significant π-stacking between pyrazolyl-

pyridine units and the aromatic spacer, and consequently dissociated in solution. This was evident as the cage could not be characterised by NMR spectroscopy or ESMS.

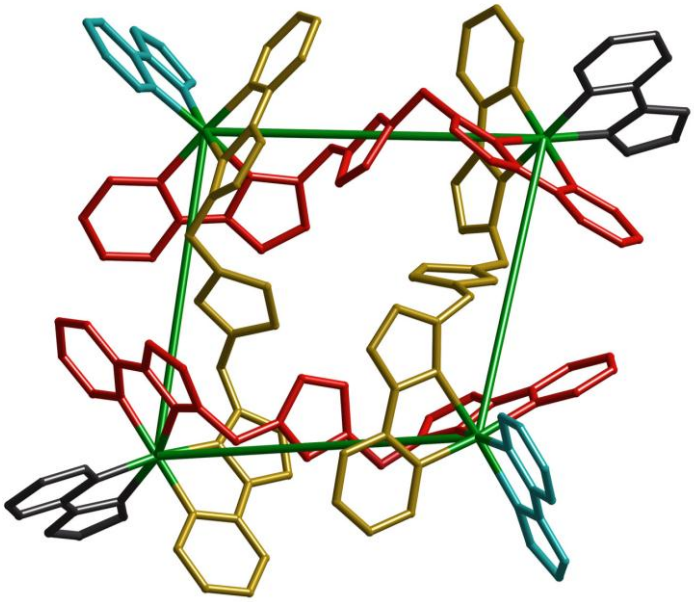

Figure 4.2.2.3 A view of one of the $Cu_4(L^{fur})_4$ cyclic helical faces with the four ligands forming the cyclic helicate in red and gold and the pillar ligands in grey and cyan receding into the page.

The central cavity of the cage accommodates one tetrafluoroborate anion. This is disordered in the crystal structure and therefore any interactions with the complex cation cannot be discussed in any great detail. There is also an anion that sits just outside the window of each face of the cube; these windows are shown clearly in the space filling view (figure 4.2.2.4).

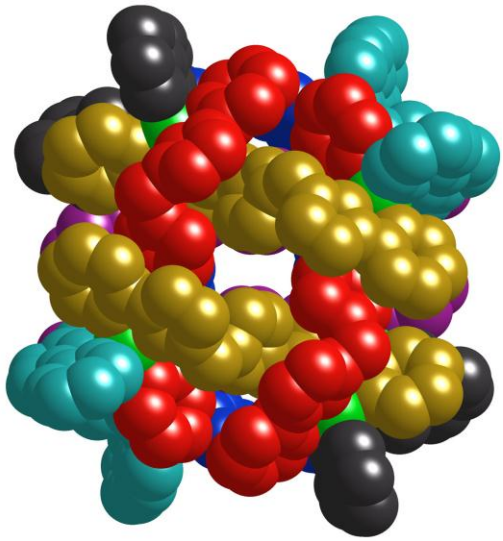

Figure 4.2.2.4 Space-filling view of the entire complex cation of $[Cu_8(L^{fur})_{12}](BF_4)_{16}$ from the same viewpoint as shown in figure 4.2.2.3.

All twelve furan units are involved in π-stacking interactions with pyrazolyl-pyridine units of adjacent ligands. These are electron rich (furan) and electron deficient (PyPz) π-stacks that are similar to many previous examples and are known to be important in cage formation and stabilising the cage assembly in solution. There are two types of π-stacking formation present in the structure: the furan groups in the ligands that are in the circular helicates are involved in a 3-layer PyPz – furan – PyPz stack, whereas the furan groups in the pillar ligands are only involved in a 2-layer PyPz – furan stack. However, the furan groups in the pillar ligands are also involved in a second interaction. The exocyclic lone pair on the furan is perpendicular to, and pointing directly at, a pyrazolyl-pyridine unit of an adjacent ligand (figure 4.2.2.5). This is presumably an area of partial positive charge given that the pyrazolyl-pyridine unit is coordinated to a 2+ metal ion. The distance between the O atom and the mean plane of the pyrazolyl-pyridine unit involved is 3.15 Å. The sum of the van der Waals radii for O and C is 3.2 Å showing that this interaction is weak although it is definitely present. None of the twelve O atoms are pointed at the anion that is located in the central cavity. This is disappointing as it means that they cannot interact with the guest in the central cavity as was hoped, although there is no reason why with a different guest in the cavity they could not interact with it. The furan groups are clearly involved in aromatic stacking which are important in the assembly of the cage and there are possibilities for further host-guest chemistry with the system in the future.

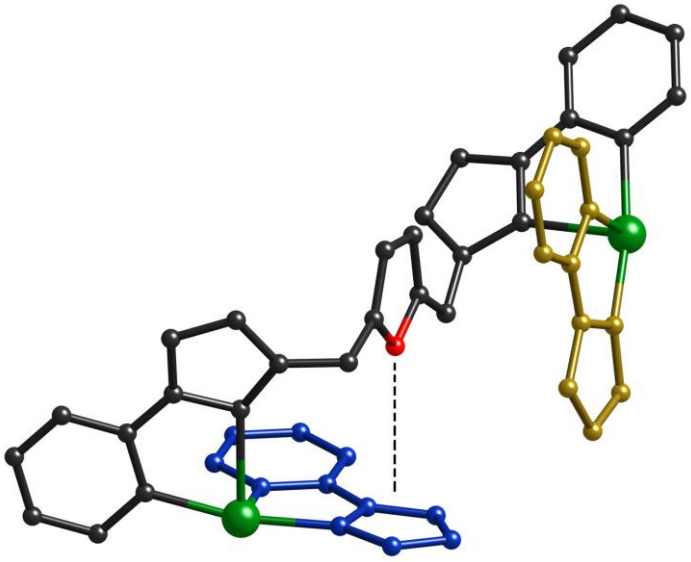

Figure 4.2.2.5 The furan ring is involved in both a side-on π-stacking interaction (with the pyrazolyl-pyridine unit shown in gold), and an interaction between its lone pair and a second pyrazolyl-pyridine unit shown in blue.

The structure with $Zn(ClO_4)_2$ is also a $[M_8(L^{fur})_{12}](ClO_4)_{16}$ cube which is isostructural with the Cu(II) example above. Although it is isostructural it crystallises in a different space group and has two complete and independent cubic cages in the asymmetric unit, therefore 16 independent Zn(II) ions. One of the independent cubes is shown in figure 4.2.2.6 with two of the pillar ligands and 5 of the expected 16 anions shown.

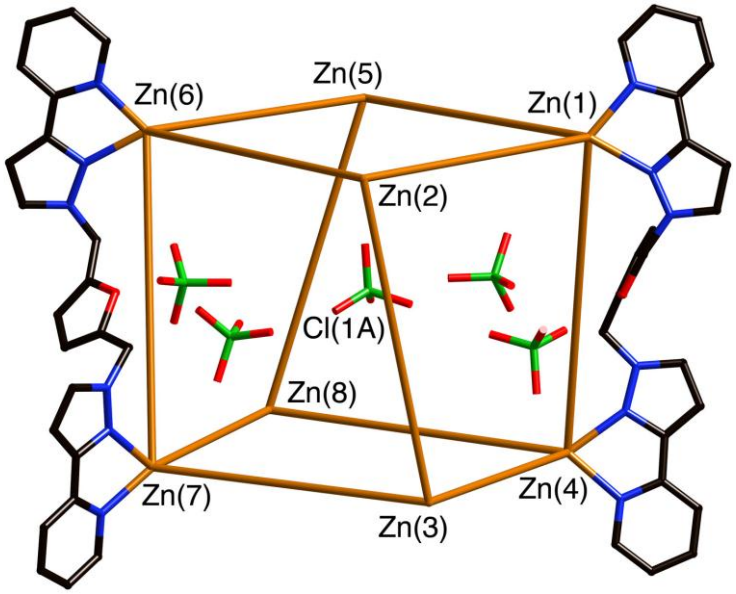

Figure 4.2.2.6 The cage with only two of the ligands shown.

As with the Cu example, the cube consists of two tetranuclear $M_4(L^{fur})_4$ helicates connected by four pillar ligands. The two helicates are offset such that they are distorted towards a square anti-prism rather than being a regular cube. There is one anion located in the central cavity and four located in the windows in 'equatorial' positions around the faces. These are clearly visible in figure 4.2.2.7, as is the distortion toward the square anti-prism structure. In the cube shown in the two figures, the Zn•••Zn separations along the edges lie in the range 9.11 Å [Zn(3)•••Zn(7)] – 10.46 Å [Zn(1)•••Zn(4)]. These are not greatly different from the Cu(II) equivalent but are shorter and longer than any in the Cu(II) structure. Zn–N bond distances lie in the range 2.10 – 2.24 Å, averaging 2.16 Å. These are not comparable to the Cu(II) equivalent as no Jahn-Teller effect is seen with the d^{10} Zn(II) ion.

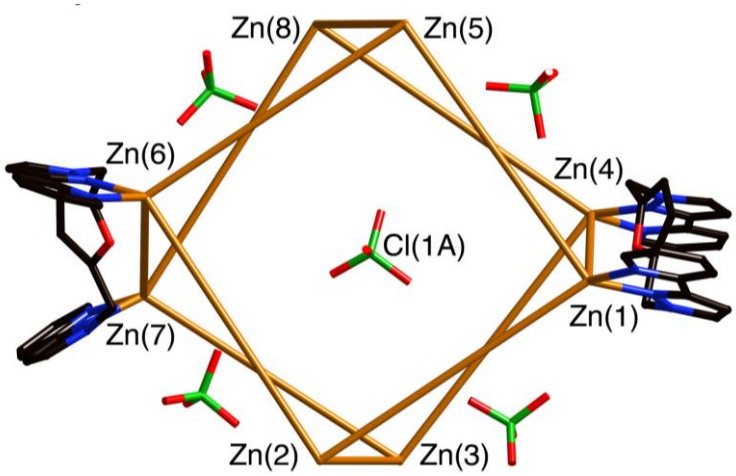

Figure 4.2.2.7 The cage from an approximately orthogonal viewpoint to figure 4.2.2.6, again showing the anions in the central cavity and the windows.

The structure of the L^{fur} complex with $Co(ClO_4)_2$ is also a $[M_8(L^{fur})_{12}](ClO_4)_{16}$ cube which is crystallographically isostructural and isomorphous with the Zn(II) cube shown above in figures 4.2.2.6 and 4.2.2.7. It has a near identical unit cell with two full cubes in the asymmetric unit; however the quality of the crystal data was relatively poor. A number of different crystal batches were tried but they were all weakly diffracting, therefore just the solution studies of this complex will be discussed (see later).

When L^{fur} was combined with $Ni(BF_4)_2$, surprisingly the crystal structure was not a $[M_8(L^{fur})_{12}]^{16+}$ cube but a $[M_4(L^{fur})_6]^{8+}$ square. The structure crystallises in the triclinic space group *P-1*, with only half the complex in the asymmetric unit. The square consists

of two equivalent but enantiomorphic double helicates connected by two cross-pieces. These cross-pieces act in a similar way to the pillar ligands in the cube structure as they are not part of a helicate but act as a link between two separate helicates. The complex cation is shown in figure 4.2.2.8 with the double helicate ligands shown in red and green and the cross-pieces shown in blue.

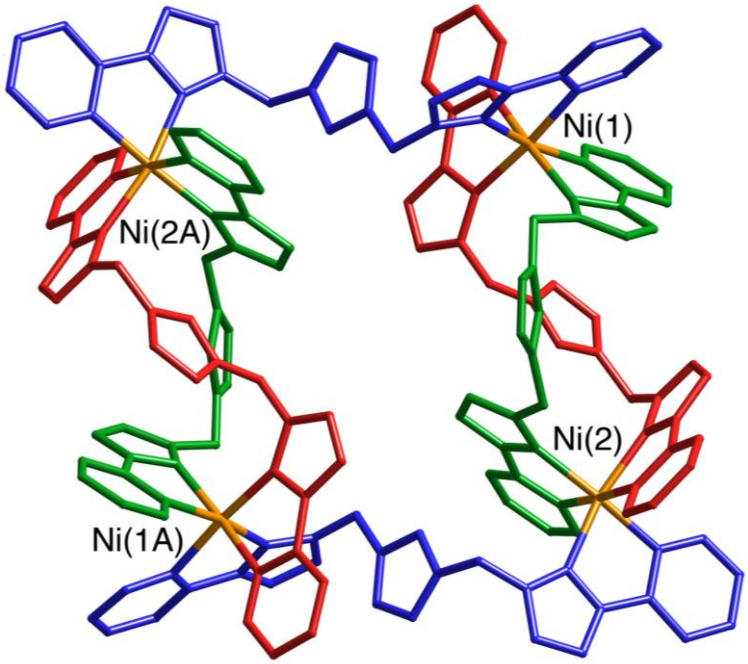

Figure 4.2.2.8 The complex cation of $[Ni_4(L^{fur})_6](BF_4)_8$.

The square can be described as an alternating sequence of one or two bridging ligands around the edges. The Ni•••Ni separations are 9.42 Å within the double helicate and 9.79 Å between the two helicates where the cross-piece ligands act as the bridge. The Ni – N distances average 2.10 Å and are fairly regular, however the two nickel centres are different configurations; Ni(1) being facial and Ni(2) being meridional.

There are two anions lying close to the central cavity, but just above and below the Ni – Ni plane as can be seen in figure 4.2.2.9. These are involved in CH•••F hydrogen bonding interactions shown in figure 4.2.2.10.

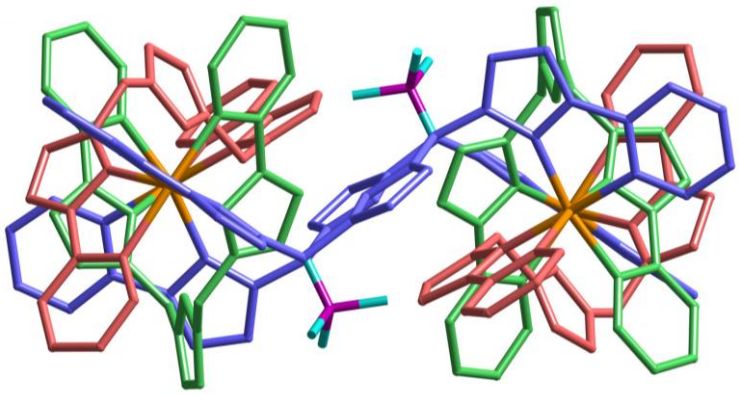

Figure 4.2.2.9 An edge-on view of the complex cation (looking down the two double helicate units) showing the arrangement of two counter-ions either side of the central cavity.

There are CH•••F interactions between F(13) and F(14X) with the methylene protons attached to C(26C), and also between F(12) and F(15X) with pyrazolyl protons attached to C(44B) and C(45B) respectively. The two C – F distances involving F(12) and F(13) are 3.17 and 3.12 Å respectively. The other two fluorine atoms are disordered over two sites and therefore, although they appear to be involved in similar interactions, detailed discussion is not appropriate.

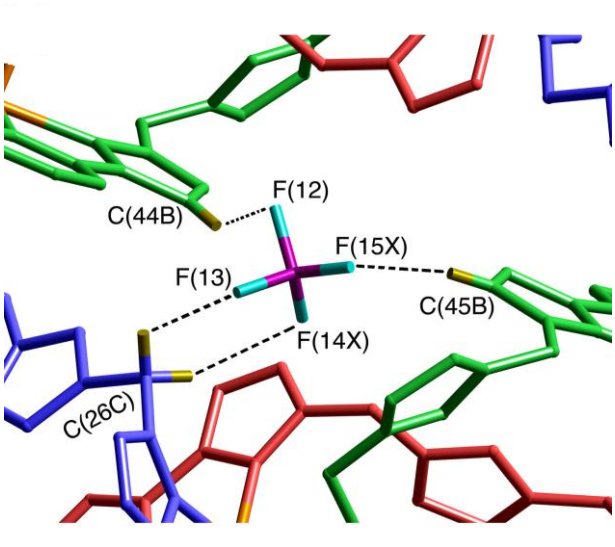

Figure 4.2.2.10 Close-up view of one of the anions showing the CH•••F hydrogen-bonding interactions in which it is involved.

M_4L_6 squares have been seen before in this group.[13] The previous example contained Ni(II) as the metal and a ligand based on 2,6-pyridine-diyl spacer with two pendant

pyrazolyl-pyridine units. Interestingly in this case the same ligand also gave $[M_8L_{12}]^{16+}$ cubes with Zn(II) and Co(II), showing that there is more than likely a specific property of Ni(II) that caused a different structure to be formed. The only significant difference between Ni(II) and the other cations is its ionic radius which is smaller (0.83 Å compared to 0.89, 0.87 and 0.88 Å for high-spin Co(II), Cu(II) and Zn(II) respectively). Possibly the smaller ionic radius results in a more compacted coordination sphere which in turn leads to a more crowded structure rather than a more open cage structure.

4.2.3 Complexes of L^{fur} with first-row transition metal dications: solution studies

It is always important in this type of work to see if the structure seen in the solid state is also stable in solution. Previous examples in the group have shown that sometimes structures observed in the solid state are not stable at all in solution,[14] and sometimes conversion from one structure to another can occur.[15] To investigate this, ESMS and, where possible, ^{1}H NMR measurements were carried out on the complexes.

ESMS studies for the Zn(II), Co(II) and Cu(II) complexes showed peaks that corresponded to the intact cube complexes; these could be confirmed by the isotope spacings which confirmed the charge at the correct *m/z* value. For example, assignment of the peak at 1576 to be $\{Zn_8(L^{fur})_{12}(ClO_4)_{12}\}^{4+}$ was confirmed by isotope spacings of ¼ of a mass unit. An $[M_4L_6]^{8+}$ square (if it existed) would also have a peak at this *m/z* value corresponding to $\{Zn_4(L^{fur})_6(ClO_4)_6\}^{2+}$ however this can be discounted as there was no peaks with ½ mass unit separation visible. However in all three cases there was clearly a high degree of fragmentation under the ESMS conditions and this led to a large number of peaks in the low *m/z* region. For example for the Zn complex, peaks were seen which corresponded to $\{Zn_n(L^{fur})_n(ClO_4)_{2n-1}\}^+$ (n = 1, 2, 3, 4, 5).

The ^{1}H NMR spectrum of $[Zn_8(L^{fur})_{12}](ClO_4)_{16}$ was far more informative however. The spectrum clearly shows that the structure remains intact in solution. The spectrum is expected to show two ligand environments, one for the ligands in the cyclic helical faces and one for the ligands that act as pillars. The ligands in the cyclic helicate, of which there are eight, have no internal symmetry because the chirality of the helix means the 'front' and 'back' end of each ligand are inequivalent. The four pillar ligands however lie astride C_2 axis and therefore do have internal symmetry. This means that they will give 9 independent ^{1}H signals and the ligands in the cyclic helicates will give

18 environments. The result therefore is that the spectrum is expected to show 27 independent ^{1}H environments, all of the same intensity (nominally 8H each). The COSY spectrum allows easy identification of pairs of coupled protons, which in particular make the pyrazolyl and methylene protons easy to identify. The pyrazolyl protons are easily distinguished because they give sharp doublets and there are three pairs in the NMR spectrum as expected. These are labelled a, b and c in figure 4.2.3.1. The other easily identifiable protons are the coupled pairs of methylene protons for the diastereotopic CH_2 groups. Although two of the peaks are partially obscured by the solvent peaks at 4.2 – 4.4 ppm the COSY spectrum proves that the peaks are definitely in that position. The three coupled pairs (as is the number expected from the number of different environments) are labelled A, B and C in figure 4.2.3.1. The other clearly identifiable protons are the protons on the furan ring. The ligands in the cyclic helicate have no internal symmetry and therefore we would expect to see a pair of doublets for the two protons. The pillar ligand with internal symmetry is expected to give a singlet and this is exactly what is seen, the pair of doublets labelled as f1 and the singlet as f2 in figure 4.2.3.1. The total number of protons is 27 as expected, in complete agreement with the crystal structure.

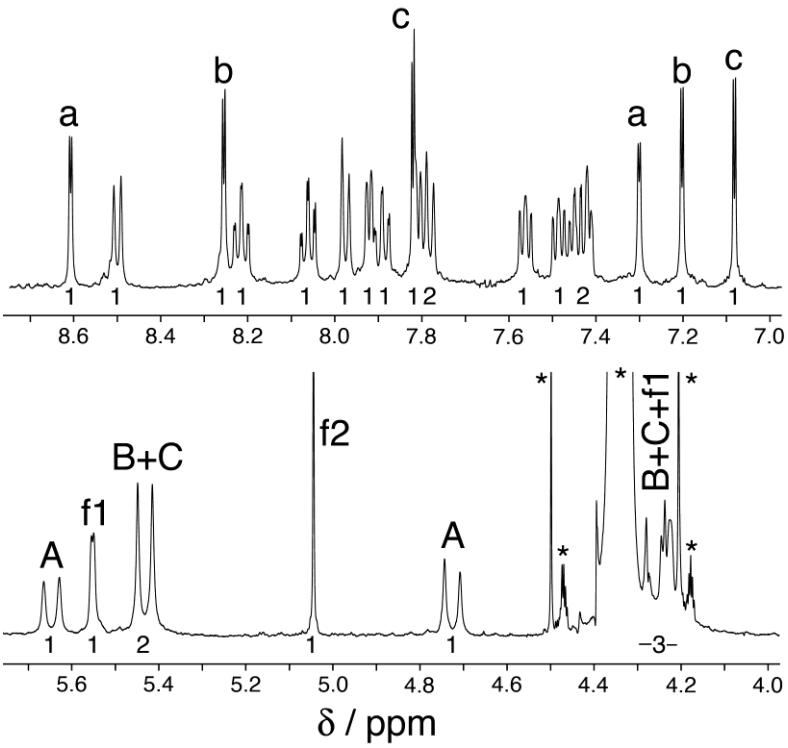

Figure 4.2.3.1 500 MHz ^{1}H NMR spectrum of $[Zn_8(L^{fur})_{12}](ClO_4)_{16}$ in CD_3NO_2. The integral values associated with each peak are shown. Solvent peaks are labelled *.

The ^{1}H NMR spectrum of $[Co_8(L^{fur})_{12}](ClO_4)_{16}$ is also consistent with the solid-state structure. As with the Zn complex, 27 signals are expected all of equal intensity as the complex will have the same symmetry. The signals though are paramagnetically shifted in the Co complex and lie between +120 and -100 ppm. The widths and intensities of these signals reflect their different τ_1 values which in turn depend on the sixth power of their distance from a high-spin Co(II) ion. A complete proton assignment of a Co cage complex has been done using this technique before[16] although is not needed here. The number of identifiable signals in the NMR spectrum is 24 as shown in figure 4.2.3.2, with the other 3 signals presumably hidden in the 0-10 ppm range by intense water or solvent peaks, or they are too broad to be distinguished from the baseline. This again confirms that the structure is retained in solution and that the conditions of the ESMS were the reason for the fragmentation.

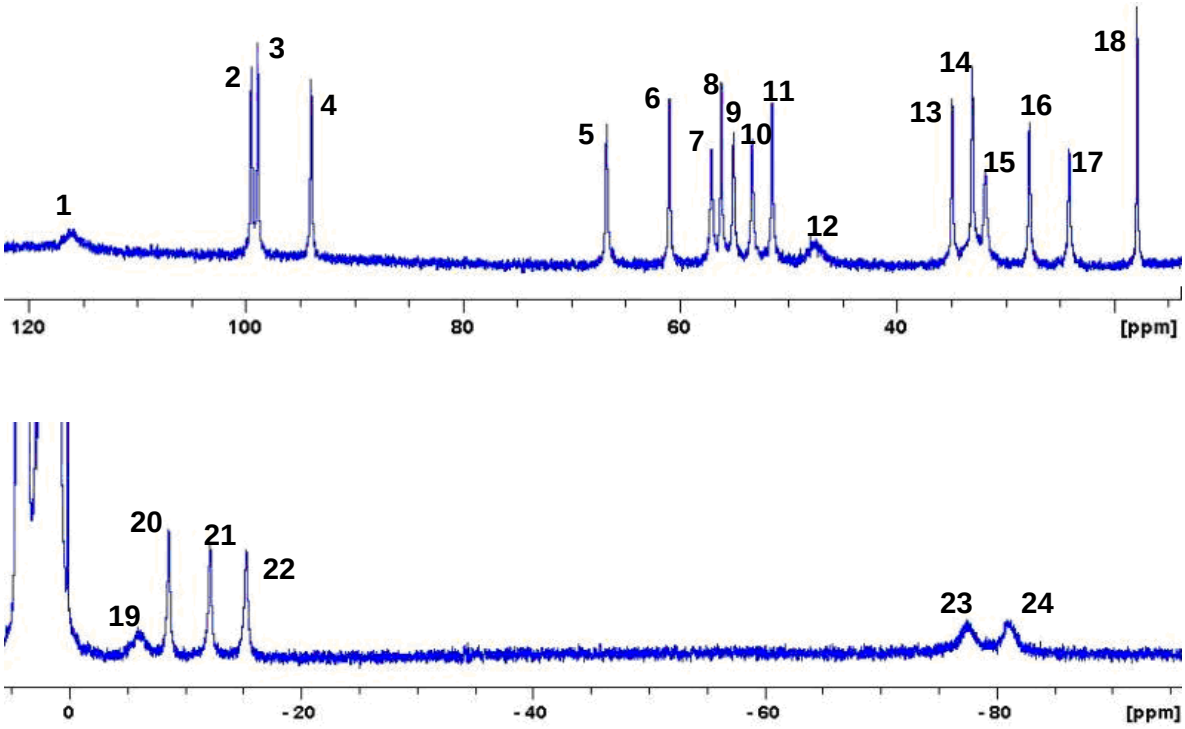

Figure 4.2.3.2 400 MHz ^{1}H NMR spectrum of $[Co_8(L^{fur})_{12}](ClO_4)_{16}$ in CD_3NO_2 showing 24 of the expected 27 peaks.

ESMS measurements on redissolved crystals of $[Cu_8(L^{fur})_{12}](BF_4)_{16}$ showed that the octanuclear cube is stable in solution, however there is also another unexpected product present. There are peaks which can be assigned unequivocally (due to the isotope spacings) which correspond to $[Cu_6(L^{fur})_9](BF_4)_{12}$. A trigonal prismatic cage has been seen with Cu(II) before and a larger cage has been shown to convert to a trigonal prismatic cage in solution[15] and so it is possible that a similar conversion is occurring in solution here. The following peaks were assigned from the ESMS unequivocally: *m/z* 2345, $\{Cu_6(L^{fur})_9(BF_4)_{10}\}^{2+}$; 2075, $\{Cu_8(L^{fur})_{12}(BF_4)_{13}\}^{3+}$;1535, overlapping $\{Cu_8(L^{fur})_{12}(BF_4)_{12}\}^{4+}$ and $\{Cu_6(L^{fur})_9(BF_4)_9\}^{3+}$; 1210, $\{Cu_8(L^{fur})_{12}(BF_4)_{11}\}^{5+}$; 1129, $\{Cu_6(L^{fur})_9(BF_4)_8\}^{4+}$; 994, $\{Cu_8(L^{fur})_{12}(BF_4)_{10}\}^{6+}$.

Redissolved crystals of $[Ni_4(L^{fur})_6](BF_4)_8$ were used to investigate the solution behaviour of this complex. The ESMS measurements were far more informative than for the cube complexes and showed clearly two sets of peaks corresponding to the tetranuclear square and the octanuclear cube. The two series of peaks do occur at the same m/z values in some cases, for example a peak at m/z = 988 could be due to either $\{Ni_4(L^{fur})_6(BF_4)_5\}^{3+}$ or $\{Ni_8(L^{fur})_{12}(BF_4)_{10}\}^{6+}$. However on the basis of isotope spacings

it was possible to determine the following peaks unequivocally: *m/z* 1525, overlapping $\{Ni_4(L^{fur})_6(BF_4)_6\}^{2+}$ and $\{Ni_8(L^{fur})_{12}(BF_4)_{12}\}^{4+}$; 1203, $\{Ni_8(L^{fur})_{12}(BF_4)_{11}\}^{5+}$; 988, $\{Ni_4(L^{fur})_6(BF_4)_5\}^{3+}$; 834, $\{Ni_8(L^{fur})_{16}(BF_4)_9\}^{7+}$; and 719, $\{Ni_4(L^{fur})_6(BF_4)_4\}^{4+}$. The abundance of the two complexes cannot reliably be determined just from ESMS, however it is clear from the spectra that the tetranuclear square is stable in solution at least to some degree. The octanuclear complex does also exist in solution which is presumably a cube like the Co(II), Cu(II) and Zn(II) analogues, although other octanuclear complexes are known with different structures.[17]

4.2.4 Complexes of L^{th} with first-row transition metal dications: crystal structures of tetranuclear squares

The ligand L^{th} was combined with the same metal salts as L^{fur}; the structures formed with first row transition metals were all tetranuclear M_4L_6 squares.

The structure of $[Co_4(L^{th})_6](BF_4)_8$ is shown below in figure 4.2.4.1. It is a tetranuclear square, similar to $[Ni_4(L^{fur})_6](BF_4)_8$ described earlier, in that it has two double helices, linked by single bridging ligands which gives an alternating sequence of one and two bridging ligands along each edge of the square. However, it does have two important differences compared to the nickel structure. The first is that all four metal centres in $[Co_4(L^{th})_6](BF_4)_8$ have a meridional tris-chelate coordination environment. The second difference is that the pair of double helical subunits are not enantiomorphic but are instead homochiral. This is because the complex lies on a C_2 axis which is perpendicular to the Co_4 plane, and does not have an inversion centre like $[Ni_4(L^{fur})_6](BF_4)_8$.

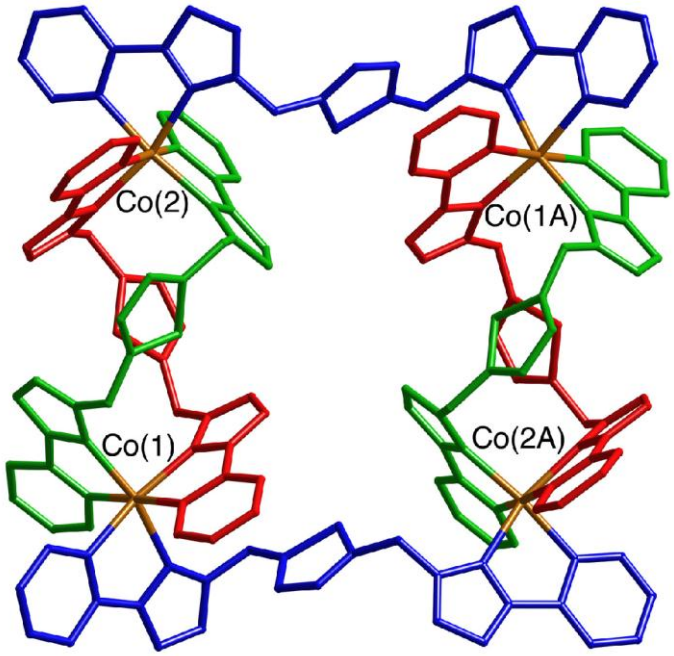

Figure 4.2.4.1 The entire complex cation of $[Co_4(L^{th})_6](BF_4)_8 \bullet 4MeNO_2$.

The two dinuclear double helicates are crystallographically equivalent and the average Co – N distance is 2.15 Å which is characteristic of a high-spin Co(II) complex. The Co•••Co distances are 9.38 Å within a dinuclear helical subunit and 10.53 Å between helical units.

The two thienyl units in the crosspiece ligands (blue in fig. 4.2.4.1) are stacked with one pyrazolyl-pyridine unit from one of the adjacent ligands of the double helical unit. The two thienyl units in the double helical unit are not π-stacked but instead are orientated so that the exocyclic lone pair is directed towards a pyrazolyl ring from the other ligand within the helical unit. The interaction between the two is clearly not strong because the distance from the S atom to the pyrazolyl is 3.52 Å (red ligand) and 3.62 Å (green ligand) which is just greater than the sum of the van der Waals radii for C and S which is 3.5 Å. This interaction is very similar to the one seen with the furan units earlier (figure 4.2.2.5).

As with the tetranuclear square $[Ni_4(L^{fur})_6](BF_4)_8$ earlier, there are anions located either side of the central cavity which are involved in CH•••F hydrogen bonding interactions. One of the $[BF_4]^-$ anions and the interactions it is involved in is shown in figure 4.2.4.2. The CH•••F distances are 3.21 Å [C(24A) – F(12A)] and 3.26 Å [C(46B) – F(13)]. The other $[BF_4]^-$ anion at the other side of the cavity is disordered and therefore the CH•••F

hydrogen bonding interactions cannot be discussed in detail although they are of a similar nature.

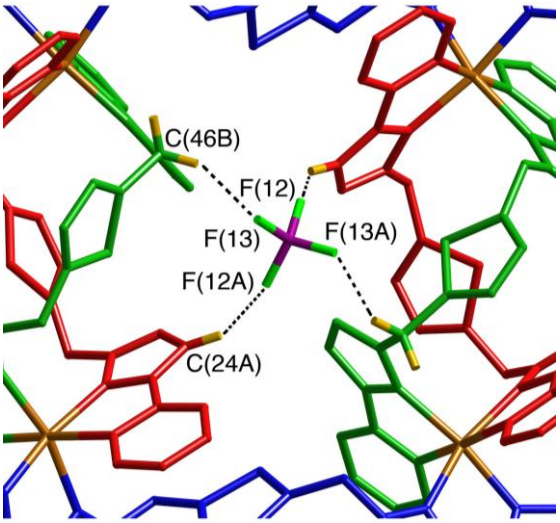

Figure 4.2.4.2 A view showing the CH•••F hydrogen-bonding interactions of the anion located near the central cavity.

The crystal structure of $[Ni_4(L^{th})_6](BF_4)_8$ is shown below in figure 4.2.4.3. It is a tetranuclear square very similar to the Co analogue although the two complexes are not crystallographically isomorphous. The two double helical subunits (Ni(1)/Ni(4) and Ni(2)/Ni(3)) in the crystal structure have the same chirality but are not crystallographically equivalent. This means that all four metal centres and all six ligands are in the asymmetric unit. All four metal centres have a mer tris-chelate coordination geometry with all Ni centres having very similar average Ni – N bond lengths (between 2.10 and 2.13 Å). The Ni – Ni distances do vary quite substantially between the double helical subunit and the single bridging unit. The distances are Ni(1)•••Ni(4), 9.43 Å; Ni(2)•••Ni(3), 9.08 Å; Ni(1)•••Ni(2), 10.29 Å; Ni(3)•••Ni(4), 10.73 Å. The structure again has $[BF_4]^-$ anions located just either side of the central cavity and the interactions are very similar to those of the Co analogue. The exocyclic lone pair on the sulphur atom is also orientated in the same way as in the Co analogue such that it is often pointed at the electron deficient pyrazolyl ring.

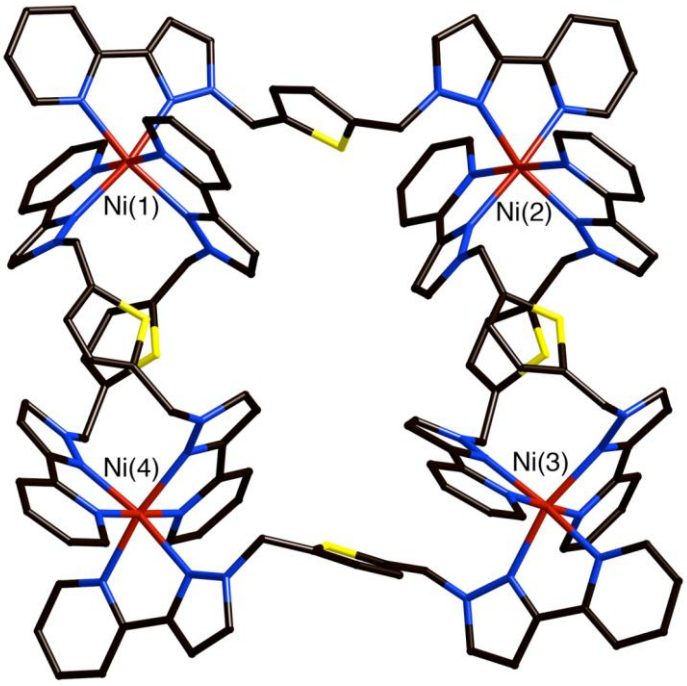

Figure 4.2.4.3 Structure of the complex cation of $[Ni_4(L^{th})_6](BF_4)_8$.

The structure of $[Cu_4(L^{th})_6](BF_4)_8$ is shown in figure 4.2.4.4 and is essentially identical to the Ni analogue except for one important difference. This is that the coordination environment around each Cu ion has Jahn-Teller distortion meaning that in each case the bond lengths in the pyrazole – pyrazole axis is elongated. This is common for Cu^{II} structures which are d^9 and results in average distance of Cu–N bonds in the equatorial plane of 2.04 Å and average distance of the long axial pair of Cu–N (pyrazole) bonds of 2.35 Å.

The structure is the same as that of the nickel analogue in that the two double helical subunits (Cu1/Cu4 and Cu2/Cu3) have the same chirality but are crystallographically inequivalent. All four metal centres are mer tris-chelate geometry and again the Cu – Cu distances are much smaller between the double helical units than for the single-bridged ligand. The distances are Cu(1)•••Cu(4), 9.16 Å; Ni(2)•••Ni(3), 9.25 Å; Cu(1)•••Cu(2), 10.14 Å; Cu(3)•••Cu(4), 11.17 Å. The tetrafluoroborate anions are located either side of the central cavity as in the nickel complex. Likewise the interactions of the sulphur exocyclic lone pairs with pyrazolyl-pyridine fragments of other ligands are also very similar to what was observed in the Ni(II) complex.

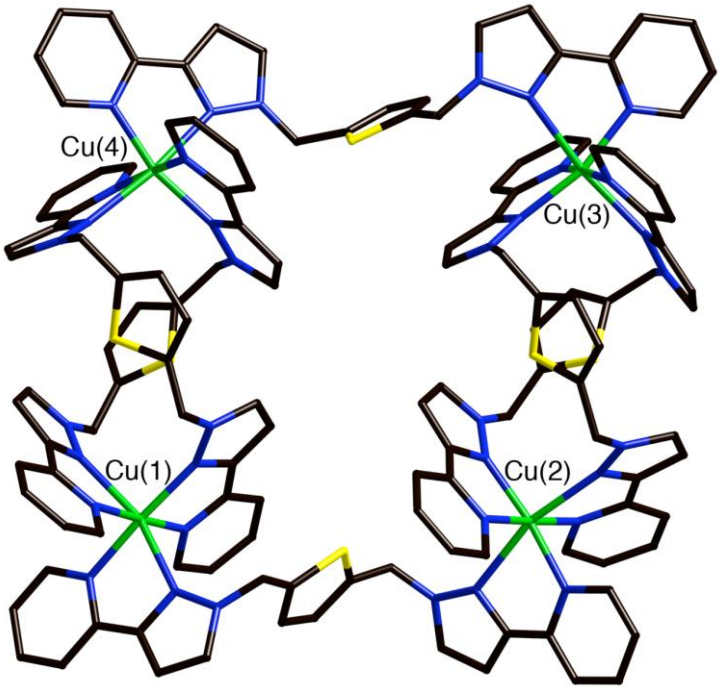

Figure 4.2.4.4 Structure of the complex cation of $[Cu_4(L^{th})_6](BF_4)_8$.

4.2.5 Complexes of L^{th} with first-row transition metal dications: solution studies

ESMS measurements and, where possible, ^{1}H NMR studies were undertaken to discover if these M_4L_6 squares with L^{th} are stable in solution. ESMS measurements of redissolved crystals of $[Co_4(L^{th})_6](BF_4)_8$ revealed three main sets of peaks. The first is the sequence corresponding to $\{[Co_4(L^{th})_6](BF_4)_{8-n}\}^{n+}$ (n = 2, 3, 4, 5, 6 at m/z = 1573, 1020, 743, 577, 466) which confirms the existence in solution of the square complex as seen in the crystal structure. The second sequence corresponds to $\{[Co_8(L^{th})_{12}](BF_4)_{16-n}\}^{n+}$ which again can be identified unambiguously due to the isotope spacings of the peaks (n = 3, 4, 5, 6 at m/z 2126, 1573, 1241, 1020). The peaks at 1573 and 1020 overlap between the two series although the peaks at 2126 and 1241 are unique and can only correspond to the octanuclear species. The final sequence of peaks is at a lower *m/z* value and presumably arises from fragmentation of the cage under the ESMS conditions. Two examples of these peaks occur at *m/z* values of 476 and 874 which correspond to $\{[Co(L^{th})]F\}^+$ and $\{[Co(L^{th})_2]F\}^+$. The fluoride has presumably arisen from decomposition of the $[BF_4]^-$ anion under the conditions of ESMS.

The ^{1}H NMR spectrum of $[Co_4(L^{th})_6](BF_4)_8$ suggests that the cage is stable in solution and was only fragmenting under the ESMS conditions. 27 peaks are expected in the ^{1}H NMR spectrum due to possible D_2 symmetry which would result in three mutually

perpendicular C_2 axes. This results in the four ligands in the double helices becoming equivalent although the two termini of the ligands are inequivalent and therefore would give 18 independent proton environments. The cross-piece ligands are also equivalent to each other and also have internal twofold symmetry such that the two termini of the ligands are equivalent. This gives 9 more environments resulting in a total of 27 environments, all of equal abundance. The ^{1}H NMR spectrum shown in figure 4.2.5.1 shows clearly 26 environments, with one presumably being obscured by residual solvent/water peaks in the 0-10 ppm region (or the peak is simply too broadened to be seen). The peaks are paramagnetically-shifted between +120 and -80 ppm and the different width of these signals reflects their different τ_1 values, which in turn depends on the sixth power of their distance from a high spin Co(II) ion.[16]

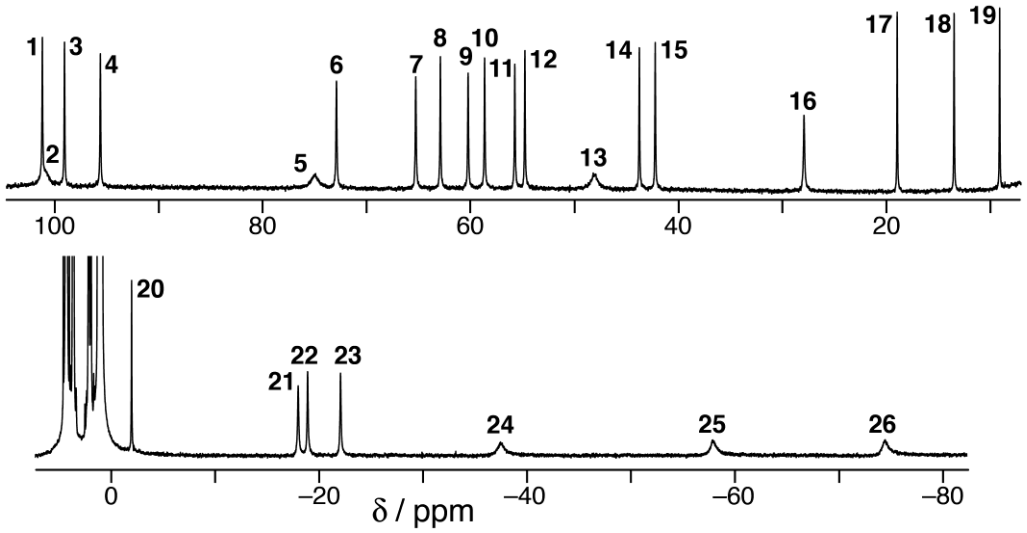

Figure 4.2.5.1 400 MHz ^{1}H NMR spectrum of $[Co_4(L^{th})_6](BF_4)_8$ in CD_3NO_2.

The ESMS of $[Ni_4(L^{th})_6](BF_4)_8$ is cleaner than that of $[Co_4(L^{th})_6](BF_4)_8$, showing a clear sequence of peaks corresponding to $\{[Ni_4(L^{th})_6](BF_4)_{8-n}\}^{n+}$ (n = 3, 4, 5, 6 at m/z 1020, 743, 577 and 476, respectively) with no evidence for any additional peaks from the $\{[Ni_8(L^{th})_{12}](BF_4)_{16-n}\}^{n+}$. For $[Cu_4(L^{th})_6](BF_4)_8$ there was significantly more fragmentation under the ESMS conditions. In fact the main peaks arose from the mononuclear fragments $\{[Cu(L^{th})]F\}^+$ and $\{[Cu(L^{th})_2]F\}^+$ (m/z 480 and 878, respectively) indicating that the square assembly is more fragile in solution and broke up under the conditions of the ESMS experiment. Whether or not the complex is stable in solution is however unclear as ^{1}H NMR spectroscopy is not useful for Cu(II) complexes.

4.2.6 Complexes of L^{fur} and L^{th} with Cd(II)

The two ligands, L^{fur} and L^{th}, were also combined with Cd(II) salts to see if the same tetranuclear and octanuclear structures resulted. Cd(II) has often given structures that are isostructural with those of the first row transition metal ions even though it has a significantly larger ionic radius (1.09 Å).[18] However in this case the two structures formed with Cd(II) are quite different from the structures seen with the first row transition metal dications.

When combined with L^{fur} the product is $[Cd(L^{fur})(BF_4)](BF_4)$ in which both pyrazolyl-pyridine units of L^{fur} are coordinated to a single Cd(II) ion (figure 4.2.6.1). There are two $[BF_4]^-$ anions, one coordinated to the Cd(II) ion and the other not. The O atom on the furan ring is directed at the Cd(II) ion; the Cd – O separation is 2.74 Å which signifies a weak interaction but one that surely plays a role in the formation of the mononuclear complex as opposed to a larger cage structure. The Cd – F distance for the coordinated $[BF_4]^-$ anion is 2.36 Å and the Cd(II) is therefore best considered as five-coordinate with a geometry approaching that of a square based pyramid ($\tau = 0.19$).[19] Selected bond distances of the complex are (Å): Cd(1)-N(42), 2.272; Cd(1)-N(22), 2.277; Cd(1)-N(31), 2.336; Cd(1)-N(11), 2.348; Cd(1)-F(62), 2.364; Cd(1)-O(55), 2.737. The ES mass spectrum showed the mononuclear complex to be the major product and showed that there were no tetra- or octa-nuclear species present; *m*/*z*; 581.6, $\{[Cd(L^{fur})][BF_4]\}^{1+}$; 247.4, $\{[Cd(L^{fur})]\}^{2+}$.

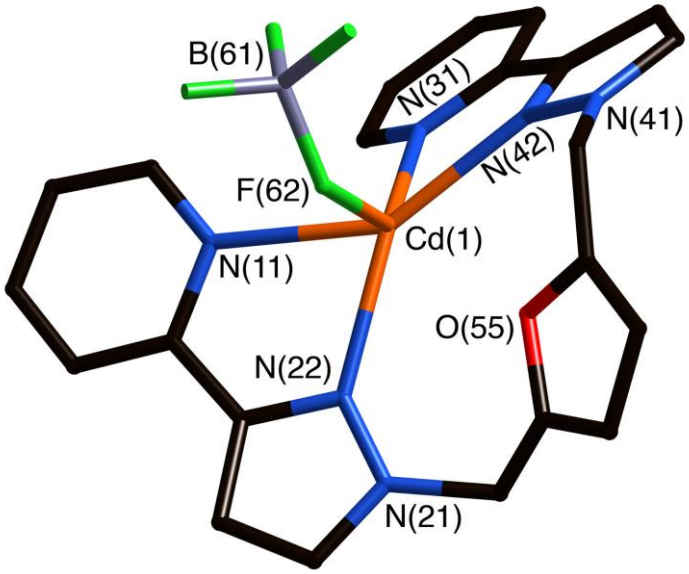

Figure 4.2.6.1 Structure of the complex cation of $[Cd(L^{fur})(BF_4)](BF_4)\bullet MeNO_2$.

The structure of the complex when Cd(II) is combined with L^{th} is quite different however; an infinite one-dimensional chain of the formula $\{[Cd_2(L^{th})_3](BF_4)_4\}_\infty$ is formed. The chain consists of double helical units which are cross-linked at each ends to different double helical units (shown in figure 4.2.6.2).

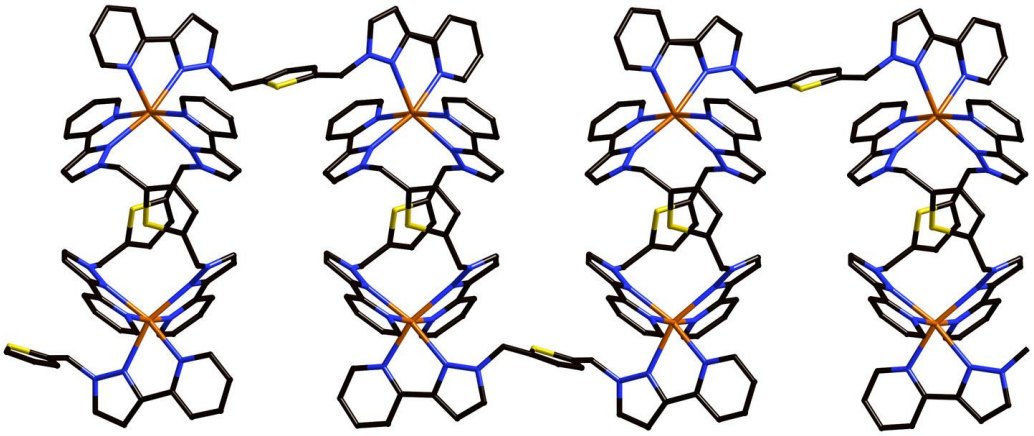

Figure 4.2.6.2 Structure of the zig-zag 'chain of double helicates' in $\{[Cd_2(L^{th})_3](BF_4)_4 \bullet 3MeNO_2\}_\infty$.

The 'crosspiece' ligands running along the top and bottom of the chain (shown in blue in Fig. 4.2.6.3) are disordered over two sites such that every pair of adjacent metal ions at the top and bottom of this view appears to be spanned by a ligand with 50% occupancy; only one component of the disorder is shown. The Cd – Cd separation within a double helical subunit is 8.76 Å and the separation between double helicates is 11.16 Å. The double helical units are C_2-symmetric and all Cd ions are crystallographically equivalent. The Cd ions have *mer* tris-chelate geometry with an average Cd – N distance of 2.34 Å.

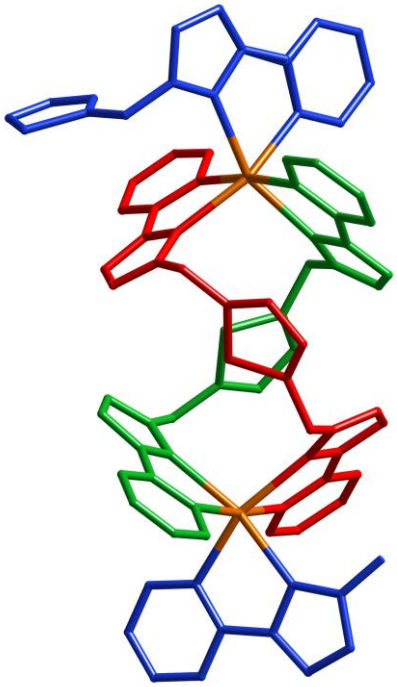

Figure 4.2.6.3 Structure of one double helical subunit in $\{[Cd_2(L^{th})_3](BF_4)_4\}_\infty$.

The infinite chain structure has many similarities to the tetranuclear square complexes described previously with this ligand. Both structures have double helical units although the way that these are connected changes. It could be imagined that one can interconvert between the two structures simply by rearranging one of the crosspiece ligands so that instead of connecting to the same double helicate it connects to a different one or *vice-versa* (figure 4.2.6.4).

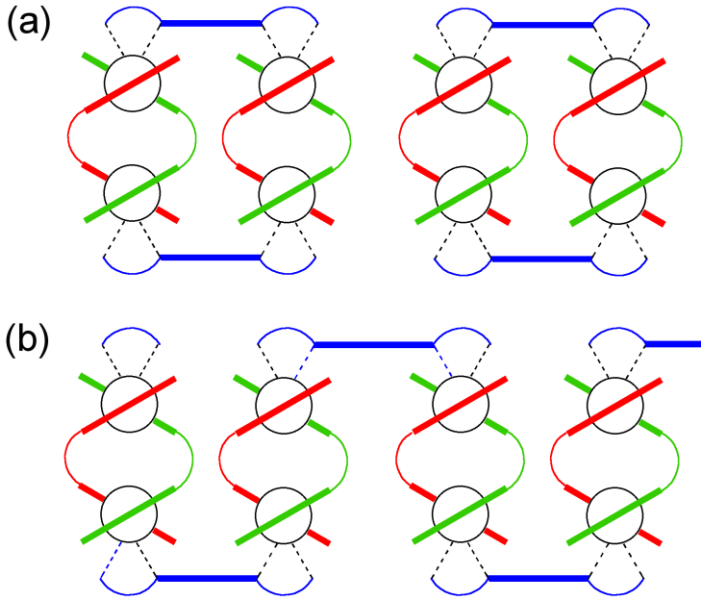

Figure 4.2.6.4 Schematic representation of the relationship between (a) squares such as $[Co_4(L^{th})_6](BF_4)_8$ and (b) the one-dimensional infinite chain of crosslinked double helicates which occurs in $\{[Cd_2(L^{th})_3](BF_4)_4\}_\infty$.

It is interesting that L^{th} does not coordinate to just one Cd(II) ion like L^{fur} does. This is most likely because the thiophene has much poorer coordination ability than furan, and therefore it is less favourable for the ligand to wrap around a single metal ion in a pentadentate coordination mode. The other reason why the mononuclear complex is less likely for L^{th} is because the distance between the two methylene carbons is much longer. The distance between these two carbons in the double helical unit of $\{[Cd_2(L^{th})_3](BF_4)_4\}_\infty$ is 5.392 Å, compared to 4.842 Å in $[Cd(L^{fur})(BF_4)](BF_4)$. The longer distance makes the two pyrazolyl-pyridine groups further apart and less likely to chelate to the same metal ion.

4.3 Conclusion

The ultimate aim of this work was to see if the exocyclic lone pair of the ligand could be utilised for host-guest chemistry inside the cavity of a coordination cage. This aim is yet to be fulfilled although there are signs that it could be achieved in the future. A series of octanuclear cubes with L^{fur} and tetranuclear squares with L^{th} were synthesised and characterised. The structures changed dramatically with Cd(II) due to the larger

ionic radius of the metal ion, which for L^{fur} allowed the ligand to wrap around a single metal ion.

The structures with L^{th} all contained double helical subunits within them although there were a range of different structures. This appeared to be the case because the sulphur atom in the thiophene ring was always pointed at a pyrazole ring of another ligand which seems to be a favourable non-covalent interaction stabilising each double helix. The structures with L^{fur} were more varied and with Cd(II) the ligand could wrap around a single metal ion and the oxygen atom was pseudo-coordinated to it. This presumably occurred with L^{fur} and not L^{th} because the oxygen in the furan ring is more nucleophilic than the sulphur in the thiophene ring and because the two pyrazolyl-pyridine groups are closer together and therefore it is easier to coordinate to the same Cd(II) ion.

It is hoped that in the future the exocyclic lone pairs of either the oxygen or the sulphur can be utilised for host-guest chemistry inside a cage or in the middle of a tetranuclear square. A series of suitable hydrogen bond acceptor guests will be tried for this purpose.

4.4 Experimental

Synthesis of L^{fur}

2,5-dimethylfuran (1.00 g, 10.4 mmol), N-Bromosuccinimide (4.00 g, 22.5 mmol) and AIBN (0.01 g) were stirred in CCl_4 (60 mL) for 16 hours at 60 °C. The excess NBS was removed by hot filtration and the CCl_4 removed *in vacuo*. The resultant white residue (undried) was reacted immediately with 3-(2-pyridyl)pyrazole (3.10 g, 21.4 mmol) and NaOH (7.50 g in 20 mL H_2O) in THF (120 mL) at 70 °C for 20 hours. The organic layer was separated, dried over $MgSO_4$ and concentrated before purification using an alumina column eluted with DCM / MeOH(1%) giving an off-white solid L^{fur} (Yield: 1.89 g, 48%).

^{1}H-NMR (400 MHz, $CDCl_3$): δ 8.64 (2H, ddd, pyridyl H^6), 7.93 (2H, dt, pyridyl H^3), 7.72 (2H, td, pyridyl H^4), 7.47 (2H, d, pyrazolyl H^5), 7.21 (2H, m, pyridyl H^5), 6.90 (2H, d, pyrazolyl H^4), 6.37 (2H, s, Furan H), 5.36 (4H, s, CH_2). ESMS m/z calc. for $[M + H]^+$ 383.1620 found 383.1626. Anal. Calcd for $C_{22}H_{18}N_6O$: C 69.1; H, 4.7; N, 22.0% Found: C, 69.3; H, 4.8; N, 21.9%.

Synthesis of L^{th}

2,5-dimethylthiophene (1.00 g, 8.9 mmol), N-Bromosuccinimide (3.74 g, 21.0 mmol) and AIBN (0.01 g) were stirred in CCl_4 (60 mL) for 16 hours at 60 °C. The excess NBS was removed by hot filtration and the CCl_4 removed *in vacuo*. The resultant white residue (undried) was reacted immediately with 3-(2-pyridyl)pyrazole (2.80 g, 19.3 mmol) and NaOH (7.00 g in 20 mL H_2O) in THF (120 mL) at 70 °C for 20 hours. The organic layer was separated, dried over $MgSO_4$ and concentrated before purification using an alumina column eluted with DCM / MeOH(1%) giving an off-white solid L^{th} (Yield: 1.63 g, 46%).

^{1}H-NMR (400 MHz, $CDCl_3$): δ 8.63 (2H, ddd, pyridyl H^6), 7.94 (2H, dt, pyridyl H^3), 7.72 (2H, td, pyridyl H^4), 7.46 (2H, d, pyrazolyl H^5), 7.21 (2H, m, pyridyl H^5), 6.94 (2H, s, thiophene H), 6.90 (2H, d, pyrazolyl H^4), 5.49 (4H, s, CH_2). ESMS m/z calc. for $[M + H]^+$ 399.1392 found 399.1385. Anal. Calcd for $C_{22}H_{18}N_6S$: C 66.3; H, 4.6; N, 21.1% Found: C, 66.0; H, 4.3; N, 21.0%.

Synthesis of L^{fur} complexes:

$[Cu_8(L^{fur})_{12}](BF_4)_{16}$

A solution of $Cu(BF_4)_2$ (0.029 g, 0.09 mmol) in MeOH (7 cm^3) was added to a solution of L^{fur} (0.050 g, 0.13 mmol) in CH_2Cl_2 (7 cm^3). The mixture was stirred at room temperature for 24 h, and the resultant precipitate was filtered off, washed with both MeOH and CH_2Cl_2, and dried *in vacuo* to give $[Cu_8(L^{fur})_{12}](BF_4)_{16}$ as a green powder in 86% yield. X-ray quality crystals were grown by slow diffusion of isopropyl ether into a solution of the complex in nitromethane.

ESMS: *m*/*z*; 2075.2, $\{[Cu_8(L^{fur})_{12})][BF_4]_{13}\}^{3+}$; 1534.7, $\{[Cu_8(L^{fur})_{12})][BF_4]_{12}\}^{4+}$; 1210.4, $\{[Cu_8(L^{fur})_{12})][BF_4]_{11}\}^{5+}$; 994.2, $\{[Cu_8(L^{fur})_{12})][BF_4]_{10}\}^{6+}$. Anal. Calcd for $Cu_8C_{264}H_{216}N_{72}O_{12}B_{16}F_{64}$: C 48.9; H, 3.4; N, 15.5% Found: C, 48.3; H, 3.3; N, 15.7%.

$[Co_8(L^{fur})_{12}](BF_4)_{16}$

A Teflon-lined autoclave was charged with $Co(BF_4)_2$ (0.030 g, 0.09 mmol), L^{fur} (0.050 g, 0.13 mmol), and methanol (9 cm^3). The mixture was heated to 100 °C for 12 h and then cooled slowly to room temperature to yield $[Co_8(L^{fur})_{12}](BF_4)_{16}$ as an orange powder in 75% yield. X-ray quality crystals were grown by slow diffusion of isopropyl ether into a solution of the complex in acetonitrile.

ESMS: *m*/*z*; 3137.7, $\{[Co_8(L^{fur})_{12})][BF_4]_{14}\}^{2+}$; 2062.9, $\{[Co_8(L^{fur})_{12})][BF_4]_{13}\}^{3+}$; 1525.5, $\{[Co_8(L^{fur})_{12})][BF_4]_{12}\}^{4+}$; 1203.0, $\{[Co_8(L^{fur})_{12})][BF_4]_{11}\}^{5+}$; 988.0, $\{[Co_8(L^{fur})_{12})][BF_4]_{10}\}^{6+}$. Anal. Calcd for $Co_8C_{264}H_{216}N_{72}O_{12}B_{16}F_{64}$: C 49.2; H, 3.4; N, 15.6% Found: C, 48.9; H, 3.6; N, 15.5%.

The crystal structure of this complex could be solved but only with a very high R-factor and therefore was not discussed, although it was clearly isostructural with that of $[Zn_8(L^{fur})_{12}](ClO_4)_{16}$.

$[Zn_8(L^{fur})_{12}](ClO_4)_{16}$

A solution of $Zn(ClO_4)_2$ (0.033 g, 0.09 mmol) in MeOH (7 cm^3) was added to a solution of L^{fur} (0.050 g, 0.13 mmol) in CH_2Cl_2 (7 cm^3). The mixture was stirred at room temperature for 24 h, and the resultant precipitate was filtered off, washed with both

MeOH and CH_2Cl_2, and dried *in vacuo* to give $[Zn_8(L^{fur})_{12}](ClO_4)_{16}$ as an off-white powder in 79% yield. X-ray quality crystals were grown by slow diffusion of isopropyl ether into a solution of the complex in nitromethane.

ESMS: *m*/*z*; 2132.8, $\{[Zn_8(L^{fur})_{12})][ClO_4]_{13}\}^{3+}$; 1574.8, $\{[Zn_8(L^{fur})_{12})][ClO_4]_{12}\}^{4+}$; 1240.1, $\{[Zn_8(L^{fur})_{12})][ClO_4]_{11}\}^{5+}$; 1016.9, $\{[Zn_8(L^{fur})_{12})][ClO_4]_{10}\}^{6+}$. Anal. Calcd for $Zn_8C_{264}H_{216}N_{72}O_{12}Cl_{16}O_{64}$: C 47.3; H, 3.2; N, 15.0% Found: C, 47.0; H, 3.0; N, 14.6%.

$[Ni_4(L^{fur})_6](BF_4)_8$

A solution of $Ni(BF_4)_2$ (0.030 g, 0.09 mmol) in MeOH (7 cm^3) was added to a solution of L^{fur} (0.050 g, 0.13 mmol) in CH_2Cl_2 (7 cm^3). The mixture was stirred at room temperature for 24 h, and the resultant precipitate was filtered off, washed with both MeOH and CH_2Cl_2, and dried *in vacuo* to give $[Ni_4(L^{fur})_6](BF_4)_8$ as a purple powder in 69% yield. X-ray quality crystals were grown by slow diffusion of isopropyl ether into a solution of the complex in nitromethane.

ESMS: *m*/*z*; 1525.0, $\{[Ni_4(L^{fur})_6)][BF_4]_6\}^{2+}$; 987.7, $\{[Ni_4(L^{fur})_6)][BF_4]_5\}^{3+}$; 719.1, $\{[Ni_4(L^{fur})_6)][BF_4]_4\}^{4+}$; 557.9, $\{[Ni_4(L^{fur})_6)][BF_4]_3\}^{5+}$; 450.5, $\{[Ni_4(L^{fur})_6)][BF_4]_2\}^{6+}$. Anal. Calcd for $Ni_4C_{132}H_{108}N_{36}O_6B_8F_{32}$: C 49.2; H, 3.4; N, 15.6% Found: C, 48.9; H, 3.3; N, 15.6%.

$[Cd(L^{fur})(BF_4)](BF_4)$

A solution of $Cd(BF_4)_2$ (0.034 g, 0.09 mmol) in MeOH (7 cm^3) was added to a solution of L^{fur} (0.050 g, 0.13 mmol) in CH_2Cl_2 (7 cm^3). The mixture was stirred at room temperature for 24 h, and the resultant precipitate was filtered off, washed with both MeOH and CH_2Cl_2, and dried *in vacuo* to give $[Cd(L^{fur})(BF_4)](BF_4)$ as a white powder in 82% yield. X-ray quality crystals were grown by slow diffusion of isopropyl ether into a solution of the complex in nitromethane.

ESMS: *m*/*z*; 581.6, $\{[Cd(L^{fur}))][BF_4]\}^{1+}$; 247.4, $\{[Cd(L^{fur}))]\ \}^{2+}$. Anal. Calcd for $CdC_{22}H_{18}N_6OB_2F_8$: C 39.5; H, 2.7; N, 12.6% Found: C, 40.0; H, 3.0; N, 12.4%.

Synthesis of L^{th} complexes:

$[Cu_4(L^{th})_6](BF_4)_8$

A solution of $Cu(BF_4)_2$ (0.027 g, 0.08 mmol) in MeOH (7 cm^3) was added to a solution of L^{th} (0.050 g, 0.12 mmol) in CH_2Cl_2 (7 cm^3). The mixture was stirred at room temperature for 24 h, and the resultant precipitate was filtered off, washed with both MeOH and CH_2Cl_2, and dried *in vacuo* to give $[Cu_4(L^{th})_6](BF_4)_8$ as a green powder in 81% yield. X-ray quality crystals were grown by slow diffusion of isopropyl ether into a solution of the complex in acetonitrile.

ESMS: *m*/*z*; 1583.0, $\{[Cu_4(L^{th})_6)][BF_4]_6\}^{2+}$; 1026.4, $\{[Cu_4(L^{th})_6)][BF_4]_5\}^{3+}$; 748.1, $\{[Cu_4(L^{th})_6)][BF_4]_4\}^{4+}$; 581.1, $\{[Cu_4(L^{th})_6)][BF_4]_3\}^{5+}$. Anal. Calcd for $Cu_4C_{132}H_{108}N_{36}S_6B_8F_{32}$: C 47.5; H, 3.3; N, 15.1% Found: C, 47.2; H, 3.2; N, 14.8%.

$[Co_4(L^{th})_6](BF_4)_8$

A Teflon-lined autoclave was charged with $Co(BF_4)_2$ (0.028 g, 0.08 mmol), L^{th} (0.050 g, 0.12 mmol), and methanol (9 cm^3). The mixture was heated to 100 °C for 12 h and then cooled slowly to room temperature to yield $[Co_4(L^{th})_6](BF_4)_8$ as an orange powder in 67% yield. X-ray quality crystals were grown by slow diffusion of isopropyl ether into a solution of the complex in nitromethane.

ESMS: *m*/*z*; 1573.8, $\{[Co_4(L^{th})_6)][BF_4]_6\}^{2+}$; 1020.2, $\{[Co_4(L^{th})_6)][BF_4]_5\}^{3+}$; 743.5, $\{[Co_4(L^{th})_6)][BF_4]_4\}^{4+}$; 577.4, $\{[Co_4(L^{th})_6)][BF_4]_3\}^{5+}$; 466.7, $\{[Co_4(L^{th})_6)][BF_4]_2\}^{6+}$. Anal. Calcd for $Co_4C_{132}H_{108}N_{36}S_6B_8F_{32}$: C 47.7; H, 3.3; N, 15.2% Found: C, 45.1; H, 3.1; N, 15.0%.

$[Ni_4(L^{th})_6](BF_4)_8$

A Teflon-lined autoclave was charged with $Ni(BF_4)_2$ (0.028 g, 0.08 mmol), L^{th} (0.050 g, 0.12 mmol), and methanol (9 cm^3). The mixture was heated to 100 °C for 12 h and then cooled slowly to room temperature to yield $[Ni_4(L^{th})_6](BF_4)_8$ as a purple powder in 72% yield. X-ray quality crystals were grown by slow diffusion of isopropyl ether into a solution of the complex in acetonitrile.

ESMS: *m*/*z*; 1573.3, $\{[Ni_4(L^{th})_6)][BF_4]_6\}^{2+}$; 1019.9, $\{[Ni_4(L^{th})_6)][BF_4]_5\}^{3+}$; 743.2, $\{[Ni_4(L^{th})_6)][BF_4]_4\}^{4+}$; 577.2, $\{[Ni_4(L^{th})_6)][BF_4]_3\}^{5+}$; 466.6, $\{[Ni_4(L^{th})_6)][BF_4]_2\}^{6+}$. Anal. Calcd for $Ni_4C_{132}H_{108}N_{36}S_6B_8F_{32}$: C 47.8; H, 3.3; N, 15.2% Found: C, 47.5; H, 3.1; N, 14.9%.

$\{[Cd_2(L^{th})_3](BF_4)_4\}_\infty$

A Teflon-lined autoclave was charged with $Cd(BF_4)_2$ (0.033 g, 0.08 mmol), L^{th} (0.050 g, 0.12 mmol), and methanol (9 cm^3). The mixture was heated to 100 °C for 12 h and then cooled slowly to room temperature to yield $\{[Cd_2(L^{th})_3](BF_4)_4\}_\infty$ as a white powder in 61% yield. X-ray quality crystals were grown by slow diffusion of isopropyl ether into a solution of the complex in nitromethane.

ESMS: *m*/*z*; 797.0, $\{[Cd_2(L^{th})_3)\ [BF_4]_2]\ \}^{2+}$; 502.4, $\{[Cd_2(L^{th})_3)\ [BF_4]]\ \}^{3+}$. Anal. Calcd for $Cd_2C_{66}H_{54}N_{18}S_3B_4F_{16}$: C 44.8; H, 3.1; N, 14.3% Found: C, 44.4; H, 3.0; N, 14.0%.

4.5 X-ray Crystallography

In each case a suitable crystal was mounted in a stream of cold N_2 on a Bruker APEX-2 or SMART CCD diffractometer equipped with graphite-monochromated Mo-Kα radiation from a sealed-tube source. Details of the crystal, data collection and refinement parameters are summarised. Data were corrected for absorption using empirical methods (SADABS)[20] based upon symmetry-equivalent reflections combined with measurements at different azimuthal angles. The structures were solved by direct methods and refined by full-matrix least squares on weighted F^2 values for all reflections using the SHELX suite of programs.[21] Non-hydrogen atoms were refined anisotropically. Hydrogen atoms were placed in calculated positions, refined using idealized geometries (riding model) and were assigned fixed isotropic displacement parameters. Several of the structures of metal complexes presented problems during data collection and refinement due to rapid solvent loss and/or anion disorder which resulted in weak scattering, necessitating extensive use of restraints during refinement to ensure reasonable geometries for counter-ions and aromatic rings. Often not all of the counter-ions could be located; in addition severely disordered solvent molecules could not be modelled satisfactorily. The resulting areas of diffuse electron density that could not be modelled were eliminated using the 'Squeeze' function in PLATON. The treatments of these issues are discussed in detail in the individual CIFs.

Crystal Data Tables

Summary of crystallographic data for the new compounds:

Compound	**$[Cu_8(L^{fur})_{12}](BF_4)_{16}$ •2($MeNO_2$)** [a]	**$[Zn_8(L^{fur})_{12}](ClO_4)_{16}$ •2.5($MeNO_2$)**	**$[Ni_4(L^{fur})_6](BF_4)_8$ •16($MeNO_2$)**
Formula	$C_{266}H_{222}B_{16}Cu_8F_{64}N_{74}O_{16}$	$C_{266.5}H_{223.5}Cl_{16}N_{74.5}O_{81}Zn_8$	$C_{148}H_{156}B_8F_{32}N_{52}Ni_4O_{38}$
Molecular weight	6608.46	13711.72	4200.57
T / *K*	100(2)	100(2)	100(2)
Crystal system	Tetragonal	Monoclinic	Triclinic
Space group	*P*–4	$P2_1/c$	*P*–1
a / Å	22.1963(4)	25.726(5)	13.0255(4)
b / Å	22.1963(4)	42.927(9)	19.7988(7)
c / Å	40.2890(11)	66.265(14)	20.0373(7)
α / °	90	90	112.172(2)
β / °	90	94.909(13)	98.864(2)
γ / °	90	90	94.268(2)
V / $Å^3$	19849.4(7)	72910(26)	4678.3(3)
Z	2	8	1
ρ / g cm^{-3}	1.106	1.168	1.491
μ / mm^{-1}	0.504	0.674	0.514
Data, restraints, parameters, R_{int}	33832 / 229 / 1480 / 0.1011	83175 / 2972 / 3090 / 0.1915	11895 / 108 / 1053 / 0.0860
Final *R*1, *wR*2 [c]	0.0807, 0.2203	0.1298, 0.3709	0.0825, 0.2390

Compound	**$[Co_4(L^{th})_6](BF_4)_8$ •4MeNO$_2$**	**$[Ni_4(L^{th})_6](BF_4)_8$ •4MeCN[b]**	**$[Cu_4(L^{th})_6](BF_4)_8$**
Formula	$C_{136}H_{120}B_8Co_4F_{32}N_{40}O_8S_6$	$C_{140}H_{120}B_8F_{32}N_{40}Ni_4S_6$	$C_{132}H_{108}B_8Cu_4F_{32}N_{36}S_6$
Molecular weight	3565.28	3484.44	3339.54
T / *K*	150(2)	150(2)	100(2)
Crystal system	Monoclinic	Orthorhombic	Monoclinic
Space group	*C*2/c	*P*mn2$_1$	*C*2/c
a / Å	25.7813(7)	43.1698(8)	54.137(9)
b / Å	18.2941(7)	18.8181(4)	18.521(3)
c / Å	39.8811(13)	20.4261(4)	43.001(12)
α / °	90	90	90
β / °	90.621(3)	90	125.747(2)
γ / °	90	90	90
V / Å^3	18808.6(11)	16593.6(6)	34993(13)
Z	4	4	8
ρ / g cm^{-3}	1.259	1.395	1.268
μ / mm^{-1}	0.502	0.618	0.638
Data, restraints, parameters, R_{int}	12291 / 868 / 940 / 0.0819	38716 / 97 / 737 / 0.0575	22867 / 1834 / 1411 / 0.1015
Final *R*1, *wR*2[c]	0.1091, 0.3369	0.1381, 0.3966	0.1071, 0.3222

Compound	**$[Cd(L^{fur})(BF_4)](BF_4)$ $\bullet MeNO_2$**	**$\{[Cd_2(L^{th})_3](BF_4)_4$ $\bullet 3(MeNO_2)\}_\infty$**
Formula	$C_{23}H_{21}B_2CdF_8N_7O_3$	$C_{69}H_{63}B_4Cd_2F_{16}N_{21}O_6S_3$
Molecular weight	729.49	1950.62
T / *K*	100(2)	150(2)
Crystal system	Triclinic	Monoclinic
Space group	*P*–1	*C*2/c
a / Å	7.1886(5)	35.6228(8)
b / Å	13.5594(10)	11.1598(2)
c / Å	15.0061(11)	22.6321(7)
α / °	104.558(3)	90
β / °	101.438(3)	108.367(2)
γ / °	102.818(3)	90
V / $Å^3$	1329.48(17)	8538.9(4)
Z	2	4
ρ / g cm^{-3}	1.822	1.517
μ / mm^{-1}	0.920	0.667
Data, restraints, parameters, R_{int}	5629 / 68 / 398 / 0.0507	9007 / 1276 / 781 / 0.0442
Final *R*1, *wR*2[c]	0.0463, 0.1199	0.1249, 0.4167

[a] Absolute structure parameter: 0.020(12)
[b] Absolute structure parameter: 0.46(2) indicating a racemic twin.
[c] The value of *R*1 is based on 'observed' data with $I>2\sigma(I)$; the value of *wR*2 is based on all data.

4.6 References

1. P. Lenain, M. Mandado, R. A. Mosquera and P. Bultinck, *J. Phys. Chem. A*, 2008, **112**, 7898.

2. M. Tominaga, K. Suzuki, M. Kawano, T. Kusukawa, T. Ozeki, S. Sakamoto, K. Yamaguchi, M. Fujita, *Angew. Chem. Int. Ed.*, 2004, **43**, 5621.

3. Q.-F. Sun, J. Iwasa, D. Ogawa, Y. Ishido, S. Sato, T. Ozeki, Y. Sei, K. Yamaguchi, M. Fujita, *Science*, 2010, **328**, 1144.

4. C. J. Kuehl, S. D. Huang and P. J. Stang, *J. Am. Chem. Soc.*, 2001, **123**, 9634.

5. D. Gupta, P. Rajakannu, B. Shankar, R. Shanmugam, F. Hussain, B. Sarkar and M. Sathiyendiran, *Dalton Trans.*, 2011, **40**, 5433.

6. F. E. Wolter, K. Schneider, B. P. Davies, E. R. Socher, G. Nicholson, O. Seitz and R. D. Süssmuth, *Org. Lett.*, 2009, **11**, 2804.

7. O. Gidron, Y. D. Posner and M. Bendikov, *J. Am. Chem. Soc.*, 2010, **132**, 2148.

8. P. Leriche, S. Roquet, N. Pillerel, G. Mabon and P. Frere, *Tetrahedron Lett.*, 2003, **44**, 1623.

9. G. A. Sotzing, J. R. Reynolds and P. J. Steel, *Chem. Mater.*, 1996, **8**, 882.

10. T. Matsuura, M. Nakajima and Y. Shimoyama, *Jpn. J. Appl. Phys*., 2001, **40**, 6945.

11. M. Morimoto and M. Irie, *Chem. Commun*., 2011, **47**, 4186.

12. Y. Liu, J. Li, H. Cao, B. Qu, Z. Chen, Q. Gong, S. Xu and S. Cao, *Polym. Adv. Technol.*, 2006, **17**, 468.

13. A. Najar, I. S. Tidmarsh, H. Adams and M. D. Ward, *Inorg. Chem.*, 2009, **48**, 11871.

14. I. S. Tidmarsh, T. B. Faust, H. Adams, L. P. Harding, L Russo, W. Clegg and M. D. Ward, *J. Am. Chem. Soc.*, 2008, **130**, 15167.

15. A. Stephenson, S. P. Argent, T, Riis-Johannessen, I. S. Tidmarsh and M. D. Ward, *J. Am. Chem. Soc.*, 2011, **133**, 858.

16. I. S. Tidmarsh, B. F. Taylor, M. J. Hardie, L. Russo, W. Clegg and M. D. Ward, *New J. Chem.*, 2009, **33**, 366.

17. A. Stephenson and M. D. Ward, *Dalton Trans.*, 2011, **40**, 7824.

18. M. D. Ward, *Chem Commun*., 2009, 4487.

19. A. W. Addison , T. N. Rao , J. Reedijk , J. van Rijn and G. C. Verschoor, *J. Chem. Soc., Dalton Trans.*, 1984, 1349.

20. G. M. Sheldrick, *SADABS*: *A program for absorption correction with the Siemens SMART system*, University of Göttingen, Germany, 1996.

21. G. M. Sheldrick, *Acta Crystallogr. Sect. A*, 2008, **64**, 112.

5. Coordination chemistry of Ag(I) with bridging ligands based on pyrazolyl-pyridine termini; polymers, helicates, a bow-tie and a 'triple helix of double helicates'

5.1 Introduction

Recent investigations by the Ward group into the self-assembly of polyhedral coordination cages has led to the identification of a large family of bis-bidentate bridging ligands which contain two pyrazolyl-pyridine termini connected *via* methylene bridges to a central aromatic core.[1] These ligands have generally been reacted with labile octahedral metal ions to form a range of polyhedral coordination cages based on a 2:3 metal-to-ligand ratio, including examples ranging from M_4L_6 tetrahedra[2] to $M_{16}L_{24}$ capped truncated tetrahedra.[3]

An alternative to using octahedral metal ions is to use Ag(I) ions which are generally four-coordinate with ligands of this type.[4] Assembly with bis-bidentate bridging ligands should afford complexes possessing a 1:1 metal-to-ligand ratio in order for coordinative saturation of the metal ions. There are various possibilities of complexes that could arise with this formula, ranging from dinuclear double helicates $[M_2L_2]$ to infinite coordination polymers $[M_1L_1]_\infty$. Ag(I) also has the additional benefits that it can be used for ^{1}H NMR and that it will not quench ligand-based luminescence.[5] Ag(I) being a d^{10} ion has no stereoelectronic preference and is particularly adaptable for different geometric requirements of different ligands. This combined with the potential Ag•••Ag interactions adds an extra dimension to the use of Ag(I) in metallosupramolecular chemistry.[6-11] Ag(I) complexes have been studied extensively and have previously been shown to have useful properties in the areas of host-guest chemistry,[12] sensing,[13] catalysis[14] and conductivity.[15]

The polyhedral coordination cages based on octahedral metal ions are largely stabilised by π-stacking between relatively electron deficient pyrazolyl-pyridine groups and relatively electron rich aromatic spacers.[1] These interactions and others such as

argentophilic Ag•••Ag interactions,[16] pyrazolyl-pyridine stacking[17] and exocyclic lone pair interactions[18] will influence the complexes that are formed.

A remarkable range of Ag(I) complexes based in part on different supramolecular interactions has emerged. The structures have been characterised by X-ray crystallography, elemental analysis and their solution behaviour studied by ^{1}H NMR and ESMS.

5.2 Results and Discussion

5.2.1 Synthesis of ligands

The ligands used in this study are shown in figure 5.2.1.1. They are all bis-bidentate and only differ in the 'spacer' between the two pyrazolyl-pyridine units.

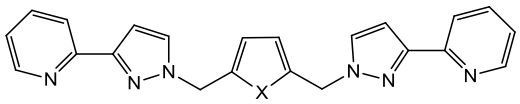

L^{fur}: X = O, L^{th}: X = S

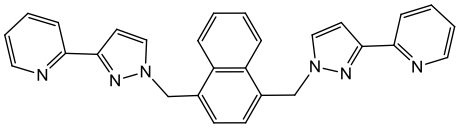

L^{14naph}

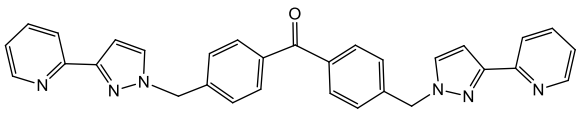

L^{bz}

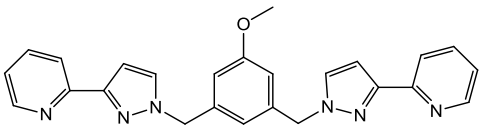

L^{OMe}

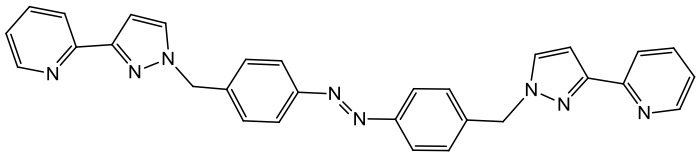

L^{azo}

Figure 5.2.1.1 The ligands combined with Ag(I).

The ligands L^{fur}, L^{th}, and L^{14naph} were synthesised as previously described in chapters 3 and 4. L^{azo}, L^{bz} and L^{OMe} were synthesised in the usual way by reaction of 3-(2-

pyridyl)pyrazole with the respective bis(bromomethyl) aromatic derivative under basic conditions. Full details are given in the experimental section.

5.2.2 A mononuclear structure with L^{fur} and Ag(I)

The ligand L^{fur} consists of two chelating pyrazolyl-pyridine termini connected to a furan-2,5-diyl spacer *via* methylene groups. It has been shown in chapter 4 to form cubic $[M_8L_{12}]^{16+}$ cages (M=Zn, Co, Cu) and a mononuclear complex with Cd(II) where the ligand wraps around a single metal ion.[19]

The structure obtained when L^{fur} was combined with $AgClO_4$ in a 1:1 ratio was also a mononuclear complex with the ligand wrapping around a single Ag(I) ion. This is perhaps unsurprising given the previous example with Cd(II) which has a smaller ionic radius than Ag(I) (1.09 compared to 1.29 Å) and the larger ionic radius of the second row transition metal was presumed to be the reason why it had not yielded a M_8L_{12} cube like the first row octahedral metal ions. The structure does have some interesting features in the crystal packing and unusually there are three crystallographically independent molecules of $[Ag(L^{fur})]ClO_4$ in the asymmetric unit as shown in figure 5.2.2.1.

All three mononuclear complexes are structurally quite similar with the two pyrazolyl-pyridine termini of L^{fur} providing irregular tetradentate chelating coordination with Ag–N distances in the range 2.23 – 2.56 Å. The central furan unit has a long, weak Ag•••O contact similar to the one seen previously in the Cd analogue (figure 5.2.2.1).

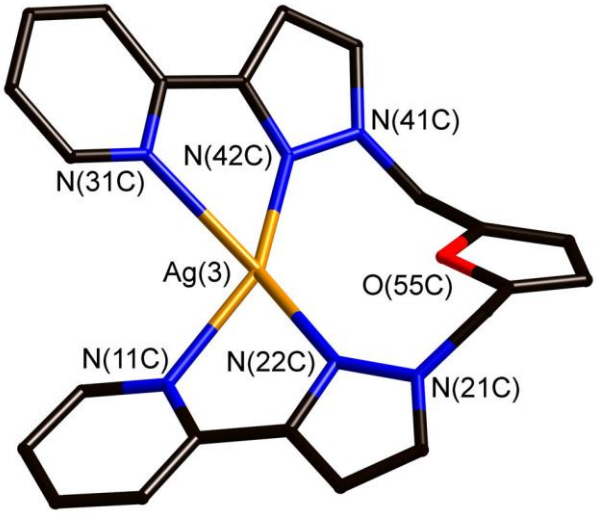

Figure 5.2.2.1 One of the mononuclear complexes showing the O atom of the furan pointing towards the Ag(I) ion.

Two of the complexes in the asymmetric unit [labelled Ag(1) and Ag(2)] form a closely-associated pair and are completely stacked with the pyrazolyl-pyridine units of each slanted so that they stack with each other in an 'overlapping' manner (figure 5.2.2.2). These two complexes also have a clear Ag•••Ag interaction with the Ag – Ag distance of 3.293 Å being shorter than twice the van der Waals radius (3.44 Å) and therefore it is likely to be a significant attractive interaction.[21]

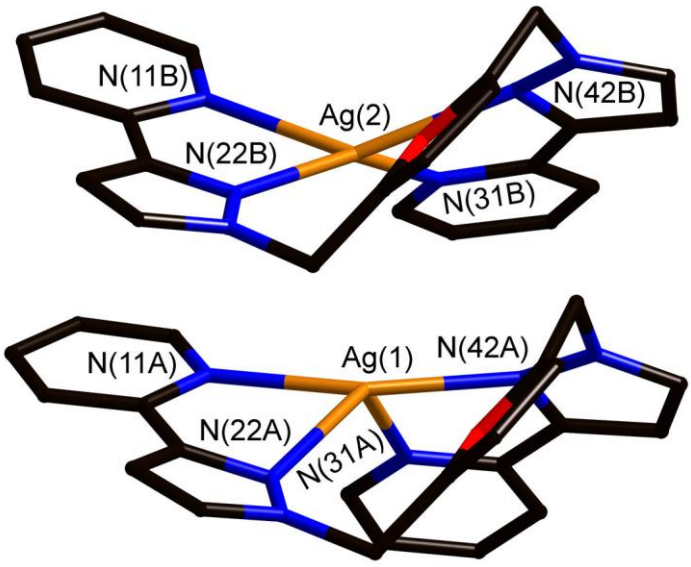

Figure 5.2.2.2 The Ag•••Ag interaction between two of the complexes and the π-stacking between the pyrazolyl-pyridine units.

Two complex cations in the asymmetric unit clearly π-stack very efficiently with each other in the 'overlapping' manner; however the third mononuclear complex is also involved in π-stacking. The crystal packing, as shown in figure 5.2.2.3, shows that the complex forms π-stacking interactions with additional symmetry-equivalent molecules in the unit cell. The offset arrangement of molecules, in contrast to the face-to-face eclipsed arrangement of Ag(1) and Ag(2) molecules, means that there cannot be any Ag•••Ag interactions involving this molecule. The Ag•••O contact distance is 2.853 Å for the Ag(3) molecule, which is shorter than in the two complexes which share the Ag•••Ag interaction (2.980 and 3.028 Å) presumably because with the lack of the Ag•••Ag interaction the Ag•••O interaction is more pronounced. Overall, all six independent chelating pyrazolyl-pyridine units are associated in π-stacking interactions although only two out of three Ag(I) ions are involved in Ag•••Ag interactions.

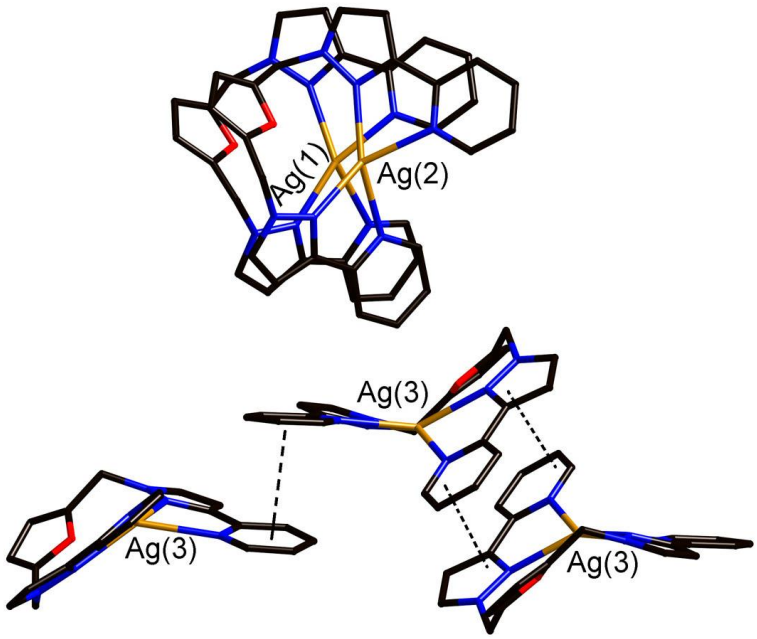

Figure 5.2.2.3 A view showing how the complexes are arranged within the unit cell and how they are orientated to maximise π-stacking between pyrazolyl-pyridine units.

ES mass spectroscopy studies reveal that the mononuclear structure is stable in solution. No multinuclear species were seen, for example dinuclear double helicates. The ^{1}H NMR spectrum also indicated that the mononuclear complex was the only product in solution, with one series of peaks corresponding to one ligand environment.

5.2.3 A dinuclear double helicate with L^{th} and Ag(I)

The ligand L^{th} consists of two chelating pyrazolyl-pyridine termini connected to a thiophene-2,5-diyl spacer *via* methylene groups. It has been shown to form M_4L_6 metallosquares (M = Zn, Co, Cu, Ni) and a 1-D zig-zag chain of double helicates with Cd(II).[19] The one common feature of both types of structure is the M_2L_2 double helix unit which is partly stabilised by the exocyclic lone pair on the thiophene pointing at the positive region in the pyrazolyl-pyridine unit.

The complex obtained when L^{th} is combined with $AgClO_4$ is a simple dinuclear double helicate as shown in figure 5.2.5. This product is perhaps what would be expected given the appearance of the double helical unit in all of the previous complexes with this ligand and the octahedral metal dications. With Ag(I) being four-coordinate this seems to be the most logical product especially given that the mononuclear complex with the ligand wrapping around a single metal ion is less favoured than with L^{fur} because the thiophene is less nucleophilic than the furan ring. The mononuclear complex is also less favoured because the distance between the two methylene carbons is longer in L^{th} than in L^{fur}.The C – C distances in the L^{th} complex are 5.388 and 5.393 Å compared to 4.829, 4.831 and 4.858 Å and this will disfavour both pyrazolyl-pyridine groups of the ligand chelating to the same Ag(I) ion.

The other reason why this structure is favourable is because the sulfur exocyclic lone pair can point directly at the relatively electron deficient pyrazolyl-pyridine units as shown in figure 5.2.3.1. This interaction is similar to the ones seen for the L^{th} complexes previously, although the interaction is slightly stronger here as the distance is shorter. The S•••pyrazolyl-pyridine distances are 3.41 and 3.46 Å in this complex compared to 3.52 and 3.62 Å in the tetranuclear Co(II) complex described previously in chapter 4.

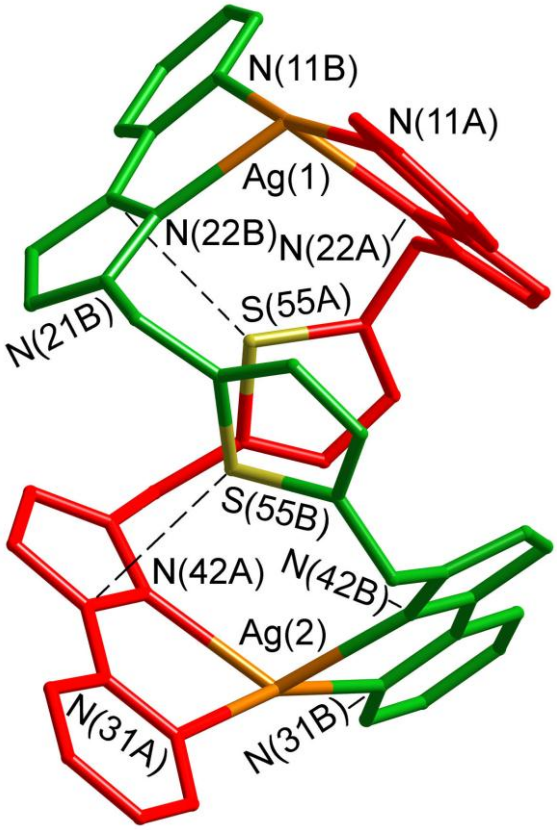

Figure 5.2.3.1: The full asymmetric unit of $[Ag_2(L^{th})_2](ClO_4)_2$.

The complex also displays π-stacking between pyrazolyl-pyridine units from different complexes. This is shown in figure 5.2.3.2 where the central complex has every pyrazolyl-pyridine unit stacked with one other pyrazolyl-pyridine unit from a different complex. The pyrazolyl-pyridine units are alternated such that the pyrazolyl ring stacks close to the pyridine ring and vice-versa. The shortest distance between stacks is 3.18 Å. In this way, the complex is similar to the mononuclear Ag complex with L^{fur} as every pyrazolyl-pyridine unit is π-stacked to one other unit. This stacking dominates the crystal packing within the structure and there are no Ag•••Ag interactions present. The Ag – Ag distance within the dinuclear helicate is 8.62 Å, the closest Ag – Ag distance between dinuclear helicates is 5.49 Å.

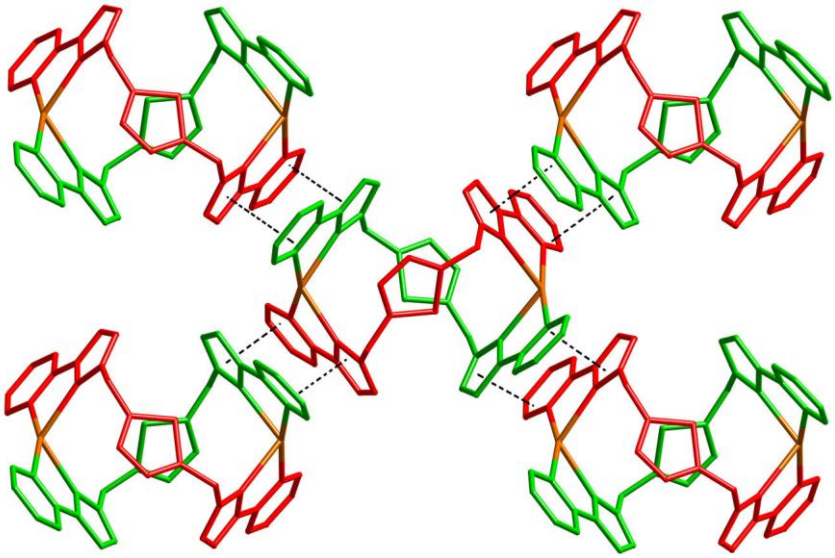

Figure 5.2.3.2 The pyrazolyl-pyridine units stack throughout the structure in 2D layers.

ES mass spectrometry confirmed the existence of the dinuclear double helicate structure in solution. Significantly, in the ^{1}H NMR spectrum both ligands are equivalent and have two fold symmetry, indicating adoption of the maximum possible molecular symmetry (D_2) for the double helix. The methylene protons appeared as a singlet rather than as a coupled pair of diastereotopic protons which are inequivalent due to the chirality of the helicate protons. This implies the presence of a dynamic process resulting in interconversion of each molecule between two enantiomeric forms that is fast on the NMR timescale, facilitated by the high kinetic lability of Ag(I).

5.2.4 A dinuclear double helicate with L^{14naph} and Ag(I)

When $AgClO_4$ and L^{14naph} are combined in a 1:1 ratio, a simple dinuclear double helicate complex, $[Ag_2(L^{14naph})_2](ClO_4)_2$ is afforded. This complex has an irregular structure with the two ligands clearly adopting substantially different conformations to allow one of the two naphthyl groups (ligand shown in blue in figure 5.2.4.1) to lie stacked between the two coordinated pyrazolyl-pyridine units of the alternate ligand. The pyridyl rings are either side of, and parallel to, the central naphthyl group and are separated from the naphthyl mean plane by *ca.* 3.5 Å (figure 5.2.4.1). This is the same type of alternating stacking (acceptor / donor / acceptor) that underpins the assembly of the polyhedral cages when this family of ligands is combined with octahedrally-coordinating transition-metal dications.[1]

The coordination geometry about the Ag(I) ions appears to be very flattened with a large gap in the coordination sphere arising from the fact that the N(pyridyl)–Ag–N(pyridyl) angles are very large [169.1˚ at Ag(1) and 165.2˚ at Ag(2)]. At Ag(1) this allows a long contact with the O atom of a perchlorate anion [Ag(1)•••O(23X), 2.812 Å], but at Ag(2) the closest Ag•••O contact [with O(14X)] is 3.26 Å such that Ag(1) can reasonably be described as five coordinate whereas Ag(2) is four-coordinate; however disorder of the perchlorate anions means that these Ag•••O distances should be regarded as approximate. The Ag•••Ag distance within the complex is 7.72 Å, shorter than in the dinuclear double helicate with L^{th} because the ligands are more distorted to maximise π-stacking.

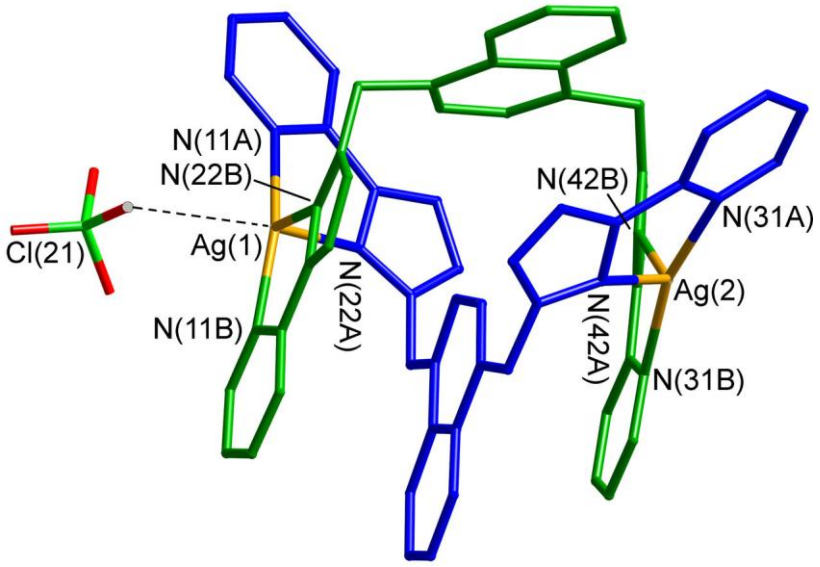

Figure 5.2.4.1 The dinuclear double helicate and one associated anion.

Again, ES mass spectrometry indicates retention of the dinuclear structure in solution, and the ^1H spectrum shows (as with the earlier double helicate) that the asymmetry observed in the solid state is lost in solution. In addition we again see that the methylene protons are equivalent rather than diastereotopic, implying a dynamic process that results in each molecule changing its chirality fast on the NMR timescale. A similar structure using the same L^{14naph} ligand and $AgNO_3$ has been reported previously.[22]

5.2.5 A 1-D coordination polymer with L^{OMe} and Ag(I)

The mixing of $AgBF_4$ with L^{OMe} in a 1:1 ratio followed by crystallisation produced a 1-D coordination polymer with a 'zigzag' topology. This is shown in figure 5.2.5.1 which

shows the alternating ligands in red and blue. Each bridging ligand spans two metal ions, presenting a bidentate N-donor site to each – as in the double helicate described above – but the ligands in this structure they alternate along the spine of Ag(I) ions to give an …Ag–L–Ag–L… infinite sequence. All Ag(I) ions are again four-coordinate, with a fairly standard geometry (figure 5.2.5.1).

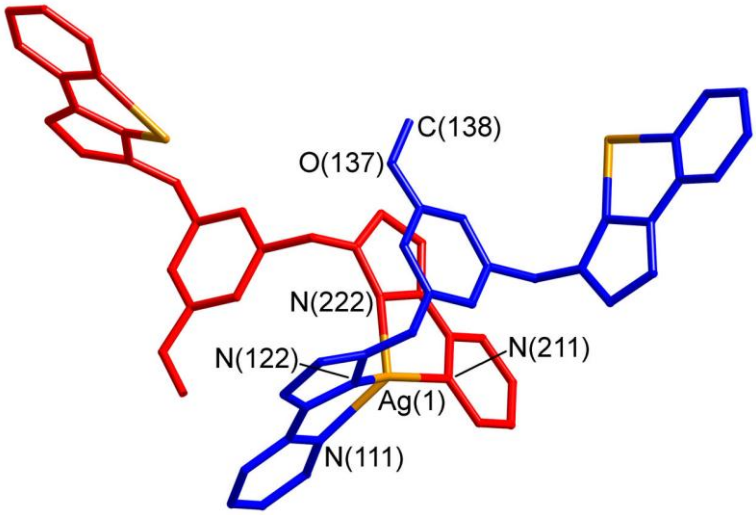

Figure 5.2.5.1 The Ag(I) coordination sphere and associated ligands.

The main non-covalent interaction to supplement the metal-ligand coordinate bonds within each chain is a π-stacking interaction between the central phenyl ring of one ligand and the pyrazole ring of a pyrazolyl-pyridine unit of a neighbouring ligand; this is emphasised in figure 5.2.5.1 with the methoxyphenyl spacer (blue) stacking with a coordinated pyrazolyl-pyridine ligand of the next ligand (in red). Every phenyl ring is stacked with an adjacent pyrazolyl-pyridine unit in this way, with a separation between parallel, overlapping aromatic fragments of 3.3 Å. As this stacking is partly charge-transfer in nature it will be facilitated by the methoxy substituent, which will make the phenyl ring more electron rich and therefore strengthen the interaction with the pyrazolyl-pyridine unit which is electron deficient by virtue of coordination to a metal cation. Within the chains we also see that the CH_3 group of the methoxy group is pointing directly at the face of a pyridine ring of a neighbouring ligand with the C(methyl)•••π(pyridyl)separation being 3.18 Å, indicative of a CH•••π interaction. There is also π-stacking between pyrazolyl-pyridine units of adjacent chains which results in the one-dimensional chains being associated into 2-D sheets (shown by dashed lines in figure 5.2.5.2).

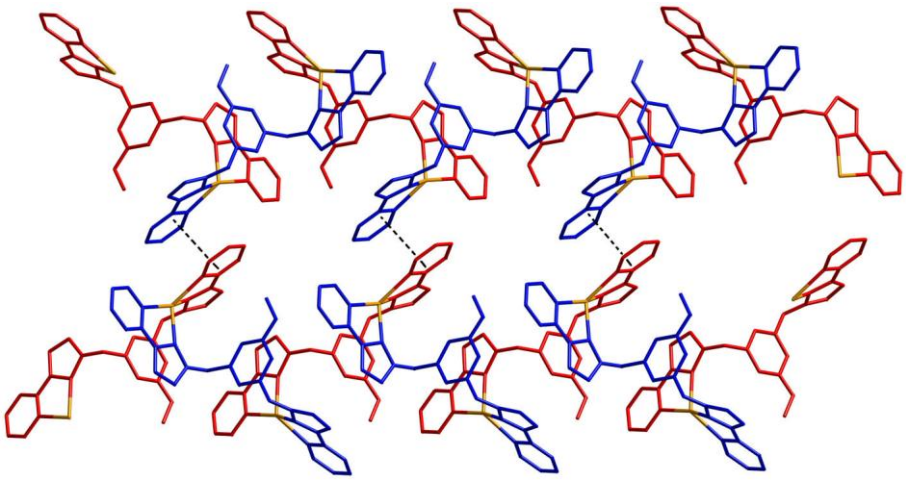

Figure 5.2.5.2 The zigzag structure of each polymer chain and the interactions between polymer chains within the crystal structure.

The anions and toluene solvent molecules in the structure both do not have any strong interactions with the Ag ions or the ligands. The ClO_4 anion and toluene molecule in the asymmetric unit are both disordered and so more detailed analysis of any hydrogen-bonding is inappropriate.

The polymer chains appear to hold together in solution with peaks in the ES mass spectrum that can be assigned to $\{Ag_4(L^{OMe})_3\}^+$, $\{Ag_3(L^{OMe})_3\}^+$, $\{Ag_3(L^{OMe})_2\}^+$, $\{Ag_2(L^{OMe})_2\}^+$, $\{Ag(L^{OMe})\}^+$. Clearly with all the different peaks for the different size fragments of the polymer chain, the chains are fragmenting under the ES conditions. However with fragments as large as $\{Ag_4(L^{OMe})_3\}$, it would appear that the polymeric structure is partially retained in solution. The ^1H NMR spectrum shows only that each ligand has twofold symmetry, which is consistent with the polymer structure.

5.2.6 A M_4L_4 'bow-tie' with L^{azo} and Ag(I)

The mixing of $AgBF_4$ with L^{azo} in a 1:1 ratio yielded a complex with an unprecedented structure in this series of $\{AgL\}_n$ complexes – a cyclic tetramer $[Ag_4(L^{azo})_4](BF_4)_4$. Such metal/ligand rings can often have a near-planar structure, however this one is based on a distorted near-tetrahedral array of Ag(I) ions with four of the six edges occupied by bridging ligands. Effectively the assembly has a 'bow-tie'-like appearance (figure. 5.2.6.1) based on the arrangement of metal ions, with all Ag(I) ions being four coordinate from the pyrazolyl-pyridine termini of two different ligands.

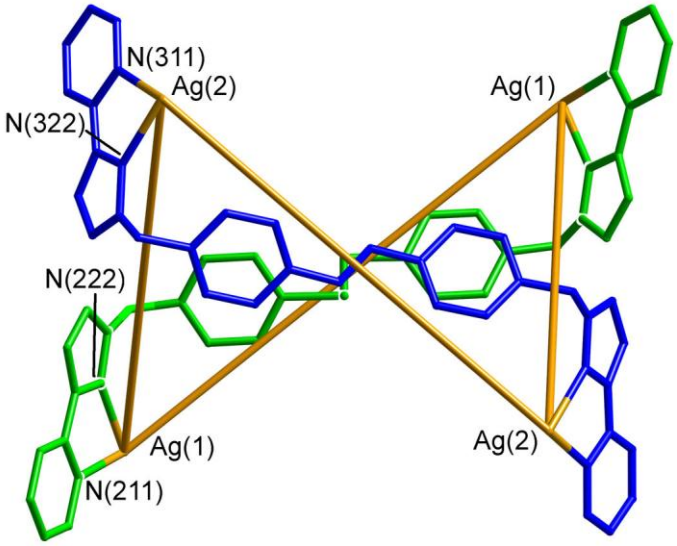

Figure 5.2.6.1 The 'bow-tie'-like topology of the complex with two of the four ligands shown.

The complex cation lies on a C_2 axis and therefore contains two independent Ag(I) ions in the asymmetric unit. Around the set of four ions in the cyclic array, successive Ag•••Ag separations are 9.71 Å [Ag(1)•••Ag(2)], 14.01 Å [Ag(2)•••Ag(2')], 9.71 Å again [Ag(2')•••Ag(1A)] and 15.39 Å [Ag(1')•••Ag(1)]. The two edges of the approximate Ag_4 tetrahedron that are not connected by bridging ligands, *i.e.* Ag(1)•••Ag(2') and Ag(1')•••Ag(2), are both 13.93 Å in length.

The main non-covalent interaction stabilising the structure is a set of two three-layer π-stacks in which an azobenzene unit from one ligand lies sandwiched between two phenyl rings of azobenzene groups from two different ligands. In figure 5.2.6.2 the (crystallographically equivalent) pair of ligands coloured pink and blue have their azobenzene units sandwiched in this way, with the orange and green ligands providing the outer phenyl rings to complete the stacks. Notably, the coordinated pyrazolyl-pyridine units are not involved in any stacking interactions within a complex molecule.

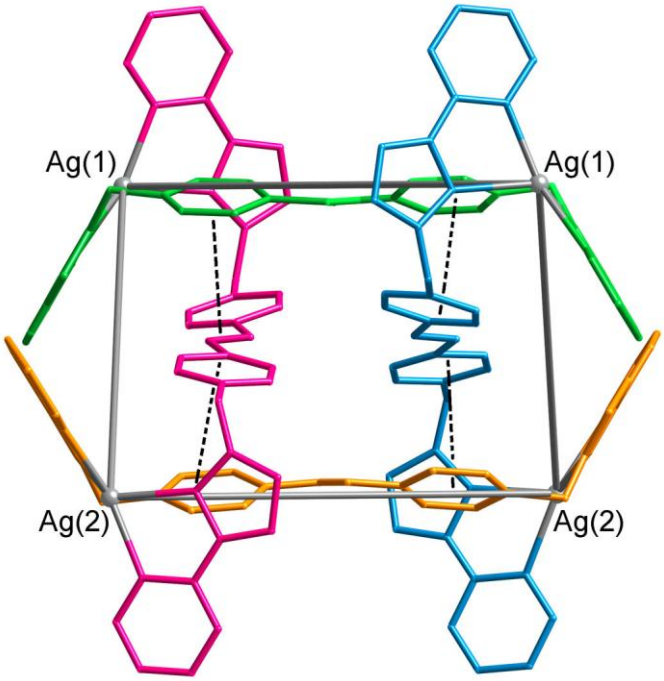

Figure 5.2.6.2 A view of the structure showing how the ligands form a square topology and how two of the azobenzene groups are stacked between phenyl groups.

In addition, there are two (crystallographically equivalent) $[BF_4]^-$ anions located at the periphery of the complex which participate in an array of CH•••F hydrogen-bonding interactions with the methylene protons of the blue and red ligands (figure 5.2.6.3). Such interactions are shown by the relatively short C•••F contacts in the range 2.7 – 2.9 Å with C(126) and C(146). Such H-bonding interactions involving these methylene protons have been shown in previous examples of polyhedral cage complexes to play an important role in recognition and binding of H-bond accepting guest molecules[23] and these interactions also clearly help to stabilise this unusual bow-tie structure.

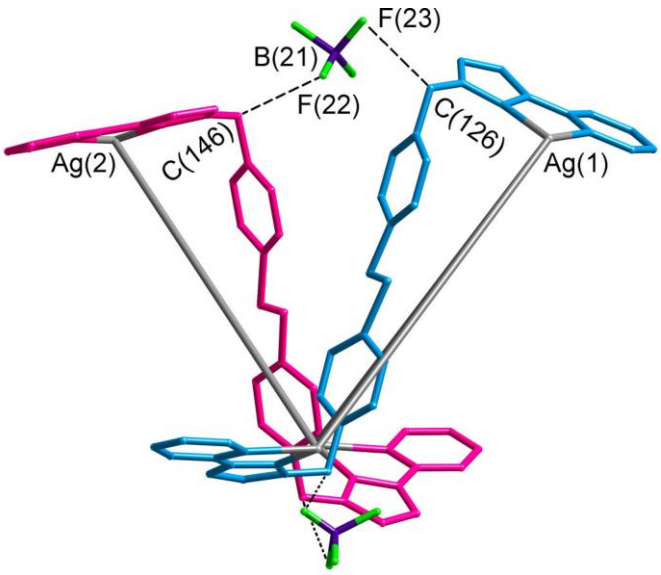

Figure 5.2.6.3 The interactions of the complex with anions (disorder not shown).

The $[Ag_4(L^{azo})_4]^{4+}$ complex cations are associated into 1-D chains *via* CH•••π interactions between the coordinated pyrazolyl-pyridine units and phenyl protons of an adjacent complex. The shortest distance between a phenyl proton and pyridine ring is 2.75 Å within a single complex and 3.05 Å between a phenyl proton of one complex and a pyridine ring of another.

The packing of the complexes results in the azobenzene groups not stacked between two phenyl rings forming a column down the centre of the channel. The azobenzene groups within a complex lie 7.33 Å apart, but the two azobenzene groups in different complexes are 3.92 Å apart. The 1-D chains associate into 2-D sheets *via* stacking interactions between pyrazolyl-pyridine units of adjacent complexes. This is shown in figure 5.2.6.4 and four of the eight pyrazolyl-pyridine units in each complex are involved in these interactions. The two pyridine rings stack and the two pyrazole rings stack, opposite to what was seen with the L^{th} complex which showed similar interactions in its crystal packing. The distance between the two pyrazolyl-pyridine units involved in the stacking is 3.33 Å.

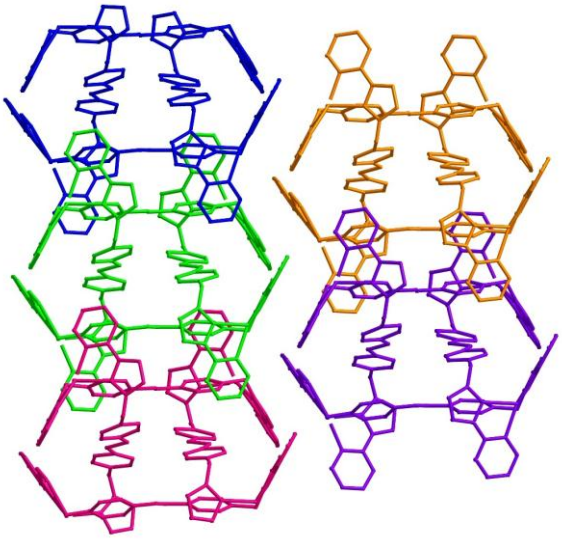

Figure 5.2.6.4 The packing of the complexes into 1-D channels and the π-stacking interactions creating 2-D sheets.

The ES mass spectrum shows only signals consistent with an $Ag_2(L^{azo})_2$ dinuclear species, possibly a double helicate: there is no trace of any signals arising from the intact tetramer. The ^1H NMR spectrum indicates formation of a symmetric species in which the ligands are all equivalent and have twofold symmetry, in agreement with the mass spectrometry data.

5.2.7 A triple helix of double helicates with L^{bz} and Ag(I)

The ligand L^{bz} was synthesised with the hope that it would form coordination cages with octahedral metal ions and a complex with a 1:1 ratio with Ag(I). The benzophenone core has the possibility for aromatic π-stacking interactions and for the carbonyl group to be functionalised.[24] The crystal structure of the ligand is shown in figure 5.2.7.1 and shows how the twist in the ligand makes it likely to form helical structures.

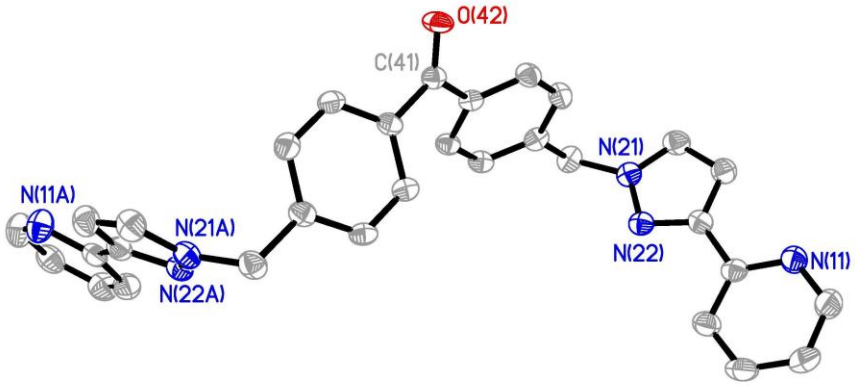

Figure 5.2.7.1 Crystal structure of L^{bz}, thermal ellipsoids at 40% probability.

The mixing of $AgPF_6$ and L^{bz} gives rise to a remarkable 'triple helix of double helicates' structure, which is based on three hierarchical levels of self-assembly. The structure is formed from $[Ag_2(L^{bz})_2]^{2+}$ dinuclear double helical units which assemble via Ag•••Ag interactions into infinite chains, three of which come together to form the triple helix of double helicates.

The dinuclear double helicate unit is shown in figure 5.2.7.2 and is quite conventional in nature. The Ag – N distances lie in the range 2.31 – 2.47 Å and the Ag – Ag distance is 11.64 Å. The double helical unit lies on a twofold axis such that only one metal ion and one ligand are in the asymmetric unit.

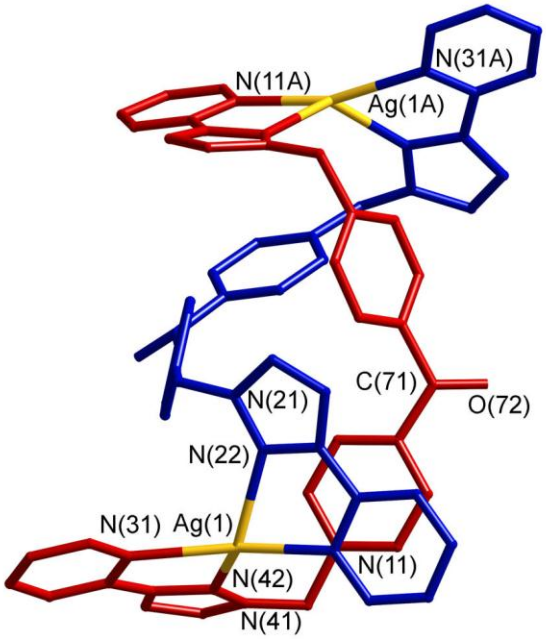

Figure 5.2.7.2 One $[Ag_2(L^{bz})_2]^{2+}$ double helical unit.

The flattened coordination geometry around each Ag(I) ion provides space for short Ag•••Ag contacts *between* units, whose distance (3.05 Å) constitutes a significant argentophilic interaction.[10] In addition this short Ag•••Ag contact results in π-stacking between the pyrazolyl-pyridine units of adjacent complex molecules, in a manner similar to that seen earlier in the complex with L^{fur} (figure 5.2.2.2). Therefore there are two interactions which result in the double helicates forming an infinite chain.

The resulting chain of double helical $[Ag_2(L^{bz})_2]^{2+}$ units (figure 5.2.7.3) has itself a shallow helical twist, with six $[Ag_2(L^{bz})_2]^{2+}$ units constituting a complete turn and a pitch length of 78.07 Å (equivalent to three times the length of the crystallographic *c* axis).

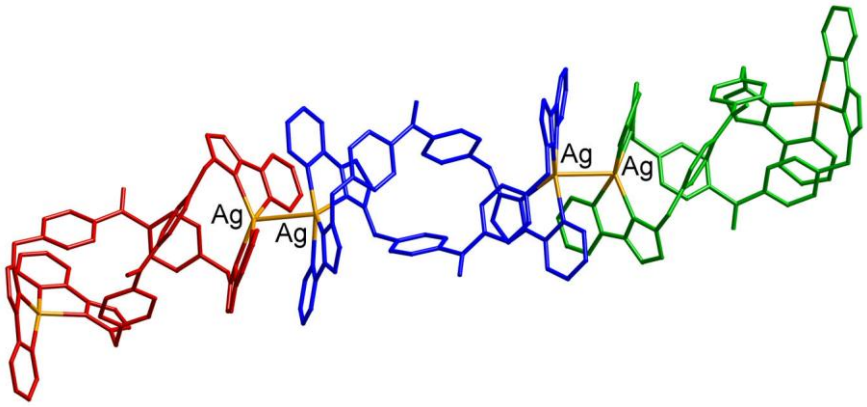

Figure 5.2.7.3 Three $[Ag_2(L^{bz})_2]^{2+}$ units connected via Ag•••Ag interactions.

The final level of organisation in this structure is that three such one-dimensional helical strands (crystallographically equivalent) are wrapped around each other to give an infinite triple helical array (figure 5.2.7.4). All three strands have the same chirality (a necessity of the chiral space group) and surprisingly the sense of twist of the triple helix is opposite to the twist of each individual double helicate.

This triple helix effectively forms a cylinder with a narrow channel down the central axis which is occupied by the hexafluorophosphate anions. Short CH•••F contacts between the F atoms and internally-directed protons from the ligands clearly stabilise the structure. The distance between successive P atoms of the anions within the central channel is 6.50 Å. The closest H•••F distances between internally-directed H atoms and the anions in the central channel are 2.31 Å to a pyrazolyl proton, 2.42 Å to a phenyl proton and 2.52 Å to a methylene proton.

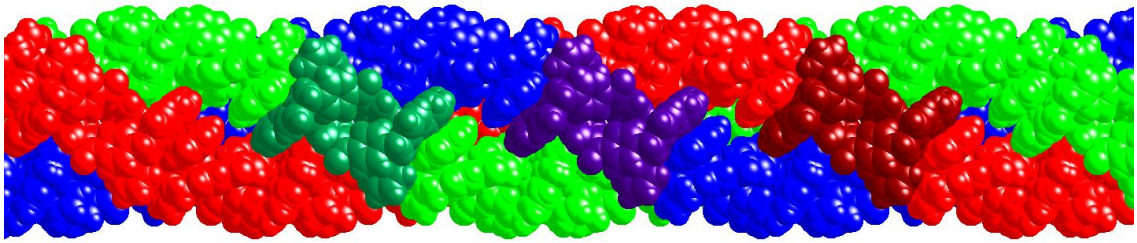

Figure 5.2.7.4 The triple helix of double helicates; one double helicate is picked out in each braid in a different colour.

Additional PF_6^- anions are located on the external surface of each triple helical cylinder, and also in the channels between the helicates. An end-on view of the cylindrical triple helicates which illustrates the hexagonal close packing of these cylinders in the extended structure is shown in figure 5.2.7.5. Accounting for the anions is somewhat complex. Within an asymmetric unit (containing one Ag(I) ion and one ligand) there are two anions with site occupancies of 1/6 which end up in the central channel of the triple helical cylinders. Another anion with 1/6 occupancy lies in the channel between triple helical cylinders and interacts equally with three such cylinders, forming CH•••F interactions (H•••F 2.55 Å) with an externally-directed pyridine H atom. The remaining anions, totalling 0.5 occupancy in the asymmetric unit, are associated with the external surface of a particular triple-helical cylinder and form CH•••F interactions with externally-directed methylene protons (H•••F, 2.63 Å).

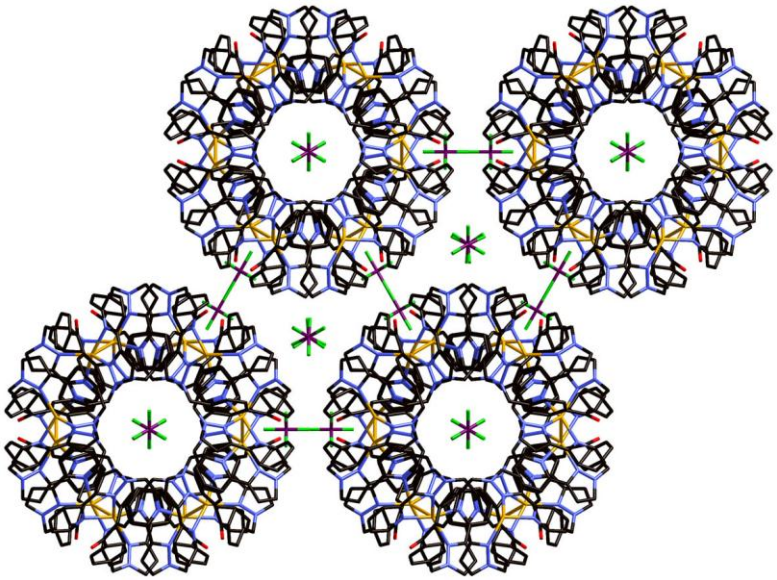

Figure 5.2.7.5 A view of the structure of $\{[Ag_2(L^{bz})_2](PF_6)_2\}_\infty$ perpendicular to that in figure 5.2.7.4, showing the arrangement of cylindrical chains, and the location of anions within the crystal packing.

The space-filling view (figure 5.2.7.6) of the structure shows the very narrow channel that is formed down the central cavity of the triple helix. The triple helix is also surrounded by anions and the weak H-bonding interactions with the anions are clearly a very dominant interaction within the structure.

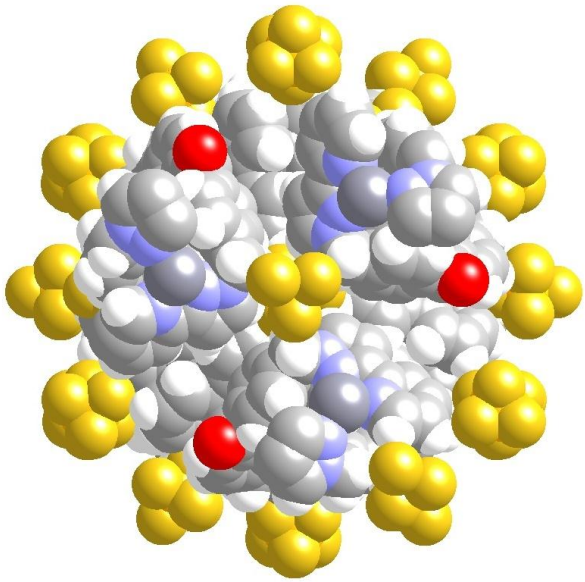

Figure 5.2.7.6 Space-filling view of one triple helix of double helix and its associated anions.

Essentially identical structures have also been observed with perchlorate and tetrafluoroborate anions. The crystal structures of these show the same triple helix of double helicate structure with the anions in the same equivalent positions in the unit cell. The fact that the same structure is obtained with all three anions implies that although the anions are involved in weak H-bonding interactions with the complex chain, the size / shape of the anion does not significantly affect this arrangement of helical chains in the crystal. To investigate this further the crystal structures of the $[Ag_2(L^{bz})_2]^{2+}$ complexes with nitrate and triflate as the anions were determined. These gave poorer quality crystals which scattered X-rays more weakly, and the structures are not included, but it was clear from the partial determinations that the gross structures are identical in every case, confirming that anion size / shape does not significantly affect the formation of these crystal structures.

The solution behaviour was studied by ES mass spectrometry which showed peaks for $[Ag_2(L^{bz})_2](X)_2$ in each case for all anions. There were no peaks which showed the dinuclear units associated with each other, for example $[Ag_4(L^{bz})_4](X)_4$ although the Ag•••Ag contacts may have been lost under the ES mass spectrometry conditions which can cause fragmentation. The ^{1}H NMR spectrum was in agreement with this showing one half equivalent of the ligand, similar to the other dinuclear double helicates described earlier.

There are two important features of the triple helix of double helicates series of structures that should be noted. First is the fact that the helical motif appears in structural chemistry in two very different forms. There is the more common series of molecular complexes based on flexible, multitopic ligands wrapping around a series of central ions such as those described by Lehn[25, 26] and others.[27-29] The other motif is based on infinite crystalline coordination polymers, when two or more infinite strands each adopt a helical twist and braid around one another.[30, 31] The two types of helical assembly have very different origins and have different requirements for them to occur. This example of the triple helix of double helicates is the first example of a single structure to include both types of structural motif to the best of our knowledge. The ligand is ideal for making a discrete double helical unit due to it being bis-bidentate and having a pre-determined twist as can be seen in its crystal structure. The Ag•••Ag contacts then allow the formation of the polymer chains which come together to form the triple helix with the H-bonding to the anions stabilising the structure. The second

important feature of the structure is that three levels of self-assembly occur in one structure. In this way it can be compared to the different organisational levels of a protein which itself has secondary, tertiary and quaternary levels of organisation.

5.3 Conclusion

In conclusion, it has been shown that six ligands all based on bis-bidentate pyrazolyl-pyridine units but different spacer groups have yielded a wide range of structures with Ag(I) ions. All complexes are based on a M_1:L_1 ratio and include a mononuclear complex $[AgL^{fur}](X)$, $[Ag_2L_2](X)_2$ dinuclear double helicates (L^{th} and L^{14naph}), a $[Ag_4L^{azo}{}_4](X)_4$ distorted 'bow-tie', a 1-D 'zig-zag' coordination polymer $\{[AgL^{OMe}](X)\}_\infty$ and a 'triple helix of double helicates' $\{[Ag_2L^{bz}{}_2](X)_2\}_\infty$. The wide range of structures is due to different favourable interactions dominating in different structures. These include Ag•••Ag interactions (especially in the complex with L^{bz}), aromatic π-stacking between PyPz units and the spacer group (L^{OMe}, L^{azo} and L^{14naph}), exocyclic lone pair interactions (L^{fur} and L^{th}) and PyPz – PyPz stacking which dictates the crystal packing in the majority of the structures. The Ag(I) ions are four coordinate with respect to the ligands in each complex, although the Ag(I) ion can adopt a flattened geometry to accommodate close contacts with either anions or other Ag(I) ions. The wide tolerance for different interactions of Ag(I) has contributed to the range of complexes seen. The most remarkable of the complexes is the 'triple helix of double helicates' with L^{bz} which has three hierarchical levels of self-assembly and has argentophilic interactions, aromatic stacking of PyPz units and weak H-bonding with anions which all help to stabilise the structure.

5.4 Experimental

The synthetic details of new ligands are given below:

Synthesis of L^{OMe}

The initial synthesis of L^{OMe} was performed by Dr Ben Hall.[32] The ligand was characterised as below:

^{1}H-NMR (400 MHz, $CDCl_3$): δ 8.62 (2H, ddd, pyridyl H^6), 7.92 (2H, dt, pyridyl H^3), 7.69 (2H, td, pyridyl H^4), 7.41 (2H, d, pyrazolyl H^5), 7.18 (2H, m, pyridyl H^5), 6.90 (2H, d, pyrazolyl H^4), 6.72 (1H, s, Phenyl H), 6.70 (2H, s, Phenyl H), 5.32 (4H, s, CH_2), 3.70 (3H, s, CH_3). ESMS *m/z* $[M + H]^+$: 423.48, $[M + Na]^+$: 445.48. Anal. Calcd for $C_{25}H_{22}N_6O$: C 71.1; H, 5.2; N, 19.9 %; found: C, 70.9; H, 5.0; N, 19.5 %.

Synthesis of L^{azo}

The synthesis of 4,4'-dimethylazobenzene and 4,4'-bis(bromomethyl)azobenzene followed previously reported methods and gave consistent analytical data.[33] The final ligand was synthesised by substitution with 3-(2-pyridyl)pyrazole under basic conditions in THF and after purification by column chromatography gave satisfactory analytical data:

^{1}H-NMR (400 MHz, $CDCl_3$): δ 8.63 (2H, ddd, pyridyl H^6), 7.95 (2H, dt, pyridyl H^3), 7.87 (4H, d, Phenyl H), 7.69 (2H, td, pyridyl H^4), 7.45 (2H, d, pyrazolyl H^5), 7.35 (4H, d, Phenyl H), 7.18 (2H, m, pyridyl H^5), 6.94 (2H, d, pyrazolyl H^4), 5.44 (4H, s, CH_2). ESMS *m/z* $[M + H]^+$: 497.58, $[M + Na]^+$: 519.53. Anal. Calcd for $C_{30}H_{24}N_8$: C 72.6; H, 4.9; N, 22.6 %; found: C, 72.2; H, 4.7; N, 22.3 %.

Synthesis of 4,4'-bis(bromomethyl)benzophenone

4,4'-dimethylbenzophenone was purchased from Alfa Aesar and used without purification. The synthesis was carried out using a modified version from previously published methods.[34-36] All characterisation data was the same as previously reported.[34]

4,4'-dimethylbenzophenone (2.00 g, 9.5 mmol) was brominated by reaction with *N*-bromosuccinimide (3.56 g, 20 mmol) in CCl_4 (80 cm^3). The mixture was refluxed for 8 hours at 77 °C in the presence of azobisisobutyronitrile (AIBN) (0.02 g) as a radical

catalyst and was activated using a tungsten lamp. Progress of the reaction was monitored by thin-layer chromatography on silica eluting with hexane:dichloromethane (80:20 v/v). The insoluble succinimide was filtered off and the remaining solution dried using $MgSO_4$. The solvent was removed under vacuum, initially yielding a pale yellow oil. The product was then recrystallised from a minimum amount of hot toluene and a solid formed on cooling. The solid was then filtered, washed with cold toluene and dried resulting in a pale yellow powder (1.61 g, 4.4 mmol, 46 %).

Synthesis of L^{benzo}

A mixture of 4,4'-bis(bromomethyl)benzophenone (1.00 g, 2.7 mmol) and 3-(2-pyridyl)pyrazole (0.78 g, 5.4 mmol; 2 equivalents) in THF (60 cm^3) containing aqueous NaOH (2.16g in 10 cm^3 H_2O) was heated to reflux for 20 hours. After cooling the solution was filtered, dried with $MgSO_4$ and reduced to dryness to yield a white powder which was washed with diethyl ether and dried (0.93 g, 1.9 mmol, 70 %).

^{1}H NMR (400MHz, $CDCl_3$): δ 8.65 (2H, ddd, J = 5.2, 1.2 and 0.8 Hz, pyridyl H_6), 7.95 (2H, dt, J = 7.9 and 1.0, pyridyl H_3), 7.77 (4H, d, J = 8.3 Hz, benzophenone H), 7.73 (2H, td, J = 7.9 and 1.8, pyridyl H_4), 7.49 (2H, d, J = 2.3 Hz, pyrazolyl H_5), 7.33 (4H, d, J = 8.3 Hz, benzophenone H), 7.22 (2H, m, pyridyl H_5), 6.96 (2H, d, J = 2.3 Hz, pyrazolyl H_4), 5.49(4H, s, CH_2). ESMS: *m/z* 497 $(M + H)^+$. Anal. Calcd for $C_{31}H_{24}N_6O$: C 75.0; H, 4.9; N, 16.9%. Found: C, 75.1; H, 4.7; N, 16.7%.

The synthetic details of the metal complexes are given below:

$[Ag(L^{fur})](ClO_4)$

A solution of $AgClO_4$ (0.029 g, 0.13 mmol) in MeOH (7 cm^3) was added to a solution of L^{fur} (0.050 g, 0.13 mmol) in CH_2Cl_2 (7 cm^3). The mixture was stirred at room temperature for 24 h, and the resultant precipitate was filtered off, washed with both MeOH and CH_2Cl_2, and dried *in vacuo* to give $[Ag(L^{fur})](ClO_4)$ as a grey powder in 70% yield. X-ray quality crystals were grown by slow diffusion of isopropyl ether into a solution of the complex in acetonitrile.

^{1}H NMR (400 MHz, CD_3CN): δ 8.49 (2H, ddd, pyridyl H^6), 7.96 (2H, dt, pyridyl H^3), 7.96 (2H, td, pyridyl H^4), 7.81 (2H, d, pyrazolyl H^5), 7.43 (2H, m, pyridyl H^5), 6.95

(2H, d, pyrazolyl H^4), 6.39 (2H, s, Furan H), 5.18 (4H, s, CH_2). ESMS: *m*/*z*; 490.3, $\{[Ag(L^{fur})]\}^+$. Anal. Calcd for $AgC_{22}H_{18}N_6OClO_4$: C 44.8; H, 3.1; N, 14.3 % Found: C, 44.6; H, 2.9; N, 14.2 %.

$[Ag_2(L^{th})_2](ClO_4)_2$

A solution of $AgClO_4$ (0.028 g, 0.12 mmol) in MeOH (7 cm^3) was added to a solution of L^{th} (0.050 g, 0.12 mmol) in CH_2Cl_2 (7 cm^3). The mixture was stirred at room temperature for 24 h, and the resultant precipitate was filtered off, washed with both MeOH and CH_2Cl_2, and dried *in vacuo* to give $[Ag_2(L^{th})_2](ClO_4)_2$ as a grey powder in 65% yield. X-ray quality crystals were grown by slow diffusion of isopropyl ether into a solution of the complex in nitromethane.

^{1}H NMR (400 MHz, CD_3CN): δ 8.30 (2H, ddd, pyridyl H^6), 7.93 (2H, dt, pyridyl H^3), 7.91 (2H, td, pyridyl H^4), 7.71 (2H, d, pyrazolyl H^5), 7.37 (2H, m, pyridyl H^5), 6.92 (2H, d, pyrazolyl H^4), 6.42 (2H, s, thiophene H), 5.11 (4H, s, CH_2). ESMS: *m*/*z*; 1111.8, $\{[Ag_2(L^{th})_2)(ClO_4)]\}^+$; 506.4, $\{[Ag_2(L^{th})_2]\}^{2+}$. Anal. Calcd for $Ag_2C_{44}H_{36}N_{12}S_2Cl_2O_8$: C 43.6; H, 3.0; N, 13.9 % Found: C, 44.0; H, 2.8; N, 14.2 %.

$[Ag_2(L^{14naph})_2](ClO_4)_2$

A solution of $AgClO_4$ (0.015 g, 0.068 mmol) in MeOH (7 cm^3) was added to a solution of L^{14naph} (0.030 g, 0.068 mmol) in CH_2Cl_2 (7 cm^3). The mixture was stirred at room temperature for 24 h, and the resultant precipitate was filtered off, washed with both MeOH and CH_2Cl_2, and dried *in vacuo* to give $[Ag_2(L^{14naph})_2](ClO_4)_2$ as a grey powder in 73% yield. X-ray quality crystals were grown by slow diffusion of diethyl ether into a solution of the complex in nitromethane.

^{1}H NMR (400 MHz, CD_3CN): δ 7.94 (4H, d; pyrazolyl H^5), 7.92 (4H, ddd; pyridyl H^6), 7.78 (4H, td; pyridyl H^4), 7.73 (4H, m; naphthyl), 7.72 (4H, dt; pyridyl H^3), 7.35 (4H, m; pyridyl H^5), 7.00 (4H, m; naphthyl), 6.92 (4H, d; pyrazolyl H^4), 5.83 (4H, s; naphthyl), 5.32 (8H, s; CH_2). ESMS: *m*/*z*; 1199.8, $\{[Ag_2(L^{14naph})_2(ClO_4)]\}^+$; 550.4, $\{[Ag_2(L^{14naph})_2]\}^{2+}$. Anal. Calcd for $Ag_2C_{56}H_{44}N_{12}Cl_2O_8$: C 51.8; H, 3.4; N, 12.9% Found: C, 51.6; H, 3.1; N, 12.5%.

$\{[Ag(L^{OMe})](BF_4)\}_\infty$

A solution of $AgBF_4$ (0.014 g, 0.071 mmol) in MeOH (7 cm^3) was added to a solution of L^{OMe} (0.030 g, 0.071 mmol) in CH_2Cl_2 (7 cm^3). The mixture was stirred at room temperature for 24 h, and the resultant precipitate was filtered off, washed with both MeOH and CH_2Cl_2, and dried *in vacuo* to give $\{[Ag(L^{OMe})](BF_4)\}_\infty$ as a grey powder in 71% yield. X-ray quality crystals were grown by slow diffusion of toluene into a solution of the complex in acetonitrile.

^{1}H-NMR (400 MHz, CD_3CN): δ 8.20 (2H, ddd, pyridyl H^6), 7.98 (2H, dt, pyridyl H^3), 7.93 (2H, td, pyridyl H^4), 7.85 (2H, d, pyrazolyl H^5), 7.39 (2H, m, pyridyl H^5), 6.98 (2H, d, pyrazolyl H^4), 6.78 (1H, s, Phenyl H), 6.57 (2H, s, Phenyl H), 5.03 (4H, s, CH_2), 3.41 (3H, s, CH_3). ESMS: *m*/*z*; 1959.3, $\{[Ag_4(L^{OMe})_3)(BF_4)_3]\}^+$; 1764.7, $\{[Ag_3(L^{OMe})_3)(BF_4)_2]\}^+$; 1342.2, $\{[Ag_3(L^{OMe})_2)(BF_4)_2]\}^+$; 1147.5, $\{[Ag_2(L^{OMe})_2)(BF_4)]\}^+$; 530.4, $\{[Ag(L^{OMe})]\}^+$. Anal. Calcd for $AgC_{25}H_{22}N_6OBF_4$: C 48.7; H, 3.6; N, 13.6% Found: C, 48.5; H, 3.2; N, 13.2%.

$[Ag_4(L^{azo})_4)](BF_4)_4$

A solution of $AgBF_4$ (0.015 g, 0.079 mmol) in MeOH (7 cm^3) was added to a solution of L^{azo} (0.040 g, 0.079 mmol) in CH_2Cl_2 (7 cm^3). The mixture was stirred at room temperature for 24 h, and the resultant precipitate was filtered off, washed with both MeOH and CH_2Cl_2, and dried *in vacuo* to give $[Ag_4(L^{azo})_4)](BF_4)_4$ as an orange powder in 63% yield. X-ray quality crystals were grown by slow diffusion of toluene into a solution of the complex in acetonitrile.

^{1}H NMR (400 MHz, CD_3CN): δ 8.45 (2H, ddd, pyridyl H^6), 7.92 (2H, m, pyridyl H^3), 7.87 (2H, d, pyrazolyl H^5), 7.87(2H, m, pyridyl H^4), 7.49 (4H, d, phenyl H), 7.34 (2H, m, pyridyl H^5), 7.21 (4H, d, phenyl H), 6.98 (2H, d, pyrazolyl H^4), 5.31 (4H, s, CH_2). ESMS: *m*/*z*; 1295.0, $\{[Ag_2(L^{azo})_2(BF_4)]\}^+$; 604.1, $\{[Ag_2(L^{azo})_2]\}^{2+}$. Anal. Calcd for $Ag_4C_{120}H_{96}N_{32}B_4F_{16}$: C 52.1; H, 3.5; N, 16.2% Found: C, 51.6; H, 3.1; N, 12.5%.

$\{[Ag_2(L^{benzo})_2](PF_6)_2\}_\infty$

A solution of $AgPF_6$ (0.015 g, 0.079 mmol) in MeOH (7 cm^3) was added to a solution of L^{benzo} (0.040 g, 0.079 mmol) in CH_2Cl_2 (7 cm^3). The mixture was stirred at room

temperature for 24 h, and the resultant precipitate was filtered off, washed with both MeOH and CH_2Cl_2, and dried *in vacuo* to give $\{[Ag_2(L^{benzo})_2](PF_6)_2\}_\infty$ as a white powder in 73% yield. X-ray quality crystals were grown by slow diffusion of toluene into a solution of the complex in nitromethane.

^{1}H NMR (400 MHz, CD_3CN): δ 8.60 (2H, ddd, pyridyl H^6), 8.01 (2H, dt, pyridyl H^3), 7.91 (2H, d, pyrazolyl H^5), 7.87 (2H, td, pyridyl H^4), 7.53 (2H, m, pyridyl H^5), 6.93 (2H, d, pyrazolyl H^4), 6.78 (4H, d, phenyl H), 6.71 (4H, d, phenyl H), 5.11 (4H, s, CH_2). ESMS: *m*/*z*; 1353.9, $\{[Ag_2(L^{benzo})_2(PF_6)]\}^+$; 604.5, $\{[Ag_2(L^{benzo})_2]\}^{2+}$. Anal. Calcd for $Ag_2C_{62}H_{48}N_{12}O_2P_2F_{12}$: C 49.7; H, 3.2; N, 11.2 % Found: C, 49.3; H, 3.3; N, 11.1%.

Synthesis of $\{[Ag_2(L^{benzo})_2](ClO_4)_2\}_\infty$

A solution of $AgClO_4$ (0.018 g, 0.079 mmol) in MeOH (7 cm^3) was added to a solution of L^{benzo} (0.040 g, 0.079 mmol) in CH_2Cl_2 (7 cm^3). The mixture was stirred at room temperature for 24 h, and the resultant precipitate was filtered off, washed with both MeOH and CH_2Cl_2, and dried *in vacuo* to give $\{[Ag_2(L^{benzo})_2](ClO_4)_2\}_\infty$ as a white powder in 67% yield. X-ray quality crystals were grown by slow diffusion of ethyl acetate into a solution of the complex in nitromethane.

^{1}H NMR (400 MHz, CD_3CN): δ 8.60 (2H, ddd, pyridyl H^6), 8.01 (2H, dt, pyridyl H^3), 7.97 (2H, d, pyrazolyl H^5), 7.87 (2H, td, pyridyl H^4), 7.52 (2H, m, pyridyl H^5), 6.93 (2H, d, pyrazolyl H^4), 6.83 (4H, d, phenyl H), 6.76 (4H, d, phenyl H), 5.22 (4H, s, CH_2). ESMS: *m*/*z*; 1307.9, $\{[Ag_2(L^{benzo})_2(ClO_4)]\}^+$; 604.5, $\{[Ag_2(L^{benzo})_2]\}^{2+}$.

Synthesis of $\{[Ag_2(L^{benzo})_2](BF_4)_2\}_\infty$

A solution of $AgBF_4$ (0.015 g, 0.079 mmol) in MeOH (7 cm^3) was added to a solution of L^{benzo} (0.040 g, 0.079 mmol) in CH_2Cl_2 (7 cm^3). The mixture was stirred at room temperature for 24 h, and the resultant precipitate was filtered off, washed with both MeOH and CH_2Cl_2, and dried *in vacuo* to give $\{[Ag_2(L^{benzo})_2](BF_4)_2\}_\infty$ as a white powder in 62% yield. X-ray quality crystals were grown by slow diffusion of ethyl acetate into a solution of the complex in nitromethane.

^{1}H NMR (400 MHz, CD_3CN): δ 8.60 (2H, ddd, pyridyl H^6), 8.01 (2H, dt, pyridyl H^3), 7.91 (2H, d, pyrazolyl H^5), 7.86 (2H, td, pyridyl H^4), 7.52 (2H, m, pyridyl H^5), 6.92

(2H, d, pyrazolyl H^4), 6.77 (4H, d, phenyl H), 6.69 (4H, d, phenyl H), 5.17 (4H, s, CH_2). ESMS: *m*/*z*; 1295.7, $\{[Ag_2(L^{benzo})_2(BF_4)]\}^+$; 604.5, $\{[Ag_2(L^{benzo})_2]\}^{2+}$.

$\{[Ag_2(L^{benzo})_2](BF_4)_2\}_\infty$ and $\{[Ag_2(L^{benzo})_2](ClO_4)_2\}_\infty$ gave variable elemental analytical data presumably due to the presence of solvent molecules and therefore are not included.

5.5 X-Ray Crystallography

Details of the crystal, data collection and refinement parameters are summarised. Data were corrected for absorption using empirical methods (SADABS)[37] based upon symmetry-equivalent reflections combined with measurements at different azimuthal angles. The structures were solved by direct methods and refined by full-matrix least squares on weighted F^2 values for all reflections using the SHELX suite of programs.[38] Non-hydrogen atoms were refined anisotropically. Hydrogen atoms were placed in calculated positions, refined using idealized geometries (riding model) and were assigned fixed isotropic displacement parameters.

The structure of $[Ag_2(L^{bz})_2](PF_6)_2$ was collected at the National Crystallography Service at the University of Southampton. The 'Squeeze' function in PLATON was used to eliminate regions of diffuse electron density in solvent-accessible voids in the structure, information is given in the CIF.

In each other case a suitable crystal was mounted in a stream of cold N_2 on a Bruker APEX-2 or SMART CCD diffractometers (at the University of Sheffield) equipped with graphite-monochromated Mo-Kα radiation from a sealed-tube source. Details of each structure are given in their individual CIFs.

Crystal Data Tables

Summary of crystallographic data for the new crystal structures:

Compound	**$[Ag(L^{fur})]_3(ClO_4)_3$ •2(MeCN)**	**$[Ag_2(L^{th})_2](ClO_4)_2$**	**$[Ag_2(L^{14naph})_2](ClO_4)_2$**
Formula	$Ag_3C_{70}H_{60}Cl_3N_{20}O_{15}$	$Ag_2C_{44}H_{36}Cl_2N_{12}O_8S_2$	$Ag_2C_{56}H_{44}C_{l2}N_{12}O_8$
Molecular weight	1851.34	1211.61	1299.67
T / *K*	120(2)	150(2)	150(2)
Crystal system	Monoclinic	Orthorhombic	Monoclinic
Space group	C2/c	Pca2(1)	P2(1)/c
a / Å	38.9323(11)	18.5223(9)	15.6463(10)
b / Å	15.4688(4)	11.5704(6)	24.0292(15)
c / Å	25.4156(6)	21.6258(11)	14.4368(9)
α / °	90	90	90
β / °	109.234(2)	90	105.090(3)
γ / °	90	90	90
V / $Å^3$	14451.8(7)	4634.6(4)	5240.6(6)
Z	8	4	4
ρ / g cm^{-3}	1.702	1.736	1.647
μ / mm^{-1}	0.998	1.119	0.919
Data, restraints, parameters, R_{int}	16509 / 297 / 1058 / 0.0487	10768 / 1 / 616 / 0.0579	12480 / 301 / 795 / 0.0489
Final *R*1, *wR*2[a]	0.0301, 0.0824	0.0387, 0.0927	0.0395, 0.0988

Compound	**$[Ag_2(L^{OMe})_2](BF_4)_2$ •(C_7H_8)**	**$[Ag_4(L^{azo})_4](BF_4)_4$ •$2(C_7H_8)$**	**$[Ag_2(L^{bz})_2](PF_6)_2$**
Formula	$Ag_2C_{57}H_{52}B_2F_8N_{12}O_2$	$Ag_4C_{134}H_{112}B_4F_{16}N_{32}$	$Ag_2C_{62}H_{48}F_{12}N_{12}O_2P_2$
Molecular weight	1326.47	2949.28	1498.80
T / *K*	100(2)	100(2)	100(2)
Crystal system	Monoclinic	Monoclinic	Hexagonal
Space group	P2(1)/n	C2/c	P6322
a / Å	10.4096(4)	34.111(6)	22.275(13)
b / Å	11.3764(5)	11.236(2)	22.275(13)
c / Å	23.0044(11)	40.686(8)	26.024(15)
α / °	90	90	90
β / °	92.754(3)	111.635(2)	90
γ / °	90	90	120
V / $Å^3$	2721.1(2)	14495(5)	11183(11)
Z	2	4	6
ρ / g cm^{-3}	1.619	1.351	1.335
μ / mm^{-1}	0.804	0.611	0.644
Data, restraints, parameters, R_{int}	3888 / 430 / 363 / 0.0694	16197 / 836 / 645 / 0.1137	3922 / 589 / 394 / 0.0963
Final *R*1, *wR*2[a]	0.0611, 0.1484	0.1167, 0.3099	0.0884, 0.2250

Compound	**$[Ag_2L_2](ClO_4)_2$ •$(MeNO_2)$**	**$[Ag_2L_2](BF_4)_2$ •$(MeNO_2)0.33(H_2O)$**	**L^{bz}**
Formula	$C_{63}H_{51}Ag_2Cl_{l2}N_{13}O_{12}$	$C_{63}H_{51.67}Ag_2B_2F_8N_{13}O_{4.33}$	$C_{31}H_{24}N_6O$
Molecular weight	1468.8	1449.5	496.56
T / *K*	100	100	100
Crystal system	Hexagonal	Hexagonal	Orthorhombic
Space group	*P*6322	*P*63	Pbcn
a / Å	21.5080(7)	21.2675(6)	8.5827(3)
b / Å	21.5080(7)	21.2675(6)	13.3565(5)
c / Å	25.7514(13)	25.9142(10)	21.0613(8)
α / °	90	90	90
β / °	90	90	90
γ / °	120	120	90
V / $Å^3$	10316.5(7)	10150.8(6)	2414.36(15)
Z	6	6	4
ρ / g cm^{-3}	1.419	1.423	1.366
μ / mm^{-1}	0.714	0.656	0.086
Data, restraints, parameters, R_{int}	4963 / 479 / 383 / 0.0786	15618 / 815 / 674 / 0.0629	2792 / 183 / 173 / 0.0715
Final *R*1, *wR*2[a]	0.0946, 0.2553	0.1200, 0.3588	0.0492, 0.1362

[a] The value of *R*1 is based on 'observed' data with $I>2\sigma(I)$; the value of *wR*2 is based on all data.

5.6 References

1. M. D. Ward, *Chem. Commun*., 2009, 4487.

2. B. R. Hall, L. E. Manck, I. S. Tidmarsh, A. Stephenson, B. F. Taylor, E. J. Blaikie, D. A. Vander Griend and M. D. Ward, *Dalton Trans.*, 2011, **40**, 12132.

3. A. Stephenson, S. P. Argent, T. Riis-Johannessen, I. S. Tidmarsh, and M. D. Ward, *J. Am. Chem. Soc.*, 2011, **133**, 858.

4. H. Fenton, I. S. Tidmarsh and M. D. Ward, *Dalton Trans*., 2009, **38**, 4199.

5. H. Fenton, I. S. Tidmarsh and M. D. Ward, *CrystEngComm.*, 2011, **13**, 1432.

6. M. Barboiu, G. Vaughan, N. Kyritsakas and J.-M. Lehn, *Chem. Eur. J.*, 2003, **9**, 763.

7. G. Baum, E. C. Constable, D. Fenske, C. E. Housecroft and T. Kulke, *Chem. Commun.*, 1998, 2659.

8. W. L. Leong and J. J. Vittal, *Chem. Rev.*, 2011, **111**, 688.

9. T. C. Mak, X.-L. Zhao, Q.-M. Wang and G.-C. Guo, *Coord. Chem. Rev.*, 2007, **251**, 2311.

10. P. Pyykkö, *Chem. Rev.*, 1997, **97**, 597.

11. A. M. Stadler, N. Kyritsakas, G. Vaughan and J.-M. Lehn, *Chem. Eur. J.*, 2007, **13**, 59.

12. G.-G. Hou , Y. Wu , J.-P. Ma and Y.-B. Dong, *CrystEngComm.*, 2011, **13**, 6850.

13. N. Gerasimchuk, A.N. Esaulenko, K.N. Dalley, C. Moore, *Dalton Trans*., 2010, **39**, 749.

14. M.-T. Chen , B. Landers and O. Navarro, *Org. Biomol. Chem*., 2012, **10**, 2206.

15. X.-F. Zheng and L.-G. Zhu, *CrystEngComm.*, 2010, **12**, 2878.

16. A. Stephenson and M. D. Ward, *Chem. Commun.*, 2012, **48**, 3605.

17. A.-M. Stadler, N. Kyritsakas, G. Vaughan, and J.-M. Lehn, *Chem. Eur. J*., 2007, **13**, 59.

18. L. Holland , W.-Z. Shen, P. von Grebe, P. J. Sanz Miguel, F. Pichierri, A. Springer, C. A. Schalley and B. Lippert, *Dalton Trans.*, 2011, **40**, 5159.

19. A. Stephenson and M. D. Ward, *Dalton Trans.*, 2011, **40**, 10360.

20. A. Stephenson and M. D. Ward, *Dalton Trans.*, 2011, **40**, 7824.

21. J. El-Bahraoui, J. M. Molina and D. P. Olea, *Phys. Chem. A*, 1998, **102**, 2443.

22. J.-L. Du, T.-L. Hu, S.-M. Zhang, Y.-F. Zeng and X.-H. Bu, *CrystEngComm*, 2008, **10**, 1866.

23. S. Turega, M. Whitehead, B. R. Hall, M. F. Haddow, C. A. Hunter and M. D. Ward, *Chem. Commun.*, 2012, **48**, 2752.

24. G. J. Summers and R. P. Quirk, *Polym. Int*., 1996, **40**, 79.

25. J.-M. Lehn, A. Rigault, J. Siegel, J. Harrowfield, B. Chevrier and D. Moras, *Proc. Natl. Acad. Sci. U. S. A.*, 2987, **84**, 2565.

26. J.-M. Lehn and A. Rigault, *Angew. Chem. Int. Ed. Engl.*, 1988, **27**, 1095.

27. C. Piguet, M. Borkovec, J. Hamacek and K. Zeckert, *Coord. Chem. Rev.*, 2005, **249**, 705.

28. S. E. Howson and P. Scott, *Dalton Trans.*, 2011, **40**, 10268.

29. M. J. Hannon and L. J. Childs, *Supramol. Chem.*, 2004, **16**, 7.

30. X.-D. Zheng and T.-B. Lu, *CrystEngComm.*, 2010, **12**, 324.

31. W. L. Leong and J. J. Vittal, *Chem. Rev.*, 2011, **111**, 688.

32. A. Stephenson and M. D. Ward, *RSC Adv.*, 2012, **2**, 10844.

33. F. Bonardi, G. London, , N. Nouwen, B. L. Feringa, and A. J. M. Driessen, *Angew. Chem. Int. Ed.*, 2010, **49**, 7234.

34. M. B. Dewal, Y. Xu, J. Yang, F. Mohammed, M. D. Smith and L. S. Shimizu, *Chem. Commun*., 2008, 3909.

35. M. Srisailas, P. Rajakumar, *Journal of Chemical Research*, 2006, **10**, 671.

36. R. S. Givens, M. K. Venkatramanan, J. Figard, *Tetrahedron Letters*, 1984, 25, 2187.

37. G. M. Sheldrick, *SADABS*: *A program for absorption correction with the Siemens SMART system*, University of Göttingen, Germany, 1996.

38. G. M. Sheldrick, *Acta Crystallogr. Sect. A*, 2008, **64**, 112.

6. Attempts to make Ir-labelled luminescent coordination cages

6.1 Introduction

The appeal of luminescent coordination cages lies in the fact that the cage might be used as an antenna group to trigger photochemical reactions of a guest bound inside the cage central cavity. This is usually done by including luminescent groups in the ligand, for example by using naphthalene or anthracene groups which has been done before by the Ward group.[1] The use of luminescent groups such as naphthalene as part of bridging ligand frameworks has also been reported in MOFs.[2]

Coordination cages with metal-based luminescence have been reported before, for example Dong and co-workers have reported a series of cages based on lanthanide metals such as La, Ce, Sm, Tb and Eu,[3]and separately cages based on Nd, Ho, Er, Tm and Yb.[4] These cages could have their emission tuned by having a different $[Ln(H_2O)_8]^{3+}$ guest species in the central cavity (figure 6.1.1). Additionally the strong luminescence from this host-guest system could be quenched or switched off by exchange of the guest with a d-block metal such as Fe^{3+} or Cu^{2+}. The cage is based on a 3,5-bis(3-benzocarboxylate)-4-amino-1,2,4-triazole ligand, which has an ideal bend angle in the ligand and the oxygen donor atoms from the carboxylate groups are excellent at coordinating to Ln(III) ions.

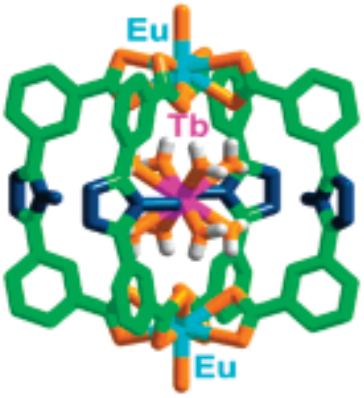

Figure 6.1.1 Crystal structure of a $[Eu_2L_4]$ cage with $[Tb(H_2O)_8]^{3+}$ guest. Reproduced from reference 3.

An example from Hamacek and co-workers showed that $[Eu_4L_4]^{12+}$ coordination cages could be synthesised containing an anion in the central cavity (figure 6.1.2). This anion could be exchanged and the system has potential for sensing using the metal-centred luminescence.[5,6] The system uses tripodal ligands, as shown in figure 6.1.2, which contain two oxygen donors and one nitrogen donor at each of the three tridentate sites. The fact that the ligands contain oxygen donors make the binding of lanthanides easier as they are known to be oxophilic.[7,8] This, along with the fact that they have high coordination numbers, makes using lanthanides with the pyrazolyl-pyridine series of ligands unlikely to yield coordination cages.

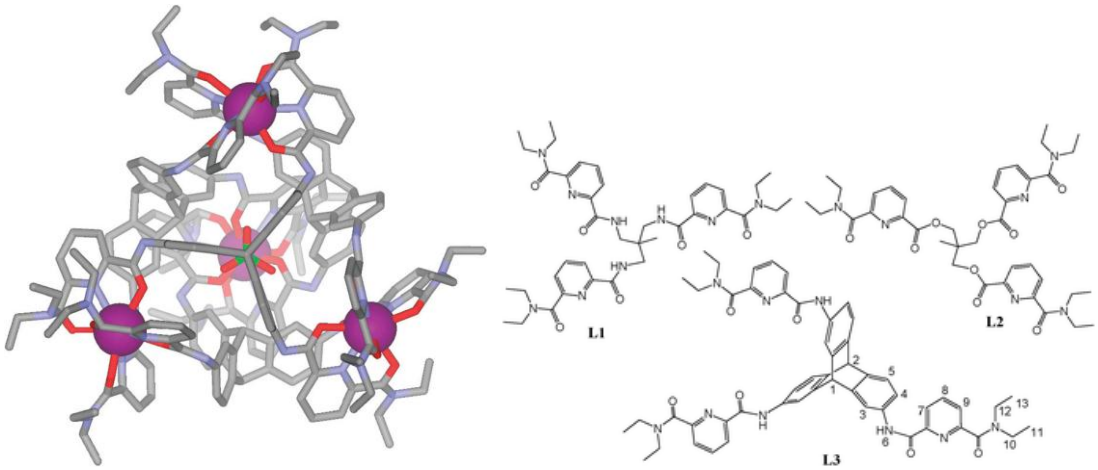

Figure 6.1.2 Molecular model of $[Eu_4(L_3)_4]^{12+}$ cage and some of the ligands used to make the cages. Reproduced from reference 6.

An alternative approach to this is to attach a luminescent metal fragment to the cage exterior, for example an Ir(phenylpyridine)$_2$ (phpy) unit which could itself act as an antenna group.

A recent example of this principle has been shown in MOFs by Lin and co-workers who have incorporated an {Ir(phpy)$_2$} unit into a MOF and used it to photoexcite Pt nanoparticles in the pores (figure 6.1.3).[9] They have achieved this by synthesising a MOF from ligands with the {Ir(phpy)$_2$} unit bound to a 2,2'-bipyridine-5,5′-dicarboxylate unit, which behaves the same as the normal biphenyl-5,5'-dicarboxylate ligand does.

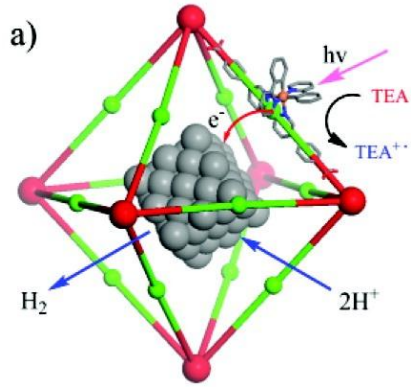

Figure 6.1.3 The photoexcitation of the Pt nanoparticles in the pores of the MOF via the {Ir(phpy)$_2$} unit. Reproduced from reference 9.

Previous work in the Ward group has shown that it is possible to use the [Ir(F_2-phpy)$_2$(pypz)]$^+$ unit to sensitise Eu(III) or Tb(III) luminescence in dinuclear Ir/Ln complexes.[10] If the unit could be attached to one pyrazolyl-pyridine unit of a tritopic ligand, the two additional 'free' pyrazolyl-pyridine units could then form a cage superstructure when the ligand was reacted with transitional metals in the usual manner. This would result in a self-assembled cage decorated with [Ir(F_2-phpy)$_2$(pypz)]$^+$ luminophores on the external surface.

This is shown in figure 6.1.4, and was done by taking a known tripodal ligand, L^{mes}, and coordinating the {Ir(F_2-phpy)$_2$} unit to one of the three pyrazolyl-pyridine units. This synthesis was done by Dr Daniel Sykes who has worked with combining the {Ir(F_2-phpy)$_2$} unit and these ligands extensively to make d-f hybrids for the purpose of making white light emitters.[11] This then leaves a ligand, $L^{mes\text{-}Ir}$, which has two vacant bis-bidentate binding sites and could conceivably make a cage with the usual M_2:L_3 ratio but have the Ir groups attached around the periphery of the cage. The ligand $L^{mes\text{-}Ir}$ will be monocationic and will have a nitrate anion associated with it.

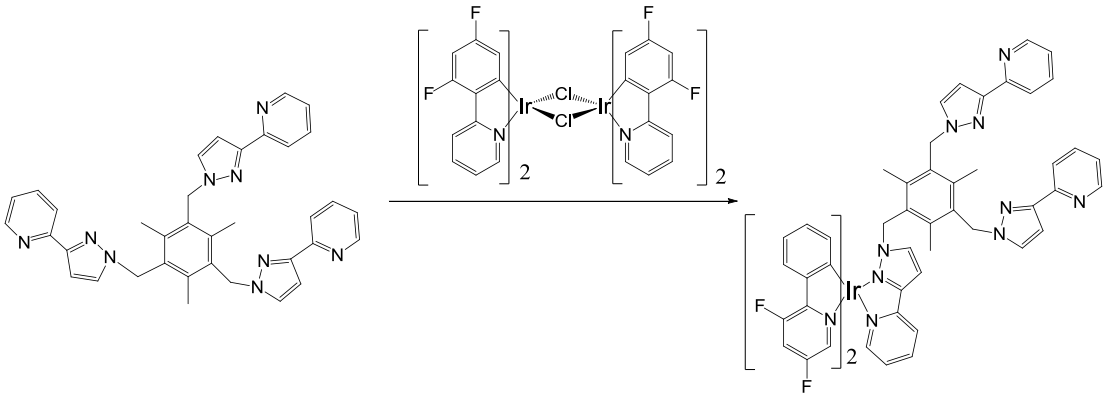

Figure 6.1.4 Synthesis of the new ligand $L^{mes\text{-}Ir}$.

6.2 Results and Discussion

6.2.1 Synthesis of ligands

The {Ir(phpy)$_2$} or {Ir(F$_2$-phpy)$_2$} antenna group has been added to four different ligands. Ligands with different numbers of pyrazolyl-pyridine units have been used to try and produce a variety of structures and to see if the idea is a plausible one. Two different tripodal ligands have been used based on the mesitylene spacer unit, one with three pyrazolyl-pyridine units ($L^{mes\text{-}Ir}$) and one with three pyridyl-triazole units ($L^{mes\text{-}Tz\text{-}Ir}$). The other ligands used are L^{pp} which will have one vacant binding pyrazolyl-pyridine unit with the Ir unit coordinated ($L^{pp\text{-}Ir}$), and L^{1245} which will have three vacant Pypz units ($L^{1245\text{-}Ir}$). Each of these ligands, shown in figure 6.2.1, has a 1+ charge due to the Ir(III) ion, and in each case there is a nitrate anion associated with the ligand.

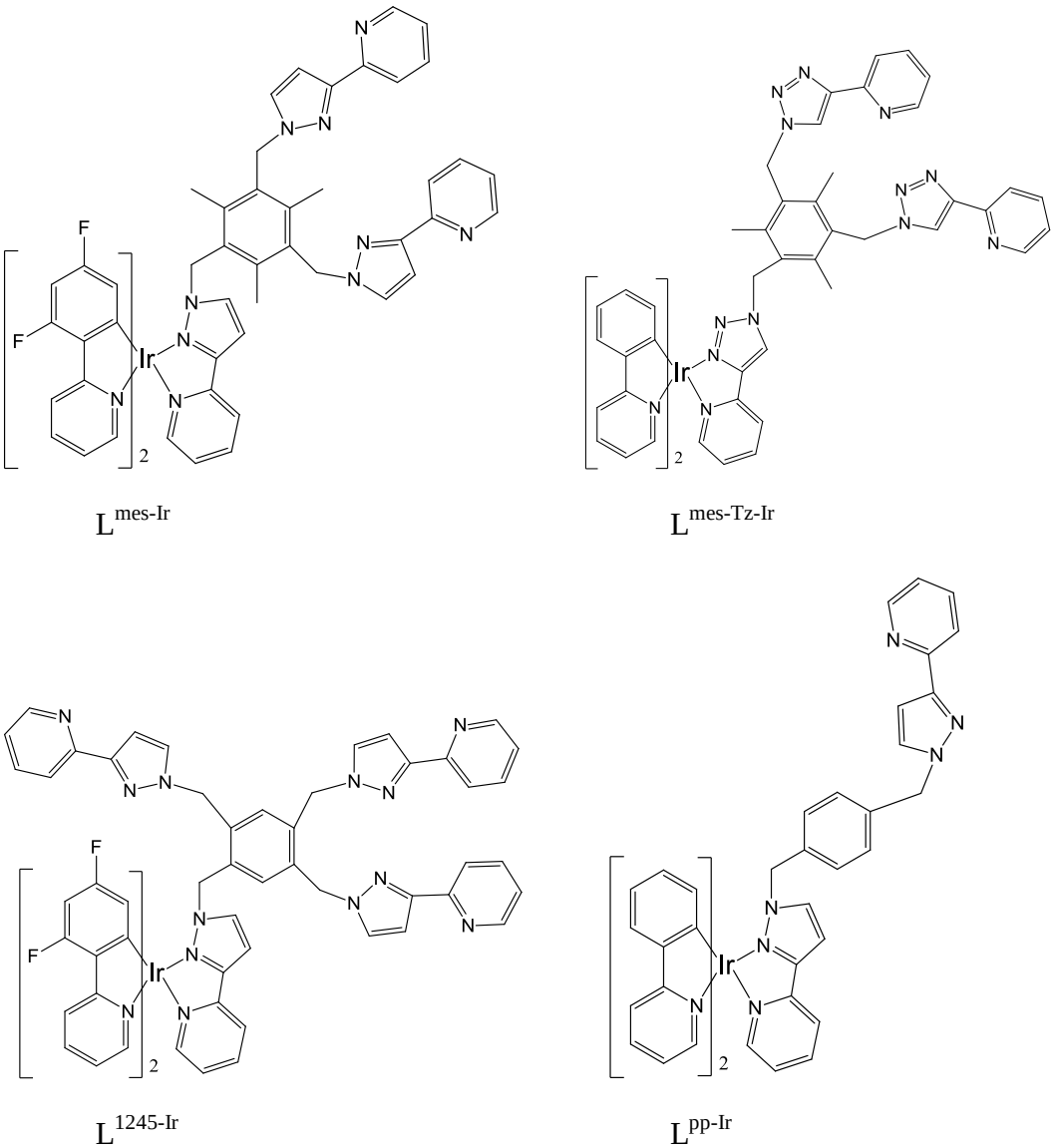

Figure 6.2.1.1 The ligands used in this study, in each case the ligand is 1+ and the counter ion was a nitrate anion.

6.2.2 A double helicate $[Cd_2(L^{mes\text{-}Ir})_2]^{6+}$ complex

When $L^{mes\text{-}Ir}$ was combined with $Cd(ClO_4)_2$ in a 3:2 ratio the product afforded was $[Cd_2(L^{mes\text{-}Ir})_2(H_2O)_4](ClO_4)_6$. The structure did not contain the 3:2 ratio as expected and a coordination cage was not obtained. The 1:1 ratio of Cd:$L^{mes\text{-}Ir}$ means that each Cd(II) ion has two coordination sites occupied by water molecules. The crystal structure is shown in figure 6.2.2.1. The structure was solved in the space group *P-1*, with only half of the complex in the asymmetric unit.

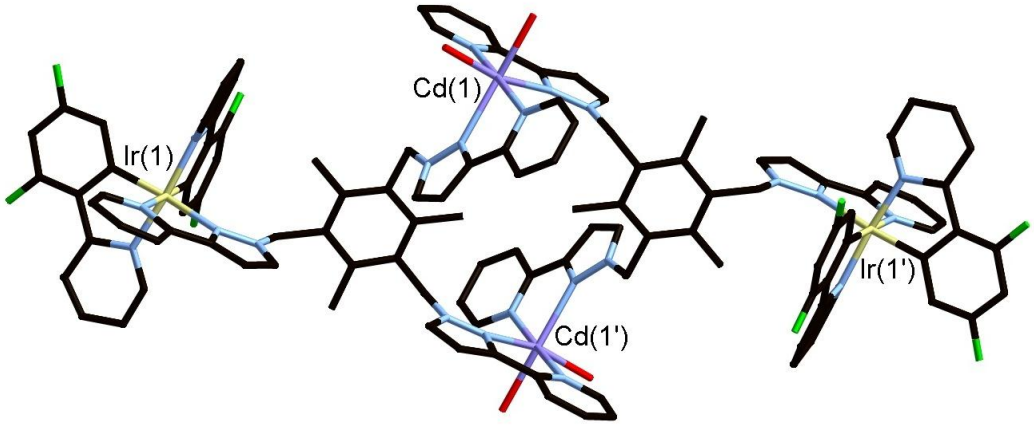

Figure 6.2.2.1 The complex cation of $[Cd_2(L^{mes\text{-}Ir})_2(H_2O)_4](ClO_4)_6$.

The metal centres form a thin rhombus shape with all metal ions in the same plane. The Cd•••Cd separation is 9.676 Å, the Ir•••Ir separation is 21.838 Å and the Cd•••Ir separations are 11.151 Å and 12.685 Å. The Cd – Ir – Cd angle is 47.4° and consequently the Ir – Cd – Ir angle is 132.6°. The $[Cd_2(\mu\text{-}L^{mes\text{-}Ir})_2]^{6+}$ structure has a helical structure and the complex may therefore be considered a $[Cd_2(\mu\text{-}L^{mes\text{-}Ir})_2]^{6+}$ double helix with pendant Ir-based luminophores.

A possible reason why this structure has formed and not a coordination cage with a 2:3 metal-to-ligand ratio is the size of the $\{Ir(F_2\text{-}phpy)_2\}$ unit. This is quite large and having six of these around the periphery of the cage may be sterically unfavourable. The space-filling view of the complex shown in figure 6.2.2.2 shows that where the vacant coordination sites are on the two Cd(II) ions (with solvent water oxygen atoms present), it may not have been possible for a single $L^{mes\text{-}Ir}$ to coordinate to both Cd(II) ions.

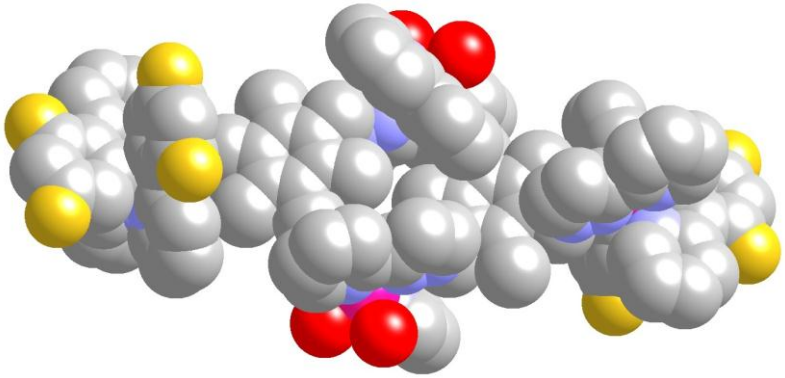

Figure 6.2.2.2 The space-filling view of $[Cd_2(L^{mes\text{-}Ir})_2](ClO_4)_6$.

Another reason why this particular structure may have formed is to maximise aromatic stacking. Although there is no aromatic π-stacking between pyrazolyl-pyridine or phenyl-pyridine units within a single complex, there is stacking between complexes in the crystal. There are two different types of stacking interactions between pyrazolyl-pyridine units of adjacent complexes. In the first stacking interaction the distance between the two groups is 3.56 Å and the two pyrazolyl-pyridine groups are stacked directly on top of one another. This interaction involves two crystallographically equivalent groups coordinated to the Cd(II) ions. The second stacking interaction involves the other pyrazolyl-pyridine group on the Cd(II) ion and the pyrazolyl-pyridine group coordinated to the Ir(III) ion. This is slightly longer at 3.64 Å and the interaction is also less pronounced as the pyrazolyl-pyridine groups are not parallel with one another and only the pyridine rings are stacked. Consequently each pyrazolyl-pyridine unit is stacked with another one to some degree. There is also π-stacking between phenyl-pyridine units of two adjacent complexes with a distance of 3.38 Å. This stacking interaction is between crystallographically equivalent units and the other phenyl-pyridine unit is not stacked at all. The stacking occurs in all three-dimensions of the crystal packing, two dimensions of which can be seen in figure 6.2.2.3.

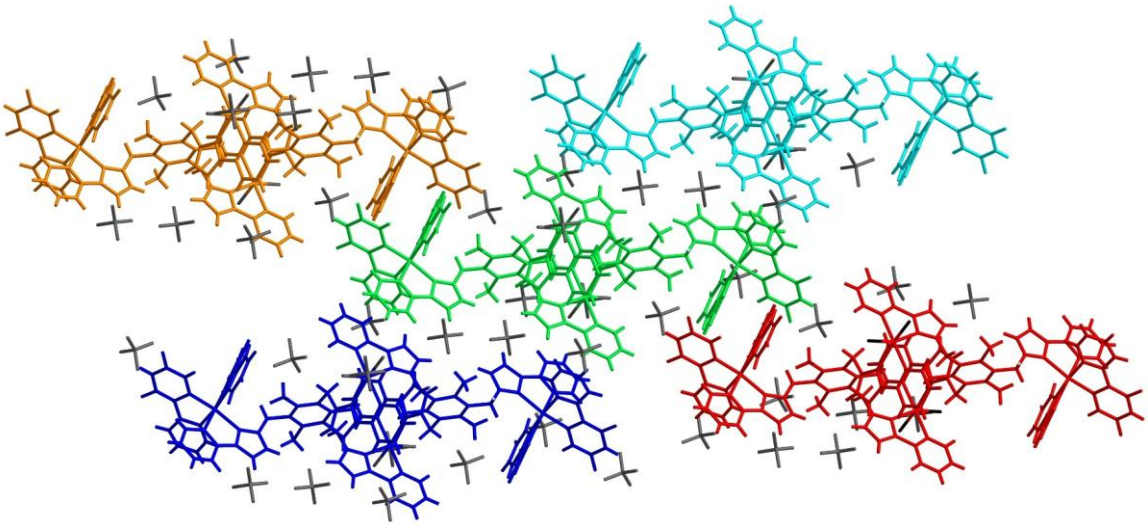

Figure 6.2.2.3 The crystal packing of $[Cd_2(L^{mes\text{-}Ir})_2](ClO_4)_6$.

No evidence for this product could be seen in solution by either ESMS or ^{1}H NMR. The main peaks in the ES mass spectrum were due to the $L^{mes\text{-}Ir}$ complex. It is possible that the structure has fragmented under the ES conditions or that free $L^{mes\text{-}Ir}$ complex was

simply able to ionise much better. It is known that Ir(III) complexes with these ligands do give very intense ES mass spectra and that they are often the most dominant peaks.

6.2.3 A trinuclear $[Cu_2(L^{1245\text{-}Ir})]^{5+}$ complex

When $L^{1245\text{-}Ir}$ was combined with $Cu(ClO_4)_2$ in a 1:1 ratio the product obtained was $[Cu_2(L^{1245\text{-}Ir})(H_2O)_2(BF_4)(NO_3)](BF_4)_3(NO_3)(CH_3CN)$, shown in figure 6.2.3.1. The idea that the ligand $L^{1245\text{-}Ir}$ could bind its three vacant pyrazolyl-pyridine units to three different metal ions and form a M_4L_4 coordination cage was not realised. This was because firstly, two of the free pyrazolyl-pyridine units were able to bind to the same Cu(II) ion, and also both Cu(II) ions in the complex were five-coordinate. The aromatic π-stacking present between the central phenyl spacer and one of the phenyl-pyridine units also means that it would be sterically unfavourable for the Cu(II) ion to be six-coordinate with three pyrazolyl-pyridine groups coordinated to it due to the stacked phenyl-pyridine unit being in such close proximity.

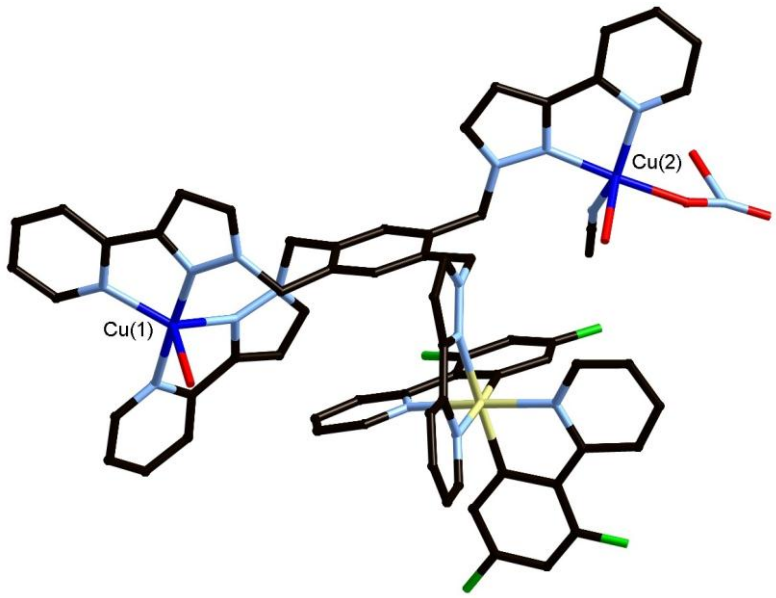

Figure 6.2.3.1 The complex cation of $[Cu_2(L^{1245\text{-}Ir})(H_2O)_2(BF_4)(NO_3)]$.

The structure crystallised in the space group *P-1*, with the whole molecule in the asymmetric unit. The two Cu(II) ions are five-coordinate with solvent molecules and anions (specifically two water molecules, an acetonitrile molecule and a nitrate anion) filling the vacant coordination sites. There is also one acetonitrile solvent molecule and four perchlorate and one nitrate anions associated with the complex.

There is aromatic π-stacking within the complex between the central phenyl ring of the ligand and a phenyl-pyridine unit coordinated to the Ir(III) ion. The distance of this interaction is 3.50 Å and is the same stacking interaction that has been seen before in many of the *d-f* hybrids with these ligands.[11] The other stacking interactions are all intermolecular between adjacent complexes. The other phenyl-pyridine unit is stacked to a pyrazolyl-pyridine unit from Cu(1) in figure 6.2.3.1, with the distance being 3.36 Å. Therefore both phenyl-pyridine units are involved in aromatic stacking, although in quite different contexts. The pyrazolyl-pyridine unit coordinated to Cu(2) is involved in a π-stacking interaction with a symmetry equivalent unit, as shown in figure 6.2.3.2. The distance between the two pyrazolyl-pyridine units is 3.45 Å and they are arranged so that a pyrazole ring is stacked with a pyridine ring and vice-versa.

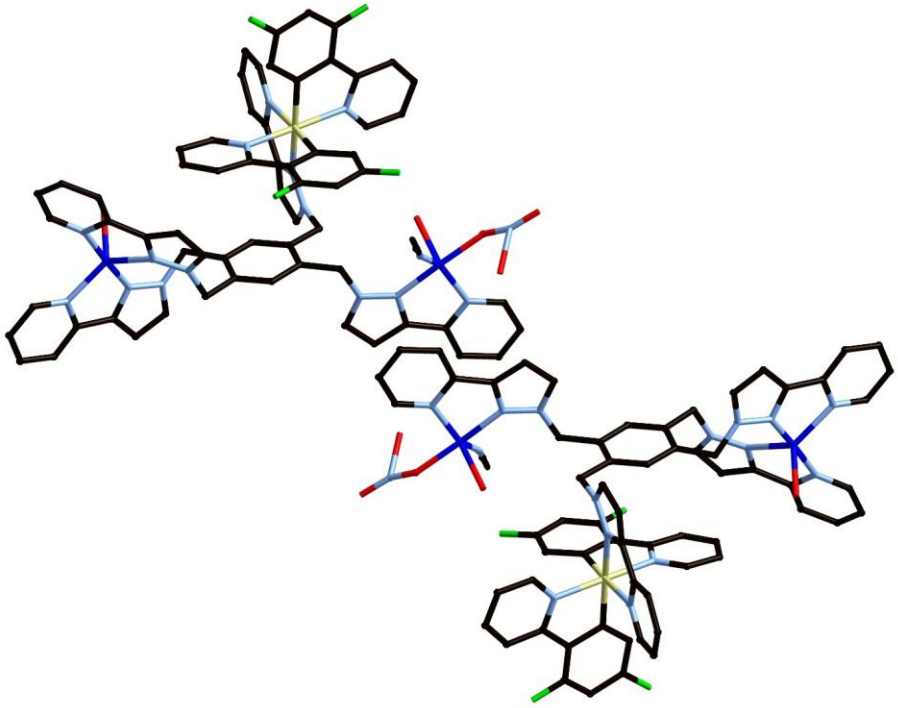

Figure 6.2.3.2 The intermolecular π-stacking of the pyrazolyl-pyridine unit coordinated to Cu(2).

The other pyrazolyl-pyridine groups in the complex are not involved in π-stacking interactions. The second pyrazolyl-pyridine group coordinated to Cu(1) is instead involved in H-bonding interactions with the perchlorate anions. The anions in the structure are disordered but a pyridine proton has a contact to a perchlorate oxygen as short as 2.24 Å and a pyrazolyl proton has a contact as short as 2.33 Å. The pyrazolyl-

pyridine unit coordinated to the Ir(I) ion is also not involved in any π-stacking interactions, but again has H-bonding interactions to anions. The pyridine proton and pyrazolyl proton contacts to a perchlorate oxygen are 2.37 and 2.42 Å respectively.

This complex could not be characterised in solution either. No peaks in the ES mass spectrum could be assigned to Cu complexes and again the only assignable peaks were due to mononuclear $L^{1245\text{-}Ir}$.

6.2.4 A trinuclear $[Zn(L^{PP\text{-}Ir})_2]^{4+}$ complex with two Ir(III) ions per Zn(II) ion

When $Zn(BF_4)_2$ was combined with $L^{pp\text{-}Ir}$ in a 1:3 ratio, the product afforded was $[Zn(L^{PP\text{-}Ir})_2(SiF_6)](NO_3)_2$. This product again did not yield the expected metal-to-ligand ratio, with the most likely product seemingly $[Zn(L^{PP\text{-}Ir})_3](X)_5$, based on a tris-chelate Zn(II) centre, however only two $L^{pp\text{-}Ir}$ units were coordinated to the Zn(II) ion. The reason for this may again be due to steric factors, because although three $Ir(phpy)_2$ units could easily fit around the Zn(II) ion, they may affect the favourable interactions within the crystal packing.

The Zn(II) ion has a distorted octahedral geometry to accommodate the bidentate coordination of an $[SiF_6]^{2-}$ anion. The L^{pp} ligands are distorted to maximise π-stacking, with the central phenyl ring of each ligand being sandwiched in a three-unit stack between a phenyl-pyridine and a pyrazolyl-pyridine. The phenyl ring from each ligand is stacked with a phenyl-pyridine coordinated to the same Ir(III) ion and a pyrazolyl-pyridine unit from the other ligand. The L^{pp} ligands are coloured differently to emphasise this in figure 6.2.4.1.

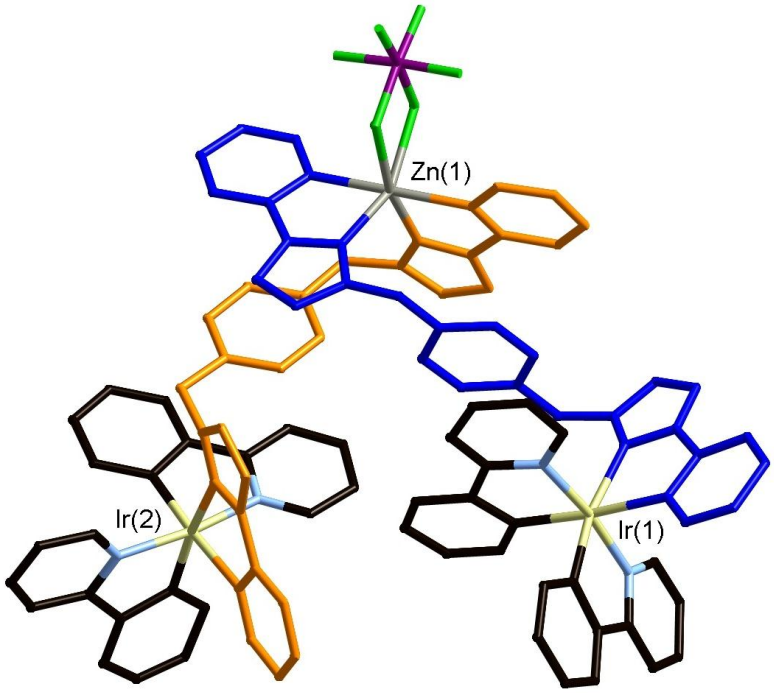

Figure 6.2.4.1 The complex cation of $[Zn(L^{PP\text{-}Ir})_2(SiF_6)]^{2+}$.

The complexes associate into dimers in the crystal packing to maximise the stacking interactions even further. Two complexes are orientated such that two three-component stacks become a single stack of six with the two pyrazolyl-pyridine units from different complexes π-stacking at a distance of 3.31 Å. The two other distances in the three-component stack are 3.25 and 3.38 Å. The stack of six units is emphasised in figure 6.2.4.2 with these units being coloured orange. The stacking is not the only favourable interaction that causes the two complexes to pack in this way. The $[SiF_6]^{2-}$ anion has F•••H H-bonding interactions to the ligand on the other complex, with F – H distances of 2.30, 2.53 and 2.63 Å to the pyridine, pyrazole and methylene protons on the ligand respectively.

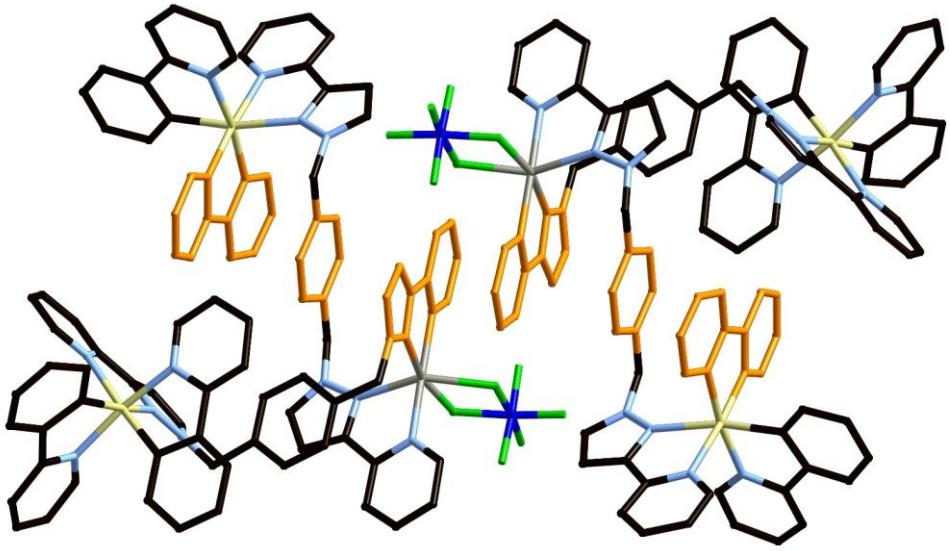

Figure 6.2.4.2 The dimer of complexes with a six-membered aromatic stack.

The remaining pyrazolyl-pyridine and phenyl-pyridine units not involved in these three-membered stacks are not involved in any aromatic π-stacking. They are however involved in various H-bonding interactions to the $[SiF_6]^{2-}$ and nitrate anions and nitromethane solvent molecules. The $[SiF_6]^{2-}$ anion has presumably arisen from decomposition of the $[BF4]^-$ anion as was seen previously with $[Ni_8(L^{pp})_{12}](BF_4)_{12}(SiF_6)_2$ in chapter 2.

There is no evidence that the product persists in solution, with the ES mass spectrum again only showing peaks for $L^{pp\text{-}Ir}$ and no assignable peaks for complexation with Zn(II).

6.2.5 A $[Cu_3(L^{mes\text{-}Tz})_2]^{6+}$ capsule with an encapsulated nitrate anion

The ligand $L^{mes\text{-}Tz\text{-}Ir}$ and $Cu(BF_4)_2$ were combined in a 3:2 ratio and reacted by the solvothermal method in MeOH. After heating at 100 °C for 12 hours and slowly cooling at 0.1 °C per minute, the reaction yielded green crystals suitable for x-ray diffraction. The data for the crystals were collected, with the complex cation expected to be similar to $[Cd_2(L^{mes\text{-}Ir})_2(H_2O)_4]$ described earlier. However the crystal structure solved as $[Cu_3(L^{mes\text{-}Tz})_2(NO_3)](BF_4)_5$ and did not contain any any of the {Ir(phpy)$_2$} unit bound to $L^{mes\text{-}Tz}$ (figure 6.2.5.1). It is apparent that due to the harsh reaction conditions, of high temperature and pressure, that the pyridyl-triazole unit coordinated to the Ir(I) ion became uncoordinated and was therefore free to coordinate to a third Cu(II) ion.

The $[Cu_3(L^{mes\text{-}Tz})_2(NO_3)](BF_4)_5$ complex is interesting because the 6+ charge of the complex cation has been balanced by five tetrafluoroborate anions and one nitrate anion, present from the original $L^{mes\text{-}Tz\text{-}Ir}$ as its nitrate salt. The nitrate is located in the centre of the capsule and is coordinated to all three Cu(II) ions, while all five tetrafluoroborate anions are located outside the central cavity. The nitrate is presumably performing a template effect, allowing the capsule to form around it.

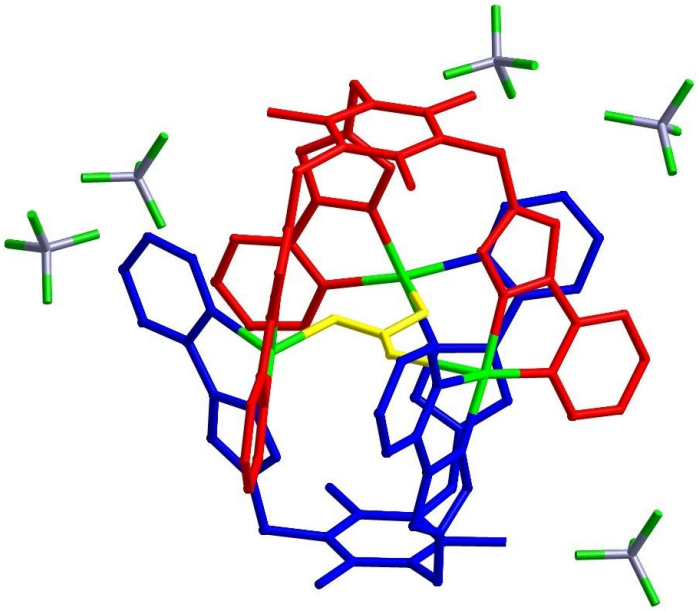

Figure 6.2.5.1 The capsule $[Cu_3(L^{mes\text{-}Tz})_2(NO_3)](BF_4)_5$.

Each Cu(II) ion is four-coordinate from two bidentate triazolyl-pyridine units, one from each ligand. This is a flattened geometry, allowing space for the Cu – O bonds to the central nitrate which are between 2.16 and 2.47 Å in length and therefore each Cu(II) ion can be considered as five-coordinate with an approximate square-pyramidal geometry. The nitrate is disordered so that each oxygen atom is located over two positions. The two ligands are effectively staggered so that each can coordinate to the Cu(II) ions at different sides. This can be seen in figure 6.2.5.2 where the methyl groups on the mesitylene are clearly in a staggered arrangement.

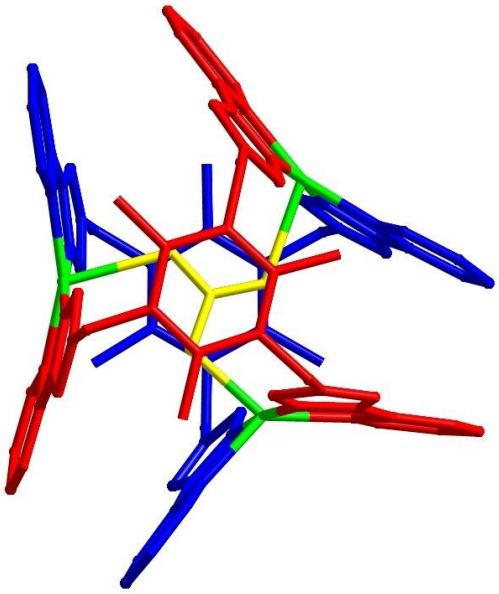

Figure 6.2.5.2 The capsule $[Cu_3(L^{mes\text{-}Tz})_2(NO_3)]$ emphasising the staggered nature of the two ligands.

The crystal packing is dominated by H-bonding interactions between the fluorine atoms of the $[BF_4]^-$ anions and the protons on the ligands. The shortest CH ••• F distances are 2.33 Å to pyridine protons, 2.39 Å to the triazole proton, 2.44 Å to the methylene protons and 2.53 Å to the methyl protons. There are no aromatic π-stacking interactions either within a single complex or between different complexes in the crystal packing.

The capsule appears to require the nitrate anion to form. When $Cu(BF_4)_2$ was reacted with $L^{mes\text{-}Tz}$ in a 3:2 ratio, no product was obtained in the solid state or could be seen in solution by ESMS. The nitrate anion is the perfect shape and size for the capsule to form around it as can be seen when the nitrate anion is in space-filling view in figure 6.2.5.3.

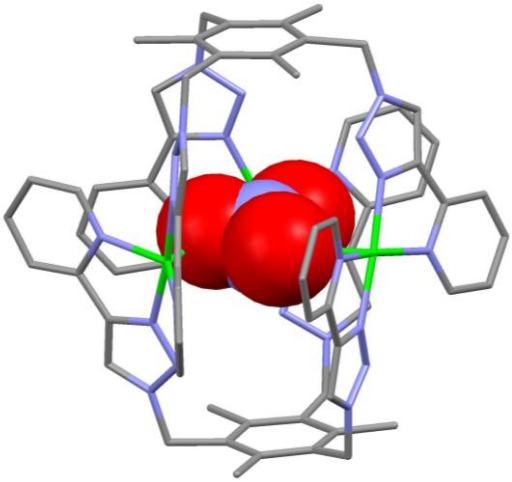

Figure 6.2.5.3 The capsule with the nitrate anion in space-filling view.

The crystals were sent for ESMS, however no peaks present in the spectrum could be assigned to the intact complex $[Cu_3(L^{mes\text{-}Tz})_2(NO_3)](BF_4)_5$ complex. It is likely that under the conditions of the ES mass spectrometry, the nitrate has been displaced from the central cavity and the capsule has fragmented.

6.3 Conclusion

The initial aim to make a luminescent coordination cage based on an $Ir(F_2\text{-phpy})_2$ or $Ir(phpy)_2$ unit coordinated to one pyrazolyl-pyridine unit of a multi-bidentate ligand has not been achieved. A series of heteronuclear structures based on these ligands and different metal salts has been described, and all show interesting features in the crystal packing. In each case the correct metal-to-ligand ratio to form a coordination cage has not been achieved. This may be due to the size of the $\{Ir(phpy)_2\}^+$ unit which will make it sterically unfavourable to have these on the exterior of a coordination cage. There are favourable aromatic π-stacking and H-bonding interactions which stabilise the complexes that are formed. With more $\{Ir(phpy)_2\}^+$ units around the metal ions, there would be less space for these favourable interactions and this could be another reason why in no occasion there is three pyrazolyl-pyridine units around a single metal ion.

The $[Cu_3(L^{mes\text{-}Tz})_2(NO_3)](BF_4)_5$ complex was achieved by serendipitous methods when under the solvothermal conditions the $\{Ir(phpy)_2\}^+$ unit originally coordinated to $L^{mes\text{-}Tz}$ was lost. The nitrate anions in the mixture appear vital to the capsule forming by acting

as a template for the capsule to form around them. The same capsule could not be seen with purely $Cu(BF_4)_2$ or $Cu(NO_3)_2$ and $L^{mes\text{-}Tz}$, suggesting that the right conditions and both anions are required for the capsule to form.

Further investigations are currently being undertaken using a $\{Pt(phpy)\}^+$ unit coordinated to one pyrazolyl-pyridine of L^{mes}. It is hoped that because only one phenyl-pyridine unit is coordinated to the square-planar Pt(II) ion this is a much smaller unit and sterically a coordination cage is more likely to form, based on the association of the remaining two pyrazolyl-pyridine units with labile metal ions.

6.4 Experimental

The ligands L^{pp} and L^{mes} were made as described previously in chapters 2 and 3 respectively. $L^{mes\text{-}Tz}$ and L^{1245} were made as previously reported.[12, 13]

Dr Daniel Sykes performed the synthesis and purification to add the $\{Ir(phpy)_2\}^+$ or $\{Ir(F_2\text{-}phpy)_2\}^+$ unit to each ligand. All complexes were prepared in the same general way; an example method is shown for $L^{pp\text{-}Ir}$.[11] A solution of L^{pp} (0.033 g, 85 μmol) was dissolved in dry CH_2Cl_2/MeOH (3:1, v/v) under N_2. To this was added a solution of $[Ir(phpy)_2(\mu\text{-}Cl)]_2$ (0.040 g, 33 μmol) in the minimum amount of CH_2Cl_2. The mixture was stirred and heated to 50 °C overnight in the dark. The mixture was cooled to room temperature and the solvent removed under reduced pressure. A saturated aqueous KPF_6 solution (20 cm^3) was added, and the resulting two-phase mixture was shaken vigorously and then separated; the aqueous residue was further extracted with several portions of CH_2Cl_2 (3 × 30 cm^3). The combined organic fractions (containing the crude complex as its hexafluorophosphate salt) were dried using sodium sulfate, and the solvent was removed. The crude yellow powder was purified by column chromatography on silica gel using MeCN and 1% aqueous KNO_3; complex $L^{pp\text{-}Ir}$ was the second yellow band to come off the column. Fractions containing the pure product were combined and reduced in volume; excess KNO_3 was precipitated by the addition of CH_2Cl_2 and filtered off. Evaporation of the resultant solution to dryness afforded pure $L^{pp\text{-}Ir}$ as its nitrate salt.

$[Cd_2(L^{mes\text{-}Ir})_2(H_2O)_4](ClO_4)_6$

A solution of $Cd(ClO_4)_2$ (0.002 g, 0.006 mmol) in MeOH (7 cm^3) was added to a solution of $L^{mes\text{-}Ir}$ (0.010 g, 0.008 mmol) in CH_2Cl_2 (7 cm^3). The mixture was stirred at room temperature for 24 h, and the resultant precipitate was filtered off, washed with both MeOH and CH_2Cl_2, and dried *in vacuo* to give $[Cd_2(L^{mes\text{-}Ir})_2(H_2O)_4](ClO_4)_6$ as a yellow powder in 65% yield. X-ray quality crystals were grown by slow diffusion of isopropyl ether into a solution of the complex in acetonitrile.

$[Cu_2(L^{1245\text{-}Ir})(H_2O)_2(BF_4)(NO_3)]\ (BF_4)_3(NO_3)\bullet(CH_3CN)$

A solution of $Cu(BF_4)_2$ (0.001 g, 0.003 mmol) in MeOH (7 cm^3) was added to a solution of $L^{1245\text{-}Ir}$ (0.005 g, 0.003 mmol) in CH_2Cl_2 (7 cm^3). The mixture was stirred at room

temperature for 24 h, and the resultant precipitate was filtered off, washed with both MeOH and CH_2Cl_2, and dried *in vacuo* to give $[Cu_2(L^{1245\text{-}Ir})(H_2O)_2(BF_4)(NO_3)](BF_4)_3(NO_3)\bullet(CH_3CN)$ as a yellow powder in 72% yield. X-ray quality crystals were grown by slow diffusion of isopropyl ether into a solution of the complex in acetonitrile.

$[Zn(L^{PP\text{-}Ir})_2(SiF_6)](NO_3)_2\bullet 2.5(CH_3NO_2)(H_2O)$

A solution of $Zn(BF_4)_2$ (0.004 g, 0.011 mmol) in MeOH (7 cm^3) was added to a solution of $L^{pp\text{-}Ir}$ (0.020 g, 0.033 mmol) in CH_2Cl_2 (7 cm^3). The mixture was stirred at room temperature for 24 h, and the resultant precipitate was filtered off, washed with both MeOH and CH_2Cl_2, and dried *in vacuo* to give $[Zn(L^{PP\text{-}Ir})_2(SiF_6)](NO_3)_2\bullet 2.5(CH_3NO_2)(H_2O)$ as a yellow powder in 58% yield. X-ray quality crystals were grown by slow diffusion of isopropyl ether into a solution of the complex in nitromethane.

$[Cu_3(L^{mes\text{-}Tz})_2(NO_3)](BF_4)_5\bullet 2(CH_3OH)$

A Teflon lined autoclave was charged with $Cu(BF_4)_2$ (0.002 g, 0.005 mmol), $L^{mes\text{-}Tz\text{-}Ir}$ (0.001 g, 0.007 mmol) and methanol (9 mL). Heating to 100 °C for twelve hours followed by slow cooling to room temperature yielded a crop of small green crystals suitable for X-ray determination.

6.5 X-ray Crystallography

Details of the crystal, data collection and refinement parameters are summarised. Data were corrected for absorption using empirical methods (SADABS)[14] based upon symmetry-equivalent reflections combined with measurements at different azimuthal angles. The structures were solved by direct methods and refined by full-matrix least squares on weighted F^2 values for all reflections using the SHELX suite of programs.[15] Non-hydrogen atoms were refined anisotropically. Hydrogen atoms were placed in calculated positions, refined using idealized geometries (riding model) and were assigned fixed isotropic displacement parameters. In each case a suitable crystal was mounted in a stream of cold N_2 on a Bruker APEX-2 or SMART CCD diffractometers (at the University of Sheffield) equipped with graphite-monochromated Mo-Kα radiation from a sealed-tube source. Details of each structure are given in their individual CIFs.

Crystal Data Tables

Summary of crystallographic data for the new crystal structures:

Compound	**$[Cd_2(L^{mes\text{-}Ir})_2(H_2O)_4](ClO_4)_6$**	**$[Cu_2(L^{1245\text{-}Ir})(H_2O)_2(BF_4)(NO_3)](BF_4)_3(NO_3)\bullet(CH_3CN)$**
Formula	$C_{116}H_{98}Cd_2Cl_6F_8Ir_2N_{22}O_{28}$	$C_{68}H_{56}B_4Cu_2F_{20}IrN_{18}O_8$
Molecular weight	3222.06	1995.83
T / *K*	100(2)	100(2)
Crystal system	Triclinic	Triclinic
Space group	P-1	P-1
a / Å	12.4512(6)	14.0399(4)
b / Å	16.1514(9)	16.5622(5)
c / Å	20.0350(9)	19.5700(6)
α / °	91.650(4)°.	96.9780(10)
β / °	99.588(3)	99.8600(10)
γ / °	111.729(4)	109.5610(10)
V / $Å^3$	3672.5(3)	4145.6(2)
Z	1	2
ρ / g cm^{-3}	1.457	1.599
μ / mm^{-1}	2.281	2.217
Data, restraints, parameters, R_{int}	10531 / 846 / 829 / 0.0788	18116 / 1132 / 1113 / 0.0292
Final *R*1, *wR*2[a]	0.0556, 0.1354	0.0674, 0.2097

Compound	**$[Zn(L^{PP\text{-}Ir})_2(SiF_6)](NO_3)_2 \cdot 2.5(CH_3NO_2)(H_2O)$**	**$[Cu_3(L^{mes\text{-}Tz})_2(NO_3)](BF_4)_5 \cdot 2(CH_3OH)$**
Formula	$C_{94.50}H_{81.50}F_6Ir_2N_{20.50}O_{12}SiZn$	$C_{68}H_{68}B_5Cu_3F_{20}N_{25}O_5$
Molecular weight	2288.16	1940.14
T / *K*	100(2)	100(2)
Crystal system	Monoclinic	Monoclinic
Space group	P2(1)/n	C2/c
a / Å	13.4782(2)	21.7160(6)
b / Å	41.4293(7)	21.2980(6)
c / Å	18.5109(3)	16.7700(5)
α / °	90	90
β / °	109.1470(10)	94.653(2)
γ / °	90	90
V / $Å^3$	9764.5(3)	7730.7(4)
Z	4	4
ρ / g cm^{-3}	1.556	1.667
μ / mm^{-1}	3.056	0.935
Data, restraints, parameters, R_{int}	22497 / 1018 / 1149 / 0.0794	8814 / 144 / 598 / 0.0641
Final *R*1, *wR*2[a]	0.0749, 0.2050	0.0506, 0.1383

[a] The value of *R*1 is based on 'observed' data with $I>2\sigma(I)$; the value of *wR*2 is based on all data

6.6 References

1. I. S. Tidmarsh, T. B. Faust, H. Adams, L. P. Harding, W. Clegg and M. D. Ward, *J. Am. Chem. Soc*., 2008, **130**, 15167.

2. Y. Cui, Y. Yue, G. Qian, and B. Chen, *Chem. Rev*., 2012, **112**, 1126.

3. Y.-B. Dong, P. Wang, J.-P. Ma, X.-X. Zhao, H.-Y. Wang, B. Tang and R.-Q. Huang, *J. Am. Chem. Soc*., 2007, **129**, 4872.

4. P. Wang, J.-P. Ma, and Y.-B. Dong, *Chem. Eur. J.*, 2009, **15**, 10432.

5 B. El Aroussi, L. Guenee, P. Pal, and J. Hamacek, *Inorg. Chem*., 2011, **50**, 8588.

6. J. Hamacek, D. Poggiali, S. Zebret, B. El Aroussi, M. W. Schneider and M. Mastalerz, *Chem. Commun*., 2012, **48**, 1281.

7. Z.-S. Meng, F.-S. Guo, J.-L. Liu, J.-D. Leng and M.-L. Tong, *Dalton Trans*., 2012, **41**, 2320.

8. S.-J. Li, S.-X. Liu, N.-N. Ma, Y.-Q. Qiu, J. Miao, C.-C. Li, Q. Tang and L. Xu *CrystEngComm.*, 2012, **14**, 1397.

9. C. Wang, K. E. deKrafft, and W. Lin, *J. Am. Chem. Soc*., 2012, **134**, 7211.

10. D. Sykes and M. D. Ward, *Chem. Commun*., 2011, **47**, 2279.

11. D. Sykes, I. S. Tidmarsh, A. Barbieri, I. V. Sazanovich, J. A. Weinstein and M. D. Ward, *Inorg. Chem*., 2011, **50**, 11323.

12. A. M. Najar, I. S. Tidmarsh and M. D. Ward, *CrystEngComm.*, 2010, **12**, 3642.

13. H. Fenton, I. S. Tidmarsh and M. D. Ward, *Dalton Trans.*, 2009, 4199.

14. G. M. Sheldrick, *SADABS*: *A program for absorption correction with the Siemens SMART system*, University of Göttingen, Germany, 1996.

15. G. M. Sheldrick, *Acta Crystallogr. Sect. A*, 2008, **64**, 112.